Group 4 amidinate complexes as olefin polymerisation catalysts

Richard T. W. Scott MChem (Oxon) AMRSC



Thesis submitted to the University of Oxford for the degree of Doctor of Philosophy, January 2013.

Statement of confidentiality

Some of the work described in this Thesis is of a commercially sensitive nature. The examiners are requested to respect the confidentiality of this information and not to disclose the information to individuals outside the Board of Examiners.

The work described in this Thesis was carried out in the Chemistry Research Laboratory, University of Oxford from October 2009 to January 2013 under the supervision of Professor Philip Mountford. All work is my own unless stated to the contrary, and has not previously been submitted for any degree at this or any other university.



Richard T. W. Scott

January 2013

Abstract

Richard T. W. Scott
Balliol College

Hilary Term 2013
D.Phil. Thesis

This Thesis describes the syntheses, structure and olefin polymerisation capability of a series of group 4 κ^1-amidinate-supported complexes.

Chapter One introduces metal-catalysed polymerisation of olefins with emphasis on the development of homogeneous molecular catalysts. The evolution of 'post-metallocene' systems, cocatalysts and the chemistry of activation are explored providing context to the work detailed in subsequent chapters.

Chapter Two describes the synthesis and characterisation of new titanium cyclopentadienyl-amidinate diene complexes and corresponding $B(C_6F_5)_3$-activated zwitterionic compounds. Their performance in small-scale ethylene-propylene-diene monomer (EPDM) copolymerisation is compared to that of a related dialkyl initiator. Some underlying chemistry of the diene/zwitterionic species is explored particularly in relation to the reversibility of zwitterion formation (activation).

Chapter Three details the synthesis and characterisation of a congeneric series of cyclopentadienyl-amidinate group 4 complexes. Combined crystallographic and DFT studies provide an insight into the nature of the amidinate-metal interaction as well as the bonding and conformational preference of the diene complexes described in Chapters Two and Three. The performance of these precatalysts in ethylene homo- and ethylene-propylene (EP) copolymerisation experiments is presented along with preliminary activation experiments giving enhanced understanding of the nature of the active species.

Chapter Four describes the synthesis and characterisation of a series of chelating cyclopentadienyl-amidinate complexes. Structural characterisation of these compounds combined with DFT calculations provide useful comparisons with the related non-*ansa* precatalysts. The EP and EPDM polymerisation performance of the bridged complexes is compared to a representative non-chelated precatalyst.

Chapter Five contains experimental details and characterising data for new compounds described in this Thesis.

CD Appendix provides crystallography .cif files

Contents

	Statement of confidentiality	ii
	Declaration	iii
	Abstract	iv
	Contents	v
	Acknowledgements	xii
	Abbreviations	xiii
	Notes	xvii
Chapter One – Introduction		1
1.1	General introduction	2
1.2	Early metal-catalysed polymerisation of olefins	2
1.3	Mechanism for homogeneous olefin polymerisation	4
1.3.1	Group 4 metallocenes and methylaluminoxane (MAO)	4
1.3.2	Proposed mechanisms	4
1.3.3	Chain transfer and termination processes	6
1.3.4	Catalyst productivity	7
1.3.5	Polymer analysis	8
1.3.5.1	Gel permeation chromatography (GPC)	8
1.3.5.2	End group analysis	10
1.4	*Ansa*-metallocenes and stereoselective propylene polymerisation	10
1.5	Constrained geometry catalysts (CGCs)	12
1.6	Non-*ansa* half-sandwich post-metallocene catalysts	15
1.7	Cyclopentadienyl-free post-metallocene catalysts	17
1.7.1	Alternative face-capping ligands	17
1.7.2	Chelated amide- and aryloxide-supported complexes	19
1.7.3	Late transition metal cyclopentadienyl-free post-metallocene systems	21
1.8	Cocatalysts and activation	22
1.8.1	Lewis acid activation of dialkyl complexes	22
1.8.2	Lewis acid activation of diene complexes	23

1.8.3	Bronsted acid activation of dialkyls and non-coordinating anions	25
1.8.4	Activation *via* alkyl abstraction	26
1.8.5	Other activation methods	27
1.9	Project introduction	27
1.9.1	Amidine and amidinate ligands	27
1.9.2	Amidinate complexes for olefin polymerisation	28
1.10	Summary and objectives	29
1.11	References for Chapter One	29
Chapter Two -		52
2.1	Overview	53
2.2	Synthesis and characterisation of cyclopentadienyl-amidinate complexes	53
2.2.1	Ligand synthesis	53
2.2.2	Synthesis of $(C_5R_5)Ti\{NC(Ph)N^iPr_2\}Cl_2$ (R = H (**2**), Me (**3**))	57
2.2.3	X-ray structures of $(C_5R_5)Ti\{NC(Ph)N^iPr_2\}Cl_2$ (R = H (**2**), Me (**3**))	59
2.2.4	Synthesis of $Cp^*Ti\{NC(Ph)N^iPr_2\}Me_2$ (**4**)	61
2.2.5	X-ray structure of $Cp^*Ti\{NC(Ph)N^iPr_2\}Me_2$ (**4**)	63
2.3	Synthesis and characterisation of cyclopentadienyl-amidinate diene complexes	63
2.3.1	Synthesis of $Cp^*Ti\{NC(Ph)N^iPr_2\}(\eta\text{-}2,3\text{-}C_4H_4Me_2)$ (**5**)	64
2.3.2	Synthesis of $Cp^*Ti\{NC(Ph)N^iPr_2\}(\eta\text{-}1,4\text{-}C_4H_4Me_2)$ (**6**)	67
2.3.3	Synthesis of $Cp^*Ti\{NC(Ph)N^iPr_2\}(\eta\text{-}1,4\text{-}C_4H_4Ph_2)$ (**7**)	69
2.3.4	Synthesis of $CpTi\{NC(Ph)N^iPr_2\}(\eta\text{-}1,4\text{-}C_4H_4Me_2)$ (**8**)	70
2.3.5	X-ray structures of diene complexes **5**-**8**	71
2.4	Synthesis and characterisation of zwitterionic cyclopentadienyl-amidinate complexes	75
2.4.1	Synthesis of $Cp^*Ti\{NC(Ph)N^iPr_2\}\{\eta^3\text{-}CH_2C(Me)C(Me)CH_2BAr^F{}_3\}$ (**9**)	75
2.4.2	Synthesis of $Cp^*Ti\{NC(Ph)N^iPr_2\}\{\eta^3\text{-}Et(CH)_3CH_2BAr^F{}_3\}$ (**10**)	78

2.4.3	Synthesis of Cp*Ti{NC(Ph)N^{i}Pr$_2$}{η^3-Me(CH)$_3$CH$_2$BAr$^{F}_3$} (**11**)	80
2.4.4	Synthesis of CpTi{NC(Ph)N^{i}Pr$_2$}{η^3-Et(CH)$_3$CH$_2$BAr$^{F}_3$} (**12**)	82
2.4.5	Attempted reaction of Cp*Ti{NC(Ph)N^{i}Pr$_2$}(η-1,4-C$_4$H$_4$Ph$_2$) (**7**) with BAr$^{F}_3$	83
2.4.6	X-ray structures of zwitterions **9**-**12**	83
2.5	Reactions of zwitterions **9** and **10** with unsaturated molecules	89
2.5.1	Reaction of Cp*Ti{NC(Ph)N^{i}Pr$_2$}{η^3-CH$_2$C(Me)C(Me)CH$_2$BAr$^{F}_3$} (**9**) with ^{t}BuNC	89
2.5.2	Reaction of Cp*Ti{NC(Ph)N^{i}Pr$_2$}{η^3-Et(CH)$_3$CH$_2$BAr$^{F}_3$} (**10**) with ^{t}BuNC	92
2.5.3	X-ray structures of zwitterionic ^{t}BuNC adducts **13** and **14**	94
2.5.4	Reactions of **9** and **10** with alkynes	97
2.5.5	Cross-over reactions with diene complexes (**5** and **6**) and zwitterions (**9** and **10**)	98
2.5.6	Variable temperature ^{19}F NMR experiments with **9** and **10**	99
2.6	Cyclopentadienyl-guanidinate titanium diene and zwitterionic complexes	100
2.6.1	Synthesis of Cp*Ti{NC(NMe$_2$)$_2$}Cl$_2$ (**15**)	100
2.6.2	Synthesis of Cp*Ti{NC(NMe$_2$)$_2$}(η-1,4-C$_4$H$_4$Me$_2$) (**16**)	102
2.6.3	Synthesis of Cp*Ti{NC(NMe$_2$)$_2$}{η^3-Et(CH)$_3$CH$_2$BAr$^{F}_3$} (**17**)	104
2.6.4	X-ray structures of **16** and **17**	105
2.7	EPDM copolymerisation experiments	109
2.8	Summary	112
2.9	References for Chapter Two	114
Chapter Three -		117
3.1	Overview	118
3.2	Zirconium and hafnium olefin polymerisation catalysts	118
3.3	Synthesis of Cp*M{NC(Ph)N^{i}Pr$_2$}Cl$_2$ (M = Zr (**18**) or Hf (**19**))	119
3.3.1	X-ray structures of Cp*M{NC(Ph)N^{i}Pr$_2$}Cl$_2$ (M = Zr (**18**) or Hf (**19**))	121

3.4	Synthesis of group 4 half-sandwich amidinate dialkyl precatalysts	123
3.4.1	Synthesis of CpTi{NC(Ph)N^{i}Pr$_2$}Me$_2$ (**20**)	124
3.4.2	Synthesis of Cp*M{NC(Ph)N^{i}Pr$_2$}Me$_2$ (M = Zr (**21**) or Hf (**22**))	124
3.4.3	Synthesis of Cp*M{NC(Ph)N^{i}Pr$_2$}(CH$_2$Ph)$_2$ (M = Ti (**23**); Zr (**24**); Hf (**25**))	125
3.4.4	X-ray structures of Cp*M{NC(Ph)N^{i}Pr$_2$}R$_2$ (M = Ti, R = CH$_2$Ph (**23**); M = Zr, R = Me (**21**); M **=** Zr, R = CH$_2$Ph (**24**); M = Hf, R = CH$_2$Ph (**25**)	127
3.5	Synthesis of zirconium diene complexes	131
3.5.1	Synthesis of Cp*Zr{NC(Ph)N^{i}Pr$_2$}(η-2,3-C$_4$H$_4$Me$_2$) (**26**)	131
3.5.2	Synthesis of Cp*Zr{NC(Ph)N^{i}Pr$_2$}(η-1,4-C$_4$H$_4$Ph$_2$) (**27**)	133
3.5.3	X-ray structures of Cp*Zr{NC(Ph)N^{i}Pr$_2$}(η-2,3-C$_4$H$_4$Me$_2$) (**26**) and Cp*Zr{NC(Ph)N^{i}Pr$_2$}(η-1,4-C$_4$H$_4$Ph$_2$) (**27**)	134
3.5.4	Synthesis of Cp*Zr{NC(Ph)N^{i}Pr$_2$}{η^3-CH$_2$C(Me)C(Me)CH$_2$BAr$^{F}_3$} (**28**)	136
3.5.5	Attempted reaction of Cp*Zr{NC(Ph)N^{i}Pr$_2$}(η-1,4-C$_4$H$_4$Ph$_2$)	138
3.5.6	X-ray structure of Cp*Zr{NC(Ph)N^{i}Pr$_2$}{η^3-CH$_2$C(Me)C(Me)CH$_2$BAr$^{F}_3$} (**28**)	138
3.5.7	Zwitterion-diene cross-over reactions	141
3.5.8	Variable temperature ^{19}F NMR experiments with **28**	141
3.5.9	Attempted reaction of Cp*Zr{NC(Ph)N^{i}Pr$_2$}(η-2,3-C$_4$H$_4$Me$_2$) (**26**) with [CPh$_3$][BAr$^{F}_4$]	142
3.6	Density functional theory calculations	142
3.6.1	Cp*M{NC(Ph)N^{i}Pr$_2$}Me$_2$ (M =Ti or Zr)	144
3.6.2	Cp*M{NC(Ph)N^{i}Pr$_2$}(η-2,3-C$_4$H$_4$Me$_2$) (M =Ti or Zr)	146
3.6.3	Calculated supine and prone isomers of Cp*M{NC(Ph)N^{i}Pr$_2$}(η-2,3-C$_4$H$_4$Me$_2$) and CpM{NC(Ph)NMe$_2$}(η-C$_4$H$_6$) (M =Ti or Zr)	148
3.6.4	Calculated supine and prone isomers of (η^5, η^1-C$_5$Me$_4$SiMe$_2$N^{t}Bu)Ti(η-2,3-C$_4$H$_4$Me$_2$) and (η^5, η^1-C$_5$H$_4$SiMe$_2$NMe)Ti(η-C$_4$H$_6$)	151

3.7	Activation chemistry of dimethyl complexes **4** and **20**-**22** with $[CPh_3][BAr^F{}_4]$	153
3.7.1	Reaction of $Cp^*Ti\{NC(Ph)N^iPr_2\}Me_2$ (**4**) with $[CPh_3][BAr^F{}_4]$	153
3.7.2	Reaction of $CpTi\{NC(Ph)N^iPr_2\}Me_2$ (**20**) with $[CPh_3][BAr^F{}_4]$	155
3.7.3	Reaction of $Cp^*M\{NC(Ph)N^iPr_2\}Me_2$ (M = Zr (**21**) or Hf (**22**)) with $[CPh_3][BAr^F{}_4]$	157
3.8	Polymerisation experiments	160
3.8.1	Ethylene homopolymerisation	160
3.8.2	Ethylene-propylene copolymerisation	164
3.9	Summary	168
3.10	References for Chapter Three	169

Chapter Four - 175

4.1	Overview	176
4.2	Synthesis and characterisation of *o*-aryl-bridged cyclopentadiene-amidine ligands	176
4.2.1	Synthetic strategy for ligand synthesis	177
4.2.2	Synthesis of ligand precursors: C_5Me_4H-2-$C_6H_4C(H)N(OMe)$ (**33**) and C_5Me_4H-2-C_6H_4CN (**34**)	178
4.2.3	Synthesis of C_5Me_4H-2-$C_6H_4C(NMe_2)NH$ (**35**)	180
4.2.4	Synthesis of C_5Me_4H-2-$C_6H_4C(N^iPr_2)NH$ (**36**) and C_5Me_4H-2-$C_6H_4C(NCy_2)NH$ (**37**)	181
4.3	Extension to indene derivatives	183
4.3.1	Synthesis of (1-C_9H_8OH)-2-$C_6H_4CH(C_2H_4O_2)$ (**38**)	183
4.3.2	Synthesis of (1-C_9H_7)-2-C_6H_4CHO (**39**)	183
4.3.3	Synthesis of (1-C_9H_7)-2-$C_6H_4C(H)N(OMe)$ (**40**)	185
4.3.4	X-ray structures of (1-C_9H_8OH)-2-$C_6H_4CH(C_2H_4O_2)$ (**38**) and (1-C_9H_7)-2-$C_6H_4C(H)N(OMe)$ (**40**)	186
4.3.5	Synthesis of (1-C_9H_7)-2-C_6H_4CN (**41**)	186
4.3.6	Attempted syntheses of (1-C_9H_7)-2-$C_6H_4C(NMe_2)NH$ and (1-C_9H_7)-2-$C_6H_4C(N^iPr_2)NH$	187

4.4	Attempted elongation of the aryl bridge	188
4.4.1	Synthesis of ±2-(((1R,2S)-1,2,3,4-tetramethyl-5-oxocyclopent-3-en-1-yl)methyl)benzonitrile (**42**)	188
4.4.2	Attempted reduction of **42**	190
4.5	Synthesis and characterisation of titanium *o*-aryl-bridged cyclopentadienyl-amidinate dichloride complexes	191
4.5.1	Synthesis of $\{\eta^5, \eta^1\text{-}C_5Me_4\text{-}2\text{-}C_6H_4C(NMe_2)N\}TiCl_2$ (**43**)	191
4.5.2	Synthesis of $\{\eta^5, \eta^1\text{-}C_5Me_4\text{-}2\text{-}C_6H_4C(N^iPr_2)N\}TiCl_2$ (**44**)	192
4.5.3	Synthesis of $\{\eta^5, \eta^1\text{-}C_5Me_4\text{-}2\text{-}C_6H_4C(NCy_2)N\}TiCl_2$ (**45**)	194
4.5.4	X-ray structures of $\{\eta^5, \eta^1\text{-}C_5Me_4\text{-}2\text{-}C_6H_4C(NR_2)N\}TiCl_2$ (R = Me (**43**), ^{i}Pr (**44**), Cy (**45**))	195
4.6	Synthesis and characterisation of titanium o-aryl-bridged cyclopentadienyl-amidinate dimethyl complexes	197
4.6.1	Synthesis of $\{\eta^5, \eta^1\text{-}C_5Me_4\text{-}2\text{-}C_6H_4C(NR_2)N\}TiMe_2$ (R = Me (**46**), ^{i}Pr (**47**), Cy (**48**))	198
4.6.2	X-ray structures of $\{\eta^5, \eta^1\text{-}C_5Me_4\text{-}2\text{-}C_6H_4C(NR_2)N\}TiMe_2$ (R = Me (**46**), ^{i}Pr (**47**), Cy (**48**))	200
4.7	Density functional theory calculations	203
4.7.1	$\{\eta^5, \eta^1\text{-}C_5Me_4\text{-}2\text{-}C_6H_4C(N^iPr_2)N\}TiMe_2$	203
4.7.2	Steric factor calculations	205
4.8	Attempted synthesis of an unconstrained chelated complex	207
4.8.1	Synthesis of 2-(2-(2,3,4,5-tetramethylcyclopentadienyl)ethyl)isoindolin-1-imine (**49**)	207
4.8.2	Attempted synthesis of $\{\eta^5, \eta^1\text{-}C_5Me_4\text{-}C_2H_4\text{-}C_8H_7N_2\}TiCl_2$ (**50**)	209
4.9	Polymerisation experiments	213
4.9.1	Productivity comparison: EP and EPDM copolymerisations	214
4.9.2	Temperature stability comparison: EP copolymerisation	216
4.9.3	Comonomer incorporation comparison: EP and EPDM copolymerisations	219
4.10	Summary	221
4.11	References for Chapter Four	222

Chapter Five - Experimental details and characterising data 225

5.1 General methods and instrumentation 226
5.2 Literature preparations and starting materials 226
5.3 Experimental details for Chapter Two 227
5.4 Experimental details for Chapter Three 240
5.5 Experimental details for Chapter Four 249
5.6 General polymerisation procedure 265
5.6.1 Reagents, cocatalysts and scavengers 265
5.6.2 Ethylene homopolymerisation 265
5.6.3 Ethylene-Propylene copolymerisation 266
5.6.4 EPDM copolymerisation 266
5.7 X-ray data collection and processing parameters 267
5.8 References for Chapter Five 267

CD Appendix

Acknowledgements

I would like express sincere thanks to my supervisor Prof. Philip Mountford for his expert supervision and guidance during my period of research in Oxford and my admiration for his unrelenting dedication to the running of his research group and the department as a whole.

I owe a debt of gratitude to the chemists at LANXESS Elastomers, The Netherlands, for my inclusion into their ACE^{TM} project and for the countless runs on the batch polymerisation reactors. In particular I would like to thank Dr Gerard van Doremaele, Dr Alexandra Berthoud, Dr Victor Quiroga, Mr Hans Leduc, Mr Ralph Franssen and Mr Philip Kenyon. Thanks also go to Dr Alex Heath, Mr Adam Russell and Mr Richard Collins who have worked with me in the Mountford group also in collaboration with LANXESS Elastomers. I acknowledge LANXESS Elastomers and the EPSRC for funding.

I wish to make special mention of Dr Andrew Schwarz for his tireless work for the group, his offering of valuable scientific advice as well as his patient proof reading of the manuscript. I would also like to acknowledge Ms Laura Groom, Ms Junjuda Unruangsri and Dr Sam Thompson for their kind efforts reading through chapters. I am particularly grateful to Drs David Watkin, Richard Cooper and Amber Thompson for their work in Chemical Crystallography. Thanks to both Dr Nick Rees for help with NMR spectroscopy and Mr Colin Sparrow for mass spectrometry; their expertise is a constant asset to the department.

Thank you to Prof. Fraser Armstrong FRS and St Johns College, Oxford, for the valuable and enjoyable teaching experience. I am obliged to Prof. Andrew Hamilton FRS and his research group for helpful discussions and exposure to interesting areas of science outside my chosen field of research. I feel fortunate for all the support and reassurance given by my family and friends and particularly my parents who have been a steadfast source of encouragement. Special thanks go to Prof. Marc Adler, Drs Sam Thompson and Hannah Lingard for their loyal friendship and all the great times in the past few years. The kindness and understanding of my new family-in-law have been overwhelming and very much appreciated. Last but most certainly not least I wish to thank my wife Victoria for her love and patience.

Abbreviations

General

Å	Ångstrom
av.	average
ca.	*circa*, about
calcd	calculated
cf.	*confer*, compare to
°C	degrees Celsius
°	degrees
d	day(s)
DFT	Density Functional Theory
equiv(s).	equivalent(s)
g	gram(s)
GPC	Gel Permeation Chromatography
h	hour(s)
η	initrinsic viscosity
k	kilo
K	Kelvin
L	litre(s)
mg	milligram(s)
min	minute(s)
mL	millilitre(s)
μL	microlitre(s)
RT	room temperature
s	second(s)
SEC	Size Exclusion Chromatography
T	temperature
T_m	melting temperature
vs.	*versus*

Chemical

Ar	aryl

Ar^F	pentafluorophenyl, C_6F_5
Ar^{F2}	2,6-$C_6H_3F_2$
BAr^F_3	tris(pentafluorophenyl)borane, $B(C_6F_5)_3$
BHT	2,6-di-*tert*-butyl-4-methylphenol
Bn	benzyl
^{n}Bu	*n*-butyl
^{t}Bu	*tert*-butyl
Cp	cyclopentadienyl
Cp*	pentamethylcyclopentadienyl
$[CPh_3][BAr^F_4]$	trityl tetrakis(pentafluorophenyl)borate
Cy	cyclohexyl
D	generic donor atom
E	carbon or silicon atom
ENB	5-ethylidenebicyclo[2.2.1]hept-2-ene
EP	ethylene-propylene
EPDM	ethylene-propylene-diene monomer
Et	ethyl
Et_2O	diethyl ether
Flu	fluorenyl, $C_{13}H_9$
i	*iso*
IBAO	isobuylaluminoxane
Ind	Indenyl, C_9H_7
L	generic ligand (set)
LDA	lithium diisopropylamide
Ln	Group 3 or lanthanide element
m	*meso*
M	metal or mol L^{-1}
MAO	methylaluminoxane
MALLS	Multiangle Laser Light Scattering
Me	methyl
Me_3[9]aneN_3	trimethyl 1,4,7-triazacyclononane
Mes	2,4,6-$C_6H_2Me_3$

M_n	number average molecular weight
M_w	weight average molecular weight
M_p	peak molecular weight
M_z	Size average molecular weight
MW	molecular weight
OAc	acetate
P	polymeryl chain
PDI	polydispersity index
Ph	phenyl
PMH	pentamethylheptane
^{i}Pr	*iso*-propyl
^{n}Pr	*n*-propyl
py	pyridine
R	generic alkyl group or hydrogen atom
rac/±	*racemic*
RI	Refractive Index
s	*syndio*
TIBA	tri(isobutyl)aluminium
THF	tetrahydrofuran
TPM(d)	tris(3,5-dimethylpyrazolyl)methane(ide)
VNB	5-vinylbicyclo[2.2.1]hept-2-ene
X	generic halide or alkyl ligand

Nuclear Magnetic Resonance Spectroscopy

app	apparent
br	broad
^{13}C-{^{1}H}	proton-decoupled ^{13}C
COSY	correlation spectroscopy
d	doublet
δ	chemical shift in ppm
HETCOR	hetereonuclear correlation
HMBC	heteronuclear multiple bond correlation
HSQC	heteronuclear single quantum coherence

Hz	Hertz
i	*ipso*
J	coupling constant
m	*meta*
m	multiplet
MHz	Megahertz
NMR	Nuclear Magnetic Resonance
nOe	nuclear Overhauser effect
o	*ortho*
p	*para*
ppm	parts per million
q	quartet or quaternary
qn	quintet
ROESY	rotating-frame nuclear Overhauser Effect spectroscopy
s	singlet
sept	septet
t	triplet
VT	variable temperature

Mass Spectrometry

EI	Electron Impact
ESI^+	Electrospray ionization (positive sweep)
FI	Field ionisation
m/z	mass to charge ratio
MS	Mass spectrometry

Infrared Spectroscopy

cm^{-1}	wavenumbers
FT-IR	Fourier transform infrared
IR	Infrared
m	medium
s	strong
w	weak

Notes

Literature compounds described in Chapter One of this Thesis are numbered **1.x**. Novel compounds are labelled **1**-**50**. X-ray crystallography data collection, refinement and .cif preparation was performed by the author aside from the structures of compounds **3**, **5**, **7**, **18**, **21** and **24** for which the data were collected by either Dr Andrew D. Schwarz or Dr Michael G. Cushion and the structures solved and refined by Prof. Philip Mountford. In all cases the molecular drawings were produced by Prof. Philip Mountford. Density functional theory (DFT) calculations were performed by Dr Betty Coussens, DSM, The Netherlands. All polymerisations were performed at LANXESS Elastomers, The Netherlands, by Mr Ralph Franssen, Mr Philip Kenyon and Mr Hans Leduc under the supervision of Drs Alexandra Berthoud and Martin Zuideveld. Mass spectra were obtained by Mr Colin Sparrow and the University of Oxford Chemistry departmental service. Elemental Analysis was performed at London Metropolitan University or Elemental Microanalysis, Devon.

Chapter One

Introduction

1.1 General introduction

The transition metal-catalysed polymerisation of olefins has been the subject of sustained investigation by academic and industrial research groups alike since its Nobel Prize-winning discovery by Karl Ziegler[1, 2] and Guilio Natta[3, 4] during the 1950s. The linear polyolefins resulting from these processes have since found utility in countless applications and are ubiquitous in contemporary society: worldwide annual production of polyolefins is currently around 125 million tons with continued growth forecasted.[5] In spite of heterogeneous catalysts providing initial breakthroughs in this field with empirical modifications leading to high productivity and selectivity,[6] development of well-defined molecular catalysts has led to enhanced mechanistic understanding along with possibility of more rational catalyst design. Such homogeneous catalyst systems also provide access to a range of polymer materials unattainable with traditional Ziegler-Natta technology.

This Thesis is concerned with the syntheses, characterisation and olefin polymerisation capability of a variety of half-sandwich κ^1-amidinate-supported group 4 complexes. Key modifications to an established catalyst system for the commercial homo- and copolymerisation of olefins[7] are described with a view to gaining better understanding of various aspects of catalyst behaviour whilst providing scope for optimisation. This work has been carried out in close collaboration with LANXESS Elastomers.

In this Chapter, an outline of olefin polymerisation is presented detailing the evolution of group 4 homogeneous catalysis. Particular attention is devoted to so-called constrained geometry catalysts (CGCs) given their significance to work in Chapter Four describing new chelated cyclopentadienyl-amidinate complexes. Advances in mechanistic understanding and precatalyst activation chemistry are presented providing context to the work described in Chapters Two and Three. An introduction to the coordination chemistry of the amidinate ligand chiefly in the context of group 4 olefin polymerisation is also discussed. For gaining a broad overview of the state-of-the-art, the reader is directed to some excellent reviews.[8-27]

1.2 Early metal-catalysed polymerisation of olefins

Free radical homopolymerisation of ethylene or propylene requires high pressure (*ca*. 2000 bar) and temperature (ca. 200 ºC) and is poorly controlled leading to low

melting point, highly branched low-density polyethylene (LDPE)[28] and atactic, low molecular weight polypropylene respectively.[29] The discovery by Ziegler and Natta that low pressure homopolymerisation of both ethylene and propylene by mixtures of aluminium alkyls and $TiCl_4$ afforded high molecular weight, linear polymers (e.g. high-density polyethylene (HDPE)) represented a breakthrough in the field of polyolefins.[1-4] The process was also shown to be stereoselective resulting in formation of largely isotactic polypropylene.[3, 4] Copolymerisation of ethylene and 1-hexene/1-octene leads to copolymers in which the composition varies with molecular weight. However, combination of vanadium compounds (e.g. VCl_4) with aluminium alkyls generates a catalyst system capable of producing random EP (ethylene-propylene) and EPDM (ethylene-propylene-diene monomer) copolymers with the proportion of monomers being uniform over the entire molecular weight range.[8, 30, 31] Unfortunately, in spite of high initial activities, rapid deactivation of this system represents a significant disadvantage.[32-35] Silica-supported chromium catalysts were developed by Phillips[36-38] and Union Carbide[39-41] which are highly active for ethylene homopolymerisation and do not require a cocatalyst. Unfortunately, these do not polymerise propylene and cannot be employed for copolymerisation of ethylene with other α-olefins.

Both Ziegler-Natta and supported-chromium systems offer distinct industrial advantages in terms of high productivity and convenient polymer processing but have drawbacks associated with their heterogeneous nature: often the diversity of active sites results in broad or multimodal polymer molecular weight distributions, mixtures of stereoregular and atactic polymers and copolymers with variable composition.[42] Furthermore, the potential for deeper mechanistic understanding and rational optimisation is limited with such catalysts leading to research into better defined homogeneous 'single-site' molecular species for polymerisation of olefins.

Wilkinson's discovery of group 4 metallocene complexes (Figure 1.1)[43] led to the independent findings of Breslow[44, 45] and Natta[46-48] that mixtures of Cp_2TiCl_2 and $AlClEt_2$ polymerise ethylene. These early homogeneous catalysts exhibited much lower activities than the Ziegler-Natta systems and did not polymerise higher α-olefins making them unsuitable for industrial application but demonstrated the principle of single-site molecular catalysis; the solubility of the active species providing scope for mechanistic investigation.[49-52]

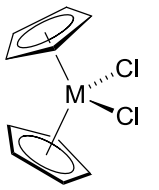

M = Ti, Zr, Hf

Figure 1.1

1.3 Mechanism for homogeneous olefin polymerisation

1.3.1 Group 4 metallocenes and methylaluminoxane (MAO)

Serendipitious discovery that addition of small quantities of water to the sluggish $Cp_2TiEtCl/AlEtCl_2$ and catalytically inactive $Cp_2ZrCl_2/AlMe_3$ systems generates in both cases a highly active catalyst for homopolymerisation of both ethylene and propylene represented yet another important breakthrough in the field.[53-60] This effect was assigned to *in situ* generation of alkylaluminoxanes by partial hydrolysis of the aluminium alkyl species: independently synthesised methylaluminoxane (MAO) in combination with Cp_2ZrCl_2 or Cp_2ZrMe_2 was shown to result in a similarly active catalytic species.[49, 56-59] The alkylaluminoxanes themselves are poorly understood, intractable and sensitive glassy materials thought to consist of oligomeric species such as linear polymers, cyclics and aggregates built from $[–Al®-O-]_n$ subunits (n ~ 5-20).[14, 61] Other routes to MAO have been explored[62, 63] aside from various hydrolytic methods[64-68] as well as the development of variants (ethylaluminoxane (EAO) and isobutylaluminoxane (IBAO)) derived from the corresponding cheaper aluminium trialkyls.[69-72] A variety of studies exploring the structure and precise role of alkylaluminoxanes in activation have been published although the details remain somewhat unclear.[73-79] In any case, these cocatalysts are thought to both alkylate and abstract chloride or alkyl ligands from neutral group 4 metal dichloride precatalysts whilst acting as scavengers of impurities such as water.

1.3.2 Proposed mechanisms

Activation chemistry of metallocenes with aluminium alkyls led to initial suggestion of a cationic active species by Shilov *et al*.[80, 81] Although supported by elegantly designed experiments, particularly the electrochemical generation of $[Cp_2TiMe]^+$ resulting in exclusive ethylene polymerisation at the cathode,[81] the invoking of a mechanism involving charge separated species in non-polar solvents was not widely

accepted. The activation of metallocenes with MAO resulted in a renaissance of the notion of a cationic active catalyst and was followed by a host of corroborating work.[82-87] Eisch demonstrated that reaction of Cp_2TiCl_2 with $AlMeCl_2$ in the presence of the alkyne, $PhCCSiMe_3$, affords the isolable and structurally characterised ion pair, $[Cp_2Ti(Me_3SiCCMePh)][AlCl_4]$ (**1.1**); the cationic titanium vinyl complex resulting from alkyne insertion into the putative $[Cp_2TiMe]^+$ intermediate (Scheme 1.1).[82]

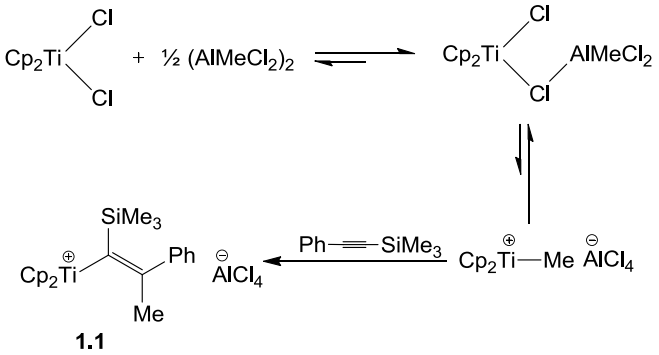

Scheme 1.1. Alkyne insertion into $[Cp_2TiMe]^+$.

It was further discovered that stable adducts could be prepared by reaction of group 4 metallocene methyl cations with Lewis bases. The first structurally characterised methyl cation was described by Jordan *et al.*: the charge separated species $[Cp_2ZrMe(THF)][BPh_4]$ was also the first example of an active ethylene polymerisation catalyst generated in the absence of an aluminium coinitiator.[83] Similarly, adducts of the related titanocene methyl cation, as well as products derived from insertion of various unsaturated substrates into the Ti-CH_3 bond, were isolated although strong interaction with the donor ligand is thought to preclude reactivity with ethylene.[84] Ethylene polymerisation was also shown to be catalysed by neutral bis(pentamethylcyclopentadienyl)-supported group 3 and lanthanide alkyl complexes; the isoelectronic relationship with group 4 alkyl cations providing further evidence for the role of such electron-deficient species in olefin polymerisation catalysis.[85-87]

The mechanism by Cossee and Arlman (Figure 1.2) proposed for Ziegler-Natta polymerisation[88, 89] is similarly relevant to the cationic molecular systems described above where the metallic active site, rather than being located at dislocations and edges of crystallites on the surface of a heterogenous catalyst, is enclosed by a set of auxilliary ligands. Coordination of an olefin to the electron deficient, ideally cationic, metal centre results in formation of a π-adduct. Subsequent migratory insertion of the alkyl ligand (or growing polymeryl chain) to the unsaturated bond of the coordinated

olefin results in simultaneous propagation and regeneration of the active species. Several alternatives to this general mechanism have since been proposed (Figure 1.2).[90-93] Investigation of transition metal alkylidene complexes led to invoking of an alternative hydride shift mechanism by Green and Rooney in which the active species is in equilibrium with a metal-alkylidene intermediate which undergoes a [2+2] cycloaddition with an olefin affording a metallacyclobutane species. Subsequent reductive elimination results in reformation of the active species.[90, 94] Although this pathway is not open to group 3, group 4 and lanthanide catalysts since at least two d-electrons are required for formal oxidative addition,[95] modified mechanisms involving α-agostic stabilisation of both ground and transition states have been suggested.[91-93] Such secondary interactions may also be integral to explanation of stereoselective polymerisation (*vide infra*) by reducing conformational flexibility in transition states.[92]

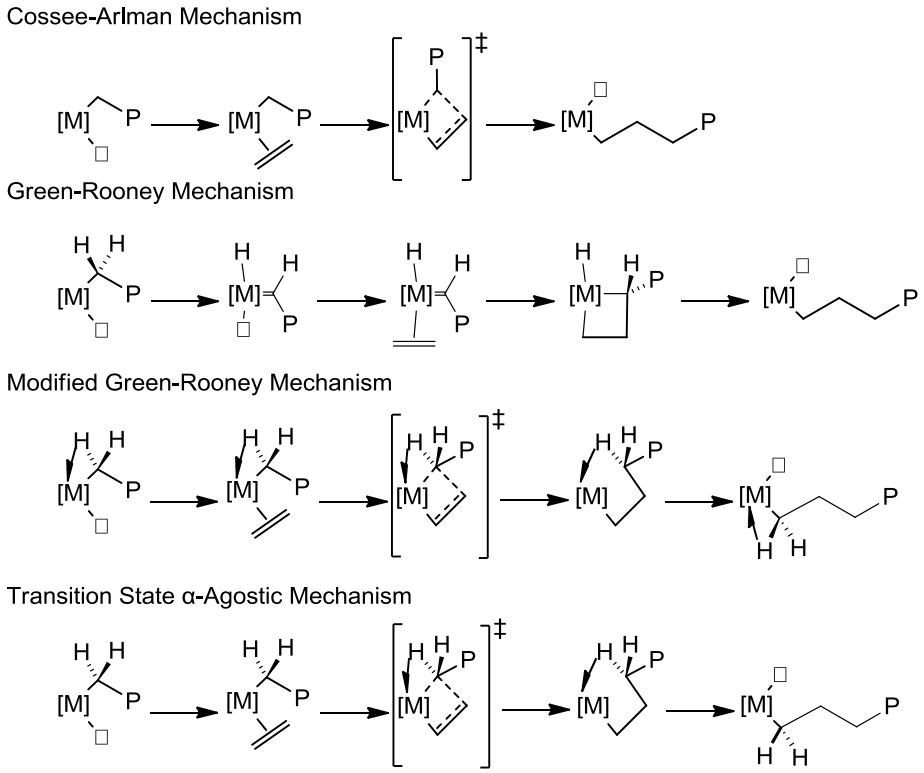

Figure 1.2. Proposed mechanisms for Ziegler-Natta catalysis. P = polymeryl chain.

1.3.3 Chain transfer and termination processes

Various chain transfer processes occur alongside the propagation pathway described above; the polymer molecular weight and molecular weight distribution (Section 1.3.5.1) are dependent on the relative rates associated with these competing

mechanisms. The growth of the polymer chain may be terminated by several mechanisms including β-hydrogen elimination or transfer to monomer[96-101] and chain transfer to aluminium in the presence of an aluminium alkyl-containing cocataylst or scavenger.[102-105] Hydrogen is often utilised as a chain transfer agent allowing control over polymer molecular weight in industrial processes.[106-108] Chain transfers involving reactivity of β-hydrogens result in vinylic polymer end groups indicated by observation of C=C vibrational bands in the FT-IR spectrum (Section 1.3.5.2) although it has been suggested that β-hydrogen transfer is more likely for metallocene and related systems.[109] Chain transfer to aluminium results in polymers with saturated chain ends following protic work-up which distinguishes this mechanism from β-hydrogen elimination or transfer. More extensive chain transfer to aluminium resulting in shorter polymer chains is observed for MAO cocatalysts containing greater concentrations of $AlMe_3$.[110] Furthermore, deactivation processes *via* formation of hetero-bimetallic resting states, exemplified by $[Cp_2Zr(\mu\text{-}Me)_2AlMe_2]^+$,[111] or reduction of titanium catalysts to +3 or +2 oxidation states have been observed from reactivity with $AlMe_3$.[112-114] Use of solid MAO, in which residual $AlMe_3$ is removed *in vacuo*, has been shown to increase catalyst productivity and polymer molecular weight[115] but is impractical for use in an industrial process. Alternatively an $AlMe_3$ scavenger such as 2,6-di-*tert*-butyl-4-methylphenol may be employed; the resulting monomethyl aluminium bisphenolate species itself acting as a scavenger of impurities such as water.[116-119]

1.3.4 Catalyst productivity

Productivity (also referred to as activity) is commonly measured in units of kg mol^{-1} h^{-1} bar^{-1} which takes into account the polymer yield (kg), the molar catalyst loading, the reaction time (h) and the pressure (bar). Importantly, this system takes no account of the kinetic profile of the polymerisation and longevity of the active species: for example, a run lasting a few minutes will result in a seemingly higher productivity than a hour long experiment for a catalyst which only remains active for thirty seconds. Furthermore, the productivity is critically dependent on the precise conditions employed for the reaction, precluding direct comparison of absolute values in the literature. For this reason Gibson developed a system whereby productivites are classified by a scale of merit (Table 1.1).[120]

Table 1.1. Rating of the effectiveness of a catalyst based on its productivity.[120]

Rating	Productivity (kg mol^{-1} h^{-1} bar^{-1})
very low	< 1
low	1 – 10
moderate	10 – 100
high	100 – 1000
very high	> 1000

1.3.5 Polymer analysis

1.3.5.1 Gel permeation chromatography (GPC)

Gel permeation chromatography (GPC), a form of size exclusion chromatography (SEC), is a powerful technique for determination of the molecular weight properties of a polymer. The chromatogram provides a convenient measure of the number average molecular weight (M_n) (Equation 1.1), the weight average molecular weight (M_w) (Equation 1.2) and the peak molecular weight (M_p), of a given polymer sample (Figure 1.3). Separation of polymers is achieved typically using a column filled with porous beads of varying pore sizes. The hydrodynamic volume of a polymer chain determines the retention time such that shorter chains, which may may more easily enter and reside in the pores of the stationary phase, are eluted more slowly than longer polymers.

The number average molecular weight (M_n) is given by:

$$M_n = \frac{\sum N_i \times M_i}{\sum N_i} \qquad \textbf{Equation 1.1}$$

where N_i is the number of molecules having molar mass of M_i. This quantity may therefore be interpreted straightforwardly as the total molar mass of the polymer molecules divided by the number of polymer molecules.

The weight average molecular weight (M_w) is given by:

$$M_w = \frac{\sum W_i \times M_i}{\sum W_i} \qquad \textbf{Equation 1.2}$$

where W_i is the mass of polymers having a molar mass of M_i.

The resulting chromatogram, plotted as weight average *vs.* molecular weight, gives both the M_n and M_w (as well as other measures of the molecular weight such as the

size average molecular weight (M_z)). The polydispersity index (PDI), defined as the M_w/M_n ratio, would be unity if all polymer chains in a sample have the same length hence molecular mass but, as discussed above, propagation for non-living catalyst systems is in competition with various chain transfer mechanisms resulting in a distribution of polymer chain lengths and increased polydispersity indices.[121] A single-site polymerisation catalyst operating simultaneously with chain transfer processes results in a Shultz-Flory distribution of polymer chains and a polymer PDI of 2.0.[122] Multi-sited catalyst behaviour is indicated by higher PDIs and multi-modal molecular weight distributions from GPC polymer analysis.

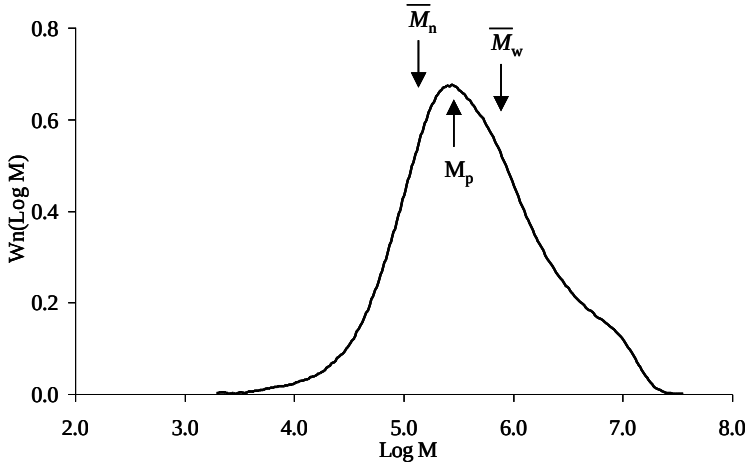

Figure 1.3. Distribution for a typical polymer sample showing M_n, M_w and M_p.

GPC instruments are usually calibrated against polystyrene samples of known molecular weight (M_n, M_w and M_p). However, the implicit assumption that the solution behaviour of a given polymer sample will be similar to polystyrene may not be valid. For this reason a universal calibration method is usually employed which accounts for the possibility that polymer species eluting at the same elution volume hence having the same hydrodynamic volume may have different molecular weights.[123] The absolute molecular weight of the polymer (M) is related to its intrinsic viscosity at infinite dilution([η]) by Equation 1.3.

$$[\eta] = K.M^{\alpha} \qquad \textbf{Equation 1.3}$$

Constants K and α are Mark-Houwink parameters which may be determined experimentally for each polymer type in a given solvent at a particular temperature. Providing these constants are known, the molecular weight may be obtained employing a standard polystyrene GPC calibration curve. Aside from the low

molecular weight polymers produced by zirconium and hafnium catalysts in Chapter Three (where a conventional calibration technique was employed), this Thesis gives polymer molecular weights derived from universal calibration.

1.3.5.2 End group analysis

Soluble lower molecular weight polymers may be characterised by ^{1}H NMR spectroscopy allowing identification of methyl or vinyl end groups resulting from chain transfer to aluminium or monomer respectively (*vide supra*). Where both mechanisms are operating, the integrals of end group proton signals indicate the prevailing termination process. As discussed in Section 1.3.3, FT-IR spectroscopy is also often utilised for end group analysis for detection of C=C bonds within polymer samples. This technique can discern both terminal and internal C=C bonds resulting from respective chain termination and isomerisation ('chain walking') processes. This technique is also useful for assessing the incorporation of non-conjugated diene comonomers in EPDM copolymerisation (Chapters Two and Four). The uptake of 5-ethylidenebicyclo[2.2.1]hept-2-ene (ENB) and 5-vinylbicyclo[2.2.1]hept-2-ene (VNB) comonomers (Figure 1.4) can be measured due to the different frequencies associated with the internal (ENB) and terminal (VNB) C=C bonds; the unsaturated bond of the bicyclic ring system is preferentially incorporated into the polymer chain due to relief of ring strain.[124-126]

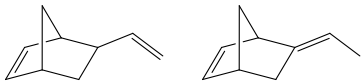

Figure 1.4

1.4 *Ansa*-metallocenes and stereoselective propylene polymerisation

Control over the regio- and stereoselectivity of propylene polymerisation leads to polymeric materials with a breadth of physical properties. Low pressure metal-catalysed reactions tend to result in enchainment *via* 1,2-insertion due to the influence of the methyl substituent on the steric properties and polarity of the monomer[13] although prevalence of 2,1-insertion for some systems has also been demonstrated.[13, 32, 127] Prochiral monomers such as propylene give rise to three main stereochemical possibilities: isotactic, syndiotactic and atactic polymer chains (Figure 1.5). The tacticity is controlled by features of the active site and itself is key in determining the

microstructure and physical properties of the polymeric material. This area has been the subject of a number of reviews.[8, 13, 128-130]

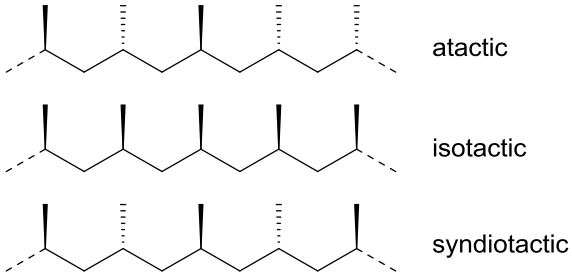

Figure 1.5

The chemical shifts of signals observed in the ^{13}C NMR spectrum of the polymer are diagnostic of the configurations of proximal stereogenic centres hence provide a valuable insight into the polymer microstructure.[131, 132] The random configuration of stereogenic centres in atactic polypropylene results in little ordering of the polymer chains and an amorphous material with limited utility. Isotactic polypropylene is in contrast a stiffer, harder and higher melting point material due to adjacent stereocentres having the same configuration leading to helical polymer strands constituting crystalline domains of the bulk material. Stereochemical alternation of neighbouring stereogenic centres along the polymer chain characterises syndiotactic polypropylene which, in spite of being softer and consequently less commercially important than the isotactic variant, is a durable material with potential medical application owing to its stability to gamma radiation.[133]

A key milestone in stereoselective homogeneous olefin polymerisation was development of *ansa*-metallocenes in which the cyclopentadienyl-type ligands are connected *via* covelent bonds to various bridging groups. It was demonstrated that such lower symmetry C_2- or C_s-symmetric catalysts (Figure 1.6) were capable of producing isotactic (**1.2**)[134] and syndiotactic (**1.3**)[135] polypropylene respectively. It was also elegantly demonstrated by Bercaw *et al.* that a highly selective chiral *ansa*-zirconocene catalyst (**1.4**) could partially resolve racemic mixtures of α-olefins containing a stereogenic centre.[8, 136] Clearly the origin of the selectivity is intimately related to the characteristics of the active site which are determined by the supporting ligand set, metal centre and the end of the growing polymeryl chain. In cases where the stereoselectivity of enchainment is influenced most strongly by the configuration of the most recently incorporated monomer, the polymer tacticity is said to be

regulated by 'chain-end' control. If the stereochemistry of each insertion is independent to that of the previous inserted monomer but is instead governed by the environment of the active site created by the auxillary ligands the origin of selectivity is described as 'enantiomorphic site-control'.[137]

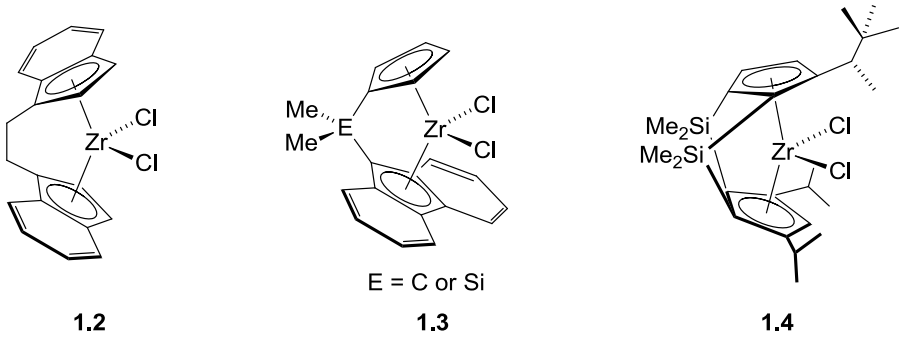

1.2 **1.3** **1.4**

Figure 1.6. Ansa-metallocene precatalysts.

These discoveries, along with MAO-activation boosting the productivity of metallocene systems to commercially viable levels, provided competition to traditional Ziegler-Natta systems. Isotactic polypropylene could be produced with better-defined molecular catalysts whilst offering possibilities beyond the scope of traditional heterogeneous catalysis such as narrower polymer PDIs and syndiotactic enchainment of prochiral α-olefins.[138, 139] Diverse new materials, such as copolymers comprised of stereoregular and atactic blocks,[140, 141] which could not have been envisaged with Ziegler-Natta catalysts were now accessible and mechanistically approachable.

1.5 Constrained geometry catalysts (CGCs)

The overwhelming success of homogeneous olefin polymerisation catalysis by group 4 metallocene complexes spawned extensive patenting of these systems which, combined with desire for better control of polymer properties and access to new polyolefinic materials, turned attention to development of new 'post-metallocene' catalysts in which one or both of the cyclopentadienyl-type ligands are replaced by alternative donor moieties combined with the possibility of replacing the group 4 metal by other transition elements or lanthanides.[11, 12, 16, 142-145]

An important class of such catalysts (Figure 1.7) was developed by both Dow[146-149] and Exxon[150-153] building on the discovery of silicon-bridged cyclopentadienyl-amido scandium[154] and titanium[155] complexes (*cf.* **1.3**) by Bercaw and Okuda respectively.

The effect of tethering the ligand moieties was a more open active site resulting in enhanced α-olefin incorporation, increased polymer molecular weight whilst improving catalyst stability. These attributes were identified by Stevens *et al.* who formulated a general definition of a constrained geometry catalyst (CGC) as a complex comprising a π-bonded moiety, such as a cyclopentadienyl-type ligand, linked to another ligand coordinated to the same metal centre making for a smaller angle between the centroid of the π-system, the metal and the other auxilliary ligand than in a comparable unchelated complex.[156]

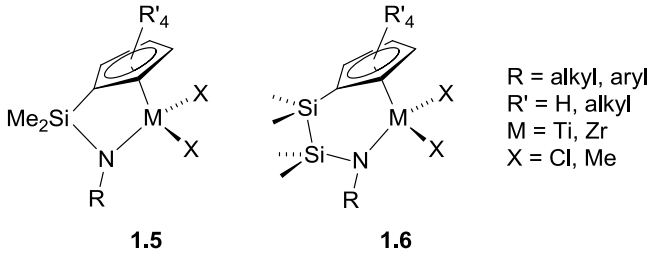

Figure 1.7. Constrained geometry precatalysts.

In comparison to the metallocenes, a more Lewis acidic metal centre is attained since a maximum of three electrons, using the neutral electron counting formalism, may be donated by the amido moiety compared to five from a cyclopentadienyl ligand.[21, 154, 157, 158] The strain imposed by the length and flexibility of the bridging moiety was claimed to be key to catalytic performance; in systems such as **1.5** and **1.6** the greater constrained character of the former results in enhanced catalyst efficiency and comonomer incorporation.[156] Similar carbon-bridged group 4 complexes incorporating C_1 (**1.7**),[159-162] C_2 (**1.8**),[163-168] C_3 (**1.9**)[169] alkyl chains or other heteroatom linkers[170-174] connecting the cyclopentadienyl and amide donors have been prepared (Figure 1.8) although have not been nearly as extensively employed in industrial processes as the original silicon-bridged CGCs. Interestingly, the opposite trend relating to the length of the linker is observed in these systems compared to the silicon-bridged species: C_2- (**1.8**) and C_3-tethered (**1.9**) *ansa*-systems offer superior actvities to more constrained C_1-linked complexes (**1.7**).[164] It seems that the length and flexibility of the *ansa* bridge combined with steric effects of the ligand subtituents are significant determining factors influencing cation-anion interactions during catalysis hence the nature and accessibility of the active site.[164, 175] Complexes supported by bifunctional *o*-aryl-bridged cyclopentadienyl-amide ligands (**1.10**)[176-182]

are of particular interest in the context of this Thesis given the work described in Chapter Four concerning similarly tethered cyclopentadienyl-amidinate species.

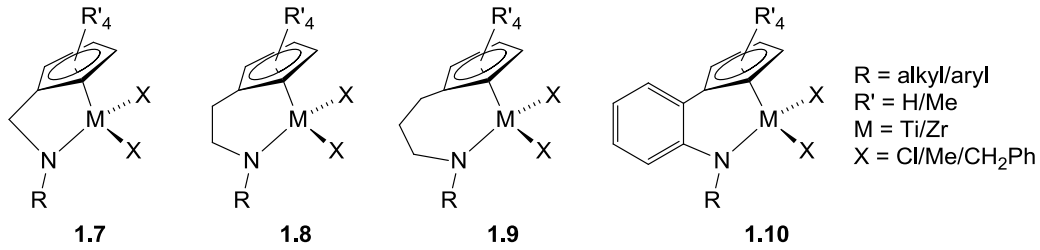

1.7 **1.8** **1.9** **1.10**

Figure 1.8. Carbon-bridged cyclopentadienyl-amide precatalysts.

The scope of such post-metallocene half-sandwich *ansa* complexes is not merely limited to variations of the cyclopentadienyl substituents and the chelate bridge. Tethered cyclopentadienyl-amine ligands[183] have been developed for chromium- and low valent titanium(+3)-catalysed olefin polymerisation.[184-186] Bifunctional ligands in which the cyclopentadienyl ring is connected to heteroatoms other than nitrogen have also been investigated: the literature documents notable examples of such ligands incorporating phosphorous-[160, 185, 187-189] and oxygen-donors.[190-199]

Coordination chemistry of such chelating ligands has been applied to many other metals. Group 3 and lanthanide alkyl and hydrido complexes[200-206] have been discovered since Bercaw's initial work with scandium.[154] Monomeric, dimeric and tetrameric constrained geometry thorium(+4) and uranium(+4) complexes have also been prepared although clearly are of limited utility in industrial olefin polymerisation.[207, 208] Consistent with successful application of vanadium compounds in Ziegler-Natta catalysis (*vide supra*) vanadium(+2, +3, +4, +5)[209-211] complexes supported by such constrained *ansa* ligands have exhibited activities which rival or exceed group 4 catalysts.[211] The heavier group 5 congeners have been employed in constrained geometry complexes although the metal exclusively adopts the group oxidation state.[212-214] Similarly, molybdenum(+4, +5, +6)[165, 215-217] and tungsten(+6)[216] complexes were prepared building on successful oligomerisation and polymerisation catalysis with chromium(+3) complexes.[142, 184, 186, 218] Developments in chemistry of the later transition metals have also resulted in synthesis of constrained geometry iron(+2) and rhenium(+3) carbonyl complexes.[155, 219, 220]

The broad field of constrained geometry complexes, which have been the subject of some useful reviews,[11, 21, 221] encompasses numerous permutations of both metal and

ligand but importantly to the field of olefin polymerisation also represents a logical step from the *ansa*-metallocene catalysts discussed in Section 1.3.6. and serves as a conceptual conduit to investigation of non-*ansa* half-sandwich post-metallocene catalysts.

1.6 Non-*ansa* half-sandwich post-metallocene catalysts

The evolution of *ansa*-metallocenes to constrained geometry systems was greatly assisted by enhanced understanding of ligand-metal bonding and the concept of isolobality.[222, 223] The σ+2π cyclopentadienyl-metal interaction (Figure 1.9) may be mimicked by other ligands which are also designed to provide a similar degree of steric protection of the metal centre. Importantly the cyclopentadienyl ring need not be tethered to the other supporting ligand; careful selection of substituents permits optimisation of the electronic properties and steric characteristics of the non-cyclopentadienyl ligand. Such non-*ansa* complexes are also advantageous due to their ease of preparation usually from reaction of readily available monocyclopentadienyl metal precursors with protio-, silylated or metallated ligands.

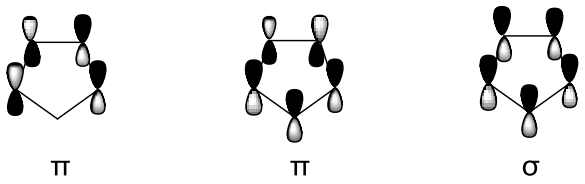

Figure 1.9. Frontier orbital symmetries of the Cp^- ligand.

Numerous non-*ansa* half-sandwich group 4 complexes have been prepared employing a host of non-cyclopentadienyl anionic ligands.[12, 16, 224, 225] Notable examples include aryl oxide- (**1.11**),[226-233] non-*ansa* amide- (**1.12**),[175, 234, 235] ketimide- (**1.13**),[236-241] guanidinate- (**1.14**),[242-244] iminoimidazolidide- (**1.15**)[242, 243] and phosphinimide-supported (**1.16**)[245-255] precatalysts (Figure 1.10).

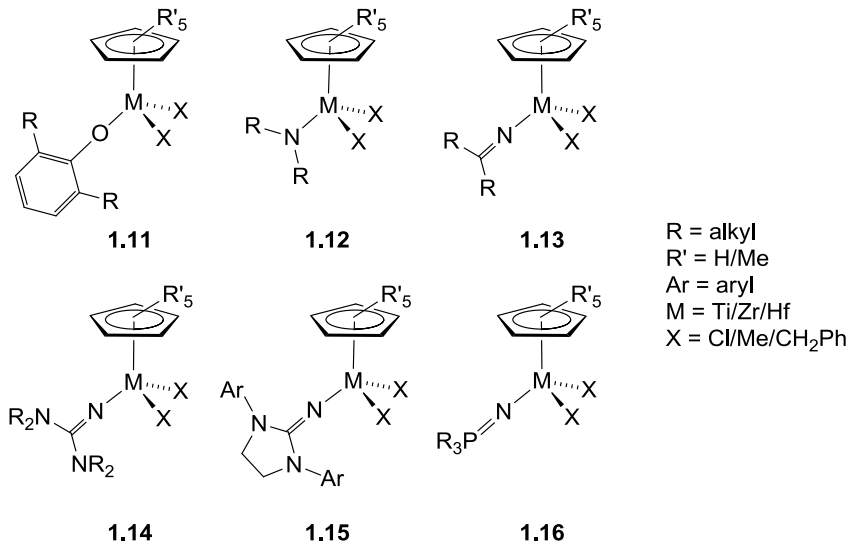

Figure 1.10. Non-*ansa* half-sandwich post-metallocene precatalysts.

The phosphinimide systems developed by Stephan (**1.16**) are prototypical of half-sandwich post-metallocene precatalysts: the linear P=N-M bond angle and shortened N-M bond length being suggestive of π-donation to the metal centre[253, 254] whilst the substituents on phosphorous providing a cone of steric protection something akin to that of a cyclopentadienyl ligand.[248, 250] These properties result in such complexes possessing good thermal stability and are successfully employed in high temperature copolymerisation processes.[255]

The relative importance of these steric and electronic ligand characteristics in determining catalytic performance is the subject of debate. The superior performance of constrained geometry cyclopentadienyl-amide complexes over the non-*ansa* variants is ascribed at least partly to the effect of the bridge in determining the immediate coordination environment around the active site and the proximity of the anion to the active site.[164, 175] Whilst it is argued for aryl oxide[226, 227] and phosphinimide[250] catalysts that steric factors are paramount, comparison of ketimide- and guanidinate-supported complexes suggests that ligands offering enhanced ligand-to-metal dπ-pπ bonding lead to higher actvities.[243, 256-258] The greater degree of π-donation in the guanidinate and phosphinimide systems is thought to stem from mesomeric donation to the donor nitrogen atom from the proximal heteroatoms (Figure 1.11).

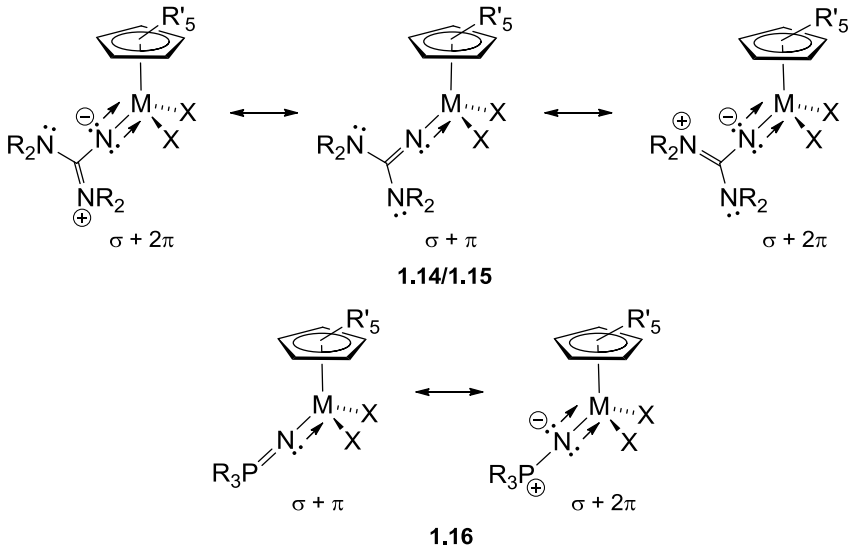

Figure 1.11. Metal-ligand bonding interactions for guanidinate- and phosphinimide-supported complexes.

Clearly both the steric and electronic characteristics of the auxilliary ligands are crucial to the nature of the active site and behaviour in catalysis. Apparently trivial modification of the ligand substituents can result in dramatic changes in performance: an important example in the context of this Thesis (see Chapter Three) is the transformation of Kretschmer's moderately/highly active Cp-guanidinate- (**1.14**) and Cp-iminoimidazolidide-supported (**1.15**) systems[242, 243] to very highly active catalysts when supported by the more bulky and electron-donating pentamethylcyclopentadienyl (Cp*) ligand.[244]

1.7 Cyclopentadienyl-free post-metallocene catalysts

Further removed from the original metallocene homogeneous olefin polymerisation catalyts are complexes which are not supported by any cyclopentadienyl-type ligands.

1.7.1 Alternative face-capping ligands

Half-sandwich-type complexes have been developed in which alternative face-capping ligands have been employed. Notably the monoanionic tris(pyrazoyl)borate (Tp) ligand (**1.17**) has received a great deal of attention since its discovery in the 1960s (Figure 1.12).[259-261] The Tp ligand bears an isolobal relationship with cyclopentadienyl-type ligands since it can interact with a transition metal *via* one σ and two π-type frontier molecular orbitals; steric characteristics may also be tuned by variation of the substituents (R_3, R_4, R_5) decorating the pyrazoyl rings. These

attractive features of Tp ligands resulted in commercial interest[262, 263] and further research into the olefin polymerisation capability of Tp-supported group 4 complexes.[264-269] Previous research in the Mountford group examined the synthesis and ethylene homopolymerisation capability of post-metallocene titanium imido- and κ^1-amidinate-supported (**1.18**) (*vide infra*) complexes supported by face-capping ligands including tris(pyrazoyl)borates (Figure 1.12).[270, 271]

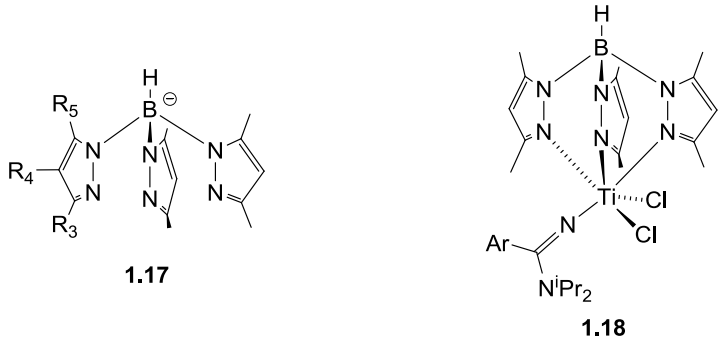

Figure 1.12

Related post-metallocene research within the group explored the scope of neutral triazacyclononane (TACN), tris(3,5-dimethylpyrazoyl)methane (TPM) and anionic tris(3,5-dimethylpyrazoyl)methanide (TPMd) face-capping ligands in combination with dianionic imido ligands supporting titanium (**1.19**-**1.21**) and vanadium (**1.19**, **1.20**) complexes as interesting isolobal alternatives to metallocenes (Figure 1.13).[272-278] This large family of imido complexes, as well as providing examples of highly active ethylene homopolymerisation catalysts,[273, 275-277] serve as useful models for understanding the ligand-metal multiple bonding characteristics of some of the post-metallocene ligands described above due to extensive study of the nature of the formal Ti-N triple bond.[279-287] This work was recently extended to cationic TACN- and TPM-supported and neutral TMPd-supported titanium complexes in which an anionic κ^1-amidinate (*vide infra*) is utilised as the other ancillary ligand (*cf.* **1.18**).[270, 288]

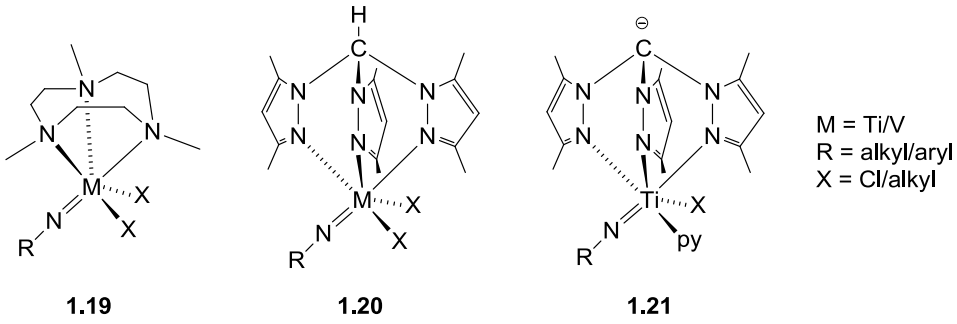

1.19 **1.20** **1.21**

Figure 1.13

1.7.2 Chelated amide- and aryloxide-supported complexes

The success of amide-supported half-sandwich complexes, particularly the constrained geometry catalysts, resulted in investigation into synthesis and application of chelated diamide complexes as potential olefin polymerisation catalysts in which the donors are connected by a variety of different bridging moieties.[16, 120, 289-306] The activated cationic species derived from such precatalyts is expected to be more electron deficient than metallocene systems due to contribution of a maximum of three electrons from each amide donor. Such highly electron deficient species are hence anticipated to be more reactive than metallocene or half-sandwich complexes but have been shown to exhibit surprising control in olefin polymerisation catalysis: low temperature living polymerisation of olefins has been demonstrated in several cases including with the C_3-bridged diamide complex **1.22**,[289] Schrock's oxygen-bridged diamide sytem **1.23**[290-298] and the imino-pyrrolide titanium complex **1.24** developed by Fujita[299, 300] (Figure 1.14). In common with all the catalyst systems discussed in this Chapter, it is difficult to overestimate the importance of the steric characteristics of the ligand, heavily influenced by the choice of substituents, on catalyst performance: for example the productivity of the MAO-activated silicon-bridged diamide precatalyst **1.25** is critically dependent on the steric protection provided by the amide substituents.[301, 302] Group 4 pyridyl-amide systems (**1.26**) have also been shown to be both highly active and stereoselective polymerisation catalysts. Control of polymer tacticity and high temperature stability have been attributed in large part to a serendipitious C-H activation during ligand complexation resulting in formation of a Hf-C_{Ar} bond which, following activation of the precatalyst, is thought to undergo insertion by the first olefin monomer.[303-306]

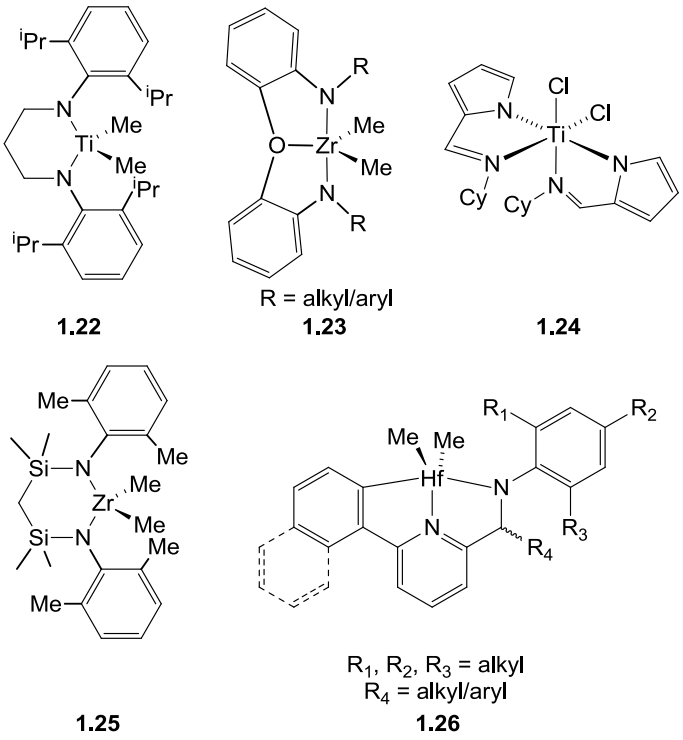

1.22 **1.23** **1.24**

1.25 **1.26**

Figure 1.14. Examples of post-metallocene chelated amide-supported precatalysts.

Reflecting the success of post-metallocene half-sandwich aryl oxide systems, non-cyclopentadienyl chelated systems incorporating phenoxide donors have also been successfully developed as olefin polymerisation catalysts.[12, 16, 307] Similarly to the amide-supported complexes a variety of difference bridges and donors are employed in conjuction with the aryl oxide. Bis(phenoxide) ligand frameworks have been developed in which the aryl rings are tethered directly by methylene, silyl (**1.27**)[308] or heterocyclic linkers (**1.28**) leading to some highly active catalyst systems (Figure 1.15) in which the combination of cocatalyst, ligand substituents and bridging moiety are key to productivity.[309-315] Other heteroatom-containing bridges have also been employed allowing incorporation of further donors to the metal centre;[307, 316-325] salan-supported C_2-symmetric zirconium complexes such as **1.29** (Figure 1.15) have been shown to catalyse the living and isospecific polymerisation of 1-hexene.[317] Phenoxy-imine-supported complexes **1.30** ('FI catalysts') are perhaps the most important examples of the non-cyclopentadienyl post-metallocene era (Figure 1.15).[18] Variation of ligand substituents has led to a raft of different desirable polymerisation behaviours such as syndiospecific polymerisation of propylene,[326, 327] copolymerisations of ethylene with propylene or α,ω-dienes[328] and living polymerisation[329] with productivities comparable to those of metallocene precatalysts.[329]

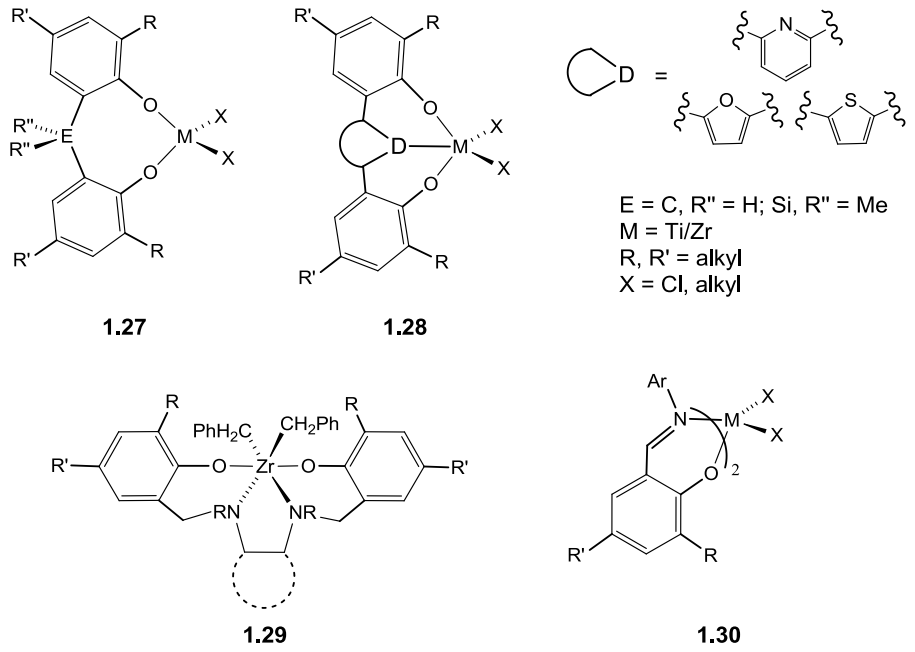

Figure 1.15. Examples of post-metallocene chelated aryl oxide-supported precatalysts.

1.7.3 Late transition metal cyclopentadienyl-free post-metallocene systems

Catalyst development has extended yet further from the original metallocene homogeneous systems: the olefin polymerisation capability of non-cyclopentadienyl late transition metal complexes has also been investigated and implemented.[12, 16] Notable cases include diimine-supported group 10 (**1.31**, **1.32**)[330-333] and related bis(imino)pyridyl-supported iron systems (**1.33**)[127, 334, 335] studied in the groups of Brookhart and Gibson (Figure 1.16). The MAO-activated nickel and iron precatalysts have displayed activities rivalling or exceeding those of the metallocenes; the palladium complexes (**1.32**) are less active and produce predominantly LDPE but are capable of incorporating polar monomers such as methyl acrylate resulting in branched copolymers with functionalised chain ends.[332, 333] By variation of the *ortho*-substituent of the aryl rings attached to the imine nitrogen, the iron complex may be switched to from a catalyst producing high molecular weight polyethylene to a highly active and selective ethylene oligomerisation catalyst.[334, 335] Tuning of ligand substituents in order to control the behaviour of the active site is the common theme to all of the molecular catalysts described in this Chapter regardless of the metal and precise nature of the supporting ligands.

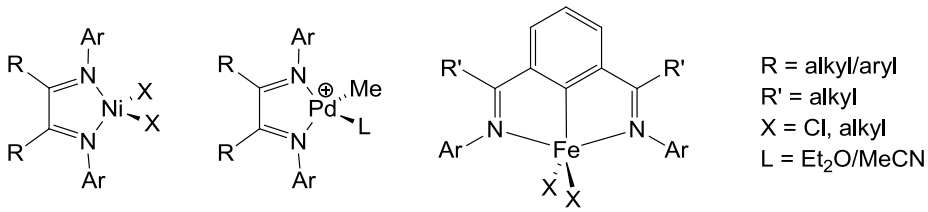

1.31 **1.32** **1.33**

Figure 1.16. Examples of post-metallocene late transition metal precatalysts.

1.8 Cocatalysts and activation

Significant advances have been made relating to cocatalysts and enhanced understanding of the chemistry of activation. The early breakthroughs in this area involved activation involving aluminium alkyls and MAO (*vide supra*) but many alternative coinitiators have since been explored.[14]

1.8.1 Lewis acid activation of dialkyl complexes

In spite of the preparation of tris(pentaflurophenyl)borane, BAr^F_3, having been published in the 1960s,[336] it was not until the early 1990s that it was discovered that it activates the zirconocene dimethyl complex by abstraction of a methyl ligand generating an active catalyst for olefin polymerisation.[337-340] The well-defined nature of such activated species has permitted useful insights into their structure *via* spectroscopic and crystallographic techniques.[341-343] Of vital importance in this chemistry is the influence of the counteranion since the ease of approach of monomers to the active site is dependent on its proximity to the electron-deficient centre. The alkyl borate (or alate if the corresponding alane, $AlAr^F_3$ is utilised)[344] will inevitably reside close to the cationic metal centre due to Coulombic attraction but the precise strength and range of the interaction depends on factors such as steric encumbrance of the ions and the electrophilicity of the cation[345, 346] Dimethyl and dibenzyl complexes have been predominantly discussed in this Chapter; both ligands may be abstracted by Lewis bases such as BAr^F_3 although the methylborate anion has been found to be more closely associated to the cationic metal centre than the bulkier benzylborate. The former may interact *via* agostic interactions between the C-H bonds of the abstracted methyl and the metal centre whereas the latter has been shown to display π-arene coordination of the benzyl ligand (Scheme 1.2).[290, 339, 340, 347-350] Stabilisation *via ipso*-interactions is also commonly observed in both neutral and cationic benzyl complexes.[351-353] Investigation of sterically crowded

perfluorarylboranes has been a topic of great interest due to the less coordinating nature of the corresponding borates during catalysis.[14, 118, 354-357] Aside from BAr^F_3 and bulky variants, simple alternative boranes, such as BF_3[358] and (N-pyrrole)$B(C_6F_5)_2$[359] have also been employed as coinitiators.

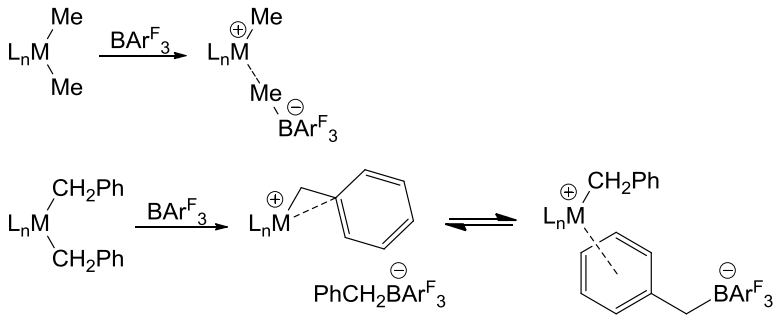

Scheme 1.2. Borane activation of dimethyl and dibenzyl precatalysts.

1.8.2 Lewis acid activation of diene complexes

An alternative activation of zirconocene and hafnocene diene complexes with BAr^F_3 was demonstrated by Erker *et al.* resulting in formation of stable well-defined zwitterionic complexes (**1.34**) which could be employed as single-component catalysts for polymerisation of ethylene and propylene.[360, 361] This chemistry offers a degree of control over anion-cation interactions which are integral to catalysis. An important feature of the structure of such metallocene allyl borate complexes is the interaction between an *ortho*-fluorine of one on the Ar^F rings and the metal centre observed both in solution and the solid state; the weak nature of this stabilising interaction (*ca.* 8.5 kcal mol^{-1})[362, 363] permits equilibration in solution with coordinatively unsaturated isomers which are catalytically active (Scheme 1.3). A number of further examples of such stabilisation *via* interactions with fluorines of Ar^F rings have also been documented.[364-367]

This discovery resulted in renewed interest in the synthesis and structure of group 4 diene complexes established during the 1980s.[368-370] Bochmann *et al.* reported reactivity of half-sandwich η^3-allyl-supported zirconium and hafnium diene complexes with BAr^F_3 resulting in zwitterion formation by reaction of the borane at the less hindered terminal carbon of the diene affording active catalysts capable of producing high molecular weight polyethylene.[371]

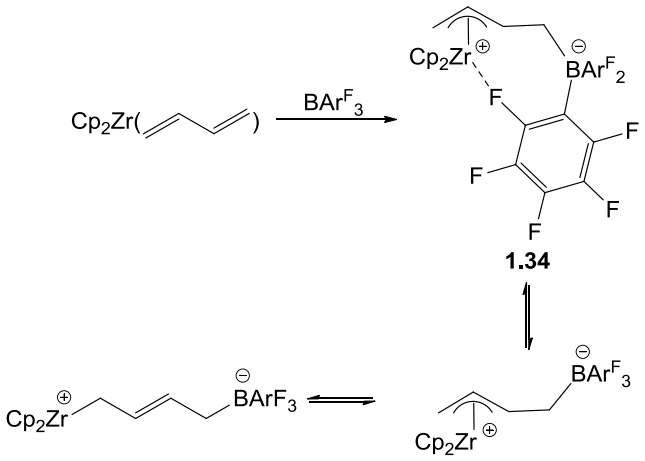

Scheme 1.3. Activation of zirconocene butadiene complex with BAr^F_3.

In the zirconium case, elimination of propene/butene with concomitant Ar^F migration results in formation of a Ar^F-supported half-sandwich boryldiene complex stabilised by an *o*-F···M interaction (**1.35**); self-activation of **1.35** generating the η^5-borole complex **1.36** (Scheme 1.4).[366] Similarly, BAr^F_3-activation of the half-sandwich benzyl-supported diene complex results in formation of **1.35** *via* abstraction of a benzyl ligand followed by loss of toluene and Ar^F transfer from boron to zirconium.[367]

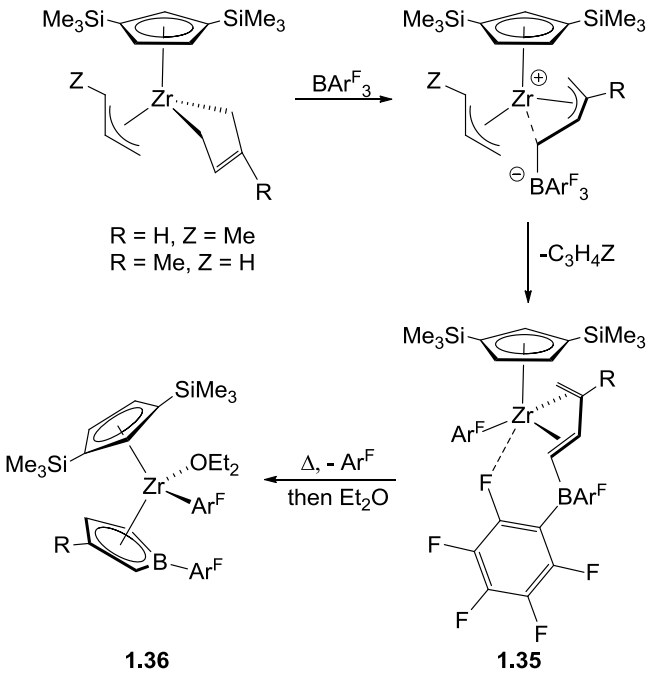

Scheme 1.4. Activation of η^3-allyl half-sandwich diene complexes.

Constrained geometry diene complexes reported by Marks *et al.* proved effective precatalysts for the copolymerisation of ethylene and 1-octene.[372, 373] Subsequent work detailed the BAr^F_3-activation of these diene complexes: well-defined

zwitterionic species were isolated and structurally characterised revealing stabilisation *via* agostic-type interactions between the $CH_2BAr^F_3$ methylene hydrogens and the metal centre rather than an *o*-F···M interaction. Furthermore, in the case of the 1,4-dimethylbutadiene complex, BAr^F_3 (or $AlAr^F_3$) activation was accompanied by rearrangment with concomitant hydrogen shift resulting in the borate becoming bonded to a newly formed terminal methylene group (Equation 1.4).[374-376]

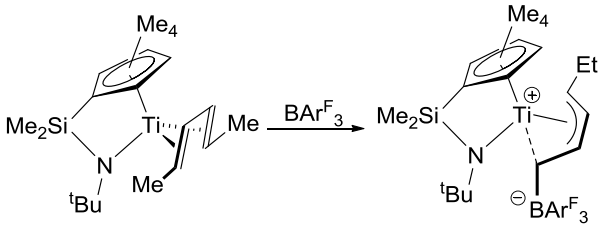

Equation 1.4

Half-sandwich phosphinimide-supported group 4 diene complexes were also developed by the group of Stephan and tested as precatalysts for ethylene polymerisation.[249, 377, 378] Stoichiometric reaction of the 2,3-dimethylbutadiene complex with BAr^F_3 appeared to afford the expected zwitterion although it was not structurally characterised.[249] In comparison to the more traditional dialkyl precatalysts, far fewer studies involving diene complexes have been reported in spite of the solubility and crystallinity of the corresponding borane-activated species and their promising olefin polymerisation capability. In view of this, one of the aims of this Thesis is to explore the scope of diene activation for half-sandwich κ^1-amidinate-supported systems (*vide infra*).

1.8.3 Bronsted acid activation of dialkyls and non-coordinating anions

A prototypical example of Bronsted acid-activation is protonolysis of titanocene dimethyl complex by $[NH_4][PF_6]$ generating $[Cp_2TiMe][PF_6]$.[84] Dialkyl precatalysts have since been activated with various Bronsted acids such as $[PhNMe_2H]^+$, $[^nBu_3NH]^+$, $[Ph_3PH]^+$ and $[H(Oet_2)_2]^+$ in order to generate the desired cationic active species.[14, 379-383] A disadvantage of this route is possible coordination of the resulting conjugate base to a vacant site on the metal centre leading to deactivation[346] although contradictory reports suggest that base coordination does not inhibit activity at low catalyst concentrations.[384, 385]

Common counter anions such as BF_4^- and PF_6^- are of limited practical use due to fluoride-transfer to metallocene alkyl cations[386, 387] while $[BPh_4]^-$ and $[C_2B_9H_{12}]^-$ anions have been demonstrated to undergo unwanted C-H activation and interact strongly with the cationic metal centre.[380, 388] Weakly coordinating anions such as tetrakis(pentafluorophenyl)borate ($[BAr^F_4]^-$) and the congeneric alate ($[AlAr^F_4]^-$) were developed and employed in conjunction with Bronsted acidic species in order to alleviate hindrance to monomers' approach of the active site.[14, 337, 379, 389] A notable exception is the thorium salt, $[Cp^*_2ThMe][BAr^F_4]$, in which two close $F\cdots Th^+$ contacts are observed in the solid state.[390] Much research, particularly in the group of Bochmann, has been devoted to preparation of non-coordinating borate anions in order to improve catlytic activity and, in some cases, stereoselectivity in polymerisation of prochiral olefins.[14, 391-395] More recently the scope of Bronsted acid activation has expanded to investigation of 'super-acidic' sulfated metal oxide solid catalyst supports which have proved efficient for activators for metallocene dialkyl precatalysts.[396-399]

1.8.4 Activation *via* alkyl abstraction

The trityl cation ($[CPh_3]^+$) is the most widely used reagent for alkide and hydride abstraction. In combination with a weakly coordinating anion such as $[BAr^F_4]^-$ it activates dialkyl precatalysts (L_nMR_2) generating the desired cationic species along with $RCPh_3$.[14, 400] Activation of the constrained geometry zirconium dibenzyl complex with $[CPh_3][BAr^F_4]$ is shown in Equation 1.5 by way of an example.[401] This cocatalyst is employed for activation of the half-sandwich κ^1-amidinate-supported precatalysts described in Chapters Three and Four. Other notable alkide abstraction agents include borate salts of aluminium and gallium dialkyl cations.[402]

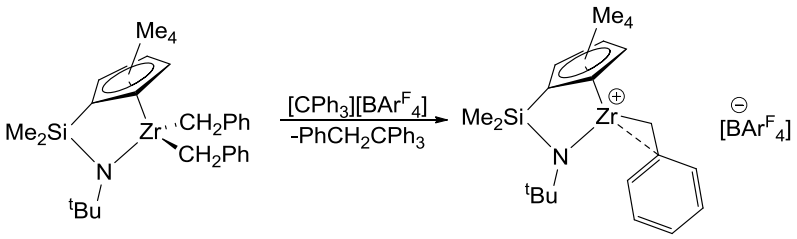

Equation 1.5

1.8.5 Other activation methods

A number of alternative catalyst activation strategies have been investigated aside from the more common protonolysis and alkyl abstraction routes described above. Cationic species may also be generated from monoalkyl-monohalide complexes by strong neutral donors such as PMe_3[84] or *via* halide-abstraction by silver or thallium salts.[386, 403] Oxidative activation of Ti(+3) alkyl species with ferrocinium or noble metal oxidising agents has been explored;[386, 404, 405] $[Cp_2Fe][BAr^F{}_4]$[406] has also been shown to activate Zr(+4) dibenzyl species *via* an oxidative process with elimination of $PhCH_2CH_2Ph$.[407]

1.9 Project introduction

A new class of post-metallocene half-sandwich precatalysts have recently been researched by LANXESS Elastomers for the commercial homo- and copolymerisation of olefins. High affinity for propylene and non-conjugated diene monomers (ENB and VNB) have resulted in these molecular systems proving viable alternatives to traditional Ziegler-Natta vanadium catalysts for production of EPDM rubber.[7, 408] The research has centred on titanium complexes (**1.37**) supported by a monoanionic κ^1-amidinate ancillary ligand capable of donating up to five electrons to the metal centre *via* $\sigma+2\pi$ interactions (*vide supra*). The steric properties of the ligand may be tuned by selection of substituents on both the amine nitrogen and aryl ring (Figure 1.17).

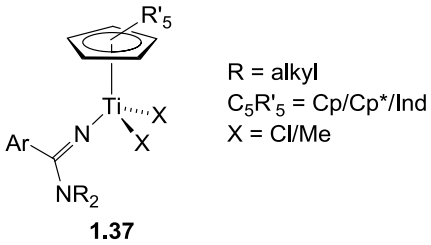

1.37

Figure 1.17

1.9.1 Amidine and amidinate ligands

The coordination chemistry of neutral amidine ligands, isoelectronic with carboxylic acids, largely involves formation of simple adducts in which donation is *via* the more basic and less sterically crowded imine nitrogen; the monoanionic amidinate ligand may bind with a variety of modes with the most common being κ^2 σ,σ-symmetrical coordination.[409-414] Such chelating amidinates may be easily prepared by nucleophilic

addition to carbodiimides. Structurally characterised examples exhibiting the κ^1-binding mode observed in the half-sandwich titanium complexes described above for **1.37** (Figure 1.17) are relatively rare. These are limited to early transition metal complexes prepared by insertion of benzonitrile into a metal-amide bond (e.g. **1.38**),[415-418] silyl migration in a TMS-substituted κ^2-amidinate complex (e.g. **1.39**)[419, 420] or reaction of a silylated amidine and $TaCl_5$ (**1.40**) (Figure 1.18).[421]

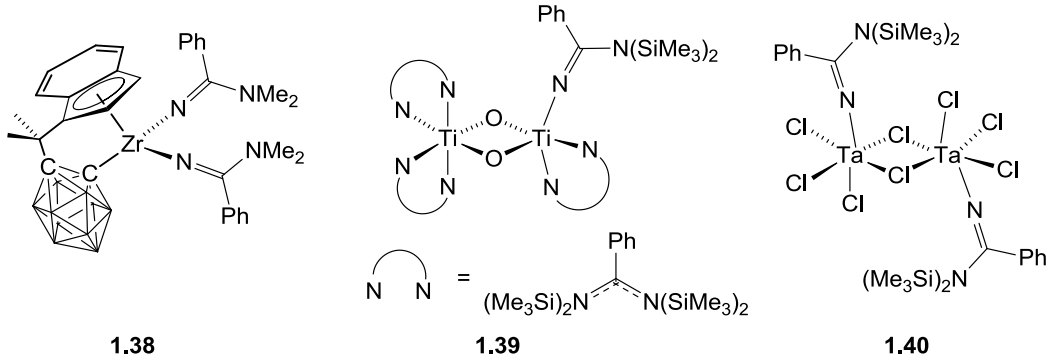

Figure 1.18. Examples of structurally characterised κ^1-amidinate complexes.

1.9.2 Amidinate complexes for olefin polymerisation

Group 4 complexes supported by κ^2-amidinate ligands have been thoroughly investigated as precatalysts for olefin polymerisation (Figure 1.19).[410, 412-414] Early progress in this area involved MAO-activation of half-sandwich complexes (**1.41**) for polymerisation of ethylene and propylene.[422-424] More recent developments have focussed on zirconium and hafnium asymmetric κ^2-amidinate complexes which have been found to be stable and stereoselective living catalysts for the polymerisation of 1-hexene.[425-428] Non-cyclopentadienyl mono- (**1.42**), bis- (**1.43**), and tris(κ^2-amidinate) (**1.44**) complexes have also been investigated for catalysing the production of a variety of polyolefins.[414, 429-433]

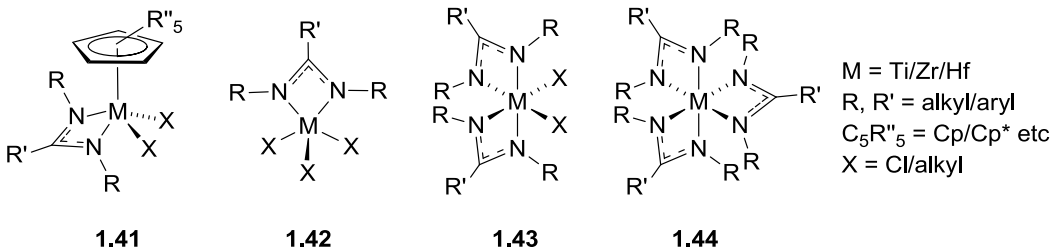

Figure 1.19. κ^2-Amidinate-supported precatalysts.

1.10 Summary and objectives

This Chapter has described the evolution of metal-catalysed olefin polymerisation catalysis from heterogeneous systems to post-metallocene molecular catalysts. A host of factors determine the polymerisation behaviour of the catalytic species such as the metal, the electronic and steric properties of the supporting ligand set and the choice of cocatalyst. This focus will be on development and understanding of new half-sandwich post-metallocene catalysts for homo- and copolymerisation of olefins. Chapter Two will explore Lewis acid (BAr^F_3) activation of half-sandwich titanium κ^1-amidinate-supported diene precatalysts for EPDM copolymerisation. The syntheses, structure, homo- and copolymerisation capability of a congeneric series of group 4 κ^1-amidinate-supported complexes is presented in Chapter Three along with insights into the trityl borate activation of the dimethyl precatalysts. Chapter Three will also present DFT calculations providing a deeper understanding of the unusual κ^1-amidinate-metal interaction. The synthesis and structure of chelated cyclopentadienyl-amidinate complexes are described in Chapter Four along with comparison of their performance in EP and EPDM copolymerisation testing with a related non-*ansa* catalyst.

1.11 References for Chapter One

1. K. Ziegler, E. Holzkamp, H. Breil and H. Martin, *Angew. Chem., Int. Ed. Engl.*, 1955, **67**, 541-547.
2. K. Ziegler, *Angew. Chem.*, 1964, **76**, 545-553.
3. G. Natta, *Angew. Chem., Int. Ed. Engl.*, 1956, **68**, 393-403.
4. G. Natta, *Angew. Chem.*, 1964, **76**, 553-566.
5. www.chemsystems.com, *Petroleum and Petrochemicals Economics Program: Petrochemicals Market Dynamics*, 2012.
6. N. Kashiwa, *J. Polym. Sci., Part A: Polym. Chem.*, 2004, **42**, 1-8.
7. E. G. Ijpeij, P. J. H. Windmuller, H. J. Arts, F. van der Burgt, G. H. J. van Doremaele and M. A. Zuideveld, *LANXESS ELASTOMERS, WO/2005/090418*, 2005.
8. H. H. Brintzinger, D. Fischer, R. Mülhaupt, B. Rieger and R. M. Waymouth, *Angew. Chem., Int. Ed. Engl.*, 1995, **34**, 1143-1170.
9. M. Bochmann, *J. Chem. Soc., Dalton Trans.*, 1996, 255-270.
10. W. Kaminsky, *J. Chem. Soc., Dalton Trans.*, 1998, 1413-1418.

11. A. L. McKnight and R. M. Waymouth, *Chem. Rev.*, 1998, **98**, 2587-2598.
12. G. J. P. Britovsek, V. C. Gibson and D. F. Wass, *Angew. Chem., Int. Ed. Engl.*, 1999, **38**, 428-447.
13. G. W. Coates, *Chem. Rev.*, 2000, **100**, 1223-1252.
14. E. Y. X. Chen and T. J. Marks, *Chem. Rev.*, 2000, **100**, 1391-1434.
15. G. W. Coates, *J. Chem. Soc., Dalton Trans.*, 2002, 467-475.
16. V. C. Gibson and S. K. Spitzmesser, *Chem. Rev.*, 2003, **103**, 283-315.
17. M. Bochmann, *J. Organomet. Chem.*, 2004, **689**, 3982-3998.
18. M. Mitani, J. Saito, S.-i. Ishii, Y. Nakayama, H. Makio, N. Matsukawa, S. Matsui, J.-i. Mohri, R. Furuyama, H. Terao, H. Bando, H. Tanaka and T. Fujita, *The Chemical Record*, 2004, **4**, 137-158.
19. P. D. Bolton and P. Mountford, *Adv. Synth. Catal.*, 2005, **347**, 355-366.
20. D. W. Stephan, *Organometallics*, 2005, **24**, 2548-2560.
21. H. Braunschweig and F. M. Breitling, *Coord. Chem. Rev.*, 2006, **250**, 2691-2720.
22. M. Bochmann, *Organometallics*, 2010, **29**, 4711-4740.
23. D. Takeuchi, *Dalton Trans.*, 2010, **39**, 311-328.
24. K. Nomura and S. Zhang, *Chem. Rev.*, 2011, **111**, 2342-2362.
25. H. Makio, H. Terao, A. Iwashita and T. Fujita, *Chem. Rev.*, **111**, 2363-2449.
26. M. Delferro and T. J. Marks, *Chem. Rev.*, 2011, **111**, 2450-2485.
27. K. Nomura and J. Liu, *Dalton Trans.*, 2011, **40**, 7666-7682.
28. A. Smedberg, T. Hjertberg and B. Gustafsson, *J. Polym. Sci., Part A: Polym. Chem.*, 2003, **41**, 2974-2984.
29. R. Mülhaupt, *Macromol. Chem. Phys.*, 2003, **204**, 289-327.
30. R. F. Jordan, F. G. A. Stone and W. Robert, in *Adv. Organomet. Chem.*, Academic Press, 1991, pp. 325-387.
31. S. Gambarotta, *Coord. Chem. Rev.*, 2003, **237**, 229-243.
32. G. Natta, I. Pasquon and A. Zambelli, *J. Am. Chem. Soc.*, 1962, **84**, 1488-1490.
33. Y. Ma, D. Reardon, S. Gambarotta, G. Yap, H. Zahalka and C. Lemay, *Organometallics*, 1999, **18**, 2773-2781.
34. K. Feghali, D. J. Harding, D. Reardon, S. Gambarotta, G. Yap and Q. Wang, *Organometallics*, 2002, **21**, 968-976.
35. S. Milione, G. Cavallo, C. Tedesco and A. Grassi, *J. Chem. Soc., Dalton Trans.*, 2002, 1839-1846.

36. J. P. Hogan and R. L. Banks, *Phillips Petroleum Co. US2825721*, 1958.
37. O. M. Bade, R. Blom and M. Ystenes, *J. Mol. Catal. A: Chem.*, 1998, **135**, 163-179.
38. A. B. Gaspar and L. C. Dieguez, *Appl. Catal., A*, 2002, **227**, 241-254.
39. G. L. Karapinka, *Union Carbide Corp., DE1808388B2*, 1976.
40. F. J. Karol, G. L. Karapinka, C. Wu, A. W. Dow, R. N. Johnson and W. L. Carrick, *J. Polym. Sci., Part A: Polym. Chem.*, 1972, **10**, 2621-2637.
41. F. J. Karol, C. Wu, W. T. Reichle and N. J. Maraschin, *J. Catal.*, 1979, **60**, 68-76.
42. Y. V. Kissin, *J. Polym. Sci., Part A: Polym. Chem.*, 2003, **41**, 1745-1758.
43. G. Wilkinson, P. L. Pauson, J. M. Birmingham and F. A. Cotton, *J. Am. Chem. Soc.*, 1953, **75**, 1011-1012.
44. D. S. Breslow, *Hercules Powder Co. US2827446*, 1958.
45. D. S. Breslow and N. R. Newburg, *J. Am. Chem. Soc.*, 1957, **79**, 5072-5073.
46. G. Natta, *Chim.e ind.(Milan)*, 1957, **39**, 19.
47. G. Natta, P. Pino, G. Mazzanti, U. Giannini, E. Mantica and M. Peraldo, *J. Polym. Sci.*, 1957, **26**, 120-123.
48. G. Natta, P. Pino, G. Mazzanti and U. Giannini, *J. Am. Chem. Soc.*, 1957, **79**, 2975-2976.
49. H. Sinn, W. Kaminsky, F. G. A. Stone and W. Robert, in *Adv. Organomet. Chem.*, Academic Press, 1980, pp. 99-149.
50. P. Pino and R. Mülhaupt, *Angew. Chem., Int. Ed. Engl.*, 1980, **19**, 857-875.
51. B. A. Krentzel and L. A. Nekhaeva, *Vysokomol. Soedin., Ser. A Ser. B*, 1994, **36**, 1607-1624.
52. J. Skupinska, *Chem. Rev.*, 1991, **91**, 613-648.
53. K. H. Reichert and K. R. Meyer, *Makromolekul. Chem.*, 1973, **169**, 163-176.
54. W. P. Long and D. S. Breslow, *Liebigs Ann.*, 1975, **1975**, 463-469.
55. A. Andresen, H.-G. Cordes, J. Herwig, W. Kaminsky, A. Merck, R. Mottweiler, J. Pein, H. Sinn and H.-J. Vollmer, *Angew. Chem., Int. Ed. Engl.*, 1976, **15**, 630-632.
56. W. Kaminsky, *Nachr. Chem., Tech. Lab.*, 1981, **29**, 373-374, 376-377.
57. W. Kaminsky, *MMI Press Symp. Ser.*, 1983, **4**, 225-244.
58. W. Kaminsky, M. Miri, H. Sinn and R. Woldt, *Makromol. Chem., Rapid Commun.*, 1983, **4**, 417-421.

59. J. Herwig and W. Kaminsky, *Polym. Bull. (Berlin)*, 1983, **9**, 464-469.
60. I. Tritto, R. Donetti, M. C. Sacchi, P. Locatelli and G. Zannoni, *Macromolecules*, 1997, **30**, 1247-1252.
61. H. Sinn, *Macromol. Symp.*, 1995, **97**, 27-52.
62. Y. V. Kissin and A. J. Brandolini, *Macromolecules*, 2002, **36**, 18-26.
63. K. Tashiro, M. Kitani, K. Sugimura and T. Ueda, *Mitsui Petrochemical Industries, JP04304202A*, 1992.
64. D. B. Malpass and A. M. Piotrowski, *Texas Alkyls, Inc., EP315234A1*, 1989.
65. Y. Tamai, R. Sugimoto and T. Asanuma, *Mitsui Toatsu Chemicals, Inc., JP01210404A*, 1989.
66. T. Tsutsui, K. Sugimura and T. Ueda, *Mitsui Petrochemical Industries, EP436399A2*, 1991.
67. S. A. Sangokoya, *Ethyl Corp., US5099050A*, 1992.
68. S. A. Sangokoya, *Ethyl Corp., US5041583A*, 1991.
69. F.-J. Wu, *Albemarle Corp., US6462212B1*, 2002.
70. F.-j. Wu and L. S. Simeral, *Albemarle Corp., US20020072578A1*, 2002.
71. Q. Wang, J. Weng, Z. Fan and L. Feng, *Eur. Polym. J.*, 2000, **36**, 1265-1270.
72. Q. Wang, J. Hong, Z. Fan and R. Tao, *J. Polym. Sci., Part A: Polym. Chem.*, 2003, **41**, 998-1003.
73. C. J. Harlan, S. G. Bott and A. R. Barron, *J. Am. Chem. Soc.*, 1995, **117**, 6465-6474.
74. M. Ystenes, J. L. Eilertsen, J. Liu, M. Ott, E. Rytter and J. A. Støvneng, *J. Polym. Sci., Part A: Polym. Chem.*, 2000, **38**, 3106-3127.
75. B. Richter, A. Meetsma, B. Hessen and J. H. Teuben, *Chem. Commun.*, 2001, 1286-1287.
76. B. Richter, A. Meetsma, B. Hessen and J. H. Teuben, *Angew. Chem., Int. Ed. Engl.*, 2002, **41**, 2166-2169.
77. D. Bianchini, J. H. Z. dos Santos, T. Uozumi and T. Sano, *J. Mol. Catal. A: Chem.*, 2002, **185**, 223-235.
78. A. Eisenhardt, B. Heuer, W. Kaminsky, K. Köhler and H. Schumann, *Adv. Synth. Catal.*, 2003, **345**, 1299-1304.
79. E. Zurek and T. Ziegler, *Prog. Polym. Sci.*, 2004, **29**, 107-148.
80. A. K. Zefirova and A. E. Shilov, *Dokl. Akad. Nauk SSSR*, 1961, **136**, 599-602.

81. Dyachkovskii, A. K. Shilova and A. E. Shilov, *J. Polym. Sci., Part A: Polym. Chem.*, 1967, 2333.
82. J. J. Eisch, A. M. Piotrowski, S. K. Brownstein, E. J. Gabe and F. L. Lee, *J. Am. Chem. Soc.*, 1985, **107**, 7219-7221.
83. R. F. Jordan, C. S. Bajgur, R. Willett and B. Scott, *J. Am. Chem. Soc.*, 1986, **108**, 7410-7411.
84. M. Bochmann, L. M. Wilson, M. B. Hursthouse and R. L. Short, *Organometallics*, 1987, **6**, 2556-2563.
85. M. E. Thompson and J. E. Bercaw, *Pure Appl. Chem.*, 1984, **56**, 1-11.
86. G. Jeske, H. Lauke, H. Mauermann, P. N. Swepston, H. Schumann and T. J. Marks, *J. Am. Chem. Soc.*, 1985, **107**, 8091-8103.
87. P. L. Watson and G. W. Parshall, *Acc. Chem. Res.*, 1985, **18**, 51-56.
88. P. Cossee, *J. Catal.*, 1964, **3**, 80-88.
89. E. J. Arlman and P. Cossee, *J. Catal.*, 1964, **3**, 99-104.
90. K. J. Ivin, J. J. Rooney, C. D. Stewart, M. L. H. Green and R. Mahtab, *J. Chem. Soc., Chem. Commun.*, 1978, 604-606.
91. R. F. Jordan, P. K. Bradley, N. C. Baenziger and R. E. LaPointe, *J. Am. Chem. Soc.*, 1990, **112**, 1289-1291.
92. W. E. Piers and J. E. Bercaw, *J. Am. Chem. Soc.*, 1990, **112**, 9406-9407.
93. R. H. Grubbs and G. W. Coates, *Acc. Chem. Res.*, 1996, **29**, 85-93.
94. M. L. H. Green, *Pure Appl. Chem.*, 1978, **50**, 27-35.
95. P. L. Watson, *J. Am. Chem. Soc.*, 1982, **104**, 337-339.
96. S. Hajela and J. E. Bercaw, *Organometallics*, 1994, **13**, 1147-1154.
97. J. J. W. Eshuis, Y. Y. Tan, J. H. Teuben and J. Renkema, *J. Mol. Catal.*, 1990, **62**, 277-287.
98. S. Miya, T. Mise and H. Yamazaki, *Stud. Surf. Sci. Catal.*, 1990, **56**, 531-534.
99. L. Resconi, F. Piemontesi, G. Franciscono, L. Abis and T. Fiorani, *J. Am. Chem. Soc.*, 1992, **114**, 1025-1032.
100. Z. Guo, D. C. Swenson and R. F. Jordan, *Organometallics*, 1994, **13**, 1424-1432.
101. L. Resconi, F. Piemontesi, I. Camurati, D. Balboni, A. Sironi, M. Moret, H. Rychlicki and R. Zeigler, *Organometallics*, 1996, **15**, 5046-5059.
102. J. C. W. Chien and A. Razavi, *J. Polym. Sci., Part A: Polym. Chem.*, 1988, **26**, 2369-2380.

103. L. Resconi, S. Bossi and L. Abis, *Macromolecules*, 1990, **23**, 4489-4491.
104. N. Naga and K. Mizunuma, *Polymer*, 1998, **39**, 5059-5067.
105. M. G. Klimpel, J. Eppinger, P. Sirsch, W. Scherer and R. Anwander, *Organometallics*, 2002, **21**, 4021-4023.
106. S. W. Ewart, M. A. Parent and M. C. Baird, *J. Polym. Sci., Part A: Polym. Chem.*, 1999, **37**, 4386-4389.
107. Y. V. Kissin, R. I. Mink, T. E. Nowlin and A. J. Brandolini, *J. Polym. Sci., Part A: Polym. Chem.*, 1999, **37**, 4281-4294.
108. H. Mori, M. Endo and M. Terano, *J. Mol. Catal. A: Chem.*, 1999, **145**, 211-220.
109. P. Margl, L. Deng and T. Ziegler, *Top. Catal.*, 1999, **7**, 187-208.
110. B. Rieger and C. Janiak, *Angew. Makromol. Chem.*, 1994, **215**, 35-46.
111. M. Bochmann and S. J. Lancaster, *Angew. Chem., Int. Ed. Engl.*, 1994, **33**, 1634-1637.
112. F. Zhu, Q. Huang and S. Lin, *J. Polym. Sci., Part A: Polym. Chem.*, 1999, **37**, 4497-4501.
113. J. C. W. Chien, Z. Salajka and S. Dong, *Macromolecules*, 1992, **25**, 3199-3203.
114. F. Zhu, Y. Huang, Y. Yang and S. Lin, *J. Polym. Sci., Part A: Polym. Chem.*, 2000, **38**, 4258-4263.
115. T. Hasan, A. Ioku, K. Nishii, T. Shiono and T. Ikeda, *Macromolecules*, 2001, **34**, 3142-3145.
116. A. P. Shreve, R. Mülhaupt, W. Fultz, J. Calabrese, W. Robbins and S. D. Ittel, *Organometallics*, 1988, **7**, 409-416.
117. M. D. Healy, D. A. Wierda and A. R. Barron, *Organometallics*, 1988, **7**, 2543-2548.
118. V. C. Williams, C. Dai, Z. Li, S. Collins, W. E. Piers, W. Clegg, M. R. J. Elsegood and T. B. Marder, *Angew. Chem., Int. Ed.*, 1999, **38**, 3695-3698.
119. R. A. Stapleton, B. R. Galan, S. Collins, R. S. Simons, J. C. Garrison and W. J. Youngs, *J. Am. Chem. Soc.*, 2003, **125**, 9246-9247.
120. G. J. P. Britovsek, V. C. Gibson and D. F. Wass, *Angew. Chem. Int. Ed.*, 1999, **38**, 428-447.
121. G. Odian, *Principles of Polymerisation*, Wiley-Interscience, 1992.
122. P. J. Flory, *Principles of Polymer Chemistry*, Cornell University Press, 1992.
123. A. Rudin and H. L. W. Hoegy, *J. Polym. Sci., Part A: Polym. Chem.*, 1972, **10**, 217-235.

124. M. Zachary, S. Camara, A. C. Whitwood, B. C. Gilbert, M. van Duin, R. J. Meier and V. Chechik, *Eur. Polym. J.*, 2008, **44**, 2099-2107.
125. M. Dees, M. van Duin, C. Twigg and H. Dikland, Smithers Rapra Technology Ltd., 2008, pp. 12/11-12/28.
126. R. Peters, M. van Duin, D. Tonoli, G. Kwakkenbos, Y. Mengerink, R. A. T. M. van Benthem, C. G. de Koster, P. J. Schoenmakers and S. van der Wal, *J. Chromatogr., A*, 2008, **1201**, 151-160.
127. B. L. Small, M. Brookhart and A. M. A. Bennett, *J. Am. Chem. Soc.*, 1998, **120**, 4049-4050.
128. L. Resconi, L. Cavallo, A. Fait and F. Piemontesi, *Chem. Rev.*, 2000, **100**, 1253-1346.
129. K. Angermund, G. Fink, V. R. Jensen and R. Kleinschmidt, *Chem. Rev.*, 2000, **100**, 1457-1470.
130. V. Busico and R. Cipullo, *Prog. Polym. Sci.*, 2001, **26**, 443-533.
131. H. N. Cheng, *Chem. Anal.* , 1991, **113**, 409-493.
132. F. A. Bovey and P. A. Mirau, *NMR of Polymers*, Academic, 1996.
133. S. E. M. Selke, *Understanding Plastics Packaging Technology*, Hanser/Gardner, Cincinnatti, 1997.
134. W. Kaminsky, K. Külper, H. H. Brintzinger and F. Wild, *Angew. Chem., Int. Ed.*, 1985, **24**, 507-508.
135. J. A. Ewen, R. L. Jones, A. Razavi and J. D. Ferrara, *J. Am. Chem. Soc.*, 1988, **110**, 6255-6256.
136. C. R. Baar, C. J. Levy, E. Y. J. Min, L. M. Henling, M. W. Day and J. E. Bercaw, *J. Am. Chem. Soc.*, 2004, **126**, 8216-8231.
137. G. Milano, G. Fiorello, G. Guerra and L. Cavallo, *Macromol. Chem. Phys.*, 2002, **203**, 1564-1572.
138. H. G. Alt and A. Köppl, *Chem. Rev.*, 2000, **100**, 1205-1221.
139. N. E. Grimmer and N. J. Coville, *S. Afr. J. Chem.*, 2001, **54**, 118-229.
140. G. W. Coates and R. M. Waymouth, *Science* 1995, **267**, 217-219.
141. V. Busico, R. Cipullo, W. P. Kretschmer, G. Talarico, M. Vacatello and C. V. van Axel, *Angew. Chem., Int. Ed.*, 2002, **41**, 505-508.
142. K. H. Theopold, *Eur. J. Inorg. Chem.*, 1998, 15-24.
143. U. Siemeling, *Chem. Rev.*, 2000, **100**, 1495-1526.
144. H. Butenschön, *Chem. Rev.*, 2000, **100**, 1527-1564.

145. J. Gromada, J.-F. Carpentier and A. Mortreux, *Coord. Chem. Rev.*, 2004, **248**, 397-410.
146. J. C. Stevens, F. J. Timmers and R. K. Rosen, *Dow Chemical Co., EP416815A2*, 1991.
147. J. C. Stevens and D. R. Neithamer, *Dow Chemical Co., EP418044A2*, 1991.
148. R. K. Rosen, P. N. Nickias, D. D. Devore and F. J. Timmers, *Dow Chemical Co., WO9319104A1*, 1993.
149. R. K. Rosen, P. N. Nickias, D. D. Devore, J. C. Stevens and F. J. Timmers, *Dow Chemical Co., US5374696A*, 1994.
150. J. A. M. Canich, *Exxon Chemical Patents Inc., EP420436A1*, 1991.
151. J. A. M. Canich, *Exxon Chemical Patents Inc., US5026798A*, 1991.
152. J. A. M. Canich, *Exxon Chemical Patents Inc., US5096867A*, 1992.
153. J. A. M. Canich, H. W. Turner and G. G. Hlatky, *Exxon Chemical Patents Inc., US5621126A* 1997.
154. P. J. Shapiro, E. Bunel, W. P. Schaefer and J. E. Bercaw, *Organometallics*, 1990, **9**, 867-869.
155. J. Okuda, *Chem. Ber.*, 1990, **123**, 1649-1651.
156. J. C. Stevens, F. J. Timmers, D. R. Wilson, G. F. Schmidt, P. N. Nickias, R. K. Rosen, G. W. Knight and S. Y. Lai, *Dow Chemical Co., EP416815A2*, 1991.
157. W. E. Piers, P. J. Shapiro, E. E. Bunel and J. E. Bercaw, *Synlett*, 1990, **1990**, 74-84.
158. D. W. Carpenetti, L. Kloppenburg, J. T. Kupec and J. L. Petersen, *Organometallics*, 1996, **15**, 1572-1581.
159. L. Duda, G. Erker, R. Fröhlich and F. Zippel, *Eur. J. Inorg. Chem.*, 1998, 1153-1162.
160. K. Kunz, G. Erker, S. Döring, R. Fröhlich and G. Kehr, *J. Am. Chem. Soc.*, 2001, **123**, 6181-6182.
161. K. Kunz, G. Erker, S. Döring, S. Bredeau, G. Kehr and R. Fröhlich, *Organometallics*, 2002, **21**, 1031-1041.
162. T. H. Kim, Y. C. Won, B. Y. Lee, D. M. Shin and Y. K. Chung, *Eur. J. Inorg. Chem.*, 2004, 1522-1529.
163. P.-J. Sinnema, L. van der Veen, A. L. Spek, N. Veldman and J. H. Teuben, *Organometallics*, 1997, **16**, 4245-4247.

164. P.-J. Sinnema, K. Liekelema, O. K. B. Staal, B. Hessen and J. H. Teuben, *J. Mol. Catal. A: Chem.*, 1998, **128**, 143-153.
165. P. T. Gomes, M. L. H. Green and A. M. Martins, *J. Organomet. Chem.*, 1998, **551**, 133-138.
166. P.-J. Sinnema, B. Hessen and J. H. Teuben, *Macromol. Rapid Commun.*, 2000, **21**, 562-566.
167. D. van Leusen, D. J. Beetstra, B. Hessen and J. H. Teuben, *Organometallics*, 2000, **19**, 4084-4089.
168. J. Chirinos, T. Rajmankina, A. Morillo, D. Ibarra, A. Parada and J. Arevalo, *Macromol. Chem. Phys.*, 2002, **203**, 1501-1505.
169. A. K. Hughes, A. Meetsma and J. H. Teuben, *Organometallics*, 1993, **12**, 1936-1945.
170. P. J. Shapiro, *Eur. J. Inorg. Chem.*, 2001, 321-326.
171. V. V. Kotov, E. V. Avtomonov, J. Sundermeyer, K. Harms and D. A. Lemenovskii, *Eur. J. Inorg. Chem.*, 2002, 678-691.
172. H. Braunschweig, F. M. Breitling, C. von Koblinski, A. J. P. White and D. J. Williams, *Dalton Trans.*, 2004, 938-943.
173. S. Bredeau, G. Altenhoff, K. Kunz, S. Döring, S. Grimme, G. Kehr and G. Erker, *Organometallics*, 2004, **23**, 1836-1844.
174. L. Truflandier, C. J. Marsden, C. Freund, B. Martin-Vaca and D. Bourissou, *Eur. J. Inorg. Chem.*, 2004, 1939-1947.
175. P.-J. Sinnema, T. P. Spaniol and J. Okuda, *J. Organomet. Chem.*, 2000, **598**, 179-181.
176. D. J. Cho, C. J. Wu, S. S, W.-S. Han, S. O. Kang and B. Y. Lee, *Organometallics*, 2006, **25**, 2133-2134.
177. D. J. Joe, C. J. Wu, T. Bok, E. J. Lee, C. H. Lee, W.-S. Han, S. O. Kang and B. Y. Lee, *Dalton Trans.*, 2006, 4056-4062.
178. U. G. Joung, C. J. Wu, S. H. Lee, C. H. Lee, E. J. Lee, W.-S. Han, S. O. Kang and B. Y. Lee, *Organometallics*, 2006, **25**, 5122-5130.
179. S. H. Lee, C. J. Wu, U. G. Joung, B. Y. Lee and J. Park, *Dalton Trans.*, 2007, 4608-4614.
180. C. J. Wu, S. H. Lee, H. Yun and B. Y. Lee, *J. Organomet. Chem.*, 2006, **691**, 5626-5634.

181. S. H. Lee, C. J. Wu, J. Yoo, J.-e. Kwak, H. Yun and B. Y. Lee, *J. Organomet. Chem.*, 2008, **693**, 457-467.
182. C. J. Wu, S. H. Lee, S. T. Yu, S. J. Na, H. Yun and B. Y. Lee, *Organometallics*, 2008, **27**, 3907-3917.
183. P. Jutzi and J. Dahlhaus, *Coord. Chem. Rev.*, 1994, **137**, 179-199.
184. A. Döhring, J. Göhre, P. W. Jolly, B. Kryger, J. Rust and G. P. J. Verhovnik, *Organometallics*, 2000, **19**, 388-402.
185. J. A. M. van Beek and G. J. M. Gruter, *DSM N.V., EP805142A1*, 1997.
186. K. Ogata, Y. Nakayama and H. Yasuda, *J. Polym. Sci., Part A: Polym. Chem.*, 2002, **40**, 2759-2771.
187. G. Altenhoff, S. Bredeau, G. Erker, G. Kehr, O. Kataeva and R. Fröhlich, *Organometallics*, 2002, **21**, 4084-4089.
188. T. Ishiyama, T. Mizuta, K. Miyoshi and H. Nakazawa, *Organometallics*, 2003, **22**, 1096-1105.
189. T. Ishiyama, T. Mizuta, K. Miyoshi and H. Nakazawa, *Chem. Lett.*, 2003, **32**, 70-71.
190. R. Fandos, J. H. Teuben, G. Helgesson and S. Jagner, *Organometallics*, 1991, **10**, 1637-1639.
191. G. Trouve, D. A. Laske, A. Meetsma and J. H. Teuben, *J. Organomet. Chem.*, 1996, **511**, 255-262.
192. Y.-X. Chen, P.-F. Fu, C. L. Stern and T. J. Marks, *Organometallics*, 1997, **16**, 5958-5963.
193. E. E. C. G. Gielens, J. Y. Tiesnitsch, B. Hessen and J. H. Teuben, *Organometallics*, 1998, **17**, 1652-1654.
194. A. Rau, S. Schmitz and G. Luft, *J. Organomet. Chem.*, 2000, **608**, 71-75.
195. K. Kunz, G. Erker, G. Kehr, R. Fröhlich, H. Jacobsen, H. Berke and O. Blacque, *J. Am. Chem. Soc.*, 2002, **124**, 3316-3326.
196. M. Gonzalez-Maupoey, T. Cuenca, L. M. Frutos, O. Castano and E. Herdtweck, *Organometallics*, 2003, **22**, 2694-2704.
197. Y. Zhang, Y. Mu, C. Lue, G. Li, J. Xu, Y. Zhang, D. Zhu and S. Feng, *Organometallics*, 2004, **23**, 540-546.
198. L. E. Turner, M. G. Thorn, P. E. Fanwick and I. P. Rothwell, *Organometallics*, 2004, **23**, 1576-1593.

199. O. Buitrago, d. A. C. Ramirez, G. Jimenez and T. Cuenca, *Organometallics*, 2004, **23**, 5873-5876.
200. Y. Mu, W. E. Piers, M.-A. MacDonald and M. J. Zaworotko, *Can. J. Chem.*, 1995, **73**, 2233-2238.
201. K. C. Hultzsch, T. P. Spaniol and J. Okuda, *Angew. Chem., Int. Ed.*, 1999, **38**, 227-230.
202. K. C. Hultzsch, P. Voth, K. Beckerle, T. P. Spaniol and J. Okuda, *Organometallics*, 2000, **19**, 228-243.
203. S. Arndt, P. Voth, T. P. Spaniol and J. Okuda, *Organometallics*, 2000, **19**, 4690-4700.
204. Z. Hou, T.-a. Koizumi, M. Nishiura and Y. Wakatsuki, *Organometallics*, 2001, **20**, 3323-3328.
205. M. Nishiura, Z. Hou, Y. Wakatsuki, T. Yamaki and T. Miyamoto, *J. Am. Chem. Soc.*, 2003, **125**, 1184-1185.
206. E. Kirillov, L. Toupet, C. W. Lehmann, A. Razavi and J.-F. Carpentier, *Organometallics*, 2003, **22**, 4467-4479.
207. J. T. Golden, D. N. Kazul'kin, B. L. Scott, A. Z. Voskoboynikov and C. J. Burns, *Organometallics*, 2003, **22**, 3971-3973.
208. B. D. Stubbert, C. L. Stern and T. J. Marks, *Organometallics*, 2003, **22**, 4836-4838.
209. P. T. Witte, A. Meetsma, B. Hessen and P. H. M. Budzelaar, *J. Am. Chem. Soc.*, 1997, **119**, 10561-10562.
210. P. T. Witte, A. Meetsma and B. Hessen, *Organometallics*, 1999, **18**, 2944-2946.
211. W. Kaminsky, B. Hinrichs and D. Rehder, *Polymer*, 2002, **43**, 7225-7229.
212. W. A. Herrmann and W. Baratta, *J. Organomet. Chem.*, 1996, **506**, 357-361.
213. M. I. Alcalde, M. P. Gomez-Sal and P. Royo, *Organometallics*, 1999, **18**, 546-554.
214. S. Gomez-Ruiz, T. Höcher, S. Prashar and E. Hey-Hawkins, *Organometallics*, 2005, **24**, 2061-2064.
215. W. A. Herrmann, W. Baratta and M. J. A. Morawietz, *J. Organomet. Chem.*, 1995, **497**, C4-C6.
216. A. K. Hughes and A. J. Kingsley, *J. Chem. Soc., Dalton Trans.*, 1997, 4139-4142.

217. P. T. Gomes, M. L. H. Green, A. M. Martins and P. Mountford, *J. Organomet. Chem.*, 1997, **541**, 121-125.
218. A. Dohring, V. R. Jensen, P. W. Jolly, W. Thiel and J. C. Weber, *Macromol. Symp.*, 2001, **173**, 117-121.
219. T.-F. Wang, C.-Y. Lai, C.-C. Hwu and Y.-S. Wen, *Organometallics*, 1997, **16**, 1218-1223.
220. T.-F. Wang, C.-C. Hwu, C.-W. Tsai and Y.-S. Wen, *Organometallics*, 1998, **17**, 131-138.
221. J. Cano and K. Kunz, *J. Organomet. Chem.*, 2007, **692**, 4411-4423.
222. R. Hoffmann, *Prix Nobel*, 1982, 173-205.
223. R. Hoffmann, *Angew. Chem., Int. Ed. Engl.*, 1982, **21**, 711-724.
224. K. Nomura, *Trends Organomet. Chem.*, 2002, **4**, 1-18.
225. K. Nomura and J.-Y. Liu, *Dalton Trans.*, 2011, **40**, 7666-7682.
226. K. Nomura, N. Naga, M. Miki, K. Yanagi and A. Imai, *Organometallics*, 1998, **17**, 2152-2154.
227. K. Nomura, N. Naga, M. Miki and K. Yanagi, *Macromolecules*, 1998, **31**, 7588-7597.
228. K. Nomura and A. Fudo, *Inorg. Chim. Acta*, 2003, **345**, 37-43.
229. K. Nomura, M. Tsubota and M. Fujiki, *Macromolecules*, 2003, **36**, 3797-3799.
230. Y. Qian, H. Zhang, X. Qian, J. Huang and C. Shen, *J. Mol. Catal. A: Chem.*, 2003, **192**, 25-33.
231. K. Nomura, Y. Hatanaka, H. Okumura, M. Fujiki and K. Hasegawa, *Macromolecules*, 2004, **37**, 1693-1695.
232. A. E. Fenwick, K. Phomphrai, M. G. Thorn, J. S. Vilardo, C. A. Trefun, B. Hanna, P. E. Fanwick and I. P. Rothwell, *Organometallics*, 2004, **23**, 2146-2156.
233. W. Wang, T. Tanaka, M. Tsubota, M. Fujiki, S. Yamanaka and K. Nomura, *Adv. Synth. Catal.*, 2005, **347**, 433-446.
234. K. Nomura and K. Fujii, *Organometallics*, 2002, **21**, 3042-3049.
235. K. Nomura and K. Fujii, *Macromolecules*, 2003, **36**, 2633-2641.
236. J. McMeeking, X. Gao, R. E. v. H. Spence, S. J. Brown and D. Jeremic, *Nova Chemicals International, WO9914250A1* 1999.
237. S. Zhang, W. E. Piers, X. Gao and M. Parvez, *J. Am. Chem. Soc.*, 2000, **122**, 5499-5509.

238. K. W. Henderson, A. Hind, A. R. Kennedy, A. E. McKeown and R. E. Mulvey, *J. Organomet. Chem.*, 2002, **656**, 63-70.
239. A. R. Dias, M. T. Duarte, A. C. Fernandes, S. Fernandes, M. M. Marques, A. M. Martins, S. J. F. da and S. S. Rodrigues, *J. Organomet. Chem.*, 2004, **689**, 203-213.
240. K. Nomura, K. Fujita and M. Fujiki, *J. Mol. Catal. A: Chem.*, 2004, **220**, 133-144.
241. M. J. Ferreira and A. M. Martins, *Coord. Chem. Rev.*, 2006, **250**, 118-132.
242. W. P. Kretschmer, *Stichting Dutch Polymer Institute, US20040192541A1*, 2004.
243. W. P. Kretschmer, C. Dijkhuis, A. Meetsma, B. Hessen and J. H. Teuben, *Chem. Commun.*, 2002, 608-609.
244. G. H. J. van Doremaele, M. A. Zuideveld, N. V. F. Quiroga and A. Leblanc, *LANXESS Elastomers, WO2011054927A1*, 2011.
245. D. W. Stephan, F. Guérin, R. E. v. H. Spence, L. Koch, X. Gao, S. J. Brown, J. W. Swabey, Q. Wang, W. Xu, P. Zoricak and D. G. Harrison, *Organometallics*, 1999, **18**, 2046-2048.
246. D. W. Stephan, J. C. Stewart, F. Guérin, R. E. v. H. Spence, W. Xu and D. G. Harrison, *Organometallics*, 1999, **18**, 1116-1118.
247. F. Guérin, J. C. Stewart, C. Beddie and D. W. Stephan, *Organometallics*, 2000, **19**, 2994-3000.
248. N. L. S. Yue and D. W. Stephan, *Organometallics*, 2001, **20**, 2303-2308.
249. N. Yue, E. Hollink, F. Guérin and D. W. Stephan, *Organometallics*, 2001, **20**, 4424-4433.
250. D. W. Stephan, J. C. Stewart, F. Guérin, S. Courtenay, J. Kickham, E. Hollink, C. Beddie, A. Hoskin, T. Graham, P. Wei, R. E. v. H. Spence, W. Xu, L. Koch, X. Gao and D. G. Harrison, *Organometallics*, 2003, **22**, 1937-1947.
251. E. Hollink, P. Wei and D. W. Stephan, *Organometallics*, 2004, **23**, 1562-1569.
252. M. Raab, J. Tirree, M. Nieger and E. Niecke, *Z. Anorg. Allg. Chem.*, 2003, **629**, 769-780.
253. K. Dehnicke and F. Weller, *Coord. Chem. Rev.*, 1997, **158**, 103-169.
254. K. Dehnicke, M. Krieger and W. Massa, *Coord. Chem. Rev.*, 1999, **182**, 19-65.
255. D. W. Stephan, J. C. Stewart and D. G. Harrison, *NOVA Chemicals International, EP 890581 A1*, 1999.

256. M. Tamm, S. Randoll, T. Bannenberg and E. Herdtweck, *Chem. Commun.*, 2004, 876-877.
257. M. Tamm, S. Randoll, E. Herdtweck, N. Kleigrewe, G. Kehr, G. Erker and B. Rieger, *Dalton Trans.*, 2006, 459-467.
258. K. Nomura, H. Fukuda, S. Katao, M. Fujiki, H. J. Kim, D.-H. Kim and S. Zhang, *Dalton Trans.*, 2011, **40**, 7842-7849.
259. S. Trofimenko, *J. Am. Chem. Soc.*, 1966, **88**, 1842-1844.
260. S. Trofimenko, *J. Am. Chem. Soc.*, 1967, **89**, 3904-3905.
261. S. Trofimenko, *J. Am. Chem. Soc.*, 1967, **89**, 6288-6294.
262. T. Obara and S. Ueki, *Toa Nenryo Kogyo K. K., JP01095110A* 1989.
263. T. H. Newman, *Dow Chemical Co., EP482934A1*, 1992.
264. H. Nakazawa, S. Ikai, K. Imaoka, Y. Kai and T. Yano, *J. Mol. Catal. A: Chem.*, 1998, **132**, 33-41.
265. L. G. Furlan, M. P. Gil and O. L. Casagrande, Jr., *Macromol. Rapid Commun.*, 2000, **21**, 1054-1057.
266. M. P. Gil, J. H. Z. dos Santos and O. L. Casagrande, Jr., *Macromol. Chem. Phys.*, 2001, **202**, 319-324.
267. M. P. Gil and O. L. Casagrande, *J. Organomet. Chem.*, 2004, **689**, 286-292.
268. M. P. Gil, J. H. Z. dos Santos and O. L. Casagrande, *J. Mol. Catal. A: Chem.*, 2004, **209**, 163-169.
269. K. Michiue and R. F. Jordan, *Organometallics*, 2004, **23**, 460-470.
270. H. Bigmore, DPhil Thesis, University of Oxford, 2007.
271. L. Clark, Part II Thesis, University of Oxford, 2008.
272. N. Hazari and P. Mountford, *Acc. Chem. Res.*, 2005, **38**, 839-849.
273. H. R. Bigmore, S. R. Dubberley, M. Kranenburg, S. C. Lawrence, A. J. Sealey, J. D. Selby, M. A. Zuideveld, A. R. Cowley and P. Mountford, *Chem. Commun.*, 2006, 436-438.
274. P. D. Bolton, E. Clot, N. Adams, S. R. Dubberley, A. R. Cowley and P. Mountford, *Organometallics*, 2006, **25**, 2806-2825.
275. H. R. Bigmore, M. A. Zuideveld, R. M. Kowalczyk, A. R. Cowley, M. Kranenburg, E. J. L. McInnes and P. Mountford, *Inorg. Chem.*, 2006, **45**, 6411-6423.
276. N. Adams, H. J. Arts, P. D. Bolton, D. Cowell, S. R. Dubberley, N. Friederichs, C. M. Grant, M. Kranenburg, A. J. Sealey, B. Wang, P. J. Wilson, M.

Zuideveld, A. J. Blake, M. Schröder and P. Mountford, *Organometallics*, 2006, **25**, 3888-3903.

277. P. D. Bolton, N. Adams, E. Clot, A. R. Cowley, P. J. Wilson, M. Schröder and P. Mountford, *Organometallics*, 2006, **25**, 5549-5565.
278. P. D. Bolton, E. Clot, A. R. Cowley and P. Mountford, *J. Am. Chem. Soc.*, 2006, **128**, 15005-15018.
279. T. R. Cundari, *Organometallics*, 1993, **12**, 4971-4978.
280. C. H. Zambrano, R. D. Profilet, J. E. Hill, P. E. Fanwick and I. P. Rothwell, *Polyhedron*, 1993, **12**, 689-708.
281. P. Mountford and D. Swallow, *J. Chem. Soc., Chem. Commun.*, 1995, 2357-2359.
282. N. Kaltsoyannis and P. Mountford, *J. Chem. Soc., Dalton Trans.*, 1999, 781-790.
283. T. R. Cundari, *Chem. Rev.*, 2000, **100**, 807-818.
284. S. C. Lawrence, M. E. G. Skinner, J. C. Green and P. Mountford, *Chem. Commun.*, 2001, 705-706.
285. P. D. Bolton, E. Clot, A. R. Cowley and P. Mountford, *Chem. Commun.*, 2005, 3313-3315.
286. C. L. Boyd, E. Clot, A. E. Guiducci and P. Mountford, *Organometallics*, 2005, **24**, 2347-2367.
287. S. C. Dunn, N. Hazari, N. M. Jones, A. G. Moody, A. J. Blake, A. R. Cowley, J. C. Green and P. Mountford, *Chem. Eur. J.*, 2005, **11**, 2111-2124.
288. A. Heath, DPhil Thesis, University of Oxford, 2011.
289. J. D. Scollard and D. H. McConville, *J. Am. Chem. Soc.*, 1996, **118**, 10008-10009.
290. R. Baumann, W. M. Davis and R. R. Schrock, *J. Am. Chem. Soc.*, 1997, **119**, 3830-3831.
291. R. Baumann and R. R. Schrock, *J. Organomet. Chem.*, 1998, **557**, 69-75.
292. R. R. Schrock, F. Schattenmann, M. Aizenberg and W. M. Davis, *Chem. Commun.*, 1998, 199-200.
293. M. Aizenberg, L. Turculet, W. M. Davis, F. Schattenmann and R. R. Schrock, *Organometallics*, 1998, **17**, 4795-4812.
294. R. Baumann, R. Stumpf, W. M. Davis, L.-C. Liang and R. R. Schrock, *J. Am. Chem. Soc.*, 1999, **121**, 7822-7836.

295. R. R. Schrock, L. C. Liang, R. Baumann and W. M. Davis, *J. Organomet. Chem.*, 1999, **591**, 163-173.
296. R. R. Schrock, R. Baumann, S. M. Reid, J. T. Goodman, R. Stumpf and W. M. Davis, *Organometallics*, 1999, **18**, 3649-3670.
297. L.-C. Liang, R. R. Schrock and W. M. Davis, *Organometallics*, 2000, **19**, 2526-2531.
298. J. T. Goodman and R. R. Schrock, *Organometallics*, 2001, **20**, 5205-5211.
299. Y. Yoshida, S. Matsui, Y. Takagi, M. Mitani, T. Nakano, H. Tanaka, N. Kashiwa and T. Fujita, *Organometallics*, 2001, **20**, 4793-4799.
300. Y. Yoshida, J. Mohri, S. Ishii, M. Mitani, J. Saito, S. Matsui, H. Makio, T. Nakano, H. Tanaka, M. Onda, Y. Yamamoto, A. Mizuno and T. Fujita, *J. Am. Chem. Soc.*, 2004, **126**, 12023-12032.
301. H. Mack and M. S. Eisen, *J. Organomet. Chem.*, 1996, **525**, 81-87.
302. V. C. Gibson, B. S. Kimberley, A. J. P. White, D. J. Williams and P. Howard, *Chem. Commun.* , 1998, 313-314.
303. T. R. Boussie, G. M. Diamond, C. Goh, K. A. Hall, A. M. LaPointe, M. K. Leclerc, V. Murphy, J. A. W. Shoemaker, H. Turner, R. K. Rosen, J. C. Stevens, F. Alfano, V. Busico, R. Cipullo and G. Talarico, *Angew. Chem., Int. Ed. Engl.*, 2006, **45**, 3278-3283.
304. D. J. Arriola, E. M. Carnahan, P. D. Hustad, R. L. Kuhlman and T. T. Wenzel, *Science* 2006, **312**, 714-719.
305. G. J. Domski, E. B. Lobkovsky and G. W. Coates, *Macromolecules*, 2007, **40**, 3510-3513.
306. R. D. J. Froese, P. D. Hustad, R. L. Kuhlman and T. T. Wenzel, *J. Am. Chem. Soc.*, 2007, **129**, 7831-7840.
307. H. Kawaguchi and T. Matsuo, *J. Organomet. Chem.*, 2004, **689**, 4228-4243.
308. A. van der Linden, C. J. Schaverien, N. Meijboom, C. Ganter and A. G. Orpen, *J. Am. Chem. Soc.*, 1995, **117**, 3008-3021.
309. M. C. W. Chan, K.-H. Tam, Y.-L. Pui and N. Zhu, *J. Chem. Soc., Dalton Trans.*, 2002, 3085-3087.
310. M. C. W. Chan, K.-H. Tam, N. Zhu, P. Chiu and S. Matsui, *Organometallics*, 2006, **25**, 785-792.
311. M. C. W. Chan, S. C. F. Kui, J. M. Cole, G. J. McIntyre, S. Matsui, N. Zhu and K.-H. Tam, *Chem. Eur. J.*, 2006, **12**, 2607-2619.

312. T. Agapie, M. W. Day and J. E. Bercaw, *Organometallics*, 2008, **27**, 6123-6142.
313. T. Agapie, L. M. Henling, A. G. DiPasquale, A. L. Rheingold and J. E. Bercaw, *Organometallics*, 2008, **27**, 6245-6256.
314. E. Kirillov, T. Roisnel, A. Razavi and J.-F. Carpentier, *Organometallics*, 2009, **28**, 5036-5051.
315. H. Aihara, T. Matsuo and H. Kawaguchi, *Chem. Commun.* , 2003, 2204-2205.
316. E. Y. Tshuva, M. Versano, I. Goldberg, M. Kol, H. Weitman and Z. Goldschmidt, *Inorg. Chem. Commun.*, 1999, **2**, 371-373.
317. E. Y. Tshuva, I. Goldberg and M. Kol, *J. Am. Chem. Soc.*, 2000, **122**, 10706-10707.
318. E. Y. Tshuva, I. Goldberg, M. Kol and Z. Goldschmidt, *Chem. Commun.* , 2001, 2120-2121.
319. E. Y. Tshuva, I. Goldberg, M. Kol and Z. Goldschmidt, *Inorg. Chem.*, 2001, **40**, 4263-4270.
320. E. Y. Tshuva, S. Groysman, I. Goldberg, M. Kol and Z. Goldschmidt, *Organometallics*, 2002, **21**, 662-670.
321. T. Toupance, S. R. Dubberley, N. H. Rees, B. R. Tyrrell and P. Mountford, *Organometallics*, 2002, **21**, 1367-1382.
322. C. Capacchione, A. Proto, H. Ebeling, R. Mülhaupt, K. Moller, T. P. Spaniol and J. Okuda, *J. Am. Chem. Soc.*, 2003, **125**, 4964-4965.
323. A. Proto, C. Capacchione, V. Venditto and J. Okuda, *Macromolecules*, 2003, **36**, 9249-9251.
324. S. Groysman, I. Goldberg, M. Kol, E. Genizi and Z. Goldschmidt, *Organometallics*, 2003, **22**, 3013-3015.
325. S. Groysman, I. Goldberg, M. Kol, E. Genizi and Z. Goldschmidt, *Inorg. Chim. Acta*, 2003, **345**, 137-144.
326. J. Tian, P. D. Hustad and G. W. Coates, *J. Am. Chem. Soc.*, 2001, **123**, 5134-5135.
327. P. D. Hustad, J. Tian and G. W. Coates, *J. Am. Chem. Soc.*, 2002, **124**, 3614-3621.
328. H. Terao, A. Iwashita, N. Matsukawa, S. Ishii, M. Mitani, H. Tanaka, T. Nakano and T. Fujita, *ACS Catal.*, **1**, 254-265.

329. J. Saito, M. Mitani, J.-I. Mohri, Y. Yoshida, S. Matsui, S.-I. Ishii, S.-I. Kojoh, N. Kashiwa and T. Fujita, *Angew. Chem., Int. Ed.*, 2001, **40**, 2918-2920.
330. L. K. Johnson, C. M. Killian and M. Brookhart, *J. Am. Chem. Soc.*, 1995, **117**, 6414-6415.
331. L. K. Johnson, C. M. Killian, S. D. Arthur, J. Feldman, E. F. McCord, S. J. McLain, K. A. Kreutzer, M. A. Bennett, E. B. Coughlin and a. et, *E. I. Du Pont de Nemours & Co., WO9623010A2*, 1996.
332. L. K. Johnson, S. Mecking and M. Brookhart, *J. Am. Chem. Soc.*, 1996, **118**, 267-268.
333. S. Mecking, L. K. Johnson, L. Wang and M. Brookhart, *J. Am. Chem. Soc.*, 1998, **120**, 888-899.
334. G. J. P. Britovsek, V. C. Gibson, B. S. Kimberley, P. J. Maddox, S. J. McTavish, G. A. Solan, A. J. P. White and D. J. Williams, *Chem. Commun.*, 1998, 849-850.
335. B. L. Small and M. Brookhart, *J. Am. Chem. Soc.*, 1998, **120**, 7143-7144.
336. A. G. Massey and A. J. Park, *J. Organomet. Chem.*, 1964, **2**, 245-250.
337. M. J. Elder and J. A. Ewen, *Fina Technology, Inc., CA2027145A1*, 1991.
338. X. Yang, C. L. Stern and T. J. Marks, *J. Am. Chem. Soc.*, 1991, **113**, 3623-3625.
339. X. Yang, C. L. Stern and T. J. Marks, *J. Am. Chem. Soc.*, 1994, **116**, 10015-10031.
340. M. Bochmann, S. J. Lancaster, M. B. Hursthouse and K. M. A. Malik, *Organometallics*, 1994, **13**, 2235-2243.
341. Y.-X. Chen, M. V. Metz, L. Li, C. L. Stern and T. J. Marks, *J. Am. Chem. Soc.*, 1998, **120**, 6287-6305.
342. J.-F. Carpentier, V. P. Maryin, J. Luci and R. F. Jordan, *J. Am. Chem. Soc.*, 2001, **123**, 898-909.
343. C. R. Landis, K. A. Rosaaen and D. R. Sillars, *J. Am. Chem. Soc.*, 2003, **125**, 1710-1711.
344. C. H. Lee, S. J. Lee, J. W. Park, K. H. Kim, B. Y. Lee and J. S. Oh, *J. Mol. Catal. A: Chem.*, 1998, **132**, 231-239.
345. J. C. W. Chien, W. Song and M. D. Rausch, *Macromolecules*, 1993, **26**, 3239-3240.
346. A. D. Horton, J. de With, A. J. van der Linden and H. van de Weg, *Organometallics*, 1996, **15**, 2672-2674.

347. C. Pellecchia, A. Immirzi, A. Grassi and A. Zambelli, *Organometallics*, 1993, **12**, 4473-4478.
348. J. I. Amor, T. Cuenca, M. Galakhov, P. Gomez-Sal, A. Manzanero and P. Royo, *J. Organomet. Chem.*, 1997, **535**, 155-168.
349. C. L. Beswick and T. J. Marks, *J. Am. Chem. Soc.*, 2000, **122**, 10358-10370.
350. S. Beck, S. Lieber, F. Schaper, A. Geyer and H.-H. Brintzinger, *J. Am. Chem. Soc.*, 2001, **123**, 1483-1489.
351. E. Kirillov, L. Lavanant, C. Thomas, T. Roisnel, Y. Chi and J.-F. Carpentier, *Chem. Eur. J.*, 2007, **13**, 923-935.
352. M. Bochmann and S. J. Lancaster, *Organometallics*, 1993, **12**, 633-640.
353. R. F. Jordan, R. E. LaPointe, N. Baenziger and G. D. Hinch, *Organometallics*, 1990, **9**, 1539-1545.
354. S. H. Strauss, *Chem. Rev.*, 1993, **93**, 927-942.
355. L. Li and T. J. Marks, *Organometallics*, 1998, **17**, 3996-4003.
356. T. J. Marks, L. Li, Y.-X. Chen, M. H. McAdon and P. N. Nickias, *Dow Chemical Company and Northwestern University, WO9906412A1*, 1999.
357. M. V. Metz, D. J. Schwartz, C. L. Stern, P. N. Nickias and T. J. Marks, *Angew. Chem., Int. Ed.*, 2000, **39**, 1312-1316.
358. Z. J. A. Komon, G. C. Bazan, C. Fang and X. Bu, *Inorg. Chim. Acta*, 2003, **345**, 95-102.
359. G. Kehr, R. Fröhlich, B. Wibbeling and G. Erker, *Chem. Eur. J.*, 2000, **6**, 258-266.
360. B. Temme, G. Erker, J. Karl, H. Luftmann, R. Fröhlich and S. Kotila, *Angew. Chem., Int. Ed. Engl.*, 1995, **34**, 1755-1757.
361. J. Karl, G. Erker and R. Fröhlich, *J. Organomet. Chem.*, 1997, **535**, 59-62.
362. J. Karl, G. Erker and R. Fröhlich, *J. Am. Chem. Soc.*, 1997, **119**, 11165-11173.
363. J. Karl, M. Dahlmann, G. Erker and K. Bergander, *J. Am. Chem. Soc.*, 1998, **120**, 5643-5652.
364. A. R. Siedle, R. A. Newmark, W. M. Lamanna and J. C. Huffman, *Organometallics*, 1993, **12**, 1491-1492.
365. Y. Sun, R. E. v. H. Spence, W. E. Piers, M. Parvez and G. P. A. Yap, *J. Am. Chem. Soc.*, 1997, **119**, 5132-5143.
366. G. Jimenez Pindado, S. J. Lancaster, M. Thornton-Pett and M. Bochmann, *J. Am. Chem. Soc.*, 1998, **120**, 6816-6817.

367. G. Jimenez Pindado, M. Thornton-Pett, M. B. Hursthouse, S. J. Coles and M. Bochmann, *J. Chem. Soc., Dalton Trans.*, 1999, 1663-1668.
368. H. Yasuda and A. Nakamura, *Angew. Chem., Int. Ed. Engl.*, 1987, **26**, 723-742.
369. B. Hessen and J. H. Teuben, *J. Organomet. Chem.*, 1988, **358**, 135-145.
370. A. Nakamura and K. Mashima, *J. Organomet. Chem.*, 2004, **689**, 4552-4563.
371. G. Jimenez Pindado, M. Thompson-Pett, M. Bouwkamp, A. Meetsma, B. Hessen and M. Bochmann, *Angew. Chem., Int. Ed. Engl.*, 1997, **36**, 2358-2361.
372. D. D. Devore, L. H. Crawford, J. C. Stevens, F. J. Timmers, R. D. Mussell, D. R. Wilson and R. K. Rosen, *Dow Chemical Co., WO9500526*, 1995.
373. D. D. Devore, F. J. Timmers, D. L. Hasha, R. K. Rosen, T. J. Marks, P. A. Deck and C. L. Stern, *Organometallics*, 1995, **14**, 3132-3134.
374. A. H. Cowley, G. S. Hair, B. G. McBurnett and R. A. Jones, *Chem. Commun.*, 1999, 437-438.
375. G. S. Hair, R. A. Jones, A. H. Cowley and V. Lynch, *Organometallics*, 2000, **20**, 177-181.
376. G. S. Hair, R. A. Jones, A. H. Cowley and V. Lynch, *Inorg. Chem.*, 2001, **40**, 1014-1019.
377. R. E. v. H. Spence, D. W. Stephan, S. J. Brown, D. Jeremic and Q. Wang, *Nova Chemicals International, WO2000005236A1*, 2000.
378. T. W. Graham, J. Kickham, S. Courtenay, P. Wei and D. W. Stephan, *Organometallics*, 2004, **23**, 3309-3318.
379. H. W. Turner, *Exxon Chemical Patents Inc., EP277004A1*, 1988.
380. G. G. Hlatky, H. W. Turner and R. R. Eckman, *J. Am. Chem. Soc.*, 1989, **111**, 2728-2729.
381. M. Brookhart, B. Grant and A. F. Volpe, Jr., *Organometallics*, 1992, **11**, 3920-3922.
382. X. Yang, W. A. King, M. Sabat and T. J. Marks, *Organometallics*, 1993, **12**, 4254-4258.
383. J. S. J. McCahill, G. C. Welch and D. W. Stephan, *Dalton Trans.*, 2009, 8555-8561.
384. M. Bochmann and S. J. Lancaster, *J. Organomet. Chem.*, 1992, **434**, C1-C5.
385. J. A. Ewen and M. J. Elder, *Makromol. Chem., Macromol. Symp.*, 1993, **66**, 179-190.

386. R. F. Jordan, W. E. Dasher and S. F. Echols, *J. Am. Chem. Soc.*, 1986, **108**, 1718-1719.
387. M. Bochmann and L. M. Wilson, *J. Chem. Soc., Chem. Commun.*, 1986, 1610-1611.
388. M. Bochmann, A. J. Jagger and J. C. Nicholls, *Angew. Chem., Int. Ed. Engl.*, 1990, **29**, 780-782.
389. I. Krossing and I. Raabe, *Angew. Chem., Int. Ed.*, 2004, **43**, 2066-2090.
390. X. Yang, C. Stern and T. J. Marks, *Organometallics*, 1991, **10**, 840-842.
391. S. J. Lancaster, A. Rodriguez, A. Lara-Sanchez, M. D. Hannant, D. A. Walker, D. H. Hughes and M. Bochmann, *Organometallics*, 2002, **21**, 451-453.
392. M. Bochmann, F. Song, A. Rodriguez and R. D. Cannon, *PMSE Prepr.*, 2002, **87**, 36-37.
393. S. Garratt, A. G. Carr, G. Langstein and M. Bochmann, *Macromolecules*, 2003, **36**, 4276-4287.
394. A. Rodriguez-Delgado, M. D. Hannant, S. J. Lancaster and M. Bochmann, *Macromol. Chem. Phys.*, 2004, **205**, 334-346.
395. F. Song, M. D. Hannant, R. D. Cannon and M. Bochmann, *Macromol. Symp.*, 2004, **213**, 173-185.
396. C. P. Nicholas, H. Ahn and T. J. Marks, *J. Am. Chem. Soc.*, 2003, **125**, 4325-4331.
397. L. A. Williams and T. J. Marks, *Organometallics*, 2009, **28**, 2053-2061.
398. L. A. Williams and T. J. Marks, *ACS Catal.*, **1**, 238-245.
399. C. P. Nicholas and T. J. Marks, *Langmuir*, 2004, **20**, 9456-9462.
400. J. C. W. Chien, W. M. Tsai and M. D. Rausch, *J. Am. Chem. Soc.*, 1991, **113**, 8570-8571.
401. Y.-X. Chen and T. J. Marks, *Organometallics*, 1997, **16**, 3649-3657.
402. J. Klosin, *Dow Chemical Company, WO2000011006A1*, 2000.
403. D. Alberti and K.-R. Pörschke, *Organometallics*, 2004, **23**, 1459-1460.
404. M. Bochmann, A. J. Jaggar, L. M. Wilson, M. B. Hursthouse and M. Motevalli, *Polyhedron*, 1989, **8**, 1838-1843.
405. R. E. LaPointe, R. K. Rosen and P. N. Nickias, *Dow Chemical Co., EP495375A2*, 1992.
406. A. R. O'Connor, C. Nataro, J. A. Golen and A. L. Rheingold, *J. Organomet. Chem.*, 2004, **689**, 2411-2414.

407. S. L. Borkowsky, N. C. Baenziger and R. F. Jordan, *Organometallics*, 1993, **12**, 486-495.
408. E. G. Ijpeij, B. Coussens, M. A. Zuideveld, G. H. J. van Doremaele, P. Mountford, M. Lutz and A. L. Spek, *Chem. Commun.*, 2010, **46**, 3339-3341.
409. J. Barker and M. Kilner, *Coord. Chem. Rev.*, 1994, **133**, 219-300.
410. E. Smolensky and M. S. Eisen, *Dalton Trans.*, 2007, 5623-5650.
411. M. P. Coles, *Dalton Trans.*, 2006, 985-1001.
412. F. T. Edelmann, *Adv. Organomet. Chem.*, 2008, **57**, 183-352.
413. F. T. Edelmann, *Chem. Soc. Rev.*, 2009, **38**, 2253-2268.
414. S. Collins, *Coord. Chem. Rev.*, 2011, **255**, 118-138.
415. C. K. Broder, A. E. Goeta, J. A. K. Howard, A. K. Hughes, A. L. Johnson, J. M. Malget and K. Wade, *J. Chem. Soc., Dalton Trans.*, 2000, 3526-3533.
416. A. E. Goeta, A. K. Hughes and J. M. Malget, *Acta Crystallogr., Sect. C*, 2001, **57**, 702-703.
417. H. Wang, H.-W. Li and Z. Xie, *Organometallics*, 2003, **22**, 4522-4531.
418. M.-M. Sit, H.-S. Chan and Z. Xie, *Dalton Trans.*, 2008, 1454-1464.
419. J. R. Hagadorn and J. Arnold, *Inorg. Chem.*, 1997, **36**, 2928-2929.
420. J. R. Hagadorn and J. Arnold, *Organometallics*, 1998, **17**, 1355-1368.
421. K. Merzweiler, D. Fenske, E. Hartmann and K. Dehnicke, *Z. Naturforsch., B: Chem. Sci.*, 1989, **44**, 1003-1006.
422. A. N. Chernega, R. Gomez and M. L. H. Green, *J. Chem. Soc., Chem. Commun.*, 1993, 1415-1417.
423. R. Gomez, R. Duchateau, A. N. Chernega, J. H. Teuben, F. T. Edelmann and M. L. H. Green, *J. Organomet. Chem.*, 1995, **491**, 153-158.
424. R. Gomez, M. L. H. Green and J. L. Haggitt, *J. Chem. Soc., Dalton Trans.*, 1996, 939-946.
425. R. J. Keaton, K. C. Jayaratne, J. C. Fettinger and L. R. Sita, *J. Am. Chem. Soc.*, 2000, **122**, 12909-12910.
426. K. C. Jayaratne and L. R. Sita, *J. Am. Chem. Soc.*, 2000, **122**, 958-959.
427. D. A. Kissounko, Y. Zhang, M. B. Harney and L. R. Sita, *Adv. Synth. Catal.*, 2005, **347**, 426-432.
428. Y. Zhang, E. K. Reeder, R. J. Keaton and L. R. Sita, *Organometallics*, 2004, **23**, 3512-3520.

429. R. Schlund, M. Lux, F. Edelmann, U. Reissmann and W. Rohde, *BASF, EP687693A1*, 1995.
430. J. C. Flores and M. D. Rausch, *University of Massachusetts, US5502128A*, 1996.
431. M. Polamo, M. Leskela, K. Hakala and B. Lofgren, *Borealis, WO9745434A1*, 1997.
432. R. Schlund, M. Lux, F. Edelmann, U. Reissmann and W. Rohde, *BASF, US5707913A*, 1998.
433. T. Elkin, S. Aharonovich, M. Botoshansky and M. S. Eisen, *Organometallics*, 2012, **31**, 7404-7414.

Chapter Two

Titanium complexes supported by cyclopentadienyl and κ^1-amidinate ligands for olefin copolymerisation

2.1 Overview

This Chapter describes the syntheses, structures and EPDM copolymerisation capability of a series of κ^1-amidinate-supported titanium complexes. The main focus concerns development of an alternative activation protocol *via* diene complexes with a view to assessing any advantage over more traditional activation of dialkyl precatalysts. Of the extensive library of ligands prepared by LANXESS Elastomers,[1] N,N-diisopropylbenzamidine was selected as a representative example and fully characterised, including by X-ray crystallography. Novel structures of $Cp^*Ti\{NC(Ph)N^iPr_2\}Cl_2$ and $Cp^*Ti\{NC(Ph)N^iPr_2\}Me_2$ are also described.

A detailed description of the synthesis and characterisation of cyclopentadienyl-amidinate-supported diene complexes is presented along with their reactivities with $B(C_6F_5)_3$ (BAr^F_3) to form well-defined zwitterionic species. Characterisation of the diene and zwitterionic complexes by X-ray diffraction was also undertaken and allows insight into the structure and bonding of these species. Some of the underlying chemistry of the diene and zwitterionic complexes is discussed; principally exploring the apparent reversibile nature of zwitterion formation. The successful diene activation chemistry is also shown to extend to a related half-sandwich guanidinate-supported system. High temperature EPDM copolymerisation experiments were performed in collaboration with LANXESS Elastomers allowing comparison to be made between the productivites of the diene complexes and a traditional dimethyl precatalyst. The zwitterionic species were shown to be very highly active single-component catalysts. Preliminary experimental work towards compounds **1**, **3** and **5-7** was described in the author's Mchem Thesis.[2] Some of the work in this Chapter has been patented.[3]

2.2 Syntheses and characterisation of cyclopentadienyl-amidinate complexes

2.2.1 Ligand synthesis

Previous work in the Mountford group centred upon preparation of post-metallocene precatalysts supported by anionic κ^1-amidinate and neutral face-capping ligands such as trimethyl 1,4,7-triazacyclononane ($Me_3[9]aneN_3$) tris(3,5-dimethylpyrazolyl)methane ($HC(Me_2pz)_3$).[4, 5] A convenient synthesis for these complexes was devised starting from silylated amidines prepared from nucleophilic attack of aryl nitriles by magnesiated secondary amines follwed by quenching with

trimethylsilyl chloride. The synthesis provides a degree of flexibility in terms of substitution of the aryl ring and amine nitrogen permitting tuning of the electronic and steric properties of the ligand although the route cannot be accessed by very sterically encumbered secondary amines such as di-*tert*-butylamine (Scheme 2.1). The silylated amidines proved convenient intermediates since they could be easily purified by crystallisation.

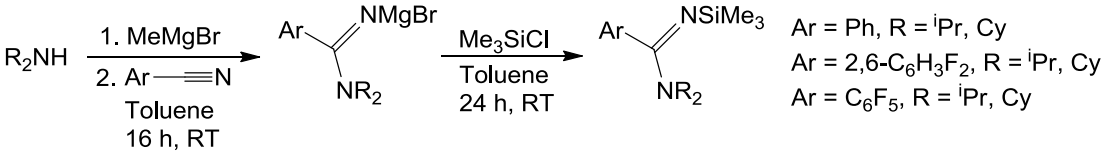

Scheme 2.1. Synthesis of silyated amidines.

Subsequent reaction of the silylated amidines with $TiCl_4$ gave titanium amidinates with the general formula $Ti\{NC(Ar)NR_2\}Cl_3$, shown to be dimeric in the solid state.[4, 5] These proved effective synthons for a family of cationic half-sandwich complexes by facile displacement of a chloride with either $Me_3[9]aneN_3$ or $HC(Me_2pz)_3$. This elegant approach also provides access to neutral half-sandwich cyclopentadienyl (Cp) and indenyl (Ind) complexes by reaction of the $Ti\{NC(Ph)N^iPr_2\}Cl_3$ synthon with the respective sodium salts of these ligands.[6] However, the yields of these salt metathesis reactions are poor (23-35 %) and the methodolgy proved incompatible with the ubiquitous pentamethylcyclopentadienyl (Cp*) ligand. Attempted reaction of the synthon with LiCp* resulted in extensive unwanted reduction to Ti(III) species while no reaction was observed with the softer transmetallating agent Cp^*SiMe_3.[6]

An alternative approach is *via* a protio-amidine of general formula, $HNC(Ar)NR_2$, prepared similarly to the silylated amidines above but quenched with an excess of water rather than trimethylsilyl chloride. Using this methodology LANXESS Elastomers has prepared a large family of amidine protio-ligands.[1] This Thesis focusses on the $HNC(Ph)N^iPr_2$ (**1**) protio-ligand prepared from diisopropylamine and benzonitrile (Scheme 2.2) as a representative example.

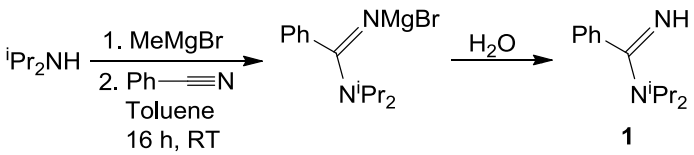

Scheme 2.2. Synthesis of $HNC(Ph)N^iPr_2$ (**1**).

Careful vacuum distillation of the crude product and subsequent drying over CaH_2 affords **1** as an analytically pure colourless solid which was fully characterised for the first time by NMR and IR spectroscopy, FI mass spectrometry and elemental analysis. Full characterising data for this and all the new compounds herein are given in Chapter Five.

The room temperature ^1H NMR spectrum of **1** in C_6D_6 has a broad singlet corresponding to the NH proton at 5.70 ppm, whilst the phenyl ring protons appear as a series overlapping multiplets spanning 7.18-7.07 ppm. Free rotation at room temperature about the C-N^{i}Pr$_2$ bond results in a single doublet being observed at 1.15 ppm along with a septet at 3.44 ppm corresponding to the methyl and methine protons repectively. This contrasts with the related silylated amidine, $Me_3SiNC(Ph)N^iPr_2$, in which restricted rotation about the C-N^{i}Pr$_2$, presumably as a result of steric interactions between the silyl methyl and *iso*-propyl groups, results in the *iso*-propyl groups appearing as a series of very broad resonances at room temperature. Cooling to -40 °C results in considerable sharpening of the signals such that two doublets and two septets are observed corresponding to the two *iso*-propyl groups differentiated by their proximity to the phenyl ring.

Compound **1** was further characterised by single crystal X-ray diffraction. Single crystals suitable for X-ray diffraction analysis were grown by slow cooling of the molten compound. The molecular structure is shown in Figure 2.1 and full crystallographic data can be found in the CD appendix. For comparison, the molecular structure of $Me_3SiNC(Ph)N^iPr_2$ is also shown in Figure 2.1 and selected bond lengths and angles of **1** and $Me_3SiNC(Ph)N^iPr_2$ are compared in Table 2.1.[6]

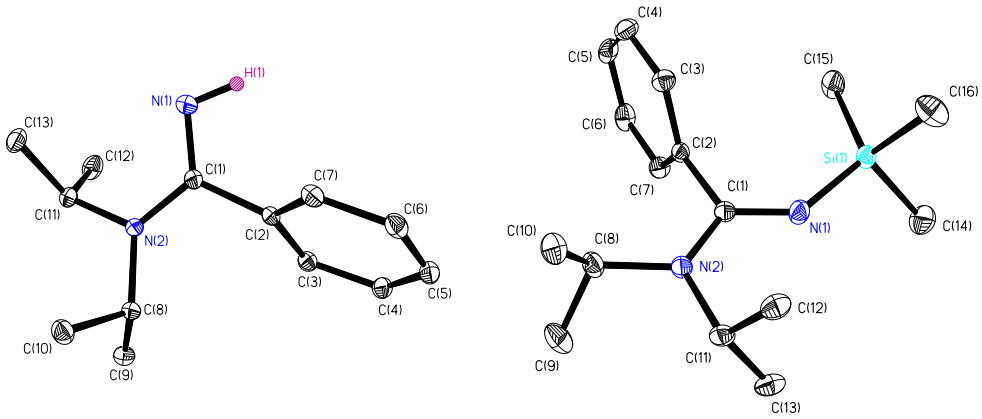

Figure 2.1. Displacement ellipsoid plots (20% probability) of HNC(Ph)N^{i}Pr$_2$ (**1**, left) and Me$_3$SiNC(Ph)N^{i}Pr$_2$ (right; 2nd molecule in asymmetric unit omitted).[6] H(1) in **1** drawn as a sphere of arbitrary radius. Other H atoms omitted for clarity.

Table 2.1. Selected bond lengths (Å) and angles (°) for HNC(Ph)N^{i}Pr$_2$ (**1**) and Me$_3$SiNC(Ph)N^{i}Pr$_2$.[6]

Parameter	**1**	Me$_3$SiNC(Ph)N^{i}Pr$_2$[†]
C(1)-N(1)	1.2922(19)	1.285(4), 1.275(4)
C(1)-N(2)	1.3627(17)	1.361(4), 1.367(4)
C(1)-C(2)	1.5024(19)	1.508(4), 1.505(4)
N(2)-C(8)	1.4763(17)	1.476(4), 1.477(4)
N(2)-C(11)	1.4766(18)	1.478(4), 1.481(4)
N(1)-C(1)-C(2)	120.51(13)	121.2(3), 120.6(3)
N(1)-C(1)-N(2)	121.23(13)	122.5(3), 122.1(3)
C(2)-C(1)-N(2)	118.17(11)	116.3(2), 117.2(2)
C(8)-N(2)-C(11)	116.37(11)	116.9(2), 116.6(2)
C(1)-N(1)-Si(1)	-	136.4(2), 134.8(2)

[†] Two molecules in the asymmetric unit.

The molecular structure, bond lengths and angles of **1** bear close resemblance to those of Me$_3$SiNC(Ph)N^{i}Pr$_2$ with the aryl ring lying perpendicular to the N=C-N^{i}Pr$_2$ plane. The coplanarity of N=C-N^{i}Pr$_2$ must stem from conjugation of amine nitrogen lone pair and the imine π bond. Further evidence for this allylic-type π-system is provided by DFT calculations of the neutral NC(Ph)N^{i}Pr$_2$ fragment detailed in Chapter Three. The aryl ring is twisted perpendicular to this plane to minimise steric interactions between the *ortho* protons and the *iso*-propyl groups.

2.2.2 Synthesis of $(C_5R_5)Ti\{NC(Ph)N^iPr_2\}Cl_2$ (R = H (2), Me (3))

Stoichiometric reaction of $CpTiCl_3$ with **1** in the presence of excess NEt_3 (Equation 2.1) provided a convenient and higher yielding route to $CpTi\{NC(Ph)N^iPr_2\}Cl_2$ (**2**) (50 %). Importantly this route proved effective for the synthesis of $Cp^*Ti\{NC(Ph)N^iPr_2\}Cl_2$ in reasonable isolated yield (54 %).

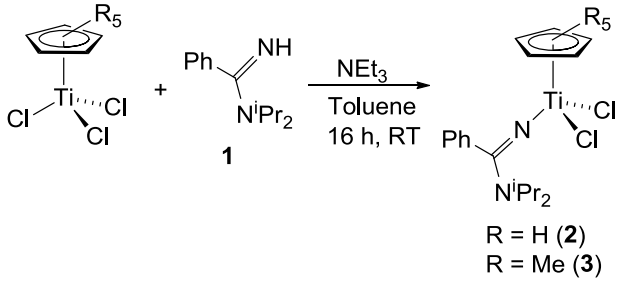

Equation 2.1

Compounds 2 and **3** have been fully characterised by NMR and IR spectroscopy, EI mass spectrometry and elemental analysis. The ^1H NMR spectra of both amidinate complexes are similar aside from signals corresponding to the different η-C_5R_5 ligands. The room temperature and low temperature (-20 °C) spectra of **2** are shown in Figure 2.2 by way of example.

The room temperature ^1H NMR spectrum of **2** in toluene-d_8 has the expected sharp singlet for the Cp protons at 6.02 ppm with the aromatic protons appearing as a series of overlapping multiplets spanning 7.13-6.92 ppm. As observed in $Me_3SiNC(Ph)N^iPr_2$, the signals for the *iso*-propyl groups are broad due to restricted rotation about the C-N^iPr_2 bond; an intermediate fluxional regime closer to the slow-exchange limit being occupied at room temperature results in observation of two broad septets (3.32 and 3.05 ppm) and two broad singlets (1.62 and 0.57 ppm) corresponding to the methine and methyl protons respectively.

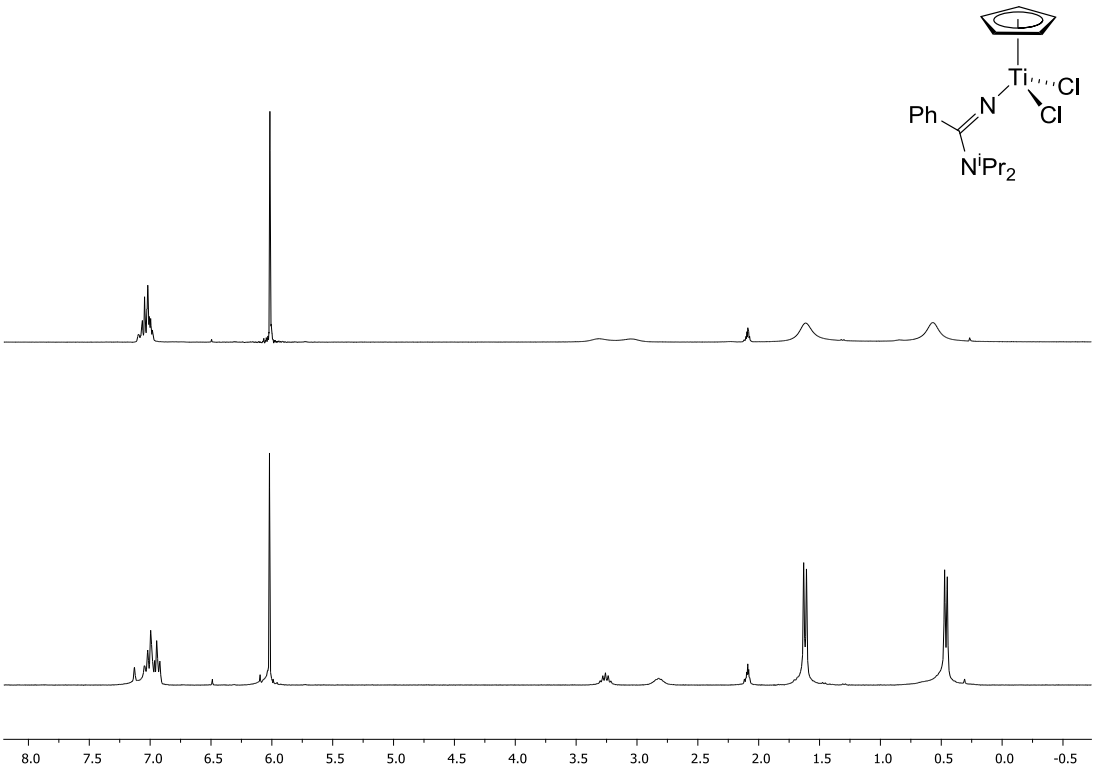

Figure 2.2. ^{1}H NMR spectra (299.9 MHz) of CpTi{NC(Ph)N^{i}Pr$_2$}Cl$_2$ (2) in toluene-d_8. Top: 293 K; bottom: 253 K. Residual protio-solvent shifts: δ = 7.09, 7.00, 6.98, 2.09 ppm.

Cooling to -20 °C permits observation of two septets (3.26 and 2.82 ppm) and two doublets (1.62 and 0.46 ppm) for the methine and methyl protons of the *iso*-propyl groups respectively. Two-dimensional COSY and ROESY spectra not only allowed assignment of the septet at 3.26 ppm and the doublet at 0.46 ppm to the same *iso*-propyl group but also identified it as being *cis* to the phenyl ring (a through-space correlation being observed with the *o*-protons of the phenyl ring) with the septet at 2.82 ppm and the doublet at 1.62 ppm being assigned to the *trans iso*-propyl group. The restricted rotation is thought to be partly electronic in origin: conjugation of the electron lone pair on the amine nitrogen with the C=N bond, lending a degree of double bond character to the C-N^{i}Pr bond, facilitating a π-interaction between the imine nitrogen and the metal. These bonding considerations will be explored in more depth in Chapter Three.

The room temperature ^{1}H NMR spectrum of **3** in toluene-d_8 is similar to that for **2** with the obvious difference being the singlet for the Cp* methyl groups at 1.94 ppm. The aromatic protons again appear as a series of overlapping multiplets spanning

7.42-7.05 ppm. As discussed for **2**, the signals for the *iso*-propyl groups are broad due to restricted rotation about the C-N^{i}Pr$_2$ bond but cooling to -40 °C permits observation of two septets (3.51 and 3.02 ppm) and two doublets (1.59 and 0.60 ppm) for the methine and methyl protons of the *iso*-propyl groups respectively. COSY and ROESY experiments allowed assignment of *cis* (3.51 and 0.60 ppm) and *trans* (3.02 and 1.59 ppm) *iso*-propyl groups relative to the phenyl ring which proved to be analgous to **2**.

2.2.3 X-ray structures of (C$_5$R$_5$)Ti{NC(Ph)N^{i}Pr$_2$}Cl$_2$ (R = H (2), Me (3))

Compound **3** was further characterised by single crystal X-ray diffraction. Single crystals suitable for X-ray diffraction analysis were grown from a toluene/n-hexanes solution at -80 °C. The molecular structure is shown in Figure 2.3 and full crystallographic data can be found in the CD appendix. For comparison, the molecular structure of **2**[6] is also shown in Figure 2.3 and selected bond lengths and angles of **2** and **3** are compared in Table 2.2.

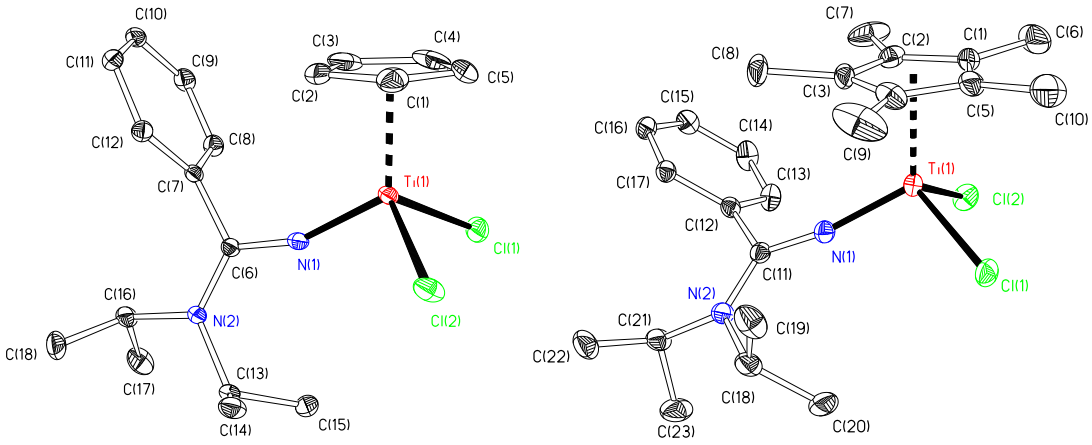

Figure 2.3. Displacement ellipsoid plots (20% probability) of CpTi{NC(Ph)N^{i}Pr$_2$}Cl$_2$ (**2**, left)[6] and Cp*Ti{NC(Ph)N^{i}Pr$_2$}Cl$_2$ (**3**, right). H atoms omitted for clarity.

Table 2.2. Selected bond lengths (Å) and angles (°) for $CpTi\{NC(Ph)N^iPr_2\}Cl_2$ (**2**)[6] and $Cp^*Ti\{NC(Ph)N^iPr_2\}Cl_2$ (**3**). $Cp(^*)_{cent}$ is the computed Cp(*) ring carbon centroid.

Parameter	**2**	**3**
$Ti(1)\text{-}Cp_{cent}$	2.05	2.05
Ti(1)-Cl(1)	2.3095(5)	2.3137(11)
Ti(1)-Cl(2)	2.3304(5)	2.3051(11)
Ti(1)-N(1)	1.7855(13)	1.800(3)
$N(1)\text{-}C_{C=N}$	1.315(2)	1.310(4)
$N(2)\text{-}C_{C=N}$	1.3279(19)	1.340(4)
$Cp(^*)_{cent}\text{-}Ti(1)\text{-}N(1)$	120.5	118.0
$Cp(^*)_{cent}\text{-}Ti(1)\text{-}Cl(1)$	114.3	113.5
$Cp(^*)_{cent}\text{-}Ti(1)\text{-}Cl(2)$	113.4	115.0
$Ti(1)\text{-}N(1)\text{-}C_{C=N}$	160.10(11)	165.2(3)
N(1)-Ti(1)-Cl(1)	101.78(5)	102.93(10)
N(1)-Ti(1)-Cl(2)	102.40(4)	104.21(10)
Cl(1)-Ti(1)-Cl(2)	102.04(2)	101.24(4)

The molecular structures of **2** and **3** show the expected *pseudo*-tetrahedral three-legged piano stool titanium centre surrounded by η^5-cyclopentadienyl and κ^1-amidinate ligands with two chlorides occupying the remaining coordination sites. Consistent with the low temperature NMR data, *cis* and *trans iso*-propyl groups with respect to the phenyl ring are also evident in the solid state. A linear $Ti(1)\text{-}N(1)\text{-}C_{C=N}$ bond angle in both **2** (160.10(11)°) and **3** (165.2(3)°) suggests a metal-amidinate dπ-pπ contribution to the bonding. This is also evidenced by respective lengthening and shortening of the $N(1)\text{-}C_{C=N}$ (1.315(2) Å (**2**), 1.310(4) Å (**3**)) and $N(2)\text{-}C_{C=N}$ (1.3279(19) Å (**2**), 1.340(4) Å (**3**)) bonds relative to the $N(1)\text{-}C_{C=N}$ (1.2922(19) Å) and $N(2)\text{-}C_{C=N}$ (1.3627(17) Å) distances observed in the protio-amidine **1**. The Ti(1)-N(1) bond lengths (1.7855(13) Å (**2**) and 1.800(3) Å (**3**)) are shorter than might be expected for a 'pure' Ti-N single bond (1.96 Å)[7] and slightly longer than the distance observed for the formal triple $T{\equiv}N_{imide}$ bond which lies in the range 1.69-1.76 Å;[8, 9] a good example for comparison being the isolobal macrocycle titanium imido dichloride complex, $Ti(N^tBu)(Me_3[9]aneN_3)Cl_2$ (1.694(2) Å).[10] It can be tentatively concluded that the extent of π-bonding may lie somewhere between these limiting

cases. Further insight into the Ti-N multiple bond character is given by DFT calculations presented in Chapter Three.

2.2.4 Synthesis of Cp*Ti{NC(Ph)N^{i}Pr$_2$}Me$_2$ (4)

Dialkyl complexes of the type L_nTiR_2 (typically R = Me, CH_2Ph) have been shown to be effective precatalysts in combination with borane or borate activators.[11] In order to assess any differences associated with the alternative activation strategy involving diene precatalysts described later in this Chapter, comparison must be made under comparable conditions with 'traditional' dialkyl precatalysts. Dimethylation of **3** with two equivalents of MeLi proceeds smoothly to give **4** in moderate isolated yield following recrystallisation from n-hexanes (40 %) (Equation 2.2).

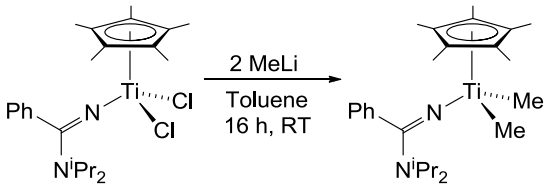

3 **4**

Equation 2.2

Compound **4** has been fully characterised by NMR and IR spectroscopy, EI mass spectrometry and elemental analysis. The room temperature and low temperature ^{1}H NMR (-50 °C) spectra are shown in Figure 2.4. The room temperature ^{1}H NMR spectrum in toluene-d_8 displays the expected signal corresponding to the methyl ligands as a singlet at 0.49 ppm; the methyl protons of the Cp* giving rise to a singlet at 1.83 ppm and the aromatic protons of the amidinate being observed as a series of multiplets spanning the range 7.24-6.95 ppm. The peak in the ^{13}C spectrum at 47.6 ppm was assigned with help of an HSQC two-dimensional experiment to the carbon of methyl ligands. A proton-coupled ^{13}C experiment allowed measurement of the $^1J_{CH}$ coupling constant for the methyl ligands (118 Hz) which lies in the range expected for monomeric neutral titanium alkyl complexes. The *iso*-propyl signals consist of a single broad septet at 3.50 ppm and a broad singlet at 1.23 ppm suggesting that the rotation about the C-N^{i}Pr$_2$ bond is closer to the fast-exchange limit (unlike in the cases of **2** and **3**). Cooling to -40 °C is required to observe the molecule in the slow-exchange limit: the *cis* and *trans* methines being observed at 3.60 and 2.91 ppm and the *cis* and *trans* methyl signals appearing at 0.64 and 1.72 ppm respectively.

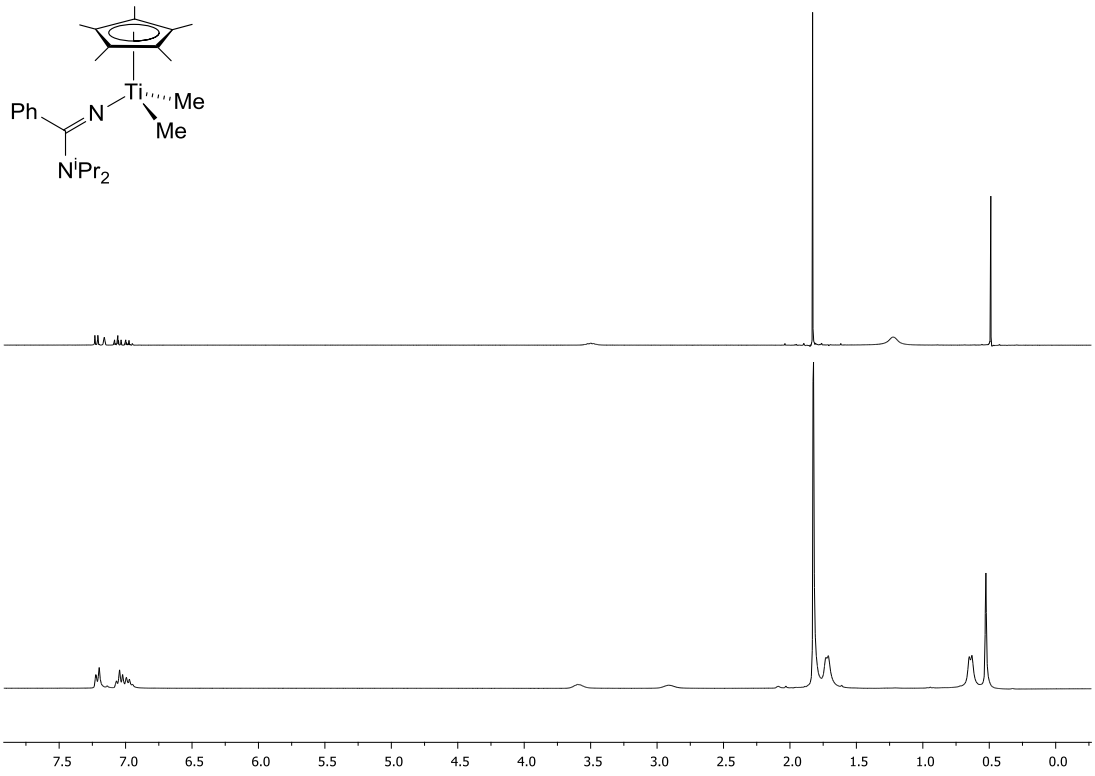

Figure 2.4. ^{1}H NMR spectra (299.9 MHz) of Cp*Ti{NC(Ph)N^{i}Pr$_2$}Me$_2$ (**4**) in toluene-d_8. Top: 293 K; bottom: 223 K.

2.2.5 X-ray structure of Cp*Ti{NC(Ph)N^{i}Pr$_2$}Me$_2$ (4)

Compound **4** was further characterised by single crystal X-ray diffraction. Single crystals suitable for X-ray diffraction analysis were grown from a pentane solution at -30 °C. The molecular structure is shown in Figure 2.5 and full crystallographic data can be found in the CD appendix. Selected bond lengths and angles of **4** are presented in Table 2.3.

The molecular structure of **4** is consistent with the low temperature NMR data and the structures of **2** and **3**. In comparison to **3**, the Cp*$_{cent}$-Ti(1) (2.07 Å) and Ti(1)-N(1) (1.8452(15) Å) distances in **4** are longer reflecting the enhanced σ-donation from methyl compared to chloride ligands. In spite of the linear geometry about the imine nitrogen (163.00(13)°) persisting in **4,** the longer Ti(1)-N(1) distance appears to result in diminished metal-amidinate dπ-pπ bonding character evidenced by the N(1)-C(11) (1.290(2) Å) and N(2)-C(11) (1.363(2) Å) bond lengths comparing closely to the corresponding distances in the protio-amidine (N(1)-C$_{C=N}$ (1.2922(19) Å), N(2)-C$_{C=N}$ (1.3627(17) Å)). This observation also explains the solution behaviour: the room

temperature rotation about the C-N^{i}Pr$_2$ bond is close the the fast-exchange limit (*vide supra*) presumably resulting from decreased double-bond character of the C-N^{i}Pr$_2$ bond (*cf.* compounds **2** and **3**).

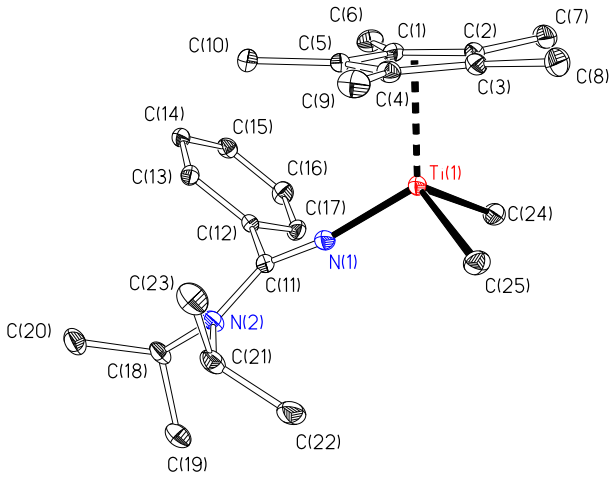

Figure 2.5. Displacement ellipsoid plot (20% probability) of Cp*Ti{NC(Ph)N^{i}Pr$_2$}Me$_2$ (**4**). H atoms omitted for clarity.

Table 2.3. Selected bond lengths (Å) and angles (°) for Cp*Ti{NC(Ph)N^{i}Pr$_2$}Me$_2$ (**4**). Cp$_{cent}$ is the computed Cp* ring carbon centroid.

Ti(1)-Cp$_{cent}$	2.07	Cp$_{cent}$-Ti(1)-N(1)	120.8
Ti(1)-C(24)	2.1227(18)	Cp$_{cent}$-Ti(1)-C(24)	113.9
Ti(1)-C(25)	2.1326(19)	Cp$_{cent}$-Ti(1)-C(25)	113.9
Ti(1)-N(1)	1.8452(15)	Ti(1)-N(1)-C(11)	163.00(13)
N(1)-C(11)	1.290(2)	N(1)-Ti(1)-C(24)	104.21(7)
N(2)-C(11)	1.363(2)	N(1)-Ti(1)-Cl(25)	104.04(7)
		C(24)-Ti(1)-C(25)	96.93(8)

2.3 Synthesis and characterisation of cyclopentadienyl-amidinate diene complexes

Group 4 diene complexes received a great deal of attention particularly during the 1980s.[12-15] A variety of routes were devised including reductive transmetallation with magnesium diene complexes[16-18] and photolysis of diaryl complexes in the presence of free 1,3-dienes.[19] Reduction with alkyl lithiums or Grignard reagents is another viable approach.[20, 21] However, it was not until the 1990s that it was discovered that they could be employed as precatalysts for olefin polymerisation; their activation with BAr$^{F}_3$ generating well-defined zwitterionic species providing unique control over

cation-anion interactions during catalysis.[22] The use of BAr^F_3 also provides an advantage due to its solubility in hydrocarbon solvents; insoluble $[CPh_3][BAr^F_4]$ must be slurried into the reactor providing a significant engineering challenge. Diene activation has been exploited for a variety of catalyst systems[22-24] and has been studied extensively for constrained geometry-type catalysts.[21, 25-27] The majority of this Chapter focusses on extending this alternative activation approach to the titanium cyclopentadienyl-amidinate system.

2.3.1 Synthesis of Cp*Ti{NC(Ph)N^{i}Pr$_2$}(η-2,3-C$_4$H$_4$Me$_2$) (5)

Half-sandwich group 4 diene complexes can exhibit a variety of binding modes of the diene: *cis* and *trans* conformations of the coordinated diene are conceivable; the *cis* conformation giving rise to supine and prone isomers which differ in the orientation of the coordinated diene with respect to the cyclopentadienyl ligand (Scheme 2.3).[12, 13, 20] However, reduction of **3** with two equivalents of ^{n}BuLi in the presence of an excess of 2,3-dimethyl-1,3-butadiene results in formation of a single isomer of the diene complex, **5** (Scheme 2.3) in reasonable isolated yield following recrystallisation (53 %). Compound **5** has been fully characterised by NMR and IR spectroscopy EI mass spectrometry and elemental analysis. The room temperature ^{1}H NMR spectrum is shown in Figure 2.6.

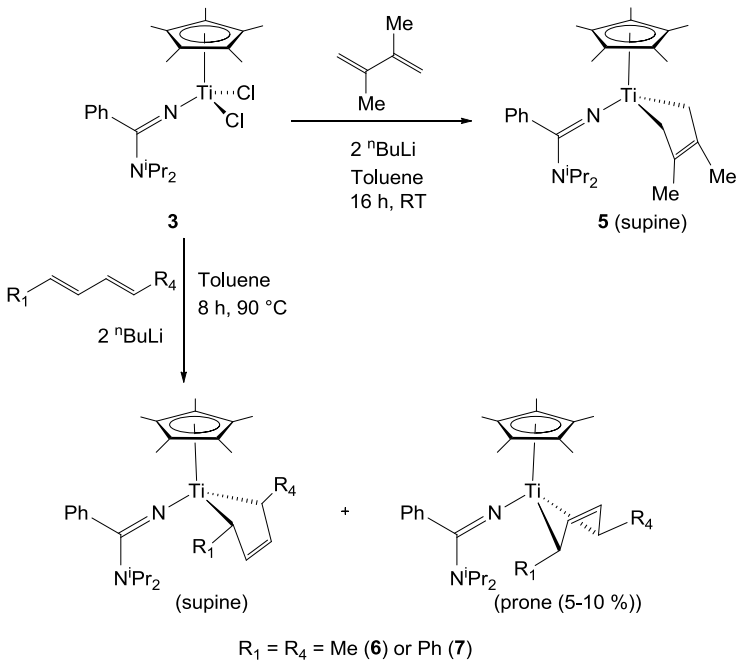

Scheme 2.3. Synthesis of diene complexes **5-7**.

The room temperature ^{1}H NMR spectrum in C_6D_6 exhibits the sharp singlet expected for the Cp* methyl groups at 1.87 ppm and the series of overlapping multiplets corresponding to the aromatic protons of the amidinate ligand (7.06-6.95 ppm). A sharp septet at 3.96 ppm and two sharp doublets at 1.05 and 1.00 ppm are assigned to the *iso*-propyl groups. Two doublets at 2.45 (^{2}J = 7.2 Hz) and 2.33 (^{2}J = 7.4 Hz) ppm and two doublets at 0.70 (^{2}J = 7.2 Hz) and 0.58 (^{2}J = 7.4 Hz) ppm are assigned to the four structurally diagnostic diastereotopic diene protons suggesting restricted rotation about the Ti-N bond with *cis*-coordination of the diene. The chemical shifts are indicative of the diene adopting the supine conformation in solution.[20] Through-space coupling (nOe) experiments have been employed to probe the diene conformation in solution: for example the prone conformation of Stephan's prone phosphinimide-supported diene complex, $CpTi(NP^tBu_3)(\eta\text{-}2,3\text{-}C_4H_4Me_2)$, was confirmed by observation of a through-space correlation between the diene methyl protons and the Cp protons.[23] In the case of **5**, no such correlation is oberved between the diene methyl and Cp* methyl groups which serves to rule out the prone conformation in agreement with the supine assignment from chemical shifts. Although the ROESY spectrum was also unable to distinguish the *syn* and *anti* terminal diene protons, these were assigned to the lower (2.45 and 2.33 ppm) and higher field (0.70 and 0.58 ppm) signals respectively due to enhanced shielding of the *anti* protons by the proximal Cp* ligand. This assignment is also consistent with examples in the literature.[23, 24, 28]

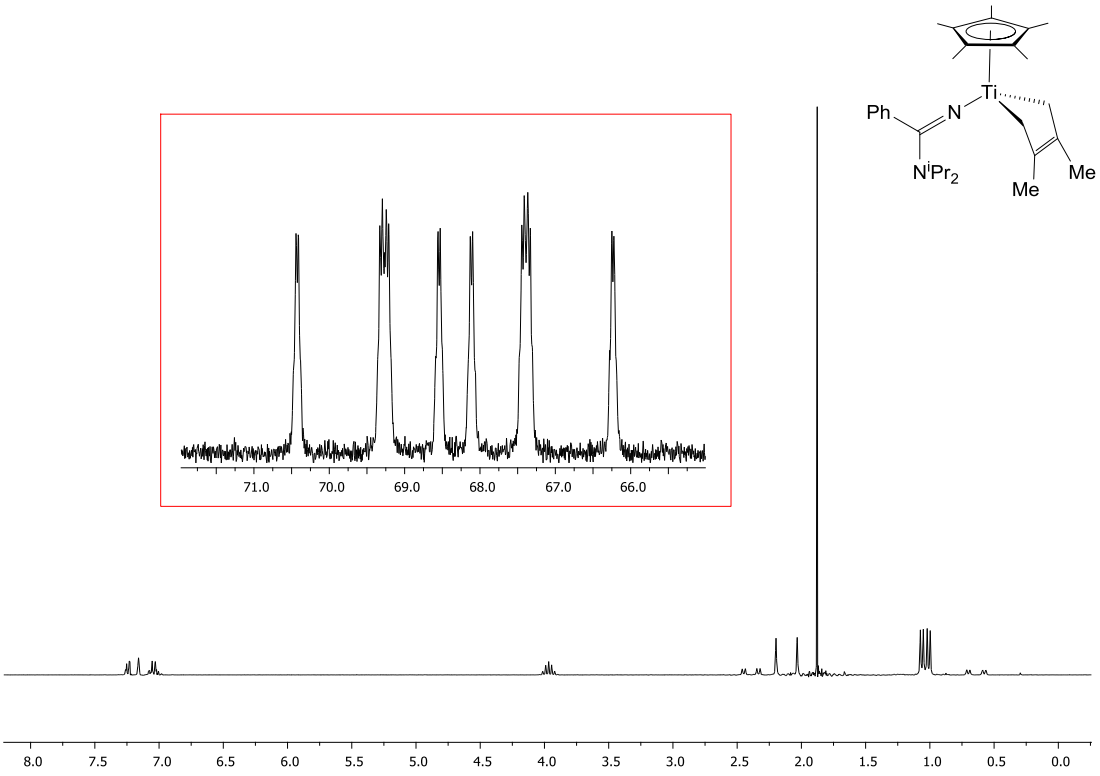

Figure 2.6. ^{1}H NMR spectrum (499.9 MHz, 293 K) of **5** in C_6D_6. Residual protio-solvent, δ = 7.16 ppm. The inset illustrates the ^{13}C (proton-coupled) spectrum (125.7 MHz) between 65.0 and 72.0 ppm.

The resonances at 67.4 and 69.3 ppm in the room temperature ^{13}C NMR spectrum were assigned using an HSQC experiment to the diastereotopic carbons of the diene ligand adjacent to Ti. The central diene carbons are observed at 128.0 and 126.3 ppm; the marked difference in chemical shift of the internal and terminal diene carbon signals supports a largely σ-bound diene and a metallocylopentene-type structure. The magnitude of ^{1}J(C^{1,4}H) for coordinated C^{1,4} carbons is often used to provide an insight into the bonding in metal-diene systems.[29, 30] The proton-coupled ^{13}C spectrum (Figure 2.6, inset) shows two doublet of doublets of quartets for each of the diastereotopic carbons adjacent to Ti. The four ^{1}J(C^{1,4}H) coupling constants were calculated to be 145 Hz. Erker *et al.* reported a ^{1}J(C^{1,4}H) of 140 Hz for $Cp_2Zr(\eta$-2,3-$C_4H_4Me_2)$ which is described as approaching the metallacyclic σ^2, π-bonding limit.[30] However, the ^{1}J(C^{1,4}H) value for **5** is significantly greater than that observed for Cp*Ti{Ph)N^{i}Pr$_2$}Me$_2$ (118 Hz). In order to aid further understanding of the bonding, **5** was characterised crystallographically (*vide infra*).

2.3.2 Synthesis of Cp*Ti{NC(Ph)N^{i}Pr$_2$}(η-1,4-C$_4$H$_4$Me$_2$) (6)

Heating **1** with two equivalents of ^{n}BuLi in the presence of excess 2,4-hexadiene results in the formation of Cp*Ti{NC(Ph)N^{i}Pr$_2$}(η-1,4-C$_4$H$_4$Me$_2$) (**6**) (Scheme 2.3). Compound **6** has been fully characterised by NMR and IR spectroscopy, EI mass spectrometry and elemental analysis. The room temperature and low temperature ^{1}H NMR (-20 °C) spectra are shown in Figure 2.7.

The room temperature ^{1}H NMR spectrum reveals the expected signals corresponding to the Cp* methyl protons (1.84 ppm) and aromatic amidinate protons (overlapping multiplets spanning the range 7.09-6.95 ppm). The *iso*-propyl resonances appear as a sharp septet at 3.55 ppm (methine) and a sharp doublet at 0.99 ppm (methyl). The resonances corresponding to the diene protons are broad but become considerably sharper on cooling to -20 °C. The room temperature ^{1}H NMR also reveals the presence of a minor isomer (*ca*. 5 %) by observation of a singlet upfield and a doublet downfield of the signals assigned to the Cp* and amidinate methyl groups respectively. The isomers cannot be separated by fractional crystallisation and the ratio of isomers appears unchanged on cooling to -80 °C; the minor prone isomer is presumed to be a kinetic product which cocrystallises with the dominant supine isomer (*vide infra*). The presence of both prone and supine isomers was also observed in, for example, (η^{5}, η^{1}-C$_5$Me$_4$SiMe$_2$NPh)Ti(η-1,4-C$_4$H$_4$Me$_2$) the prone isomer predominating in that case.[21]

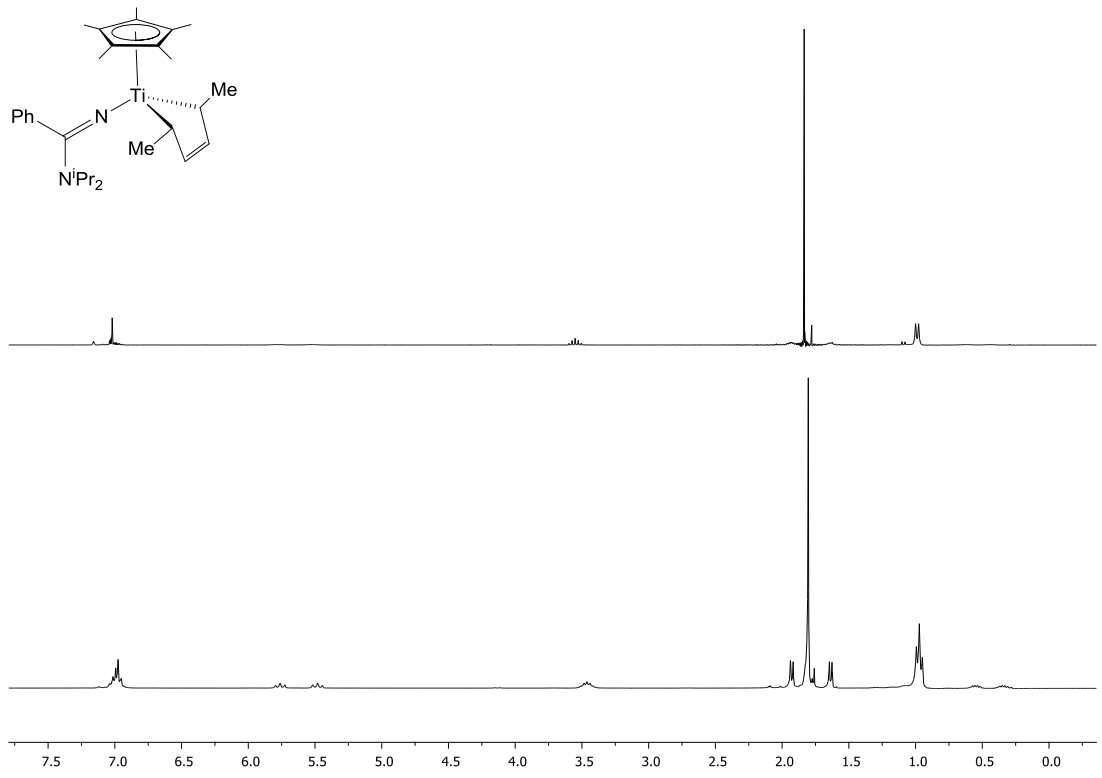

Figure 2.7. ^{1}H NMR spectra (299.9 MHz) of Cp*Ti{NC(Ph)N^{i}Pr$_2$}(η-1,4-$C_4H_4Me_2$) **(6)** in toluene-d_8. Top: 293 K; bottom: 253 K.

The low temperature (-20 °C) ^{1}H NMR spectrum reveals two sets of multiplets at 5.84 and 5.55 ppm which are assigned to the vinylic protons of the metallocyclopentene, with two sets of multiplets at 0.60 and 0.38 ppm being observed for the diene protons on the carbons adjacent to titanium. The methyl groups of the diene fragment appear as two doublets at 1.99 and 1.70 ppm. The sharpening of the diene signals at low temperature presumably corresponds to slowing rotation about the Ti-N bond; at the fast rotation limit the molecule will have time-averaged C_s-symmetry and the diene protons are no longer diastereotopic. At low temperature, two partially overlapping doublets for the *iso*-propyl methyl groups are observed (*cf*. compound **5**). The chemical shifts of the high-field diene protons are similar to those seen for **5** suggesting a supine conformation of the diene fragment in solution in the case of the major isomer of **6**. This was confirmed by observation of a through-space correlation between the protons on the diene carbon adjacent to titanium and the Cp* methyls in the low temperature ROESY spectrum. No cross-peaks were observed correlating the vinylic protons of the diene and the methyl groups of the Cp* ligand.

2.3.3 Synthesis of Cp*Ti{NC(Ph)N^{i}Pr$_2$}(η-1,4-C$_4$H$_4$Ph$_2$) (7)

It was found that Cp*Ti{NC(Ph)N^{i}Pr$_2$}(η-1,4-C$_4$H$_4$Ph$_2$) (**7**) could be prepared either from reduction of **1** with ^{n}BuLi in the presence of one equivalent of 1,4-diphenyl-1,3-butadiene, as in the cases of **5** and **6** (Scheme 2.3), or by reaction of **1** with Mg(η-1,4-C$_4$H$_4$Ph$_2$)(THF)$_3$.[31] The former method proved to be the higher yielding (39 %). Purification of **7** was more challenging due to the presence of unreacted 1,4-diphenyl-1,3-butadiene. Fractional crystallisation proved ineffective owing to the similar solubilities of the free diene and diene complex. Fortunately the uncomplexed diene could be removed by sublimation with no noticeable decomposition of **7**.

Compound **7** has been fully characterised by NMR and IR spectroscopy, EI mass spectrometry and elemental analysis. The room temperature ^{1}H NMR spectrum of **7** displays key similarities with that of **6**. The Cp* methyl resonance appears as a sharp singlet at 1.70 ppm while the aromatic protons correspond to overlapping multiplets (some broad) between 7.26 and 6.89 ppm. Fast rotation about the Ti-N bond results in a sharp septet (3.79 ppm) and doublet (0.96 ppm) being observed for the methine and methyl protons of the *iso*-propyl goups respectively. The signals for the diene protons are very broad at room temperature. A further similarity with **6** is the presence of what is thought to be a minor isomer (10 %): signals at 1.61 and 1.00 ppm correspond to Cp* and amidinate methyl groups respectively. The isomers cannot be separated by fractional crystallisation and their relative concentrations appear unchanged with temperature.

Cooling to -20 °C in toluene-d_8 allows observation of the signals corresponding to the diastereotopic diene protons: the vinylic protons are observed as two multiplets at 6.25 and 5.87 ppm while the diene protons adjacent to Ti are observed as two multiplets at 2.20 and 1.98 ppm. The chemical shifts of the former signals are similar to those observed in **6**. The downfield shift of the diene proton resonances adjacent to Ti in **7** compared to **6** must result from the electron-withdrawing effect of the phenyl substituents. The dominant isomer of **7** is presumed to be supine given the similarity of the spectra of **6** and **7** along with structural characterisation of **5**-**7** (*vide infra*). As may be expected there is considerable sharpening of the signals in the aromatic region on cooling to -20 °C. Similarly to the behaviour observed in **6**, cooling also results in

the amidinate methyl groups splitting into two partially overlapping doublets with some broadening of the methine septet.

2.3.4 Synthesis of CpTi{NC(Ph)N^{i}Pr$_2$}(η-1,4-C$_4$H$_4$Me$_2$) (8)

With a view to gaining a better understanding of any influence of slight changes in the steric demands and electronic properties of the η-C_5R_5 ring substituents on the conformation of the coordinated diene, as well on performance in polymerisation testing, CpTi{NC(Ph)N^{i}Pr$_2$}(η-1,4-C$_4$H$_4$Me$_2$) (**8**) was prepared similarly to **6** by reduction of **2** with two equivalents of ^{n}BuLi in the presence of excess 2,4-hexadiene (Equation 2.3).

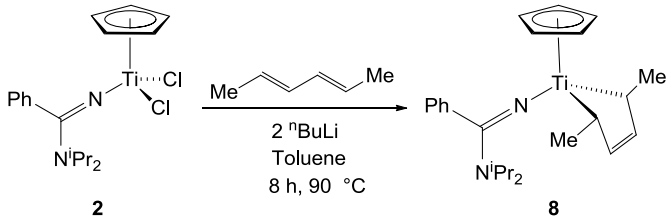

2 **8**

Equation 2.3

Compound **8** has been fully characterised by NMR and IR spectroscopy, EI mass spectrometry and elemental analysis. The room temperature ^{1}H NMR spectrum in C_6D_6 is shown in Figure 2.8. The spectrum exhibits the singlet corresponding to the Cp protons at 5.74 ppm with the aromatic protons of the amidinate appearing as a series of overlapping multiplets (7.07-6.82 ppm). Fast rotation about the Ti-N bond, presumably as a result of the less sterically demanding Cp ligand, results in a sharp septet (3.20 ppm) and doublet (1.01 ppm) being observed for the amidinate methine and methyl protons respectively. The time-resolved C_s-symmetry of the molecule at room temperature further results in observation of one multiplet for the diene vinylic protons (5.67 ppm), one multiplet for the diene protons adjacent to Ti (0.70 ppm) and a doublet for the diene methyl groups (1.83 ppm). The spectrum of **8** is assigned, by analogy to **6**, to the supine isomer but with significantly less of the prone isomer evident in solution.

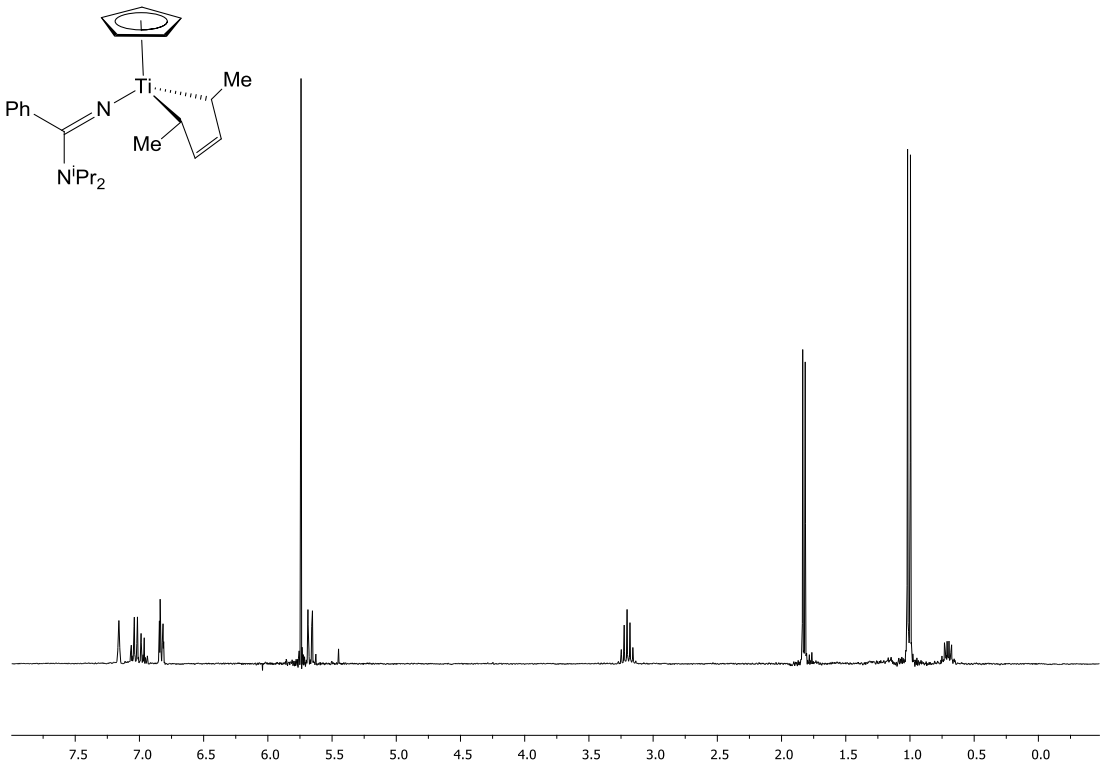

Figure 2.8. ^{1}H NMR spectrum (299.9 MHz, 293 K) of CpTi{NC(Ph)N^{i}Pr$_2$}(η-1,4-$C_4H_4Me_2$) (**8**) in C_6D_6. Residual protio-solvent, δ = 7.16 ppm.

2.3.5 X-ray structures of diene complexes 5-8

Compounds **5**-**8** were further characterised by single crystal X-ray diffraction. Single crystals of **5** suitable for X-ray diffraction analysis were grown from a pentane solution at room temperature while crystals of compounds **6**-**8** were grown from pentane solutions cooled to -30 °C. The molecular structures are shown in Figure 2.9 and full crystallographic data can be found in the CD appendix. Selected distances and angles are listed in Tables 2.4 and 2.5.

The molecular structures of **5**-**8** are monomeric consisting of a *pseudo*-tetrahedral titanium surrounded by η^5-cyclopentadienyl, κ^1-amidinate and η^4-diene ligands. The diene is coordinated in a *cis* fashion and adopts the supine conformation in the solid state for all four complexes. The C-C bonding sequence in the coordinated diene for **5**-**8** suggests metallocyclopentene character with the central C-C bond (1.387(3) Å (**5**), 1.395(3) Å (**6**), 1.385(4) Å (**7**), 1.388(3) Å (**8**)) being shorter than the peripheral C-C bonds (1.443(3), 1.447(2) Å (**5**), 1.427(3), 1.419(4) Å (**6**), 1.435(4), 1.421(4) Å (**7**), 1.425(3), 1.429 Å (**8**)) in direct contrast to the bond length alternation in the free

diene. This is markedly different to the molecular structure of (η^5, η^1-$C_5Me_4SiMe_2N^tBu$)Ti(η-1,4-$C_4H_4Me_2$) in which the diene is in the prone conformation and the internal diene bond lengths (1.402(9), 1.404(9), 1.391(9) Å) are all the same within error; the diene being suggested to be predominantly π-bound.[21] The Ti(1)-C(24) (2.1779(18) Å (**5**), 2.216(2) Å (**6**)) and Ti(1)-C(27) (2.1641(18) Å (**5**), 2.209(2) Å (**6**)) bond lengths in **5** and **6** are only slightly longer than the Ti(1)-C(24) (2.1227(18) Å) and Ti(1)-C(25) (2.1326(19) Å) distances observed in **4**. The Ti(1)-C(24) (2.244(3) Å) and Ti(1)-C(27) (2.269(3) Å) bond lengths in **7** are longer than in **5** and **6** reflecting the steric demands and enhanced electron withdrawing properties of the diene phenyl rings.

The Ti(1)-Cp^*_{cent} (and Ti(1)-Cp_{cent} in the case of **8**) distances (2.07 Å) are typical for Ti(+4) half-sandwich complexes and the same as that observed for the dimethyl complex, **4**. Structural characterisation of **5-8** appears to suggest that, whilst the formal oxidation state of the metal is +2, extensive reduction of the diene ligand results in significant dianionic character and predominant σ-binding to the metal centre; the oxidation state of titanium lying closer to the +4 limit. The dependence of the extent of reduction on the conformation of the diene is also of interest given the opposite conclusion drawn for the structurally characterised prone complex, (η^5, η^1-$C_5Me_4SiMe_2N^tBu$)Ti(η-1,4-$C_4H_4Me_2$).[21] These considerations will be elaborated upon with aid of DFT calculations in Chapter Three.

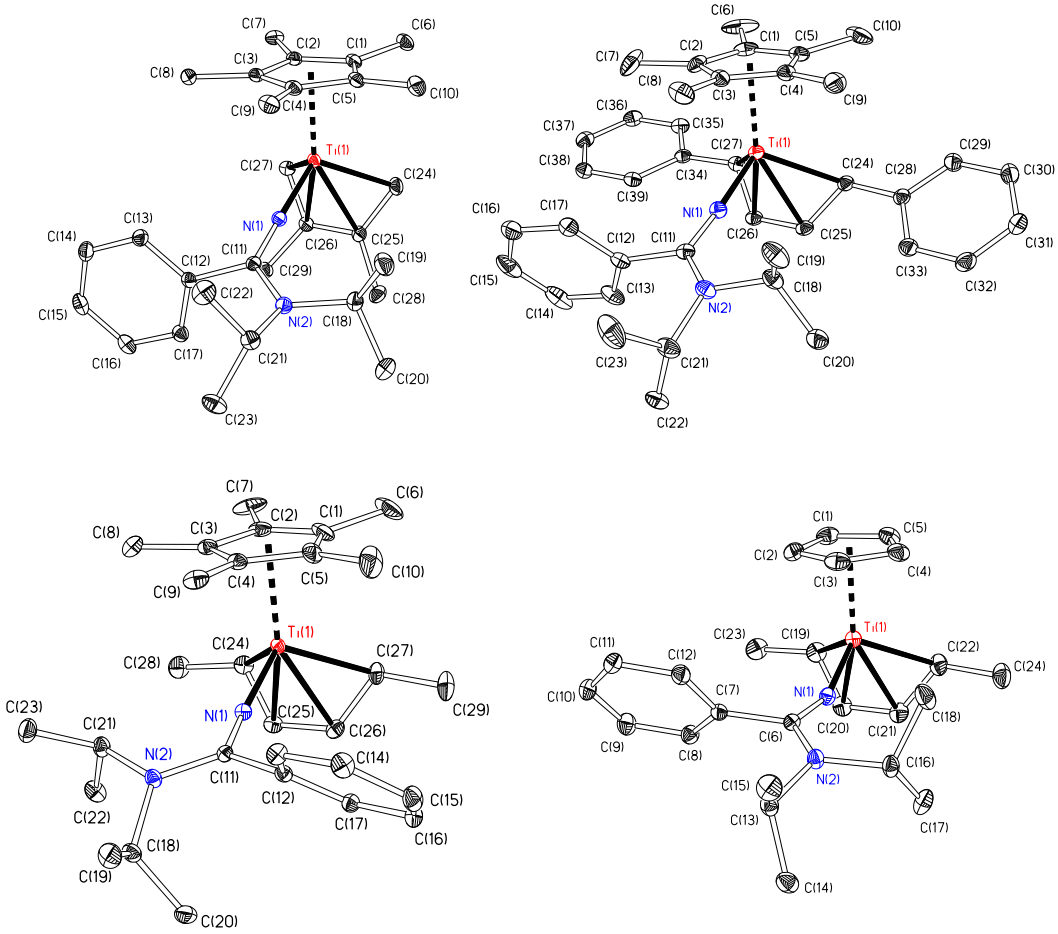

Figure 2.9. Displacement ellipsoid plots of Cp*Ti{NC(Ph)N^{i}Pr$_2$}(η-2,3-C$_4$H$_4$Me$_2$) (**5**, top left), Cp*Ti{NC(Ph)N^{i}Pr$_2$}(η-1,4-C$_4$H$_4$Me$_2$) (**6**, bottom left), Cp*Ti{NC(Ph)N^{i}Pr$_2$}(η-1,4-C$_4$H$_4$Ph$_2$) (**7**, top right) and CpTi{NC(Ph)N^{i}Pr$_2$}(η-1,4-C$_4$H$_4$Me$_2$) (**8**, bottom right). H atoms omitted for clarity. Ellipsoids are drawn at the 20% probability level.

The Ti(1)-N(1)-C(11) bond angle of the κ^1-amidinate ligand (158.60(13)°-174.61(12)°) in complexes **5-8** is comparable to that observed in **4** (163.00(13)°). Interestingly, the N(1)-C(11) bond lengths (1.273(2)-1.281(3) Å) are comparable while the N(2)-C(11) distances (1.376(2)-1.389(2) Å) are a little longer in **5-7** than in **4** (1.290(2) Å; 1.363(2) Å) suggesting that the extent of amidinate π-donation to the metal centre is somewhat diminished in the diene complexes. This may be suggested to be symptomatic of the longer Ti(1)-N(1) bonds being observed for **5-7** (1.873(2)-1.8907(14) Å) compared to **4** (1.8452(15) Å). However, closer approach of the amidine ligand (Ti(1)-N(1): 1.8619(14) Å) to the more open metal centre in **8** does

not seem to result in enhanced amidinate π-donation: similar internal amidinate bond distances are observed (N(1)-C(6): 1.283(2) Å, N(2)-C(6): 1.374(2) Å).

Table 2.4. Selected bond lengths (Å) and angles (º) for Cp*Ti{NC(Ph)N^{i}Pr$_2$}(η-2,3-$C_4H_4Me_2$) (**5**), Cp*Ti{NC(Ph)N^{i}Pr$_2$}(η-1,4-$C_4H_4Me_2$) (**6**) and Cp*Ti{NC(Ph)N^{i}Pr$_2$}(η-1,4-$C_4H_4Ph_2$) (**7**). Cp_{cent} is the computed Cp* ring carbon centroid.

Parameter	**5**	**6**	**7**
Ti(1)-Cp_{cent}	2.07	2.07	2.07
Ti(1)-N(1)	1.8907(14)	1.8761(17)	1.873(2)
N(1)-C(11)	1.273(2)	1.275(3)	1.281(3)
N(2)-C(11)	1.389(2)	1.389(2)	1.376(3)
Ti(1)-C(24)	2.1779(18)	2.216(2)	2.244(3)
Ti(1)-C(27)	2.1641(18)	2.209(2)	2.269(3)
Ti(1)-C(25)	2.3530(17)	2.302(2)	2.290(3)
Ti(1)-C(26)	2.3448(16)	2.300(2)	2.307(3)
C(24)-C(25)	1.443(3)	1.427(3)	1.435(4)
C(25)-C(26)	1.387(3)	1.395(3)	1.385(4)
C(26)-C(27)	1.447(2)	1.419(4)	1.421(4)
Cp_{cent}-Ti(1)-N(1)	114.2	114.2	114.2
Cp_{cent}-Ti(1)-C(24)	115.5	115.6	116.8
Cp_{cent}-Ti(1)-C(27)	113.3	115.6	114.5
Ti(1)-N(1)-C(11)	174.61(12)	169.64(15)	173.0(2)
N(1)-Ti(1)-C(24)	114.28(7)	112.83(8)	111.20(10)
N(1)-Ti(1)-C(27)	113.89(7)	113.05(9)	114.88(10)
C(24)-Ti(1)-C(27)	81.88(8)	84.75(10)	82.81(11)
Ti(1)-C(24)-C(25)	78.17(10)	74.90(13)	73.32(15)
Ti(1)-C(27)-C(26)	78.22(10)	75.17(13)	73.39(15)
C(24)-C(25)-C(26)	120.11(17)	123.8(2)	124.4(3)
C(25)-C(26)-C(27)	120.51(16)	124.0(2)	123.7(3)

Table 2.5. Selected bond lengths (Å) and angles (º) for $CpTi\{NC(Ph)N^iPr_2\}(\eta\text{-}1,4\text{-}C_4H_4Me_2)$ (**8**). Cp_{cent} is the computed Cp ring carbon centroid.

Ti(1)-Cp_{cent}	2.07	Ti(1)-C(20)	2.294(2)
Ti(1)-N(1)	1.8619(14)	Ti(1)-C(21)	2.296(2)
N(1)-C(6)	1.283(2)	C(19)-C(20)	1.425(3)
N(2)-C(6)	1.374(2)	C(20)-C(21)	1.388(3)
Ti(1)-C(19)	2.2067(18)	C(21)-C(22)	1.429(3)
Ti(1)-C(22)	2.212(2)		
Cp_{cent}-Ti(1)-N(1)	112.4	C(19)-Ti(1)-C(22)	85.34(9)
Cp_{cent}-Ti(1)-C(19)	113.3	Ti(1)-C(19)-C(20)	74.92(11)
Cp_{cent} –Ti(1)-C(22)	114.6	Ti(1)-C(22)-C(21)	74.76(12)
Ti(1)-N(1)-C(6)	158.60(13)	C(19)-C(20)-C(21)	124.2(2)
N(1)-Ti(1)-C(19)	116.06(7)	C(20)-C(21)-C(22)	124.4(2)
N(1)-Ti(1)-C(22)	112.54(8)		

2.4 Synthesis and characterisation of zwitterionic cyclopentadienyl-amidinate complexes

Erker *et al.* first discovered that reaction of zirconocene diene complexes with BAr^F_3 resulted in well-defined zwitterionic species, shown to be stabilised by an interaction between an *ortho*-F of one of the aryl rings of the borate and Zr, which could be utilised as single-component olefin polymerisation catalysts.[22] This chemistry has since been successfully applied to a variety of catalyst systems most notably the constrained geometry-type systems resulting in similar zwitterionic species being formed which are stabilised *via* agostic interactions between the methylene hydrogens adjacent to the borate and the metal (Ti, Zr) centre.[25, 26]

2.4.1 Synthesis of $Cp^*Ti\{NC(Ph)N^iPr_2\}\{\eta^3\text{-}CH_2C(Me)C(Me)CH_2BAr^F_3\}$ (9)

Stoichiometric reaction of **5** with BAr^F_3 immediately generates the zwitterionic species, $Cp^*Ti\{NC(Ph)N^iPr_2\}\{\eta^3\text{-}CH_2C(Me)C(Me)CH_2BAr^F_3\}$ (**9**) in which the borate moiety is found to be located on a terminal CH_2 with the other three diene carbons forming an allylic ligand; the diene methyl substituents are spectators in the reaction (Equation 2.4).

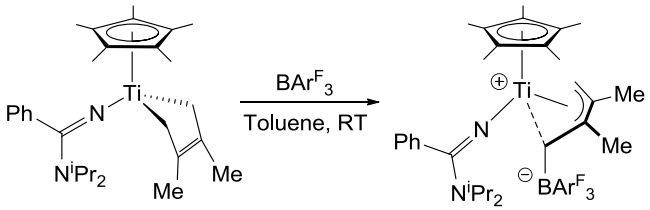

5 **9**

Equation 2.4

Compound **9** has been fully characterised by NMR and IR spectroscopy, EI mass spectrometry and elemental analysis. The low temperature (-40 °C) ^{1}H NMR spectrum is shown in Figure 2.10. The room temperature ^{1}H NMR spectrum in toluene-d_8 is broad, presumably due to restricted rotation about the Ti-N bond, but displays the familiar signals for the Cp* methyls (1.62 ppm) and aromatic amidinate protons (7.28-6.87 ppm). The singlets corresponding to the methyl groups of the allyl borate are observed at 1.88 and 1.20 ppm. Observation of the upfield methyl groups is aided by the overlapping amidinate methyl group (1.18 ppm) being broad. Three other broad singlets (1.12, 0.78 and 0.74 ppm) are assigned to the remaining amidinate methyl groups; broad singlets at 4.31 and 3.27 ppm account for the methine protons. The observation of four signals for the *iso*-propyl methyl groups suggest slow rotation about C-N^{i}Pr$_2$ and C-Ph bonds presumably as a result of the steric demands of the allyl borate ligand. The allyl protons are mostly obscured by the broad signals at room temperature but can be more easily seen at low temperature (-40 °C).

On cooling to -40 °C, the amidinate signals sharpen considerably: the septets at 4.26 and 3.16 ppm are better defined (although the upfield resonance is broader as observed with **2**-**4)** and the amidinate methyl group doublets sharpen into two sets of apparent triplets at 1.14 and 0.68 ppm. The singlets at 1.88 and 1.11 ppm are assigned to the diene methyl groups but the upfield signal is partially obscured in the low temperature spectrum by the nearby amidinate methyl resonance. Importantly the spectrum recored at -40 °C allows identification of the signals corresponding to the allylic protons farthest from the borate which are observed as two doublets at 1.78 and 1.25 ppm (^{2}J = 8.3 Hz) and the methylene protons adjacent to BAr$^F_3$ which appear as broad signals at 0.89 and -0.51 ppm. The chemical shifts of the latter protons are similar to those observed in the related constrained geometry-type zwitterionic species, (η^5, η^1-C$_5$Me$_4$SiMe$_2$N^{t}Bu)Ti{η^3-CH$_2$C(Me)C(Me)CH$_2$BAr$^F_3$} (0.94 and 0.07 ppm) which was shown to be stabilised by agostic interactions between the CH$_2$-

BAr^F_3 hydrogens and titanium.[25] The presence of similar interactions for **9** was confirmed by structural characterisation (*vide infra*).

A two-dimensional ROESY experiment was also performed at -40 °C providing an insight into the conformation of the allyl borate ligand. Through-space correlations were observed between the Cp* methyl protons and one of the terminal allylic protons and with a CH_2-BAr^F_3 proton but not with either allylic methyl groups. This suggests that the supine conformation of the diene complex (**5**) is preserved in **9**. Structural characterisation of **9** (*vide infra*) supports the solution-phase observations.

The room temperature ^{19}F NMR spectrum is broad and complicated suggesting restricted rotation about the B-CH_2 bond. Heating the sample to 80 °C in toluene-d_8 results in simplification of the ^{19}F NMR spectrum: three multiplets are observed at -130.1, -160.8 and -165.4 ppm which are assigned to the *ortho*-, *para*- and *meta*-fluorine atoms respectively. No high field (*ca.* -200 ppm) resonance is observed for **9** implying the absence of the kind of Ti···F interaction seen in Erker's $Cp_2Zr\{\eta^3$-$CH_2(CH)_2CH_2BAr^F_3\}$ zwitterion.[22] As discussed, **9** appears to be stabilised by agostic-type interactions between CH_2-BAr^F_3 hydrogens and the metal centre. A sharp singlet in the room temperature ^{11}B NMR spectrum at -12.0 ppm is indicative of the expected tetra-coordinate boron.

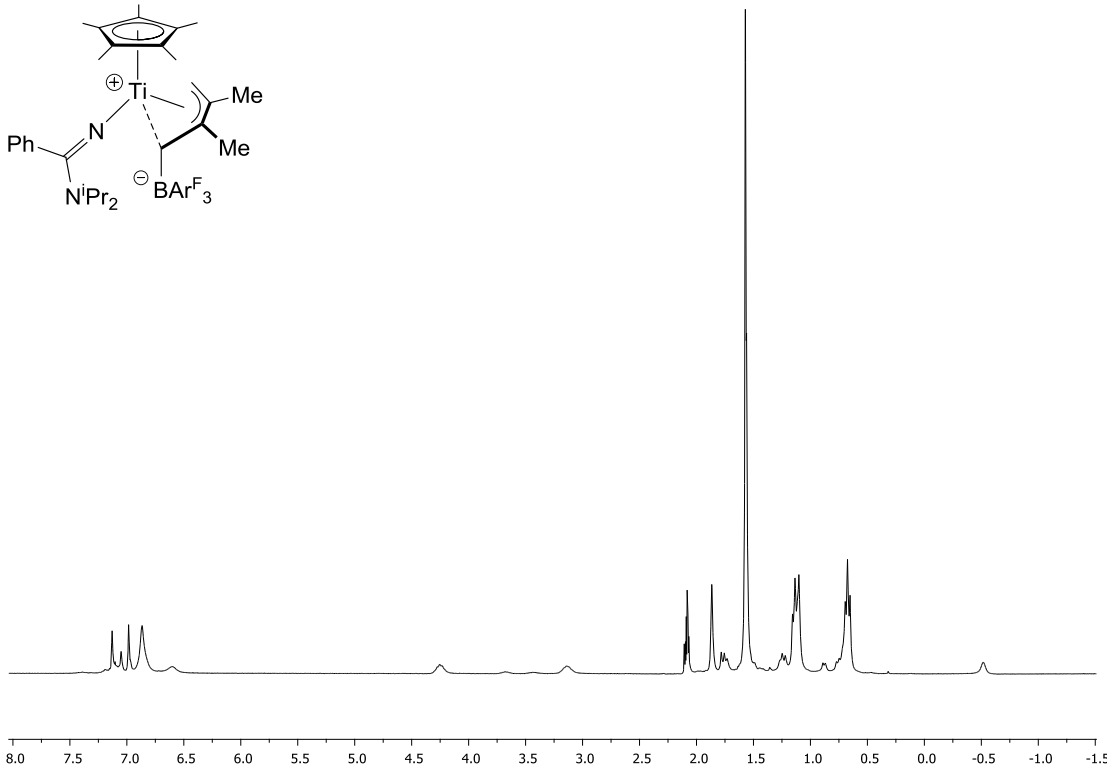

Figure 2.10. ^{1}H NMR spectrum (299.9 MHz, 233 K) of Cp*Ti{NC(Ph)N^{i}Pr$_2$}{η^3-CH$_2$C(Me)C(Me)CH$_2$BAr$^F_3$} (**9**) in toluene-d_8. Residual protio-solvent shifts: δ = 7.09, 7.00, 6.98, 2.09 ppm.

2.4.2 Synthesis of Cp*Ti{NC(Ph)N^{i}Pr$_2$}{η^3-Et(CH)$_3$CH$_2$BAr$^F_3$} (10)

Stoichiometric reaction of **6** with BAr$^F_3$ proceeds differently to the reaction shown in Equation 2.4. The formation of the zwitterion, Cp*Ti{NC(Ph)N^{i}Pr$_2$}{η^3-Et(CH)$_3$CH$_2$BAr$^F_3$} (**10**), occurs *via* migration of the borane with a concomitant hydrogen shift resulting in the BAr$^F_3$ becoming attached to a newly formed terminal methylene group (previously a CH_3) which connects to the allylic moiety; the other peripheral allylic carbon bearing an ethyl group (Equation **2.5**). Such a rearrangement observed during the formation of **10** is also seen in the reaction of (η^5, η^1-C$_5$Me$_4$SiMe$_2$N^{t}Bu)Ti(η-1,4-C$_4$H$_4$Me$_2$) with BAr$^F_3$.[25]

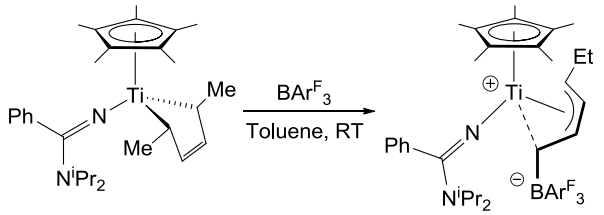

6 **10**

Equation 2.5

Compound **10** has been fully characterised by NMR and IR spectroscopy, EI mass spectrometry and elemental analysis. The high temperature (70 °C) ^{1}H NMR spectrum is shown in Figure 2.11. Similarly to compound **10**, restricted rotation about the Ti-N bond results in the room temperature ^{1}H NMR spectrum being broad; the resonances for amidinate methyl groups and the ethyl protons of the allyl borate in particular. The expected signals for the Cp* protons (1.51 ppm) and the aromatic amidinate protons (7.13-6.91 ppm) are observed along with broad signals corresponding to the allylic protons (5.08, 4.24 and 2.91 ppm). The sample was cooled to -40 °C in order to obtain sharper spectra with some success. However, heating to 70 °C, resulting in fast rotation about the Ti-N bond, permitted recording of a sharper and more easily assigned ^{1}H NMR spectrum (Figure 2.11). The amidinate *iso*-propyl signals are observed as a broad septet at 3.94 ppm (methine) and two doublets at 0.94 and 0.85 ppm (methyls). A two-dimensional COSY spectrum assisted assignment of the allylic protons. These signals are observed at 5.22 (double doublet assigned to the central allylic CH), 4.24 (CH adjacent to $CH_2BAr^F_3$) and 3.00 (CH adjacent to Et) ppm. The $CH_2BAr^F_3$ protons, presumably agostically interacting with Ti in solution as discussed for **9**, appear as broad singlets at 0.20 and 0.03 ppm. The triplet expected for the terminal methyl group of the allyl borate appears at 0.52 ppm with the adjacent methylene protons corresponding to a broad signal at 0.75 ppm.

A two-dimensional ROESY experiment was performed at -40 °C providing an insight into the conformation of the allyl borate ligand. Through-space correlations are observed between the Cp* methyl protons and the protons attached to the central allylic carbon and that adjacent to CH_2-BAr^F_3. Cross-peaks between the Cp* methyls and CH_2-BAr^F_3 and the allylic proton adjacent to CH_2CH_3 are not observed. This appears to suggest that a switch from the supine conformation in **6** has also occurred on reaction with BAr^F_3. The two central diene protons being closer to the Cp* implies

a prone-type conformation in **10**. Structural characterisation of **10** (*vide infra*) supports these solution-phase observations.

In contrast to **9**, the room temperature ^{19}F NMR spectrum shows the expected three multiplets corresponding to the *ortho*-, *para*- and *meta*-fluorines (-126.9, -156.0, -160.0 ppm respectively) suggesting free rotation about the B-CH_2 bond. This must be partly due to the absence of substituents on the diene central carbons and the switch to a prone-type conformation resulting in reduced steric interactions of the allylic moiety with the aryl rings of the borate. A sharp singlet at -12.1 ppm in the room temperature ^{11}B NMR spectrum corresponds to the expected tetra-coordinate boron.

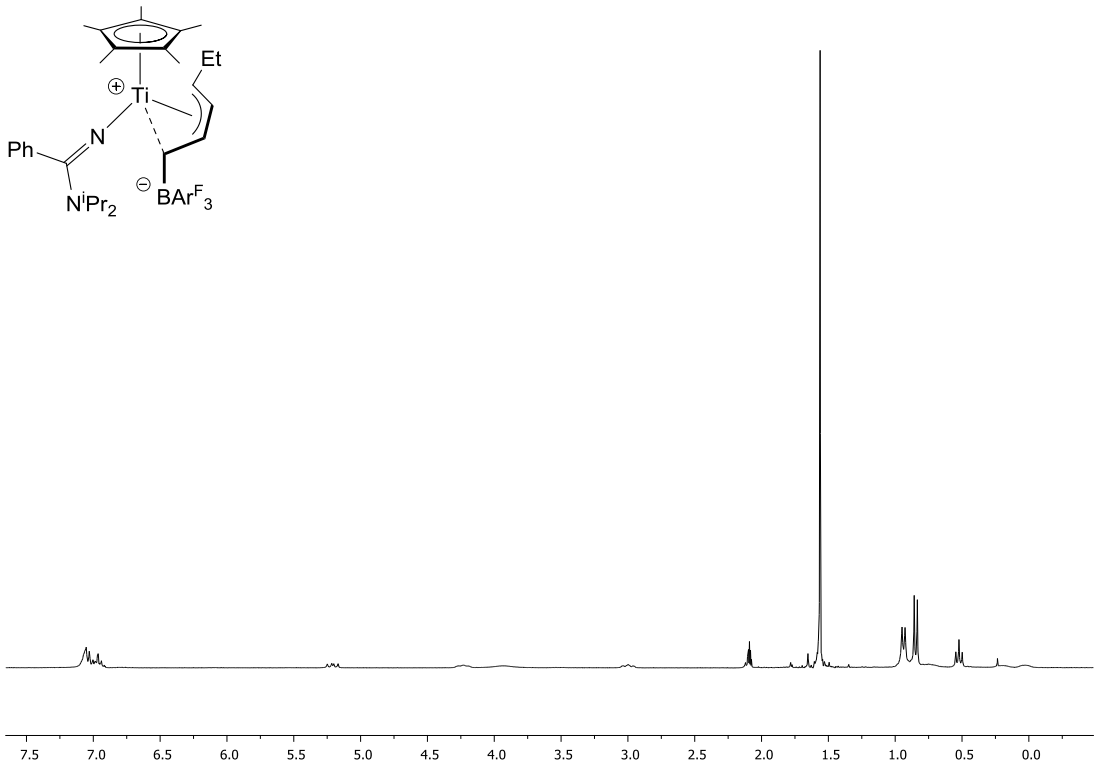

Figure 2.11. ^1H NMR spectrum (299.9 MHz, 343 K) of Cp*Ti{NC(Ph)N^{i}Pr$_2$}{η^3-Et(CH)$_3$CH$_2$BAr$^F{}_3$} (**10**) in toluene-d_8. Residual protio-solvent shifts: δ = 7.09, 7.00, 6.98, 2.09 ppm.

2.4.3 Synthesis of Cp*Ti{NC(Ph)N^{i}Pr$_2$}{η^3-Me(CH)$_3$CH$_2$BAr$^F{}_3$} (11)

Attempts to isolate Cp*Ti{NC(Ph)N^{i}Pr$_2$}(η-1-C_4H_4Me) (**11_INT**) were hampered owing to its oily nature; attempted short-path distillation of the dark green oil resulted in significant decomposition. Fortunately, the corresponding zwitterion,

Cp*Ti{NC(Ph)N^{i}Pr$_2$}{η^3-Me(CH)$_3$CH$_2$BAr$^F{}_3$} (**11**), could be isolated as a crystalline solid by reaction of **11_INT** with BAr$^F{}_3$ *in situ*. (Scheme 2.4).

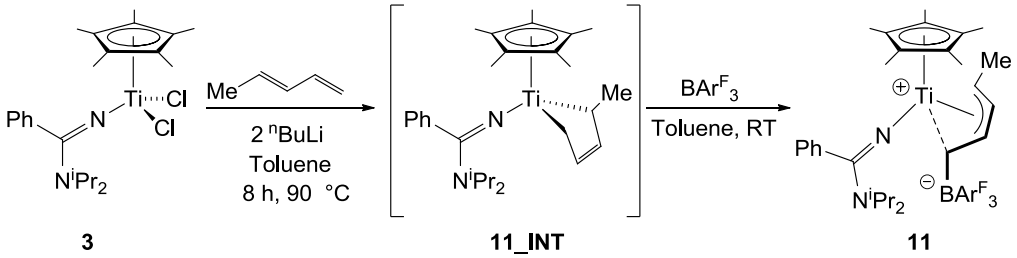

3 **11_INT** **11**

Scheme 2.4. Synthesis of Cp*Ti{NC(Ph)N^{i}Pr$_2$}{η^3-Me(CH)$_3$CH$_2$BAr$^F{}_3$} (**11**).

Compound **11** has been fully characterised by NMR and IR spectroscopy, EI mass spectrometry and elemental analysis. The room temperature spectrum of **11** is similar, as may be expected, to that of **10**. The room temperature spectrum is broad but cooling to -30 °C and use of a COSY spectrum allows the signals to be assigned. The Cp* methyl protons correspond to a singlet at 1.41 ppm and the protons of the phenyl ring of the amidinate are observed as a series of overlapping multiplets (7.24-6.67 ppm). As with the low temperature spectrum of **9**, rotation about the C-N^{i}Pr$_2$ and C-Ph bonds is slow resulting in observation of two methines (3.67 and 2.98 ppm) and four distinct methyl groups (1.16, 0.91, 0.65 and 0.30 ppm) for the amidinate *iso*-propyl groups. The allylic protons are observed at 5.03 (central CH), 3.97 (CH adjacent to CH$_2$-BAr$^F{}_3$) and 3.00 ppm (CH adjacent to CH$_3$). The terminal methyl group corresponds to a broad signal at 0.62 ppm with the methylene protons immediately adjacent to the borate being observed at 0.48 and -0.51 ppm.

The room temperature ^{19}F NMR spectrum of **11** in toluene-d_8 was similar to that seen for **10**. Three separate multiplets at -132.0, -161.1 and -165.2 ppm were observed indicating fast rotation about the B-CH$_2$ bond. The room temperature ^{11}B NMR spectrum also exhibited a sharp singlet at -7.1 ppm for the tetra-coordinate boron. The overall similarity of the NMR spectra of **11** with those recorded for **10** suggests that a prone-type conformation of the allyl borate moiety is also adopted in **11** similarly with agostic interactions between the methylene hydrogens adjacent to boron and the titanium centre. This was confirmed crystallographically (*vide infra*).

2.4.4 Synthesis of CpTi{NC(Ph)N^{i}Pr$_2$}{η^3-Et(CH)$_3$CH$_2$BAr$^{F}_3$} (12)

For comparison with the reactivity of the Cp*-supported diene complexes detailed in the synthesis of compounds **9-11**, CpTi{NC(Ph)N^{i}Pr$_2$}(η-1,4-C$_4$H$_4$Me$_2$) (**8**) was similarly 'activated' by stoichiometric reaction with BAr$^{F}_3$. Interestingly, the zwitterionic species (CpTi{NC(Ph)N^{i}Pr$_2$}{η^3-Et(CH)$_3$CH$_2$BAr$^{F}_3$} (**12**)) formed is analogous to **10**. In both cases a rearrangment results in the borate being linked to the allylic moiety *via* a newly-formed methylene group.

Compound **12** has been fully characterised by NMR and IR spectroscopy, EI mass spectrometry and elemental analysis. The room temperature ^{1}H NMR spectrum in toluene-d_8 exhibits the expected signals corresponding to the Cp ligand (5.44 ppm) and the aromatic amidinate protons which appear as a series of multiplets spanning 7.10-6.72 ppm. The resonances for the *iso*-propyl groups are observed as a broad septet (3.15 ppm) for the methine protons, partially overlapping with an allylic CH signal, and a broad singlet (0.82 ppm) corresponding to the methyl groups, slightly obscured by a multiplet corresponding to the methylene protons of the terminal ethyl group (0.85 ppm) of the allyl borate. The allylic protons are observed at 4.96 (central allylic CH), 3.98 (CH adjacent to CH$_2$BAr$^{F}_3$) and 3.19 (CH adjacent to Et) ppm. The familiar CH$_2$BAr$^{F}_3$ agostic protons appear as broad resonances at 0.33 and -1.02 ppm. The signal corresponding to the terminal methyl group of allyl borate is observed as a triplet at 0.50 ppm. Given the close analogy between the ^{1}H NMR spectrum of **12** with that of **10**, a prone-type conformation is assigned to the allylic moiety. Structural characterisation of **12** (*vide infra*) is in agreement with this assumption.

Cooling to -50 °C had little effect on the appearance of the allylic borate peaks aside from slight changes in chemical shift. However, similarly to **9** and **11**, the broad signal corresponding to the amidinate methyl groups at room temperature separated into four distinct resonances (1.37, 1.02, 0.57 and 0.49 ppm) with two signals for the methine protons being observed (3.03 and 2.61 ppm). The possible presence of the minor (supine) isomer (10 %) is observed in solution by the presence of a weak signal slightly downfield of the major Cp resonance. The relative concentrations are constant with temperature. Unfortunately no other peaks corresponding to this possible minor isomer could be observed in the ^{1}H NMR spectrum possibly due to overlap with signals for the dominant prone isomer. However, further evidence is found in the ^{19}F NMR spectrum: weak peaks (-132.8, -160.3 and -164.9 ppm) are observed adjacent to

each of the main *ortho*-, *para*- and *meta*-fluorine signals (-132.4, -160.9 and -165.1 ppm respectively). Free rotation about the B-CH_2 bond at room temperature results in observation of the three sharp multiplets for the major isomer as observed for **10** and **11**. The ^{11}B NMR spectrum showed a single peak at -12.4 ppm due to possible overlap of the signals corresponding to the two isomers.

2.4.5 Attempted reaction of Cp*Ti{NC(Ph)N^{i}Pr$_2$}(η-1,4-C$_4$H$_4$Ph$_2$) (7) with BAr$^F_3$

Unlike the diene complexes **5**, **6** and **8**, Cp*Ti{NC(Ph)N^{i}Pr$_2$}(η-1,4-$C_4H_4Ph_2$) (**7**) did not react immediately with BAr^F_3 at room temperature to form a well-defined zwitterionic species. Heating at 60 °C for 3 h or reaction at room temperature for several days resulted in the formation of a mixture of products observed from the ^{1}H, ^{19}F and ^{11}B NMR spectra including liberation of the free diene. The greater steric bulk of the diene in the case of **7** appears to preclude zwitterion formation; rearrangement as seen in formation of **10** and **12** is also prohibited in the case of the phenyl-substituted diene.

2.4.6 X-ray structures of zwitterions 9-12

Compounds **9**-**12** were further characterised by single crystal X-ray diffraction. Single crystals of **9** and **11** suitable for X-ray diffraction were grown from benzene solutions at room temperature. Single crystals of **10** and **12** were grown from pentane solutions at -30 °C and room temperature respectively. The molecular structures are shown in Figure 2.12 and full crystallographic data can be found in the CD appendix. Selected distances and angles are listed in Tables 2.6-2.8.

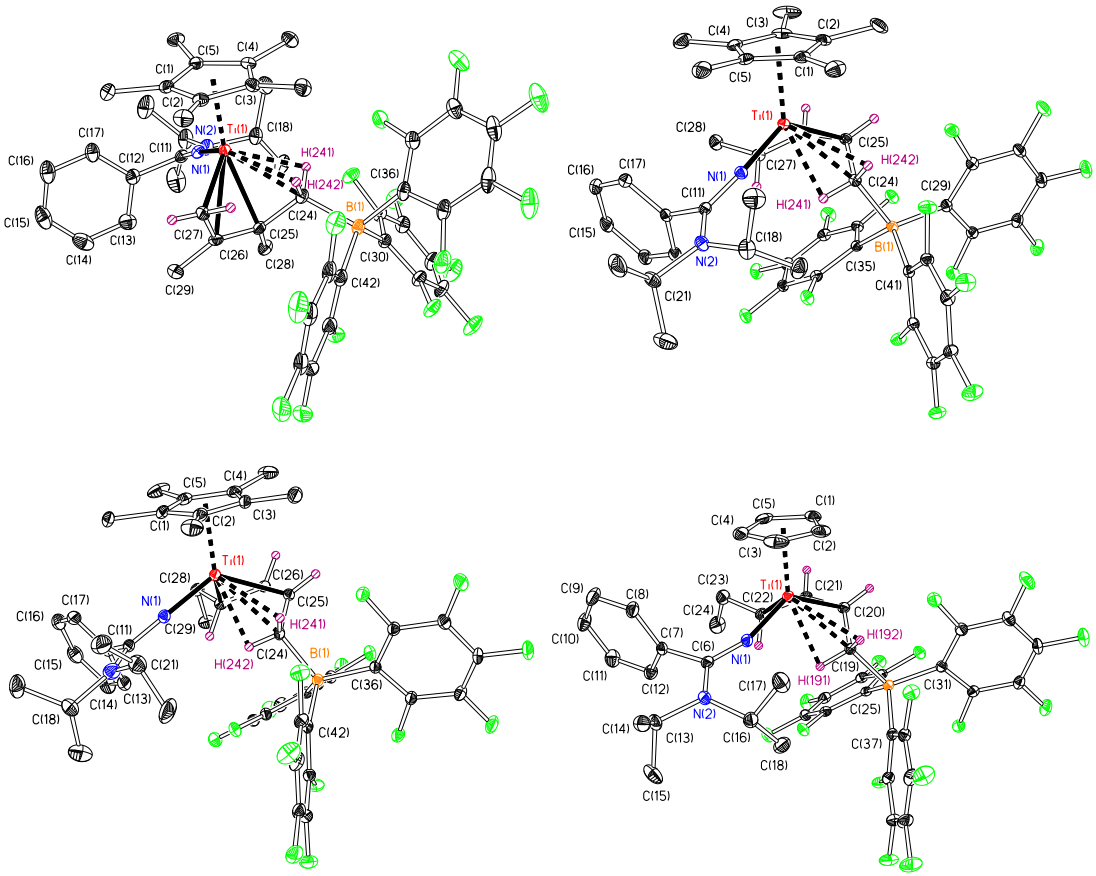

Figure 2.12. Displacement ellipsoid plots of Cp*Ti{NC(Ph)N^{i}Pr$_2$}{ η^3-$CH_2C(Me)C(Me)CH_2BAr^F_3$} (**9**, top left), Cp*Ti{NC(Ph)N^{i}Pr$_2$}{η^3-$Et(CH)_3CH_2BAr^F_3$} (**10**, bottom left), Cp*Ti{NC(Ph)N^{i}Pr$_2$}{η^3-$Me(CH)_3CH_2BAr^F_3$} (**11**, top right) and CpTi{NC(Ph)N^{i}Pr$_2$}{η^3-$Et(CH)_3CH_2BAr^F_3$} (**12**, bottom right). H atoms except those on allyl borate omitted for clarity. Ellipsoids are drawn at the 20% probability level.

Table 2.6. Selected bond lengths (Å) and angles (º) for Cp*Ti{NC(Ph)N^{i}Pr$_2$}{ η^3-CH$_2$C(Me)C(Me)CH$_2$BAr$^{F}_3$} (**9**) and Cp*Ti{NC(Ph)N^{i}Pr$_2$}{η^3-Et(CH)$_3$CH$_2$BAr$^{F}_3$} (**10**). Cp$_{cent}$ is the computed Cp* ring carbon centroid.

Parameter	**9**	**10**	Parameter	**9**	**10**
Ti(1)-Cp$_{cent}$	2.06	2.04	N(1)-Ti(1)-C(27)	117.97(12)	90.70(18)
Ti(1)-N(1)	1.855(2)	1.852(4)	C(24)-Ti(1)-C(27)	80.33(10)	81.51(16)
N(1)-C(11)	1.288(4)	1.268(6)	C(24)-Ti(1)-C(25)	37.38(10)	36.66(17)
N(2)-C(11)	1.374(4)	1.326(7)	C(24)-Ti(1)-C(26)	64.90(10)	65.16(16)
Ti(1)-C(24)	2.380(3)	2.445(4)	C(25)-Ti(1)-C(26)	34.56(10)	35.48(17)
Ti(1)-H(241)	2.22(3)	2.47(5)	C(25)-Ti(1)-C(27)	65.49(11)	66.21(17)
Ti(1)-H(242)	2.30(3)	2.23(6)	C(26)-Ti(1)-C(27)	35.92(11)	35.37(17)
Ti(1)-C(27)	2.201(3)	2.308(5)	Ti(1)-C(24)-C(25)	69.52(14)	64.3(2)
Ti(1)-C(25)	2.330(3)	2.243(4)	Ti(1)-C(25)-C(24)	73.10(15)	79.1(3)
Ti(1)-C(26)	2.374(3)	2.331(5)	Ti(1)-C(25)-C(26)	74.42(16)	75.7(3)
C(24)-C(25)	1.510(4)	1.487(7)	Ti(1)-C(26)-C(25)	71.03(15)	68.8(3)
C(25)-C(26)	1.398(4)	1.396(7)	Ti(1)-C(26)-C(27)	65.41(15)	71.4(3)
C(26)-C(27)	1.420(4)	1.409(7)	Ti(1)-C(27)-C(26)	78.67(16)	73.2(3)
C(24)-B(1)	1.699(4)	1.690(6)	C(24)-C(25)-C(26)	122.5(3)	126.4(4)
Cp$_{cent}$-Ti(1)-N(1)	112.5	116.67	C(25)-C(26)-C(27)	121.1(3)	124.8(4)
Cp$_{cent}$-Ti(1)-C(25)	159.7	115.14	Ti(1)-C(24)-B(1)	170.2(2)	166.1(3)
Cp$_{cent}$-Ti(1)-C(26)	144.4	114.2	B(1)-C(24)-C(25)	115.7(2)	113.6(4)
Cp$_{cent}$-Ti(1)-C(27)	108.5	126.28	C(24)-B(1)-C(30)	114.7(2)	99.9(3)
Ti(1)-N(1)-C(11)	175.9(2)	170.8(4)	C(24)-B(1)-C(36)	112.7(2)	114.0(4)
N(1)-Ti(1)-C(24)	109.94(10)	96.06(16)	C(24)-B(1)-C(42)	100.4(2)	113.4(4)

Table 2.7. Selected bond lengths (Å) and angles (º) for Cp*Ti{NC(Ph)N^{i}Pr$_2$}{η^3-Me(CH)$_3$CH$_2$BAr$^{F}_3$} (**11**). Cp$_{cent}$ is the computed Cp* ring carbon centroid.

Parameter		Parameter	
Ti(1)-Cp$_{cent}$	2.03	N(1)-Ti(1)-C(27)	90.09(8)
Ti(1)-N(1)	1.8575(19)	C(24)-Ti(1)-C(27)	81.80(8)
N(1)-C(11)	1.294(3)	C(24)-Ti(1)-C(25)	37.20(8)
N(2)-C(11)	1.360(3)	C(24)-Ti(1)-C(26)	65.38(8)
Ti(1)-C(24)	2.415(2)	C(25)-Ti(1)-C(26)	35.12(8)
Ti(1)-H(241)	2.20(3)	C(25)-Ti(1)-C(27)	65.58(8)
Ti(1)-H(242)	2.44(3)	C(26)-Ti(1)-C(27)	34.75(8)
Ti(1)-C(27)	2.331(2)	Ti(1)-C(24)-C(25)	69.52(14)
Ti(1)-C(25)	2.245(2)	Ti(1)-C(25)-C(24)	77.61(12)
Ti(1)-C(26)	2.346(2)	Ti(1)-C(25)-C(26)	76.42(13)
C(24)-C(25)	1.495(3)	Ti(1)-C(26)-C(25)	68.46(13)
C(25)-C(26)	1.388(3)	Ti(1)-C(26)-C(27)	72.06(13)
C(26)-C(27)	1.397(3)	Ti(1)-C(27)-C(26)	73.18(13)
C(24)-B(1)	1.692(3)	C(24)-C(25)-C(26)	126.2(2)
Cp$_{cent}$-Ti(1)-N(1)	116.5	C(25)-C(26)-C(27)	125.8(2)
Cp$_{cent}$-Ti(1)-C(25)	114.9	Ti(1)-C(24)-B(1)	165.75(15)
Cp$_{cent}$-Ti(1)-C(26)	114.3	B(1)-C(24)-C(25)	113.62(18)
Cp$_{cent}$-Ti(1)-C(27)	125.9	C(24)-B(1)-C(29)	113.21(17)
Ti(1)-N(1)-C(11)	164.41(17)	C(24)-B(1)-C(35)	99.78(17)
N(1)-Ti(1)-C(24)	97.31(8)	C(24)-B(1)-C(41)	112.57(17)

Table 2.8. Selected bond lengths (Å) and angles (º) for CpTi{NC(Ph)N^{i}Pr$_2$}{η^3-Et(CH)$_3$CH$_2$BAr$^{F}_3$} (**12**). Cp$_{cent}$ is the computed Cp ring carbon centroid.

Parameter		Parameter	
Ti(1)-Cp$_{cent}$	2.01	N(1)-Ti(1)-C(22)	90.95(9)
Ti(1)-N(1)	1.8499(19)	C(19)-Ti(1)-C(22)	82.75(9)
N(1)-C(6)	1.292(3)	C(19)-Ti(1)-C(20)	37.13(8)
N(2)-C(6)	1.357(3)	C(19)-Ti(1)-C(21)	65.38(8)
Ti(1)-C(19)	2.422(2)	C(20)-Ti(1)-C(21)	34.87(9)
Ti(1)-H(191)	2.29(3)	C(20)-Ti(1)-C(22)	66.21(9)
Ti(1)-H(192)	2.38(2)	C(21)-Ti(1)-C(22)	35.57(9)
Ti(1)-C(22)	2.276(2)	Ti(1)-C(19)-C(20)	65.70(12)
Ti(1)-C(20)	2.264(2)	Ti(1)-C(20)-C(19)	77.17(13)

Table 2.8. cont.

Parameter		Parameter	
Ti(1)-C(21)	2.337(2)	Ti(1)-C(20)-C(21)	75.49(14)
C(19)-C(20)	1.499(3)	Ti(1)-C(21)-C(20)	69.64(13)
C(20)-C(21)	1.380(4)	Ti(1)-C(21)-C(22)	69.85(13)
C(21)-C(22)	1.410(3)	Ti(1)-C(22)-C(21)	74.58(14)
C(19)-B(1)	1.683(3)	C(19)-C(20)-C(21)	126.4(2)
Cp_{cent}-Ti(1)-N(1)	116.1	C(20)-C(21)-C(22)	125.4(2)
Cp_{cent}-Ti(1)-C(20)	114.6	Ti(1)-C(19)-B(1)	173.98(17)
Cp_{cent}-Ti(1)-C(21)	110.5	B(1)-C(19)-C(20)	111.95(18)
Cp_{cent}-Ti(1)-C(22)	120.1	C(19)-B(1)-C(25)	101.42(17)
Ti(1)-N(1)-C(6)	162.47(17)	C(19)-B(1)-C(31)	113.96(18)
N(1)-Ti(1)-C(19)	98.43(8)	C(19)-B(1)-C(37)	110.97(18)

The molecular structures of **9**-**12** are consistent with the spectroscopic data revealing the expected monomeric complex with titanium coordinated by η^5-cyclopentadienyl, κ^1-amidinate and η^3-allyl borate ligands; secondary agostic-type interactions between methylene hydrogens adjacent to the borate moiety and the metal centre are also observed (*vide infra*). The rearrangement described for formation of **10** and **12** which results in the borane becoming attached to what was previously a terminal methyl group of the diene is confirmed crystallographically. In agreement with solution-phase NMR experiments, the supine conformation of the coordinated diene in **5** is maintained in the corresponding zwitterion, **9**. The switch to a prone-type conformation during formation of **10** and **12**, predicted from the low temperature ROESY spectrum of **10**, is clearly evident from the molecular structures.

The distances between the terminal η^3-allyl carbons (C(25) and (C(27)) and titanium (2.330(3) and 2.201(3) Å (**9**), 2.243(4) and 2.308(5) Å (**10**), 2.245(2) and 2.331(2) Å (**11**)) are shorter than the bond lengths observed between titanium and the central allylic carbon (C(26)) (2.374(3) Å (**9**), 2.331(5) Å (**10**), 2.346(2) Å (**11**)). This is commonly observed for allyl complexes of the early transition metals.[13] The internal C(25)-C(26) and C(26)-C(27) bond lengths of the allylic moiety (1.398(4) and 1.420(4) Å (**9**), 1.396(7) and 1.409(7) Å (**10**), 1.388(3) and 1.397(3) Å (**11**)) and the C(25)-C(26)-C(27) angles (121.1(3)º (**9**), 124.8(4)º (**10**), 125.8(2)º (**11**)) are also similar to those of published η^3-allyl complexes.[22, 25, 26] The allyl moiety exhibits a *Z*-configuration with respect to the C(25)-C(26) π-bond. This configuration brings C(24) into a favourable position for agostic interactions between H(241) and H(242) and

titanium. The hydrogen atoms of C(24) were located from a Fourier difference map and positionally and isotropically refined. The Ti(1)-H(241) and Ti(1)-H(242) bond lengths are relatively short (2.22(3) and 2.47(5) Å (**9**), 2.30(3) and 2.23(6) Å (**10**), 2.20(3) and 2.44(3) Å (**11**)) and lie towards the upper limit of the range (*ca.* 1.8-2.3 Å)[32] expected for classical agostic interactions.[32-34] Combined with the apparent linearity of the Ti(1)-C(24)-B(1) bond angles (170.2(2)º (**9**), 166.1(3)º (**10**), 165.75(15)º (**11**)), the structural features appear strongly indicative of agostic-type interactions between the $CH_2BAr^F_3$ hydrogens and titanium. Furthermore, no Ti···F interaction is observed in the solid-state in agreement with solution-phase observations. Interestingly, Erker observed an E-configuration of the allyl moiety which presumably facilitates the Zr···F interaction observed in $Cp_2Zr\{\eta^3$-$CH_2(CH)_2CH_2BAr^F_3\}$.[22] These considerations of the allyl borate moiety in **9**-**11** also apply to **12**; the relevant bond lengths and angles for **12** are not detailed in the text due to a differing numbering scheme required by the unsubstituted cyclopentadienyl ligand but may be found in Table 2.8. Also noteworthy is the narrowing of one of the H_2C-B-C(Ar^F) bond angles (99.78(17)º-101.42(17)º) compared to the others (110.97(18)º-114.7(2)º) in **9**-**12** which acts to bring the plane of one of the perfluorinated aryl rings parallel to that of the allylic cation moiety which may be described as a type of intramolecular π-stacking interaction. The preference of perfluorinated aryl rings for π-stacking interactions is well-documented in supramolecular chemistry[35-37] and beautifully exemplified by the 1:1 benzene–perfluorobenzene complex which, due to such arene-perfluoroarene interactions, has a significantly higher melting point (24 ºC) than either neat benzene (5.5 ºC) or perfluorobenzene (4 ºC).[38]

The $Cp^{(*)}_{cent}$-Ti distances are shorter for these zwitterionic species (2.06 Å (**9**), 2.04 Å (**10**), 2.03 Å (**11**), 2.01 Å (**12**)) than their diene precursors (2.07 Å (**5**, **6**, **8**)) which may be expected given the cationic nature of the metal. A longer Cp^*_{cent}-Ti distance in **9** compared to the other zwitterions must stem from the adoption of a different (supine) conformation of the allyl borate. The Ti(1)-N(1) distances for the zwitterionic compounds (1.855(2) Å (**9**), 1.852(4) Å (**10**), 1.8575(19) Å (**11**), 1.8499(19) Å (**12**)) are also shorter in comparison with the neutral diene complexes (1.8907(14) Å (**5**), 1.8761(17) Å (**6**), 1.8619(14) Å (**8**)). The expected approximately linear geometry about N(1) persists in compounds **9**-**12**. Comparable N(1)-C(11)

(N(1)-C(6) for **8** and **12**) bond lengths are observed in the zwitterions (1.288(4) Å (**9**), 1.268(6) Å (**10**), 1.294(3) Å (**11**), 1.292(3) Å (**12**)) and diene complexes (1.273(2) Å (**5**), 1.275(3) Å (**6**), 1.283(2) Å (**8**). Slightly shorter N(2)-C(11) (N(2)-C(6) for **8** and **12**) bond lengths are seen in the zwitterions (1.374(4) Å (**9**), 1.326(7) Å (**10**), 1.360 (3) Å (**11**), 1.357(3) Å (**12**)) compared to the diene complexes (1.389(2) Å (**5**), 1.389(2) Å (**6**), 1.374(2) Å (**8**). This suggests broadly similar bonding between amidinate and titanium in the zwitterionic complexes compared to the diene compounds although the shorter N(2)-C(11) (N(2)-C(6) for **12**) distances in **9**-**12** perhaps indicate a slightly superior π-donation from the amidinate ligand to the cationic titanium.

2.5 Reactions of zwitterions 9 and 10 with unsaturated molecules

Whilst an exhaustive study into the underlying chemistry of the zwitterionic species described above is beyond the scope of this Thesis, experiments were undertaken in order understand some of the chemistry of the 'activated' zwitterionic species. Research into group 4 alkyl cation chemistry has long made use of unsaturated molecules as mimics of olefin coordination and insertion. The reactivity of bis(cyclopentadienyl) group 4 alkyl cation complexes with isonitriles have been studied in detail by Bochmann[39-41] while trapping reactions of alkyl cations with alkynes have also received a great deal of attention most notably in the work of Eisch.[42] More recently some of the coordination/insertion behaviour for η^3-allyl zwitterionic systems has been examined by probing reactivity of these systems with CO, ^{t}BuNC and PMe_3.[27] With a view to exploring reactivity of the zwitterionic systems described above, experiments were designed to assess the reactivity **9** and **10** (as representative examples) with ^{t}BuNC and alkynes.

2.5.1 Reaction of Cp*Ti{NC(Ph)N^{i}Pr$_2$}{η^3-CH$_2$C(Me)C(Me)CH$_2$BAr$^F_3$} (9) with ^{t}BuNC

Reaction of **9** with one equivalent of ^{t}BuNC in toluene at room temperature results in the solution immediately changing from green to dark red with crystallisation of a red-orange solid on addition of n-hexanes and leaving to stand at room temperature for three hours. The product was shown to be the adduct, Cp*Ti{NC(Ph)N^{i}Pr$_2$}{η^3-CH$_2$C(Me)C(Me)CH$_2$BAr$^F_3$}(^{t}BuNC) (**13**). Steric factors are thought to preclude an insertion reaction affording an iminoacyl species. A similar result was noted for

reaction of (η^5, η^1-$C_5Me_4SiMe_2N^tBu$)Ti{η^3-$Me(CH)_3CH_2BAr^F_3$} with ^{t}BuNC.[27] Surprisingly, heating the isolated adduct (**13**) in C_6D_6 at 70 ºC for three hours results in quantitative formation of the neutral diene complex **9** and ^{t}BuNC·BAr^F_3 (Scheme 2.5). Reaction of (η^5, η^1-$C_5Me_4SiMe_2N^tBu$)Ti{η^3-$Me(CH)_3CH_2BAr^F_3$} with Pme_3 also resulted in reformation of the neutral diene complex (and $Me_3P·BAr^F_3$) presumably *via* an adduct which was not observed.[27]

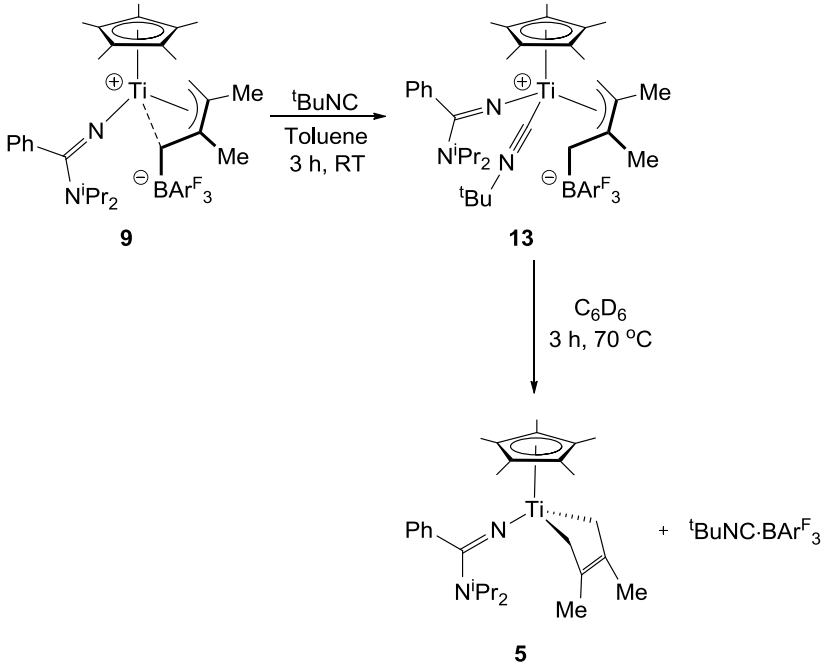

Scheme 2.5. Synthesis of adduct **13** and reformation of diene complex **5**.

Compound **13** has been fully characterised by NMR and IR spectroscopy, EI mass spectrometry and elemental analysis. The low temperature (-30 °C) ^{1}H NMR spectrum is shown in Figure 2.13. The room temperature ^{1}H NMR spectrum in CD_2Cl_2 is very broad which is postulated to result from reversible ^{t}BuNC dissociation. Cooling to -30 ºC sharpens the signals considerably and reveals the presence of two diastereomers which are thought to correspond to the occupancy of the ^{t}BuNC ligand in two possible coordination sites. Assignment was assisted greatly by use of two-dimensional COSY and ROESY spectra. The ratio of the diastereomers denoted **13A** and **13B** in solution at -30 ºC is *ca*. 3:1 in favour of **13A**. In both isomers, the aromatic protons appear as overlapping multiplets spanning the range 7.42-6.88 ppm. The major singlets assigned to the Cp* protons are observed at 1.55 (**13A**) and 1.83 (**13B**) ppm with the ^{t}Bu group signals appearing at 1.71 (**13A**) and 1.30 (**13B**) ppm. Restricted rotation about the C-N^{i}Pr$_2$ and C-Ph bonds in **13A** results in observation of

two methine septets (4.68 and 3.46 ppm) and four methyl doublets (1.20, 1.12, 1.02 and 0.91 ppm) for the amidinate *iso*-propyl groups. For **13A**, the singlets corresponding to the allyl methyl groups are located at 2.05 and 1.48 ppm with the terminal allylic protons appearing as a doublet at 1.91 and a peak at 0.87 ppm which is obscured by the amidinate methyl signals of **13B**. The $CH_2BAr^F{}_3$ protons are located as doublets at 2.36 and -0.27 ppm; the former signal is located significantly downfield in comparison with chemical shifts observed in **9** which may be indicative of loss of agostic interaction with titanium in **13A**.

The amidinate *iso*-propyl signals in **13B** are observed as a septet (3.39 ppm) and two doublets (0.85 and 0.81 ppm). The allylic resonances for **13B** are at similar chemical shifts to those observed for **13A**: the methyl groups correspond to two singlets (1.86 and 1.68 ppm), the terminal allylic and $CH_2BAr^F{}_3$ protons appear at 2.17 and 1.23 ppm and 2.01 and -0.38 ppm respectively. The room temperature ^{19}F spectrum consists of three relatively broad peaks at -130.1, -164.2 and -167.4 ppm corresponding to the *ortho*, *para* and *meta* fluorine environments of the borate aryl groups. At -30 °C the spectrum broadens and peaks corresponding to both isomers begin to appear but further cooling failed to resolve the ^{19}F signals corresponding to **13A** and **13B**. The ^{11}B NMR spectra recorded at room temperature and -30 °C both showed a single peak at -13.4 ppm showing that the two diastereomers cannot be distinguished by ^{11}B NMR.

Several attempts were made to grow single crystals of each diastereomer but only one of them could be structurally characterised (*vide infra*). It seems that **13** crystallises as a single diastereomer but isomerises in solution. This is reinforced by observation of a single υ**(**C≡N) in the IR spectrum of the solid material (Nujol mull) at 2171 cm^{-1}. This value is consistent with that observed for the closely related literature compound: (η^5, η^1-$C_5Me_4SiMe_2N^tBu$)Ti{η^3-$Me(CH)_3CH_2BAr^F{}_3$}(^{t}BuNC) (2191 cm^{-1}).[27] The higher frequency vibration observed in the adduct **13** compared to the free isonitrile (2125 cm^{-1}) is consistent with the absence of back-bonding expected for a d^0 titanium complex.

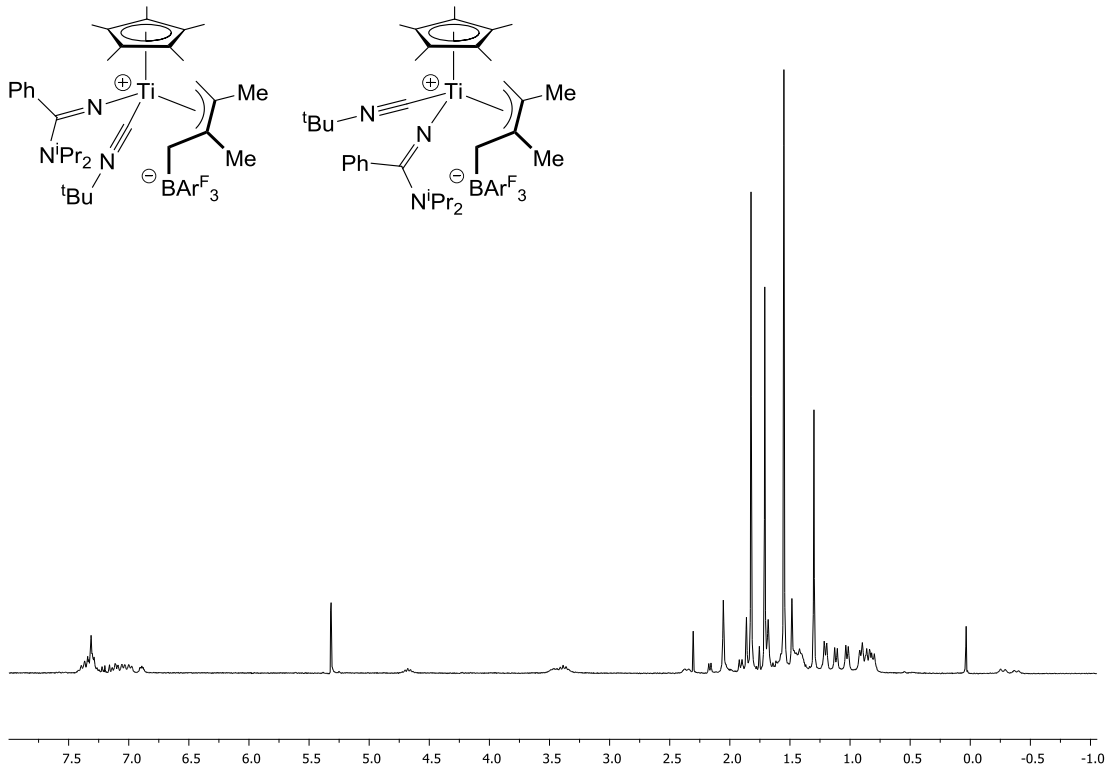

Figure 2.13. ^{1}H NMR spectrum (299.9 MHz, 243 K) of Cp*Ti{NC(Ph)N^{i}Pr$_2$}{η^3-Et(CH)$_3$CH$_2$BAr$^F{}_3$}(^{t}BuNC) (**13**) in CD_2Cl_2. Residual protio-solvent, δ = 5.32 ppm.

2.5.2 Reaction of Cp*Ti{NC(Ph)N^{i}Pr$_2$}{η^3-Et(CH)$_3$CH$_2$BAr$^F{}_3$} (10) with ^{t}BuNC

Similarly, reaction of **10** with one equivalent ^{t}BuNC in toluene results in the formation of the adduct, Cp*Ti{NC(Ph)N^{i}Pr$_2$}{η^3-Et(CH)$_3$CH$_2$BAr$^F{}_3$}(^{t}BuNC) (**14**). Heating the isolated adduct, **14**, in toluene-d_8 at 80 ºC for up to 16 h does not result in generation of ^{t}BuNC·BAr$^F{}_3$, as is the case for **13**, and the diene complex **6** (or a rearranged diene complex). Extended heating results in decomposition of **14** to a mixture of products evident from ^{1}H, ^{19}F and ^{11}B NMR spectra. The apparently more facile reversibility to the diene complex in the case of **9** compared to **10** is further explored below. Reaction of **14** with one equivalent of BAr$^F{}_3$ immediately regenerates **10** with elimination of ^{t}BuNC·BAr$^F{}_3$; potential utility of **14** as a precatalyst is implied by this reaction. These observations are summarised in Scheme 2.6. Interestingly, **14**, whether as the isolated solid or in solution displays remarkable resistance to hydrolysis which is attributed to coordinative saturation of titanium and the steric protection provided by the ligands. The compound survives for days in the solid state in air and a satisfactory ^{1}H NMR spectrum may even be recorded in 'wet' bench $CDCl_3$.

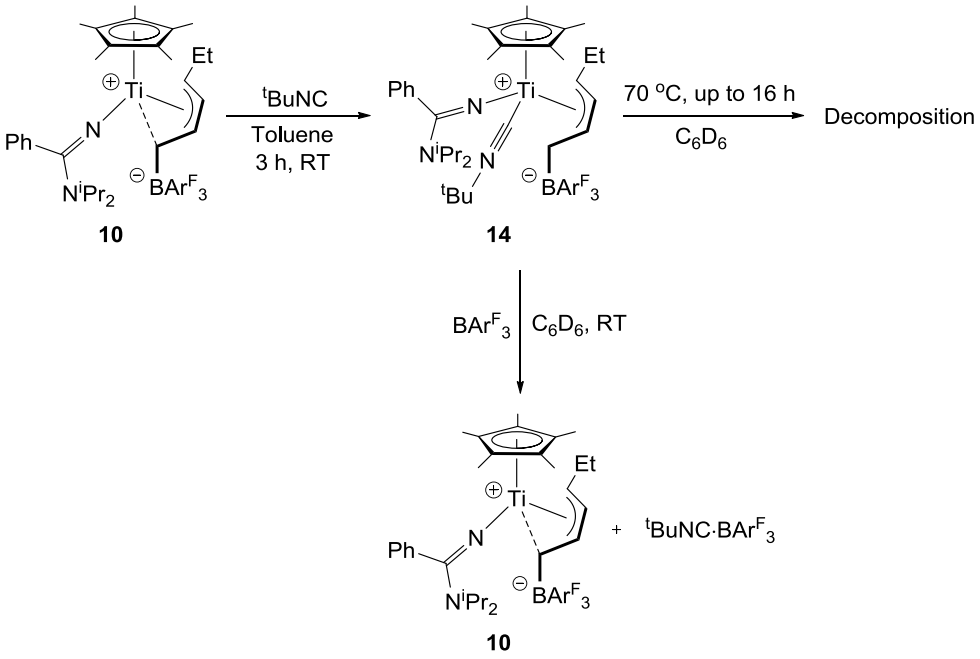

Scheme 2.6. Synthesis of adduct **14** and reformation of base-free **10** by reaction with BAr^F_3.

Compound **14** has been fully characterised by NMR and IR spectroscopy, EI mass spectrometry and elemental analysis. The room temperature ^{1}H NMR spectrum in CD_2Cl_2 shows a single diastereomer of **14**. The singlets for the Cp* and ^{t}Bu protons are observed at 1.69 and 1.60 ppm respectively whilst the amidinate phenyl protons correspond to a series of multiplets spanning 7.35-6.97 ppm. The broad doublets corresponding to the methylene protons adjacent to boron (1.88 and 3.08 ppm) are shifted significantly from the chemical shifts observed in **10** (0.20 and 0.03 ppm). As with **13**, this oberservation is speculated to suggest that **14** is not stabilised by the agostic-type interactions observed in the zwitterionic complexes **9-12**. This was confirmed by structural characterisation of **14** (*vide infra*). The other signals observed for the allylic moiety are similar to those of the base-free zwitterion, **10**: the double doublet corresponding to the central allylic proton is located at 4.44 ppm and multiplets for the allylic protons adjacent to the ethyl and $CH_2BAr^F_3$ groups are found at 3.08 and 2.39 ppm respectively. A multiplet at 1.46 ppm (CH_2) and a sharp triplet at 0.81 ppm (CH_3) correspond to signals for the terminal ethyl group of the allyl borate.

The room temperature ^{19}F NMR spectrum exhibits the expected three multiplets corresponding to the *ortho*, *meta* and *para* environments of the borate aryl rings

(-131.3, -162.8, -166.3 ppm). The ^{11}B spectrum displays a sharp singlet for the tetra-coordinate boron at -12.3 ppm. A single υ(C≡N) is observed in the IR spectrum (Nujol mull) at 2177 cm^{-1} which is, as discussed for **13**, at higher frequency compared to the related band observed in free ^{t}BuNC (2125 cm^{-1}).

2.5.3 X-ray structures of zwitterionic ^{t}BuNC adducts 13 and 14

Compounds **13** and **14** were further characterised by single crystal X-ray diffraction. Single crystals of **13** and **14** suitable for X-ray diffraction were grown from toluene/n-hexanes solutions at room temperature. The molecular structures are shown in Figure 2.14 and full crystallographic data can be found in the CD appendix. Selected distances and angles are listed in Table 2.9.

The supine-type conformation of the allyl borate persists in **13** with retention of the Z-configuration of the allyl moiety with respect to the C(25)-C(26) π-bond. In contrast, coordination of ^{t}BuNC is accompanied by a switch to *trans*-type conformation in **14**; a similar rearrangement is observed for (η^5, η^1-$C_5Me_4SiMe_2N^tBu$)Ti{η^3-$CH_3(CH)_3CH_2BAr^F_3$}(^{t}BuNC).[27] In both **13** and **14** the Ti is no longer within bonding distance of C(24) with loss of linearity of the Ti(1)-C(24)-B(1) bond angle (121.6(2)º (**13**), 124.6(3)º (**14**)). As predicted from spectroscopic data, the agostic interactions between the $CH_2BAr^F_3$ protons and titanium are absent; stabilisation of the complex by secondary bonding interactions are no longer required due to coordination of the ^{t}BuNC ligand. The Ti(1)-C(25) (2.718(3) Å (**13**), 2.566(3) Å (**14**)) and Ti(1)-C(26) (2.430(3) Å (**13**), 2.365(3) Å (**14**)) bond lengths are longer than those observed in the base-free zwitterions (Ti(1)-C(25): 2.330(3) Å (**9**), 2.243 Å (**10**); Ti(1)-C(26): 2.374(3) Å (**9**), 2.331(5) Å (**10**)). This is suggested to be as a result of steric interactions of the aryl rings of the borate with the nearby methyl groups of the ^{t}BuNC. This effect is not noticeable for the other terminal allylic carbon (C(27)) given that it is further from the borate and ^{t}Bu moieties: similar Ti(1)-C(27) distances are seen in **9** (2.201(3) Å) and **13** (2.206(3) Å) with a shorter bond length in **14** (2.246(3) Å) than seen in **10** (2.308(5) Å). This shorter Ti(1)-C(27) distance is thought to arise from different (E-) configuration of the η^3-allyl ligand in **14**. The distances in the allyl borate are also broadly similar to those observed in (η^5, η^1-$C_5Me_4SiMe_2N^tBu$)Ti{η^3-$CH_3(CH)_3CH_2BAr^F_3$}(^{t}BuNC).[27]

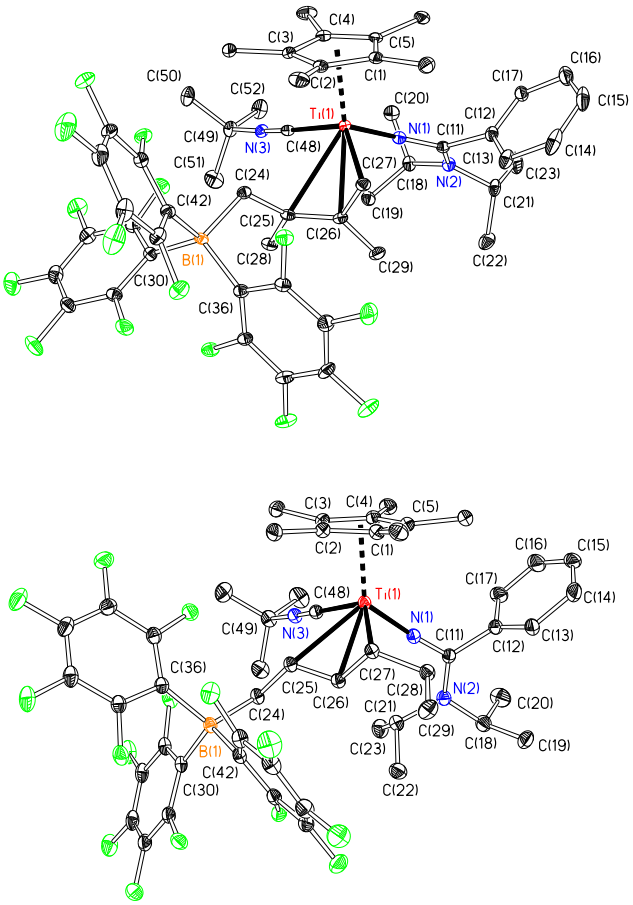

Figure 2.14. Displacement ellipsoid plots of Cp*Ti{NC(Ph)N^{i}Pr$_2$}{ η^3-$CH_2C(Me)C(Me)CH_2BAr^F{}_3$}(^{t}BuNC) (**13**) (top) and Cp*Ti{NC(Ph)N^{i}Pr$_2$}{η^3-$Et(CH)_3CH_2BAr^F{}_3$}(^{t}BuNC) (**14**) (bottom). H atoms (and toluene of crystallisation in the case of **14**) omitted for clarity. Ellipsoids are drawn at the 25% and 20% probability level for **13** and **14** respectively.

Table 2.9. Selected bond lengths (Å) and angles (º) for Cp*Ti{NC(Ph)N^{i}Pr$_2$}{ η^3-CH$_2$C(Me)C(Me)CH$_2$BAr$^{F}_3$}(^{t}BuNC) (**13**) and Cp*Ti{NC(Ph)N^{i}Pr$_2$}{η^3-Et(CH)$_3$CH$_2$BAr$^{F}_3$}(^{t}BuNC) (**14**). Cp$_{cent}$ is the computed Cp* ring carbon centroid.

Parameter	**13**	**14**	Parameter	**13**	**14**
Ti(1)-Cp$_{cent}$	2.08	2.08	Cp$_{cent}$-Ti(1)-C(27)	109.9	108.9
Ti(1)-N(1)	1.848(2)	1.827(2)	Cp$_{cent}$-Ti(1)-C(48)	105.7	105.4
N(1)-C(11)	1.294(4)	1.297(4)	Ti(1)-N(1)-C(11)	164.5(2)	175.9(2)
N(2)-C(11)	1.359(3)	1.359(4)	N(1)-Ti(1)-C(25)	108.95(9)	110.90(10)
N(3)-C(48)	1.162(4)	1.146(4)	N(1)-Ti(1)-C(26)	91.17(10)	91.15(10)
Ti(1)-C(25)	2.718(3)	2.566(3)	N(1)-Ti(1)-C(27)	99.43(10)	95.34(11)
Ti(1)-C(26)	2.430(3)	2.365(3)	C(25)-Ti(1)-C(26)	30.47(9)	32.03(9)
Ti(1)-C(27)	2.206(3)	2.246(3)	C(25)-Ti(1)-C(27)	58.91(9)	61.25(9)
Ti(1)-C(48)	2.176(3)	2.171(3)	C(26)-Ti(1)-C(27)	35.77(9)	35.56(10)
C(24)-C(25)	1.511(4)	1.495(4)	Ti(1)-C(25)-C(26)	63.16(14)	65.89(15)
C(25)-C(26)	1.381(4)	1.374(4)	Ti(1)-C(26)-C(25)	86.36(16)	82.08(17)
C(26)-C(27)	1.440(4)	1.413(4)	Ti(1)-C(26)-C(27)	63.59(14)	67.62(15)
C(24)-B(1)	1.689(4)	1.655(4)	Ti(1)-C(27)-C(26)	80.64(15)	76.82(15)
C(30)-B(1)	1.659(4)	1.661(4)	C(24)-C(25)-C(26)	123.6(2)	123.5(3)
C(36)-B(1)	1.658(4)	1.665(4)	Ti(1)-C(24)-B(1)	121.6(2)	124.6(3)
C(42)-B(1)	1.662(4)	1.646(4)	B(1)-C(24)-C(25)	115.2(2)	111.6(2)
Cp$_{cent}$-Ti(1)-N(1)	118.1	128.8	C(24)-B(1)-C(30)	115.7(2)	109.9(2)
Cp$_{cent}$-Ti(1)-C(25)	133	120.3	C(24)-B(1)-C(36)	104.4(2)	114.0(2)
Cp$_{cent}$-Ti(1)-C(26)	141.4	133.8	C(24)-B(1)-C(42)	108.4(2)	104.0(2)

The Ti(1)-C(48) (2.176(3) Å (**13**), 2.171(3) Å **(14)**) bond lengths are comparable to to those of the related isonitrile compounds $[Cp_2Ti\{\eta^2\text{-}C(N^tBu)Me\}(^tBuNC)]^+$ (2.192(6) Å),[39] $Cp^*_2Ti\{\eta^2\text{-}C(N^tBu)CH_2CH_2\text{-}CORe_2(CO)_9\}(^tBuNC)$ (2.17(2) Å)[43] and (η^5, η^1-$C_5Me_4SiMe_2N^tBu)Ti\{\eta^3\text{-}CH_3(CH)_3CH_2BAr^F_3\}(^tBuNC)$.[27] The N(3)-C(48) (1.162(4) Å (**13**), 1.146(4) Å (**14**)) distances are also typical of coordinated isonitriles (*ca.* 1.16Å).[27, 39, 40]

Steric effects must also account for the slightly longer Ti(1)-Cp^*_{cent} distances (2.08 Å) in the adducts as compared with the base-free compounds. The Ti-N(1) bond length in **13** (1.848(2) Å) is similar to that seen in **9** (1.855(2) Å) while the distance observed in **14** (1.827(2) Å) is actually shorter than in **10** (1.852(4) Å). This difference must partly derive from the different configuration of the allyl borate ligand. The Ti(1)-N(1)-C(11) bond angles are very similar in **13** (164.5(2)º) and **14** (175.9(2) º) to those in **10** (174.61(12)º) and **12** (169.64(15)º) (and the other structures presented in this Chapter). The N(1)-C(11) distances in the adducts (1.294(4) Å (**13**), 1.297(4) Å (**14**)) are comparable to those in the base-free complexes (1.288(4) Å (**9**), 1.268(6) Å (**10**)). Close agreement is also observed with the N(2)-C(11) bond lengths (1.374(4) Å (**9**), 1.326(7) Å (**10**), 1.359(3) Å (**13**), 1.359(4) Å (**14**)) suggesting a similar degree of amidinate π-donation to the metal centre. The intramolecular π-stacking interaction observed in the base-free zwitterions (**9-12**) evidenced by the narrowing of one of the $H_2C\text{-}B\text{-}C(Ar^F)$ angles bringing the plane of an aryl ring closer to the allylic moiety is also observed in **13** and **14**.

2.5.4 Reactions of 9 and 10 with alkynes

No reaction was observed in attempted NMR tube reactions of **9** with 2-butyne or phenylacetylene; extended heating resulted in decomposition of the zwitterion. Similarly, no reaction was observed between **10** and phenylacetylene but reaction with 2-butyne resulted in a slow colour change from dark green to red after 3 days at room temperature. The ^1H NMR spectrum confirmed complete reaction of the zwitterion although the complexity of the spectrum precluded identification of major product(s) of the reaction.

2.5.5 Cross-over reactions with diene complexes (5 and 6) and zwitterions (9 and 10)

The reformation of **5** from the adduct **13** (Scheme 2.6) suggests a degree of diene-zwitterion reversability which was further explored by way of NMR tube cross-over experiments. Equivalent quantities of **6** and **9** were combined in C_6D_6 resulting in immediate conversion to **5** and **10** at room temperature as observed in the ^{1}H and ^{19}F NMR spectra. The room temperature ^{1}H NMR spectra for isolated **5**, **10** and for the products of mixing **6** and **9** in C_6D_6 at room temperature are shown in Figure 2.15. No reaction was observed upon mixing stoichiometric quantities of **5** and **10**. These observations are summarised in Equation 2.6.

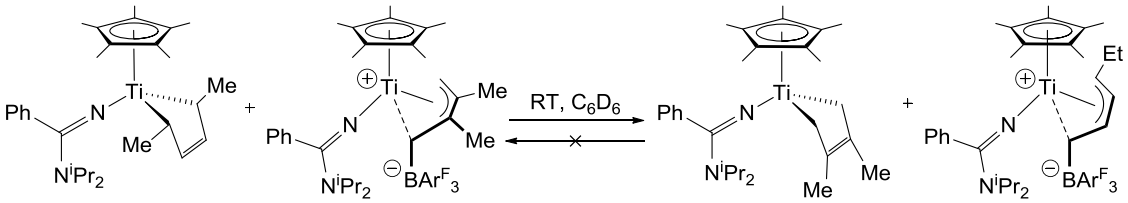

6 **9** **5** **10**

Equation 2.6

This result not only appears to support the hypothesized reversibility of the reaction between the diene complex and BAr^F_3 but appears to suggest greater stability of **10** compared to **9** with respect to the reverse reaction reforming the diene precatalyst.

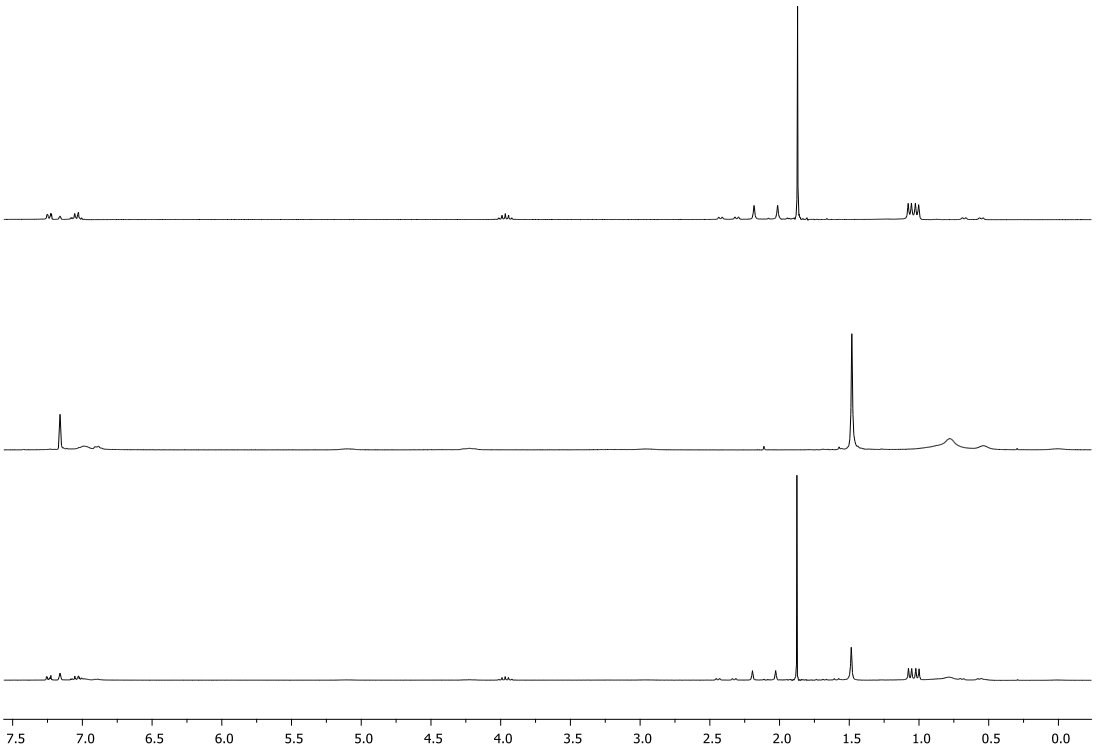

Figure 2.15 ^{1}H NMR spectra (299.9 MHz, 293 K) of Cp*Ti{NC(Ph)N^{i}Pr$_2$}(η-2,3-$C_4H_4Me_2$) (**5**, top), Cp*Ti{NC(Ph)N^{i}Pr$_2$}{η^3-Et(CH)$_3$CH$_2$BAr$^F_3$} (**10**, middle) and the products observed by reaction of **6** and **9** (bottom). Residual protio-solvent, δ = 7.16 ppm.

2.5.6 Variable temperature ^{19}F NMR experiments with 9 and 10

Comparison between the stabilities of **9** and **10** with respect to diene reformation was also examined qualitatively by variable temperature ^{19}F experiments. Heating **9** in the presence of one equivalent of BAr$^F_3$ results in significant broadening of the free borane ^{19}F resonances above *ca.* 60 ºC indicating exchange of free and associated borane. However, heating to 90 ºC is required in order to see any appreciable line broadening of the ^{19}F signals when **10** is heated in the presence of BAr$^F_3$. The kinetic barrier to reformation of the diene complex appears higher for **10** compared to **9**. The more facile dissociation of BAr$^F_3$ in **9** may well be as a result of steric interactions between the borane aryl rings and the diene methyl substituents (which also serve to restrict rotation about the B-CH$_2$ bond in **9**).

2.6 Cyclopentadienyl-guanidinate titanium diene and zwitterionic complexes

2.6.1 Synthesis of Cp*Ti{NC(NMe$_2$)$_2$}Cl$_2$ (15)

Recently LANXESS Elastomers have assessed κ^1-guanidinates as potential supporting ligands in half-sandwich titanium copolymerisation precatalysts.[44] It was deemed a logical step to attempt to extend the scope of the diene and zwitterion chemistry to these new precatalysts in parallel with development of understanding of the underlying alkyl cation chemistry of these systems.[45] The synthetic route to the half-sandwich dichlordes is straightforward and commercially available ligands may be employed such as 1,1,3,3-tetramethylguanidine. *In situ* deprotonation of this protio-guanidine with ^{n}BuLi followed by reaction with Cp*TiCl$_3$ gives the guanidinate complex, Cp*Ti{NC(NMe$_2$)$_2$}Cl$_2$ (**15**) in good yield (87 %) (Scheme 2.7).

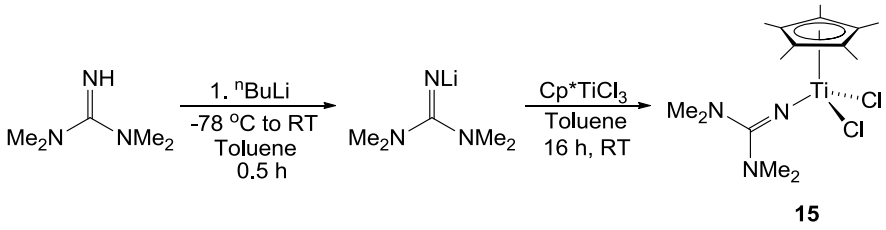

Scheme 2.7. Synthesis of Cp*Ti{NC(NMe$_2$)$_2$}Cl$_2$ (**15**).

Compound **15** has been fully characterised by NMR and IR spectroscopy, EI mass spectrometry and elemental analysis in collaborative work involving the author and Mr Adam Russell.[45] The room temperature ^{1}H NMR spectrum of **15** is straightforward due to fast rotation about Ti-N and C-NMe$_2$ bonds: two singlets are observed at 2.34 and 2.09 ppm corresponding to the guanidinate and Cp* methyl protons respectively. Compound **15** was further characterised by single crystal X-ray diffraction. Single crystals were grown from a benzene solution at room temperature. The molecular structure is shown in Figure 2.16 and full crystallographic data can be found in the CD appendix. Selected distances and angles are listed in Table 2.10.

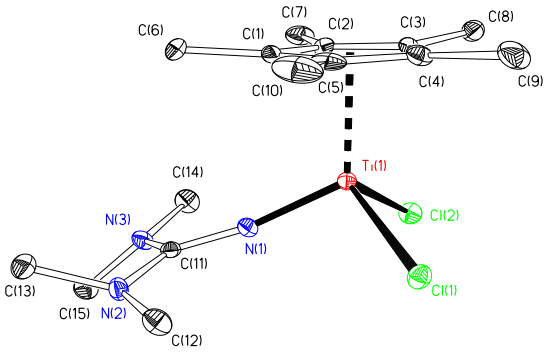

Figure 2.16. Displacement ellipsoid plot (20% probability) of Cp*Ti{NC(NMe$_2$)$_2$}Cl$_2$ (**15**). H atoms omitted for clarity.

The monomeric structure of **15** exhibits similar three-legged piano stool, *pseudo*-tetrahedral coordination around titanium to that observed in the half-sandwich κ^1-amidinate dichloride complexes **2** and **3**. The coordinated guanidinate is largely planar but with one of the NMe$_2$ groups twisted slightly out of the plane which appears similar to the perpendicular orientation of the phenyl ring with respect to the N=C-N^{i}Pr$_2$ plane in **2** and **3**. The molecular structure of **15** exhibits the linear Ti(1)-N(1)-C(11) bond angle (170.3(3)°) also observed in titanium cyclopentadienyl-amidinate dichloride complexes **2** (160.10(11)°) and **3** (165.2(3)°), suggesting a metal-amidinate dπ-pπ contribution to the bonding as discussed above. Similar Ti(1)-N(1) distances are observed in **15** (1.782(3) Å) and the amidinate dichlorides **2** (1.7855(13) Å) and **3** (1.800(3) Å). The N(1)-C(11) bond length in **15** (1.324(5) Å) is also comparable to that observed in **3** (1.310(4) Å) and the N(1)-C(6) distance (1.315(2) Å) in **2**. Similarly, the N(2)-C(11) (1.361(5) Å) and N(3)-C(11) (1.357(5) Å) guanidinate distances are comparable to, if slightly longer than the N(2)-C(11) (1.340(4) Å) and N(2)-C(6) (1.3279(19) Å) bond lengths observed in **3** and **2** respectively. The calculated Ti(1)-Cp$_{cent}$ distances for all three complexes **2**, **3** and **15** are the same (2.05 Å). Overall, judging by the similarities between the structure of **15** with those of **2** and **3**, it may be surmised that the electronic properties of the guanidinate are akin to those of the κ^1-amidinate ligand.

Table 2.10. Selected bond lengths (Å) and angles (°) for Cp*Ti{NC(NMe$_2$)$_2$}Cl$_2$ (**15**). Cp$_{cent}$ is the computed Cp* ring carbon centroid.

Ti(1)-Cp$_{cent}$	2.05	Cp*$_{cent}$-Ti(1)-Cl(1)	114.9
Ti(1)-Cl(1)	2.3181(11)	Cp*$_{cent}$-Ti(1)-Cl(2)	114.2
Ti(1)-Cl(2)	2.3149(11)	Cp*$_{cent}$-Ti(1)-N(1)	117.5
Ti(1)-N(1)	1.782(3)	Ti(1)-N(1)-C(11)	170.3(3)
N(1)-C(11)	1.324(5)	N(1)-Ti(1)-Cl(1)	102.87(11)
N(2)-C(11)	1.361(5)	N(1)-Ti(1)-Cl(2)	103.45(11)
N(3)-C(11)	1.357(5)	Cl(1)-Ti(1)-Cl(2)	101.91(4)

The structure of **15** compares closely to the cyclic guanidinate-supported half-sandwich titanium dichloride complex, CpTi{Ph$_2$(CH$_2$N)$_2$C=N}Cl$_2$, reported by Kretschmer *et al*: the short Ti-N$_{C=N}$ (1.792(2) Å) bond length combined with the N$_{amine}$-C$_{C=N}$ bonds being *ca.* 0.1 Å shorter than the N$_{amine}$-C$_{ring}$ distances are suggested to be indicative of significant guanidinate π-donation.[46] More extensive π-bonding is observed with the related half-sandwich cyclopentadienyl-imidazolin-2-iminato titanium complexes; enhanced donation from the unsaturated cyclic imidazolin-2-iminato ligand results in shorter Ti-N$_{C=N}$ bond lengths (1.765(3)-1.778(2) Å) than observed in **15** and the Kretschmer guanidinate complexes.[46-48]

2.6.2 Synthesis of Cp*Ti{NC(NMe$_2$)$_2$}(η-1,4-C$_4$H$_4$Me$_2$) (16)

As in the synthesis of diene compounds **6** and **8**, the half-sandwich dichloride complex **15** was reduced with two equivalents of ^{n}BuLi in the presence of excess 2,4-hexadiene affording Cp*Ti{NC(NMe$_2$)$_2$}(η-1,4-C$_4$H$_4$Me$_2$) (**16**) in moderate isolated yield (43 %). Compound **16** has been fully characterised by NMR and IR spectroscopy, EI mass spectrometry and elemental analysis. The room temperature ^{1}H NMR spectrum in C$_6$D$_6$ is shown in Figure 2.17. The spectrum reveals the presence of peaks corresponding to two isomers with the ratio of the major to minor isomer (*ca.* 3:1) being greater than observed for diene complexes **6** and **7**. The signals for the guanidinate and Cp* methyl groups for the dominant isomer are observed at 2.24 and 1.93 ppm respectively; free-rotation about the Ti-N bond results in time-averaged C$_s$-symmetry of the molecule. The diene proton resonances of the major isomer are observed at 5.32 and 1.57 ppm and are assigned to the vinylic protons of the central diene carbons and the protons on the peripheral carbons adjacent to titanium respectively. The diene methyl protons are observed as a doublet at 1.87 ppm. Two

singlets corresponding to the guanidinate and Cp* methyl groups of the minor isomer are observed at 2.56 and 1.79 ppm respectively; the doublet for the diene methyl groups is located at 2.06 ppm. The multiplet corresponding to the vinylic diene protons is shifted slightly upfield (4.22 ppm) in comparison to the signal for the major isomer. The diene protons adjacent to titanium are observed at higher chemical shift (1.57 ppm) in comparison to the corresponding resonance for the dominant isomer.

A two-dimensional ROESY experiment was used in order to assign the isomers as supine and prone as in the cases of **5** and **6**. Through-space correlations are observed for the major isomer between the Cp* protons and the diene methyl protons as well as with the diene protons adjacent to titanium. The dominant isomer is therefore assigned as supine similarly to the amidinate-supported diene complexes **5**-**8**. The minor isomer is thought to be the prone isomer; a through-space correlation between the diene and guanidinate methyl groups was observed but a cross-peak with the Cp* protons was not. It was attempted to grow single crystals of both isomers but only the major supine isomer was crystallographically characterised (*vide infra*).

The resonances in the ^{13}C spectrum corrsponding to the diene carbons adjacent to titanium were assigned using a two-dimensional HSQC experiment: 73.1 (supine) and 70.3 (prone) ppm. The $^{1}J_{CH}$ coupling constant was measured for both isomers using a proton-coupled ^{13}C spectrum (Figure 2.17, inset). It was anticipated that the coupling constants might be different reflecting different extents of reduction of titanium depending on the isomer.[21] However, the coupling constant for each isomer was found to be 138.5 Hz. This value is slightly smaller than for **5** (145 Hz) perhaps indicating greater reduction of the diene in the guanidinate complex.

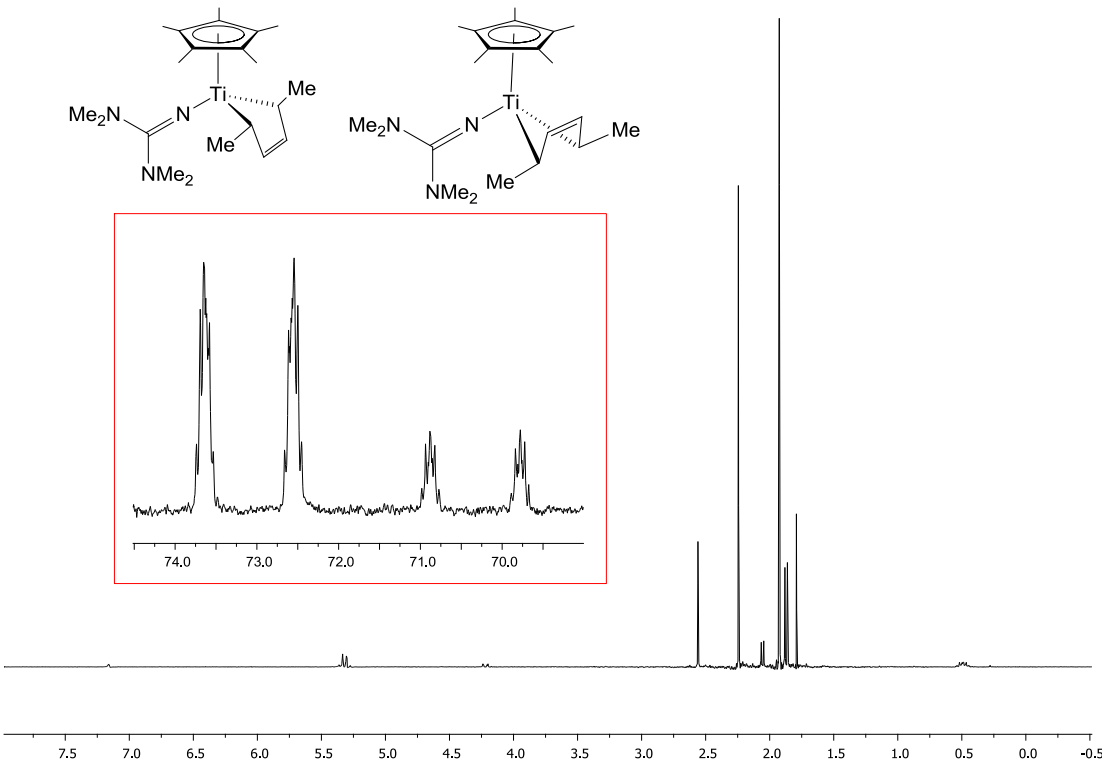

Figure 2.17. ^{1}H NMR spectrum (299.9 MHz, 293 K) of the (**16**) in C_6D_6. Residual protio-solvent, δ = 7.16 ppm. The inset illustrates the ^{13}C (proton-coupled) spectrum (125.7 MHz) between 69.0 and 72.5 ppm.

2.6.3 Synthesis of Cp*Ti{NC(NMe$_2$)$_2$}{η^3-Et(CH)$_3$CH$_2$BAr$^F_3$} (17)

For comparison with the reactivity of the amidinate-supported diene complexes with BAr$^F_3$, Cp*Ti{NC(NMe$_2$)$_2$}{η^3-Et(CH)$_3$CH$_2$BAr$^F_3$} (**17**) was similarly prepared by stoichiometric reaction of **16** with BAr$^F_3$ (Equation 2.7). As observed with compounds **10** and **12**, a rearrangment results in the borate being linked to the allylic moiety *via* a newly-formed methylene group.

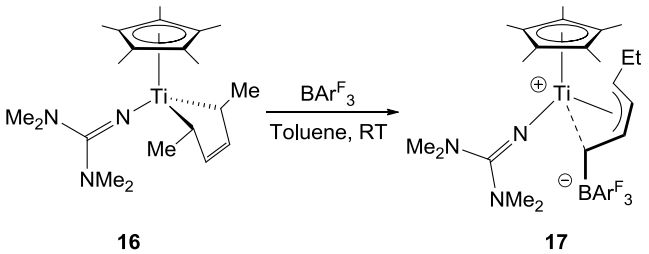

Equation 2.7

Compound **17** has been fully characterised by NMR and IR spectroscopy, EI mass spectrometry and elemental analysis. The room temperature ^{1}H NMR spectrum in

C_6D_6 shows the single resonance corresponding to the Cp* protons at 1.49 ppm with two singlets at 2.33 and 2.15 ppm for the guanidinate methyl groups suggesting restricted rotation about the Ti-N bond due to steric interactions of the guanidinate and allyl borate ligands. The central allylic proton is observed as a double doublet at 5.35 ppm with the allylic protons adjacent to the $CH_2BAr^F_3$ and ethyl groups being observed at 4.07 and 3.34 ppm respectively. The ethyl group protons correspond to a multiplet at 1.36 ppm (CH_2) and a triplet at 0.87 ppm (CH_3). The methylene protons adjacent to the borate are observed as broad signals at 1.25 and -0.48 ppm. As with zwitterions **9**-**12**, these hydrogens are expected to interact agostically with the metal centre. This was confirmed by structural characterisation of **17** (*vide infra*). Fast rotation about the B-CH_2 bond results in observation of three separate multiplets at -132.1, -160.8 and -165.0 ppm in the room temperature ^{19}F NMR spectrum corresponding to the *ortho, para* and *meta* aryl fluorines respectively. The ^{11}B NMR spectrum shows the expected sharp singlet for tetra-coordinate boron at -12.7 ppm.

2.6.4 X-ray structures of 16 and 17

Compounds **16** and **17** were further characterised by single crystal X-ray diffraction. Single crystals of **16** and **17** suitable for X-ray diffraction were grown from benzene solutions at room temperature. The molecular structures are shown in Figure 2.18 and full crystallographic data can be found in the CD appendix. Selected distances and angles are listed in Tables 2.11 and 2.12.

The molecular structure of **16** is consistent with the spectroscopic data for the major isomer in solution: the diene ligand is coordinated is a *cis* fashion and adopts the supine conformation in the solid state. The C-C bonding sequence in the coordinated diene in **16** suggests metallocyclopentene character with the central C-C bond length (1.399(3) Å) being similar to one (1.413(3) Å) and slightly shorter than the other of the peripheral C-C bonds (1.419(3) Å). This behaviour is observed in the amidinate diene complexes **5**-**8** which also adopt the supine conformation in the solid state. The Ti(1)-C(16) and Ti(1)-C(19) bond lengths in **16** (2.223(2), 2.2122(19) Å) are similar to the corresponding Ti(1)-C(24) and Ti(1)-C(27) oberved in **6** (2.216(2), 2.209(2) Å).

The Ti-Cp_{cent} distance (2.07 Å) is typical for Ti(+4) half-sandwich complexes and similar to that observed for **15**. As observed for diene complexes **5**-**8**, in spite of the formal oxidation state of the metal being +2, the diene ligand displays significant σ-

bound dianionic character in **16** with the metal oxidation state lying closer to the +4 limit.

The Ti(1)-N(1)-C(11) bond angle of the κ^1-guanidinate ligand (176.40(16)°) in **16** is close to that observed in **15** (170.3(3)°). The N(1)-C(11) bond length in **16** (1.8820(16) Å) is comparable to that observed in **6** (1.8761(17) Å) but significantly longer than that observed in the dichloride complex, **15** (1.782(3) Å). Combined with a shorter N(1)-C(11) distance in **16** (1.264(3) Å) in comparison to **15** (1.324(5) Å) and longer N(2)-C(11) and N(3)-C(11) distances in **16** (1.410(3), 1.449(3) Å) than in **15** (1.361(5), 1.357(5) Å), the degree of guanidinate π-donation appears markedly diminished in **16** compared to **15**. A similar effect was noted for the amidinate diene complexes (**5**-**8**) in comparison to the dichloride (**2**, **3**) and dimethyl (**4**) complexes (*vide supra*).

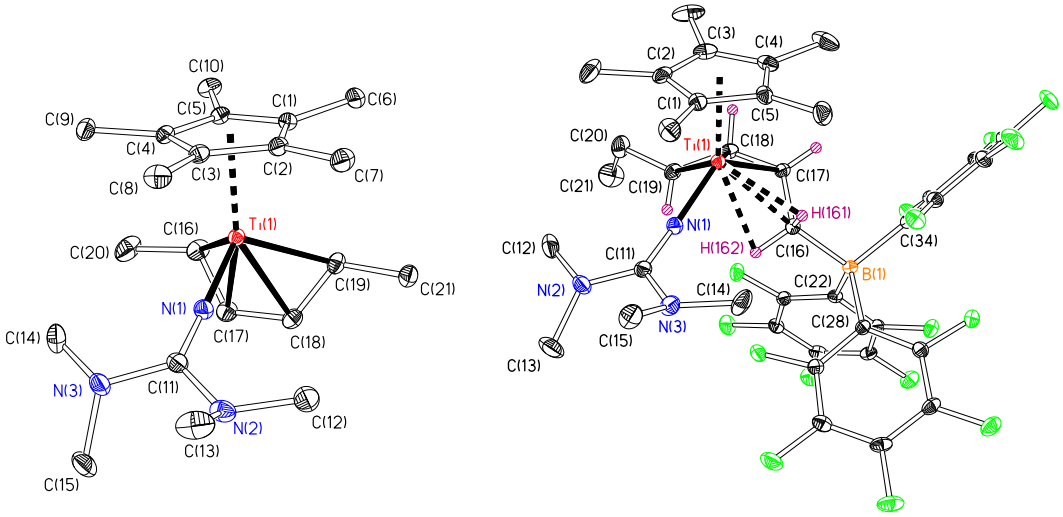

Figure 2.18. Displacement ellipsoid plots of Cp*Ti{NC(NMe$_2$)$_2$}(η-1,4-C$_4$H$_4$Me$_2$) (**16**) (left) and Cp*Ti{NC(NMe$_2$)$_2$}{η^3-Et(CH)$_3$CH$_2$BAr$^F_3$} (**17**) (right). H atoms omitted for clarity. Ellipsoids are drawn at the 20% probability level.

Table 2.11. Selected bond lengths (Å) and angles (°) for Cp*Ti{$NC(NMe_2)_2$}(η-1,4-$C_4H_4Me_2$) (**16**). Cp_{cent} is the computed Cp* ring carbon centroid.

Ti(1)-Cp_{cent}	2.07	Ti(1)-C(19)	2.2122(19)
Ti(1)-N(1)	1.8820(16)	Ti(1)-C(17)	2.299(2)
N(1)-C(11)	1.264(3)	Ti(1)-C(18)	2.299(2)
N(2)-C(11)	1.410(3)	C(16)-C(17)	1.413(3)
N(3)-C(11)	1.449(3)	C(17)-C(18)	1.399(3)
Ti(1)-C(16)	2.223(2)	C(18)-C(19)	1.419(3)
Cp_{cent}-Ti(1)-N(1)	113.1	C(16)-Ti(1)-C(19)	83.50(8)
Cp_{cent}-Ti(1)-C(16)	115.9	Ti(1)-C(16)-C(17)	74.75(12)
Cp_{cent}-Ti(1)-C(19)	115.0	Ti(1)-C(19)-C(18)	75.01(11)
Ti(1)-N(1)-C(11)	176.40(16)	C(16)-C(17)-C(18)	123.2(2)
N(1)-Ti(1)-C(16)	113.73(9)	C(17)-C(18)-C(19)	123.34(19)
N(1)-Ti(1)-C(19)	112.50(7)		

The molecular structure of **17** is consistent with the spectroscopic data and the structures of the related zwitterions **10** and **12**. The rearrangement observed for **10** and **12** is also confirmed crystallographically for **17**. Similarly to **10** and **12**, the prone-type conformation predicted from the ROESY spectrum of **17** is also observed in the solid state.

As with the amidinate-supported zwitterions, **9**-**12**, the distances between the terminal η^3-allyl carbons (C(17) and (C(19)) and titanium (2.317(4) and 2.294(4) Å) are shorter than the bond length observed between titanium and the central allylic carbon (C(18)) (2.368(3) Å)). The internal C(17)-C(18) and C(18)-C(19) bond lengths of the allylic moiety (1.392(5) and 1.400(5) Å) and the C(17)-C(18)-C(19) angle (126.6(3)º) are also similar to those of **9**-**12** and published η^3-allyl complexes.[22, 25, 26] Furthermore, as observed for zwitterions **9**-**12**, the allyl moiety exhibits a *Z*-configuration with respect to the C(18)-C(19) π-bond which brings C(16) into a favourable position for agostic interactions between H(161) and H(162) and titanium. As with the amidinate-supported base-free zwitterions, the Ti(1)-H(161) and Ti(1)-H(162) bond lengths are relatively short (2.17(4) and 2.38(4) Å) and the Ti(1)-C(16)-B(1) bond angle (169.7(2)º) is fairly linear. The presence of agostic-type interactions between the $CH_2BAr^F_3$ hydrogens and titanium is therefore thought to provide stabilisation in **17** just as in the cases of **9**-**12**. The similarities also extend to the presence of an intramolecular π-stacking interaction between one of the perfluorinated aryl rings and

the allylic cation which has the effect of narrowing one of the H_2C-B-C(Ar^F) bond angles: the C(16)-B(1)-C(34) bond angle (105.0(3) º) is smaller than the C(16)-B(1)-C(22) (112.0(3)º) and C(16)-B(1)-C(28) (110.8(3)º) angles.

Table 2.12. Selected bond lengths (Å) and angles (°) for Cp*Ti{$NC(NMe_2)_2$}{η^3-$Et(CH)_3CH_2BAr^F_3$} (**17**). Cp_{cent} is the computed Cp* ring carbon centroid.

Parameter		Parameter	
Ti(1)-Cp_{cent}	2.04	N(1)-Ti(1)-C(19)	94.89(14)
Ti(1)-N(1)	1.822(3)	C(16)-Ti(1)-C(19)	83.25(12)
N(1)-C(11)	1.290(4)	C(16)-Ti(1)-C(17)	36.70(11)
N(2)-C(11)	1.358(5)	C(16)-Ti(1)-C(18)	65.21(12)
N(3)-C(11)	1.391(5)	C(17)-Ti(1)-C(18)	34.55(12)
Ti(1)-C(16)	2.413(3)	C(17)-Ti(1)-C(19)	65.48(13)
Ti(1)-H(161)	2.17(4)	C(18)-Ti(1)-C(19)	34.90(13)
Ti(1)-H(162)	2.38(4)	Ti(1)-C(16)-C(17)	68.14(18)
Ti(1)-C(19)	2.294(4)	Ti(1)-C(17)-C(16)	75.16(19)
Ti(1)-C(17)	2.317(4)	Ti(1)-C(17)-C(18)	74.7(2)
Ti(1)-C(18)	2.368(3)	Ti(1)-C(18)-C(17)	70.7(2)
C(16)-C(17)	1.492(5)	Ti(1)-C(18)-C(19)	69.7(2)
C(17)-C(18)	1.392(5)	Ti(1)-C(19)-C(18)	75.4(2)
C(18)-C(19)	1.400(5)	C(16)-C(17)-C(18)	126.6(3)
C(16)-B(1)	1.675(5)	C(17)-C(18)-C(19)	126.6(3)
Cp_{cent}-Ti(1)-N(1)	116.6	Ti(1)-C(16)-B(1)	169.7(2)
Cp_{cent}-Ti(1)-C(17)	116.4	B(1)-C(16)-C(17)	115.7(3)
Cp_{cent}-Ti(1)-C(18)	113.4	C(16)-B(1)-C(22)	112.0(3)
Cp_{cent}-Ti(1)-C(19)	122.3	C(16)-B(1)-C(28)	110.8(3)
Ti(1)-N(1)-C(11)	173.0(3)	C(16)-B(1)-C(34)	105.0(3)
N(1)-Ti(1)-C(16)	94.27(12)		

The Cp^*_{cent}-Ti distance in **17** (2.04 Å) is shorter than in the diene complex **16** (2.07 Å) (and the same as in the related zwitterion **10**) which is expected given the cationic nature of the metal. The Ti(1)-N(1) (1.822(3) Å) distance in **17** is also shorter than that observed for the diene complex **16** (1.8820(16) Å). The approximately linear geometry about N(1) persists in **17** (173.0(3)°) but the N(1)-C(11) (1.290(4) Å) distance is longer compared to **16** (1.264(3) Å) and the N(2)-C(11) distances in **17** (1.358(5), 1.391(5) Å) are shorter than those seen in **16** (1.410(3), 1.449(3) Å). This is consistent with the comparisons made between the amidinate-supported diene and

zwitterionic complexes: the data suggests slightly superior guanidinate π-donation to the cationic titanium in **17**.

2.7 EPDM copolymerisation experiments

EPDM (ethylene, propylene, dienes: 5-ethylidenebicyclo[2.2.1]hept-2-ene (ENB) and 5-vinylbicyclo[2.2.1]hept-2-ene (VNB)) copolymerisation testing of diene complexes **5**-**8** and zwitterionic complexes **9**-**12** and **14** were performed in a small-scale batch reactor under industrially relevant conditions at LANXESS Elastomers, The Netherlands. Comparison was made under the same conditions with the dimethyl complex, Cp*Ti{NC(Ph)N^{i}Pr$_2$}Me$_2$ (**4**). Activation of the dimethyl and neutral diene precatalysts was achieved with one, two and five equivalents of BAr^F_3. The zwitterionic complexes were used as single-component catalysts (overall [B]:[Ti] = 1) or with four extra equivalents of BAr^F_3 (overall [B]:[Ti] = 5). (Pre)catalysts were assessed using low (0.14 μmol) loadings in order to maintain isothermal conditions (exotherms < 3 ºC) and to reduce the possibility of mass-transport limitations. Hydrogen was also fed to the reactor together with the ethylene and propylene reactant gases in order to avoid reactor fouling by formation of too high molecular weight polymers.[49-51] Full experimental details are given in Chaper 5. Titanium complexes **7**, **8** and **12** were unproductive under these conditions. The composition of the polymers was analysed using FT-IR and the molecular weight and polydispersity index (PDI) were obtained from GPC data. The results for the active catalysts are summarised in Table 2.13.

The FT-IR data indicate fairly equal incorporation of ethylene and propylene with a slight preference for the former monomer under these conditions. The ENB and VNB incorporations are around 1.0 and 0.7 wt.% respectively. The GPC data reveal fairly high molecular weights (M_n = 100-130 kg mol^{-1}) and fairly narrow (PDI: 2.1-2.6), monomodal molecular weight distributions indicative of single-site behaviour.[52, 53] The polymer composition and molecular weights are within error regardless of the nature of the activating group. It may therefore be concluded that it is the Cp* and κ^1-amidinate supporting ligands which influence the nature of the polymer rather than an activator effect. The similar polymer properties also allow comparison of the productivities of the dimethyl, diene and zwitterionic initiators. The productivities presented in Table 2.13 are very high on the Gibson scale[54] although the temperature

profiles indicate short-lived catalysts which are very active for approximately the first four minutes but subsequently deactivate over the subsequent six minutes of the run. Diene complexes **5** and **6** are highly productive precatalysts for EPDM copolymerisation with comparable productivities to the dimethyl complex **4**. Compound **5** is slightly less productive than the dimethyl and the isomeric diene complex **6** which displays similar productivities in comparison to **4** at [B]:[Ti] ratios of 1 and 2. Slightly enhanced productivities are observed for **6** with higher cocatalyst concentrations ([B]:[Ti] = 5) in comparison to **4**. In the cases of compounds **4**, **5** and **6** the productivities increase with higher [B]:[Ti] ratios.

Zwitterionic complexes **9** and **10** are active single-component 'drop-in' catalysts with **10** being more productive than **9** which is consistent for the trend with the *in situ* activated diene complexes. The poorer productivity of the zwitterionic catalysts in comparison to the corresponding diene precatalysts, particuarly in the case of **9**, is due to the greater sensitivity of the preactivated compounds and the associated difficulties during catalyst dosing to the reactor. Just as in the cases of the diene precatalysts, the productivity of **10** is also enhanced by addition of four extra equivalents of BAr^F_3.

Table 2.13. EPDM polymerisation results[a]

(Pre)catalyst	[B]:[Ti]	Yield/ g	Productivity/ kg mol^{-1} h^{-1} bar^{-1}	Polymer Analysis					
				C2/wt.%	C3/wt.%	ENB/wt.%	VNB/wt.%	M_n/ kg mol^{-1}	M_w/M_n
4	1	7.5	46000	53.4	45.0	0.96	0.66	100	2.6
	2	9.6	59000	51.8	46.5	0.99	0.71	-	-
	5	10.1	62000	51.9	46.4	1.02	0.70	-	-
5	1	5.4	33000	53.2	45.1	1.00	0.72	120	2.3
	2	6.3	39000	53.5	44.7	1.07	0.73	-	-
	5	7.0	43000	53.5	44.8	0.98	0.70	110	2.3
9	1	2.7	17000	52.7	45.6	1.06	0.71	-	-
	5[c]	3.0	18000	54.1	44.2	1.05	0.69	-	-
6	1	8.0	49000	53.0	45.2	1.09	0.75	120	2.4
	2	10.3	63000	52.6	45.7	1.03	0.71	-	-
	5	13.0	80000	52.4	45.9	1.00	0.69	-	-
10	1	7.4	45000	58.6	39.6	1.10	0.78	120	2.3
	5[c]	8.8	54000	58.6	39.5	1.11	0.75	-	-
14	1	5.3	33000	54.0	44.3	1.03	0.72	125	2.1
	2[b]	8.9	54000	48.9	49.5	0.99	0.67	-	-
11	1	8.2	50000	58.3	39.9	1.08	0.76	130	2.4
	5[c]	7.5	46000	55.2	43.3	0.89	0.59	-	-

[a]Conditions: T= 90 °C, Pressure: 7 bar Scavenger: IBAO-65 ([Al] = 0.45 mM), 10 minute reaction time. Solvent pentamethylheptane (1 L) C_3/C_2 = 80/40, H_2 flow: 3.5 NL/h , ENB: 0.7 mL, VNB: 0.7 mL. [b]2 extra equivalents of $BAr^F{}_3$ are added. [c]4 extra equivalents of $BAr^F{}_3$ are added. All polymer yields given are reproducible to within 10 % in duplicate runs.

Overall, the data are consistent with the experiments probing the zwitterion-diene reversibility: the reformation of the inactive diene complex is more facile in the case of **9** than **10** which may help explain the poorer productivty of **5**+BAr^F_3/**9** compared to **6**+BAr^F_3/**10** due to less titanium entering the catalytic cycle in the former catalyst system. Furthermore, it helps to explain the enhanced productivities observed by the addition of extra equivalents of borane cocatalyst; even to a preactivated single-component catalyst. Comparing **10** and **11** we see similar productivities as may be expected from the structural similarities. The productivites of the ^{t}BuNC adduct (see below) **14** are also comparable as expected with those of **12**; the ^{t}BuNC dissociating under polymerisation conditions, presumably by reaction with aluminium alkyl species, to generate **12** *in situ*. With addition of an extra equivalent of BAr^F_3 ([B]:[Ti] = 2) the productivity of **14** is slightly increased probably due to more efficient generation of **10** (and ^{t}BuNC·BAr^F_3 (*vide supra*)).

The explanation for compound **7** being inactive when BAr^F_3 is employed as the cocatalyst must be partly explained by its inability, presumably due to sterics, to react cleanly with the borane to form a zwitterion as discussed in Section 2.4.5. This does not adequately rationalise the inactivity of the unsubstituted cyclopentadienyl diene complex, **8**, since it reacts immediately to form the zwitterion **12**. However, **12** is also inactive whether employed as a single-component catalyst or with added borane cocatalyst. This may be explained by deactivation processes *via* formation of amidinate-bridged dimers with titanium or aluminium permitted by less steric protection to the metal centre provided by the unsubstituted cyclopentadienyl ligand (See Chapter Three).

2.8 Summary

This Chapter has detailed the investigation of an alternative catalyst activation *via* borane activation of diene precatalysts. The protio-amidine ligand (**1**) and half-sandwich dichloride precursors (**2** and **3**) were prepared and fully characterised. Synthesis of the corresponding dimethyl precatalyst (**4**) was required in order to assess any advantage offered by the diene complexes in polymerisation testing. Furthermore, structural characterisation of compounds **1**-**4** provided an insight into the bonding of the amidinate ligand and proved useful for structural comparison with the diene and zwitterionic complexes synthesised later in the Chapter.

Synthesis of diene complexes **5**-**8** was successfully achieved making use of the ^{n}BuLi reduction method favoured by Marks.[21] Structural characterisation of all four diene complexes revealed exclusive *cis*-coordination of the diene with a supine conformation. Inspection of the bond lengths of the diene ligand suggest it is predominantly σ-bound with the oxidation state of titanium lying close to the +4 limit. Reactions of **5**, **6** and **8** with BAr^{F}_{3} afforded well-defined zwitterionic species; no such species was isolated in the case of **7** which is attributed to steric limitations imposed by the phenyl substituents of the diene. Difficulties encountered during attempts to isolate the oily 1,3-pentadiene complex (**11_INT**) were overcome by *in situ* reaction with BAr^{F}_{3} affording the zwitterion **11** as a crystalline solid. Crystal structures of all four zwitterionic complexes were obtained providing an enhanced insight into the activation of the diene precatalysts. This activation chemistry was also shown to extend to half-sandwich guanidinate complexes which are currently under investigation by LANXESS Elastomers.

Some of the underlying chemistry of the zwitterionic species was studied particularly with regard to reversibility of zwitterion formation (activation). In a series of experiments it was observed that **9** had a much greater propensity to reform **5** than the isomer **10** to reform **6**. This behaviour seemed to explain differences observed in high temperature EPDM copolymerisation testing.

Diene compounds **5** and **6** and zwitterions **9**-**11** and **14** were very highly active in EPDM copolymerisation; the zwitterions were shown to be effective single-component catalysts. Particularly surprising was the high productivity of the base-stabilised zwitterion **14** which was shown to be very robust with respect to hydrolysis. Whether activated *in situ* or employed as a preactivated zwitterion, **6** was shown to be consistently more productive than **5** which is thought to reflect the relative tendencies of activated zwitterions **9** and **10** to reform the respective inactive neutral diene complexes (**5** and **6**). Pleasingly the productivity of **6** matched that of the dimethyl complex (**4**) with the diene compound proving more productive than the dimethyl precatalyst at higher [B]:[Ti] ratios.

2.9 References for Chapter Two

1. E. G. Ijpeij, P. J. H. Windmuller, H. J. Arts, F. van der Burgt, G. H. J. van Doremaele and M. A. Zuideveld, *LANXESS ELASTOMERS, WO/2005/090418*, 2005.
2. R. T. W. Scott, Part II Thesis, University of Oxford, 2009.
3. M. A. Zuideveld, G. H. J. Doremaele, P. Mountford, R.T.W. Scott and A. Heath, *LANXESS ELASTOMERS, WO/2011/076775* 2011.
4. H. Bigmore, DPhil Thesis, University of Oxford, 2007.
5. A. Heath, DPhil Thesis, University of Oxford, 2011.
6. L. Clark, Part II Thesis, University of Oxford, 2008.
7. J. R. Hagadorn and J. Arnold, *Organometallics*, 1998, **17**, 1355-1368.
8. F. H. Allen, O. Kennard, J. J. Galloy, O. Johnson and D. G. Watson, *Chem. Des. Autom. News*, 1993, **8**, 1 & 31.
9. D. A. Fletcher, R. F. McMeeking and D. Parkin, *J. Chem. Inf. Comput. Sci.*, 1996, **36**, 746-749.
10. P. J. Wilson, A. J. Blake, P. Mountford and M. Schröder, *Chem. Commun.*, 1998, 1007-1008.
11. E. Y. X. Chen and T. J. Marks, *Chem. Rev.*, 2000, **100**, 1391-1434.
12. H. Yasuda, K. Tatsumi and A. Nakamura, *Acc. Chem. Res.*, 1985, **18**, 120-126.
13. H. Yasuda and A. Nakamura, *Angew. Chem., Int. Ed. Engl.*, 1987, **26**, 723-742.
14. K. Mashima and A. Nakamura, *J. Organomet. Chem.*, 2002, **663**, 5-12.
15. G. Erker, C. Krüger and G. Müller, in *Adv. Organomet. Chem.*, 1985, pp. 1-39.
16. H. Yasuda, Y. Kajihara, K. Mashima, K. Nagasuna, K. Lee and A. Nakamura, *Organometallics*, 1982, **1**, 388-396.
17. H. Yasuda, Y. Kajihara, K. Mashima, K. Lee and A. Nakamura, *Chem. Lett.*, 1981, **10**, 519-522.
18. U. Dorf, K. Engel and G. Erker, *Organometallics*, 1983, **2**, 462-463.
19. G. Erker, J. Wicher, K. Engel, F. Rosenfeldt, W. Dietrich and C. Krüger, *J. Am. Chem. Soc.*, 1980, **102**, 6344-6346.
20. J. Chen, Y. Kai, N. Kasai, H. Yamamoto, H. Yasuda and A. Nakamura, *Chem. Lett.*, 1987, 1545-1548.
21. D. D. Devore, F. J. Timmers, D. L. Hasha, R. K. Rosen, T. J. Marks, P. A. Deck and C. L. Stern, *Organometallics*, 1995, **14**, 3132-3134.

22. B. Temme, G. Erker, J. Karl, H. Luftmann, R. Fröhlich and S. Kotila, *Angew. Chem., Int. Ed. Engl.*, 1995, **34**, 1755-1757.
23. T. W. Graham, J. Kickham, S. Courtenay, P. Wei and D. W. Stephan, *Organometallics*, 2004, **23**, 3309-3318.
24. N. Yue, E. Hollink, F. Guérin and D. W. Stephan, *Organometallics*, 2001, **20**, 4424-4433.
25. A. H. Cowley, G. S. Hair, B. G. McBurnett and R. A. Jones, *Chem. Commun.*, 1999, 437-438.
26. G. S. Hair, R. A. Jones, A. H. Cowley and V. Lynch, *Inorg. Chem.*, 2001, **40**, 1014-1019.
27. G. S. Hair, R. A. Jones, A. H. Cowley and V. Lynch, *Organometallics*, 2000, **20**, 177-181.
28. H. Yamamoto, H. Yasuda, K. Tatsumi, K. Lee, A. Nakamura, J. Chen, Y. Kai and N. Kasai, *Organometallics*, 1989, **8**, 105-119.
29. L. J. Guggenberger, P. Meakin and F. N. Tebbe, *J. Am. Chem. Soc.*, 1974, **96**, 5420-5427.
30. C. Krüger, G. Müller, G. Erker, U. Dorf and K. Engel, *Organometallics*, 1985, **4**, 215-223.
31. Y. Kai, N. Kanehisa, K. Miki, N. Kasai, K. Mashima, H. Yasuda and A. Nakamura, *Chem. Lett.*, 1982, **11**, 1277-1280.
32. M. Brookhart, M. L. H. Green and G. Parkin, *Proceedings of the National Academy of Sciences*, 2007, **104**, 6908-6914.
33. M. Brookhart and M. L. H. Green, *J. Organomet. Chem.*, 1983, **250**, 395-408.
34. M. Brookhart, M. L. H. Green and L.-L. Wong, *Prog. Inorg. Chem.*, 1988, **36**, 1.
35. G. R. Desiraju, *Crystal Engineering: The Design of Organic Solids*, Elsevier, New York, 1989.
36. G. R. Desiraju, ed., *The Crystal as a Supramolecular Entity*, John Wiley, New York, 1996.
37. C. A. Hunter, K. R. Lawson, J. Perkins and C. J. Urch, *J. Chem. Soc., Perkin Trans. 2*, 2001, 651-669.
38. C. R. Patrick and G. S. Prosser, *Nature*, 1960, **187**, 1021-1021.
39. M. Bochmann, L. M. Wilson, M. B. Hursthouse and R. L. Short, *Organometallics*, 1987, **6**, 2556-2563.

40. M. Bochmann, L. M. Wilson, M. B. Hursthouse and M. Motevalli, *Organometallics*, 1988, **7**, 1148-1154.
41. Z. Guo, D. C. Swenson, A. S. Guram and R. F. Jordan, *Organometallics*, 1994, **13**, 766-773.
42. J. J. Eisch, A. M. Piotrowski, S. K. Brownstein, E. J. Gabe and F. L. Lee, *J. Am. Chem. Soc.*, 1985, **107**, 7219-7221.
43. K. Mashima, K. Jyodoi, A. Ohyoshi and H. Takaya, *Organometallics*, 1987, **6**, 885-887.
44. G. H. J. Doremaele, M. A. Zuideveld, V. F. Quiroga Norambuena and A. Leblanc, *LANXESS ELASTOMERS, WO/2011/054927 A1*, 2011.
45. A. F. Russell and P. Mountford, in *Unpublished Results*, 2012.
46. W. P. Kretschmer, C. Dijkhuis, A. Meetsma, B. Hessen and J. H. Teuben, *Chem. Commun.*, 2002, 608-609.
47. M. Tamm, S. Randoll, T. Bannenberg and E. Herdtweck, *Chem. Commun.*, 2004, 876-877.
48. M. Tamm, S. Randoll, E. Herdtweck, N. Kleigrewe, G. Kehr, G. Erker and B. Rieger, *Dalton Trans.*, 2006, 459-467.
49. S. W. Ewart, M. A. Parent and M. C. Baird, *J. Polym. Sci., Part A: Polym. Chem.*, 1999, **37**, 4386-4389.
50. Y. V. Kissin, R. I. Mink, T. E. Nowlin and A. J. Brandolini, *J. Polym. Sci., Part A: Polym. Chem.*, 1999, **37**, 4281-4294.
51. H. Mori, M. Endo and M. Terano, *J. Mol. Catal. A: Chem.*, 1999, **145**, 211-220.
52. P. J. Flory, *Principles of Polymer Chemistry*, Cornell University Press, 1992.
53. G. Odian, *Principles of Polymerisation*, Wiley-Interscience, 1992.
54. G. J. P. Britovsek, V. C. Gibson and D. F. Wass, *Angew. Chem., Int. Ed. Engl.*, 1999, **38**, 428-447.

Chapter Three

Titanium, zirconium and hafnium complexes supported by cyclopentadienyl and κ^1-amidinate ligands for olefin homo- and copolymerisation

3.1 Overview

This Chapter describes the syntheses, characterisation, homo- and copolymerisation capability of a congeneric series of group 4 cyclopentadienyl amidinate complexes. The preparation of both dialkyl and diene precatalysts is described with the intention of probing possible activator effects in polymerisation studies. Combined crystallographic and DFT studies of these complexes provide an insight into the nature of the amidinate-metal interaction as well as an enhanced understanding of the bonding in the diene compounds. The reactivity of the zirconium diene complexes is further explored by reactions with BAr^F_3 revealing similarities with the titanium zwitterionic species described in Chapter Two. The influence of the group 4 metal on polymer productivity and propylene incorporation in EP copolymerisation is discussed in the context of preliminary activation experiments with $[CPh_3][BAr^F_4]$. Preliminary experimental work towards compounds **18**, **21**, **24** and **27** was described in the author's Mchem Thesis.[1]

3.2 Zirconium and hafnium olefin polymerisation catalysts

The majority of early transition metal catalysts which operate under commercially relevant conditions result from activation of titanium or zirconium complexes.[2-6] The greater stability of the Hf-C bond associated with higher calculated barriers with respect to insertion hence poorer aptitude for chain propagation[7, 8] seem to have resulted in fewer reported hafnium catalysts. However, selection of the appropriate supporting ligand the insertion barrier may be minimised[7] leading to the recent successful development of post-metallocene hafnium catalysts by Mitsui[9-12] and Dow.[13-15] Of the group 4 chelated diamide complexes developed by Schrock *et al.* for the low temperature living polymerisation of 1-hexene,[16-28] the titanium congeners are inactive[17, 19] whilst the relative performance of the zirconium and hafnium systems depends primarily on stability of the active species with respect to β-hydride elimination. This is exemplified by comparison of the diaryl amido pyridine-supported complexes: borate-activation of hafnium dialkyls (possessing β-hydrogens) generates well-defined cationic species which are stable to β-hydride elimination below 10 ºC whereas the cationic zirconium species are unstable with respect to this process at 0 ºC. Activation of the zirconium dimethyl complex has also been shown to result in formation of inactive μ-Me dimeric species.[22, 24]

The group of Nomura has recently described the ethylene homo- and ethylene-octene/2-methyl-1-pentene copolymerisation capability of a series of MAO-activated half-sandwich aryl oxide-supported titanium, zirconium and hafnium complexes.[29, 30] Catalyst activity was observed to follow the trend Ti > Zr > Hf with the titanium catalyst producing higher molecular weight polymer than the heavier congeners. The titanium systems were also shown have greater affinity for the higher α-olefins. A similar activity trend is observed for borate-activated group 4 half-sandwich phosphinimide complexes: hafnium catalysts exhibit moderate activity[31] although are less active than titanium congeners.[32-34]

3.3 Synthesis of Cp*M{NC(Ph)N^{i}Pr$_2$}Cl$_2$ (M = Zr (18) or Hf (19))

As described in Chapter Two, the titanium half-sandwich amidinate dichlorides, CpTi{NC(Ph)N^{i}Pr$_2$}Cl$_2$ (**2**) and Cp*Ti{NC(Ph)N^{i}Pr$_2$}Cl$_2$ (**3**) were successfully prepared by stoichiometric reaction of the protio-amidine, HNC(Ph)N^{i}Pr$_2$ (**1**) with CpTiCl$_3$ or Cp*TiCl$_3$ respectively in the presence of an excess of Net$_3$. This approach proved unsuccessful for the synthesis of the zirconium and hafnium congeners. The silylated amidine, Me$_3$SiNC(Ph)N^{i}Pr$_2$, was similarly unreactive with Cp*ZrCl$_3$ and Cp*HfCl$_3$. Such dehalosilylation reactions have been successfully employed for synthesis of titanium phosphinimide compounds but very high temperatures and use of alkali metal fluorides were required for preparation of zirconium and hafnium complexes.[35] More convenient routes to phopshinimide complexes of the heavier group 4 elements were *via* salt metathesis.[31] Hence, a successful synthesis was devised *via* transmetallation of the magnesiated amidinate with Cp*MCl$_3$ affording Cp*M{NC(Ph)N^{i}Pr$_2$}Cl$_2$ (M = Zr (**18**) or Hf (**19**)) in good isolated yield (77-83 %). The preparation of **18** and **19** is shown in Scheme 3.1.

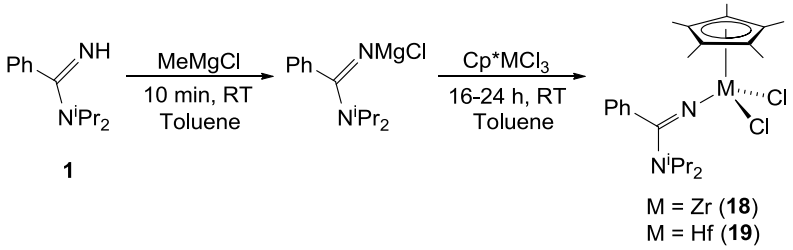

Scheme 3.1. Synthesis of Cp*M{NC(Ph)N^{i}Pr$_2$}Cl$_2$ (M = Zr (**18**) or Hf (**19**)).

Compounds **18** and **19** have been fully characterised by NMR and IR spectroscopy, EI mass spectrometry and elemental analysis. As may be expected, the ^{1}H NMR spectra

of the zironium and hafnium congeners are similar. The low temperature (-20 °C) spectrum of **19** is shown in Figure 3.1 by way of example. Just as in the cases of the titanium half-sandwich dichlorides, **2** and **3**, the room temperature ^{1}H NMR spectra in toluene-d_8 of compounds **18** and **19** show very broad signals corresponding to the *iso*-propyl protons of the amidinate due to restricted rotation about the C-N^{i}Pr$_2$ bond. Compounds **18** and **19** were characterised at -20 °C since slow rotation about the C-N^{i}Pr$_2$ bond at this temperature results in observation of considerably sharper signals for the *iso*-propyl groups. For **18** the singlet corresponding to the Cp* protons is located at 1.89 ppm and the aromatic amidinate protons are observed as a series of multiplets spanning 7.31-6.98 ppm. Two septets (3.51 and 2.95 ppm) and two doublets (1.55 and 0.56 ppm) are observed for the *iso*-propyl methine and methyl groups respectively. A two-dimensional ROESY spectrum confirmed the assignment of *cis* (3.51 and 0.56 ppm) and *trans* (2.95 and 1.55 ppm) *iso*-propyl signals with respect to the phenyl ring consistent with the assignments made for **2** and **3** (Chapter Two).

The low temperature (-20 °C) spectrum of **19** (Figure 3.1) is very similar to that of **18** as may be expected. The Cp* singlet is observed at 1.93 ppm and the aromatic amidinate protons correspond to a series of multiplets (7.30-6.99 ppm). The *iso*-propyl signals are located at 3.56 (methine, *cis*), 2.98 (methine, *trans*), 1.55 (methyl, *trans*), 0.60 (methyl, *cis*) ppm.

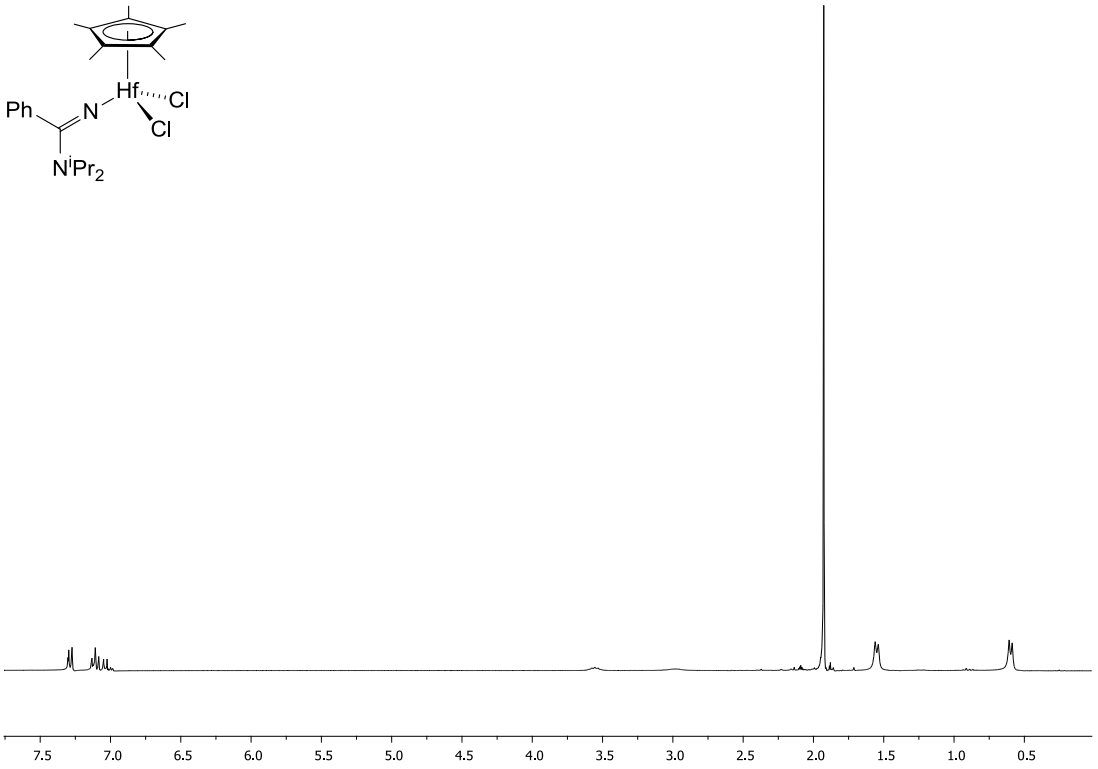

Figure 3.1. ^{1}H NMR spectrum (299.9 MHz, 253 K) of Cp*Hf{NC(Ph)N^{i}Pr$_2$}Cl$_2$ (**19**) in toluene-d_8.

3.3.1 X-ray structures of Cp*M{NC(Ph)N^{i}Pr$_2$}Cl$_2$ (M = Zr (18) or Hf (19))

Compounds **18** and **19** were further characterised by single crystal X-ray diffraction. Single crystals suitable for X-ray diffraction analysis were grown from toluene (**18**) and n-hexanes (**19**) solutions at room temperature. The structures of **18** and **19** are isomorphous, consistent with the chemical similarities of zirconium and hafnium. The molecular structure of **19** is shown in Figure 3.2 and full crystallographic data can be found in the CD appendix. Selected bond lengths and angles of **18** and **19** are presented in Table 3.1.

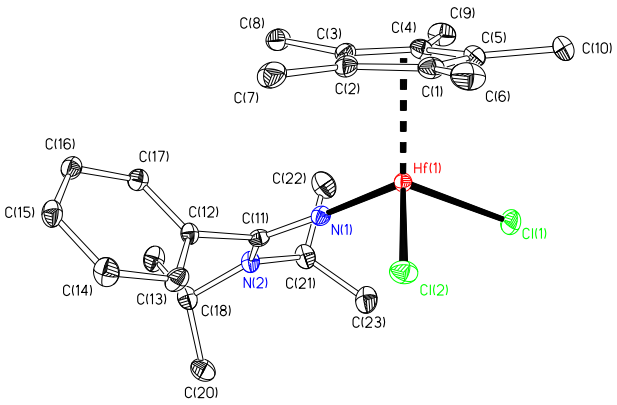

Figure 3.2. Displacement ellipsoid plot (20% probability) of $Cp^*Hf\{NC(Ph)N^iPr_2\}Cl_2$ (**19**, left). H atoms omitted for clarity.

The molecular structures of **18** and **19** are consistent with the low temperature NMR data and the structure of the titanium congener (**3**). The M(1)-Cp^*_{cent} bond lengths of compounds **3** (2.05 Å), **18** (2.19 Å) and **19** (2.17 Å) reflect the increase in ionic radius from titanium to zirconium followed by the slight decrease to hafnium due to the effect of the lanthanide contraction. This is further exemplified in the M(1)-N(1) bond lengths (1.800(3) Å (**3**), 1.943(6) Å (**18**), 1.930(4) Å (**19**)) and the M-Cl distances. In spite of the increased M(1)-N(1) bond length in **18** and **19**, coupled with poorer energy match between the nitrogen 2p and 4d/5d metal orbitals, the extent of the metal-amidinate π-interaction does not appear significantly diminished evidenced by similar N(1)-C(11) (1.310(4) Å (**3**), 1.286(9) Å (**18**), 1.298(6) Å (**19**)) and N(2)-C(11) (1.340(4) Å (**3**), 1.363(9) Å (**18**), 1.356(5) Å (**19**)) distances in **18** and **19** compared to **3**. The linearity of the M(1)-N(1)-C(11) bond angles (162.9(5)° (**18**), 163.8(3)° (**19**)) is also indicative of some degree of dπ-pπ bonding in **18** and **19**.

Table 3.1. Selected bond lengths (Å) and angles (°) for Cp*M{NC(Ph)N^{i}Pr$_2$}Cl$_2$ (M = Ti (**3**), Zr (**18**), Hf (**19**)). Cp$_{cent}$ is the computed Cp* ring carbon centroid.

Parameter	**3**	**18**	**19**
M(1)-Cp$_{cent}$	2.05	2.19	2.17
M(1)-Cl(1)	2.3137(11)	2.423(2)	2.3987(12)
M(1)-Cl(2)	2.3051(11)	2.4222(19)	2.3914(12)
M(1)-N(1)	1.800(3)	1.943(6)	1.930(4)
N(1)-C(11)	1.310(4)	1.286(9)	1.298(6)
N(2)-C(11)	1.340(4)	1.363(9)	1.356(5)
Cp$_{cent}$-M(1)-N(1)	118.0	114.9	116.1
Cp$_{cent}$-M(1)-Cl(1)	113.5	113.9	114.1
Cp$_{cent}$-M(1)-Cl(2)	115.0	112.9	113.3
M(1)-N(1)-C(11)	165.2(3)	162.9(5)	163.8(3)
N(1)-M(1)-Cl(1)	102.93(10)	105.45(18)	104.66(11)
N(1)-M(1)-Cl(2)	104.21(10)	105.39(18)	104.77(12)
Cl(1)-M(1)-Cl(2)	101.24(4)	103.29(8)	102.44(5)

Several other early transition metal κ^1-amidinate complexes have been structurally characterised in the literature.[36-41] Of particular interest in this case are the zirconium half-sandwich carborane complexes mentioned in Chapter One, {[η^5, σ-Me$_2$C(C$_5$H$_4$)(C$_2$B$_{10}$H$_{10}$)]Zr[μ-N=C(Ph)N(Me)(CH$_2$)$_3$N(Me)(Ph)C=N]}$_2$ (in which the κ^1-amidinates are the termini of bridges between the zirconium centres in the bimetallic complex)[38] and [η^5, σ-Me$_2$C(C$_9$H$_6$)(C$_2$B$_{10}$H$_{10}$)]Zr[N=C(Ph)NMe$_2$]$_2$,[39] both formed from insertion of benzonitrile into Ti-NMe$_2$ bonds. Along with the approximate linearity of the C-N-Zr bonds (154.0(3)-169.1(6)°), the Zr-N (1.958(9)-1.972(2) Å), amidinate N=C (1.274(9)-1.317(12) Å) and C-NR$_2$ (1.329(12)-1.388(10) Å) bond lengths are comparable to those observed in **18** and **19** in spite of the different supporting ligands and amidinate substituents.

3.4 Synthesis of group 4 half-sandwich amidinate dialkyl precatalysts

Dialkyl complexes are often employed as precatalysts in combination with various cocatalysts.[42] A congeneric series of group 4 half-sandwich amidinate dialkyl complexes was prepared in order to assess the influence of changes in size and electronic properties of the metal on polymerisation performance and polymer properties. In particular it was hoped to develop an understanding of the effect of the more open metal centre expected for zirconium and hafnium congeners on propylene

incorporation in EP copolymerisation. Both dimethyl and dibenzyl complexes were synthesised for evaluation of potential activator effects under industrially relevant polymerisation conditions.

3.4.1 Synthesis of CpTi{NC(Ph)N^{i}Pr$_2$}Me$_2$ (20)

Similarly to the synthesis of Cp*Ti{NC(Ph)N^{i}Pr$_2$}Me$_2$ (**4**), addition of two equivalents of MeLi to CpTi{NC(Ph)N^{i}Pr$_2$}Cl$_2$ (**2**) affords CpTi{NC(Ph)N^{i}Pr$_2$}Me$_2$ (**20**) in reasonable isolated yield (57 %) (Equation 3.1). Compound **20** has been fully characterised by NMR and IR spectroscopy, EI mass spectrometry and elemental analysis. Due to familiar broadening of the *iso*-propyl signals at room temperature, compound **20** was characterised by ^{1}H and ^{13}C NMR at -40 °C. The low temperature spectrum displays the expected signals corresponding to the Cp protons (5.80 ppm) with the aromatic amidinate resonances appearing as a series of overlapping multiplets spanning the range 7.01-6.84 ppm. The two *iso*-propyl groups assigned as *cis* and *trans* to the phenyl ring correspond to septets at 3.42 (*cis*) and 2.97 (*trans*) ppm and doublets at 1.85 (*trans*) and 0.61 (*cis*) ppm. A singlet located at 0.75 ppm is observed for the methyl ligands.

3.4.2 Synthesis of Cp*M{NC(Ph)N^{i}Pr$_2$}Me$_2$ (M = Zr (21) or Hf (22))

Likewise, the zirconium and hafnium dimethyl complexes, **21** and **22** respectively, were prepared by reaction of the half-sandwich dichloride with two equivalents of MeLi or MeMgCl in moderate isolated yield (40-49 %) (Equation 3.1); slightly superior yields were noted with the former. Conversion to the dimethyl compounds appears quantitative when tested in NMR tube-scale reactions; the isolated yields are lower due to the highly soluble nature of **21** and **22**.

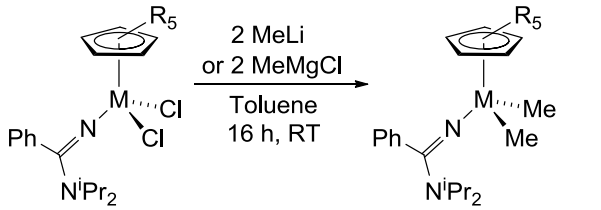

M = Ti; R = H (**2**)
M = Zr; R = Me (**18**)
M = Hf; R = Me (**19**)

M = Ti; R = H (**20**)
M = Zr; R = Me (**21**)
M = Hf; R = Me (**22**)

Equation 3.1

Compounds **21** and **22** have been fully characterised by NMR and IR spectroscopy, EI mass spectrometry and elemental analysis. As with **20**, compounds **21** and **22** were characterised by NMR at low temperature (-40 to -50 °C); restricted rotation about the C-N^{i}Pr$_2$ bond results in broadening of the *iso*-propyl signals at room temperature. The low temperature spectra of **21** and **22** in toluene-d_8 are very similar to that of the titanium congener, **4**. Comparable chemical shifts are observed for the Cp* methyl group singlets (1.88 ppm (**21**); 1.90 ppm (**22**)) and multiplets corresponding to the aromatic amidinate protons (7.19-6.98 ppm (**21**); 7.21-6.97 ppm (**22**)). As with **4**, two sets (*cis* and *trans* with respect to the amidinate phenyl group) of *iso*-propyl signals are observed in the slow C-N^{i}Pr$_2$ rotation regime: the methine septets (3.56 (*cis*) and 2.84 (*trans*) ppm (**21**); 3.59 (*cis*) and 2.87 (*trans*) ppm (**22**)) and methyl doublets (1.72 (*trans*) and 0.60 (*cis*) (**21**); 1.68 (*trans*), 0.62 (*cis*) ppm (**22**)) being observed at similar chemical shifts for both zirconium and hafnium congeners. The signals for the Me ligand protons are observed at 0.29 and 0.10 ppm for **21** and **22** respectively; an HSQC experiment allowed assignment of the corresponding signals in the ^{13}C NMR spectrum (35.6 ppm (**21**), 45.2 ppm (**22**)). Not only are there slight differences in the chemical shifts associated with the methyl ligands of the titanium (**4**), zirconium (**21**) and hafnium (**22**) congeners, the $^{1}J_{CH}$ coupling constants for the zirconium and hafnium dimethyl complexes (113 Hz and 112 Hz respectively) are significantly smaller than oberved for the titanium congener (118 Hz). As the metal centre becomes more electropositive descending the group, the contribution of the carbon 2s orbital in the M-C bond increases with an associated decrease in the C-H bonds (Bent's rule) resulting in smaller $^{1}J_{CH}$ coupling constants.[43]

3.4.3 Synthesis of Cp*M{NC(Ph)N^{i}Pr$_2$}(CH$_2$Ph)$_2$ (M = Ti (23); Zr (24); Hf (25))

Reaction of the half-sandwich dichlorides (**3** (Ti), **18** (Zr) or **19** (Hf)) with two equivalents of PhCH$_2$MgCl affords the desired congeneric series of dibenzyl precatalysts Cp*M{NC(Ph)N^{i}Pr$_2$}(CH$_2$Ph)$_2$ (M = Ti (**23**); Zr (**24**); Hf (**25**)) in reasonable isolated yields (58-88 %) (Equation 3.2).

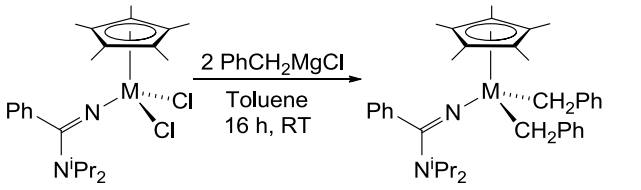

M = Ti (**23**), Zr (**24**), Hf (**25**)

Equation 3.2

Compounds **23-25** have been fully characterised by NMR and IR spectroscopy, EI mass spectrometry and elemental analysis. As with **20**, compounds **24** and **25** were characterised by NMR at low temperature (-60 °C) in the slow C-N^{i}Pr$_2$ bond rotation regime. The low temperature spectrum of **23** is complicated presumably due to the effect of *ipso*-carbon interactions observed in the solid state (*vide infra*) resulting in inequivalence of the benzyl ligands. At higher temperatures the spectrum is more easily interpreted and assigned hence **23** was characterised by NMR in the fast rotation regime at 60 °C. The room temperature and high temperature (60 °C) spectra of **23** are shown in Figure 3.3.

The room temperature spectrum of **23** in toluene-d_8 displays the expected Cp* singlet (1.88 ppm) and multiplets (7.33-7.01 ppm) corresponding to the aromatic amidinate and benzyl protons. Broad signals at 4.22 and 1.23 ppm are observed for the *iso*-propyl methine and methyl protons respectively. The four methylene protons of the benzyl ligands are observed as an AB quartet at 2.31 ppm. Warming to 60 °C (Figure 3.3) results in free rotation about the C-N^{i}Pr$_2$ bond allowing observation of one septet (4.32 ppm) and one doublet (1.24 ppm) for the amidinate *iso*-propyl groups.

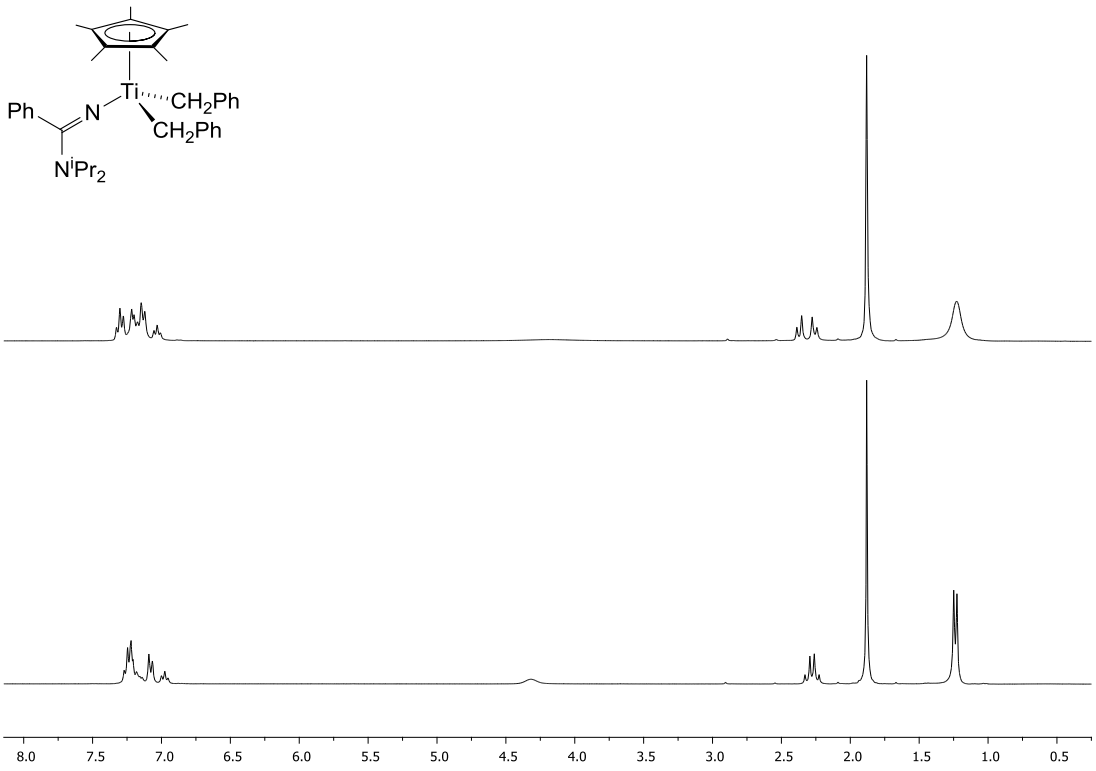

Figure 3.3. ^{1}H NMR spectra (299.9 MHz) of Cp*Ti{NC(Ph)N^{i}Pr$_2$}(CH$_2$Ph)$_2$ (**23**) in toluene-d_8. Top: 293 K; bottom: 333 K.

The low temperature (-60 °C) ^{1}H NMR spectra of **24** and **25** in toluene-d_8 reveal the expected signals corresponding to the Cp* protons (1.72 ppm (**24**) 1.71 ppm (**25**)) with the aromatic amidinate and benzyl protons appearing as a series of overlapping multiplets (7.39-6.93 ppm (**24**), 7.32-6.93 ppm (**25**)). As discussed, slow rotation about the C-N^{i}Pr$_2$ at this temperature results in observation of two methine septets (3.39 (*cis*) and 2.67 (*trans*) ppm (**24**); 3.44 (*cis*) and 2.74 (*trans*) ppm (**25**)) and two methyl doublets (1.51 (*trans*) and 0.53 (*cis*) ppm (**24**); 1.49 (*trans*) and 0.57 (*cis*) ppm (**25**)). The methylene protons of the benzyl ligands correspond to a broad signal (2.11 ppm (**24**), 1.91 ppm (**25**)) in the low temperature spectrum.

3.4.4 X-ray structures of Cp*M{NC(Ph)N^{i}Pr$_2$}R$_2$ (M = Ti, R = CH$_2$Ph (23); M = Zr, R = Me (21); M = Zr, R = CH$_2$Ph (24); M = Hf, R = CH$_2$Ph (25)

Compounds **21** and **23-25** were further characterised by single crystal X-ray diffraction. Single crystals suitable for X-ray diffraction were grown at room temperature from pentane (**21**, **23, 24**) and benzene (**25**) solutions. The crystal structure of the zirconium dimethyl complex, **21** is isomorphous with that of **4** and, similarly to the zirconium and hafnium half-sandwich dichlorides, dibenzyl

compounds **24** and **25** are also isomorphous. The molecular structures of **21**, **23** and **25** are shown in Figure 3.4 and full crystallographic data can be found in the CD appendix. Selected bond lengths and angles of **21** and the titanium congener **4** for comparison are presented in Table 3.2. Selected bond lengths and angles for **23**-**25** are presented in Table 3.3.

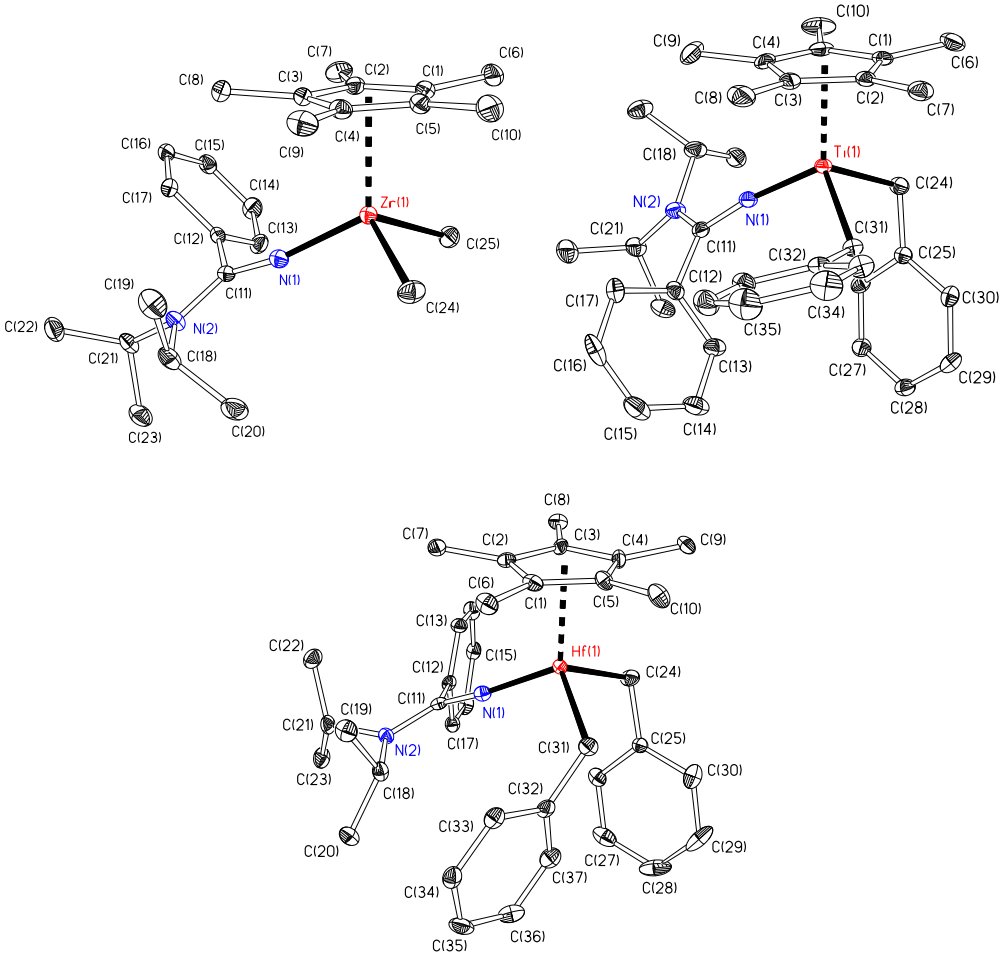

Figure 3.4. Displacement ellipsoid plots of Cp*Zr{NC(Ph)N^{i}Pr$_2$}Me$_2$ (**21**, top left), Cp*Ti{NC(Ph)N^{i}Pr$_2$}(CH$_2$Ph)$_2$ (**23**, top right) and Cp*Hf{NC(Ph)N^{i}Pr$_2$}(CH$_2$Ph)$_2$ (**25**, bottom). H atoms omitted for clarity. Ellipsoids are drawn at the 20% probability level.

Table 3.2. Selected bond lengths (Å) and angles (°) for Cp*M{NC(Ph)N^{i}Pr$_2$}Me$_2$ (M = Ti, (**4**) or Zr (**21**)). Cp$_{cent}$ is the computed Cp* ring carbon centroid.

Parameter	**4**	**21**
M(1)-Cp$_{cent}$	2.07	2.22
M(1)-N(1)	1.8452(15)	1.984(2)
N(1)-C(11)	1.290(2)	1.287(3)
N(2)-C(11)	1.363(2)	1.373(3)
M(1)-C(24)	2.1227(18)	2.263(3)
M(1)-C(25)	2.1326(19)	2.259(3)
Cp$_{cent}$-M(1)-N(1)	120.8	119.1
Cp$_{cent}$-M(1)-C(24)	113.9	111.8
Cp$_{cent}$-M(1)-C(25)	113.9	111.6
M(1)-N(1)-C(11)	163.00(13)	164.56(18)
N(1)-M(1)-C(24)	104.21(7)	104.82(10)
N(1)-M(1)-C(25)	104.04(7)	107.96(10)
C(24)-M(1)-C(25)	96.93(8)	99.57(11)

As may be expected from the structure of **21** being isomorphous with that of **4**, the molecular structures are similar aside from differences associated with the larger ionic radius of zirconium. The Zr(1)-Cp$_{cent}$ (2.22 Å) and Zr(1)-N(1) (1.984(2) Å) distances are significantly longer than the Ti(1)-Cp$_{cent}$ (2.07 Å) and Ti(1)-N(1) (1.8452(15) Å) bond lengths observed in **4**. The M(1)-C(24) (2.1227(18) Å (**4**), 2.263(3) Å (**21**)) and M(1)-C(25) (2.1326(19) Å (**4**), 2.259(3) Å (**21**)) distances are also consistent with the expected trend reflecting the ionic radii of the titanium and zirconium congeners. The M(1)-N(1) bond lengths are longer than observed in the corresponding half-sandwich dichlorides, **3** (1.800(3) Å) and **18** (1.943(6) Å) which as discussed for **4** in Chapter Two reflects the more powerful σ-donation of the methyl ligands.

Compound **21** exhibits the familiar linear Zr(1)-N(1)-C(11) angle (164.56(18)°) expected from other structurally characterised κ^1-amidinate complexes in this Thesis as well as in the literature.[36-41, 44] The internal amidinate N(1)-C(11) (1.290(2) Å (**4**), 1.287(3) Å (**21**)) and N(2)-C(11) (1.363(2) Å (**4**), 1.373(3) Å (**21**)) distances are, however, very similar implying a similar degree of amidinate-metal π-interaction in spite of the longer M(1)-N(1) bonds observed in **21**. This will be further discussed in the context of DFT calculations (*vide infra*).

Table 3.3. Selected bond lengths (Å) and angles (°) for $Cp^*M\{NC(Ph)N^iPr_2\}(CH_2Ph)_2$ (M = Ti (**23**); Zr (**24**); Hf (**25**)). Cp_{cent} is the computed Cp* ring carbon centroid.

Parameter	**23**	**24**	**25**
M(1)-Cp_{cent}	2.08	2.23	2.20
M(1)-N(1)	1.8379(18)	1.976(3)	1.960(6)
N(1)-C(11)	1.295(3)	1.297(5)	1.286(9)
N(2)-C(11)	1.356(3)	1.364(5)	1.370(9)
M(1)-C(24)	2.180(2)	2.290(5)	2.250(7)
M(1)-C(31)	2.158(2)	2.307(4)	2.289(6)
Cp_{cent}-M(1)-N(1)	120.3	116.7	118.1
Cp_{cent}-M(1)-C(24)	113.7	109.2	110.2
Cp_{cent}-M(1)-C(31)	116.2	110.8	114.1
M(1)-N(1)-C(11)	172.19(16)	168.7(3)	168.3(5)
N(1)-M(1)-C(24)	103.62(9)	102.54(18)	102.6(3)
N(1)-M(1)-C(31)	102.99(8)	109.54(16)	108.3(2)
C(24)-M(1)-C(31)	96.72(9)	107.48(18)	105.0(3)
M(1)-C(24)-C(25)	110.48(15)	105.1(3)	108.7(5)
M(1)-C(31)-C(32)	126.23(15)	118.8(3)	119.4(5)

Similar trends are observed for the congeneric series of half-sandwich dibenzyl complexes (**23**, **24** and **25**) as for the dichloride compounds (**3**, **18** and **19**): the M(1)-Cp_{cent} (2.08 Å (**23**), 2.23 Å (**24**), 2.20 Å (**25**)) and M(1)-N(1) (1.8379(18) Å (**23**), 1.976(3) Å (**24**), 1.960(6) Å (**25**)) bond lengths demonstrate the expected increase in ionic radius from titanium to zirconium followed by the slight decrease to hafnium. This trend is also obvious from the M(1)-C(24) and M(1)-C(31) (2.180(2), 2.158(2) Å (**23**), 2.290(5), 2.307(4) Å (**24**), 2.250(7), 2.289(6) Å (**25**)) distances. The M(1)-N(1) distances are, however, longer than in the corresponding dichloride compounds (1.800(3) Å (**3**), 1.943(6) Å (**18**), 1.930(4) Å (**19**)) which is thought to derive from the enhanced σ-donation of benzyl ligands in comparison to chlorides.

In all three complexes, the M(1)-C(24)-C(25) bond angle (110.48(15)° (**23**), 105.1(3)° (**24**), 108.7(5)° (**25**)) is significantly more acute than the corresponding M(1)-C(31)-C(32) angle (126.23(15)° (**23**), 118.8(3)° (**24**), 119.4(5)° (**25**)) which is suggestive of an *ipso*-carbon interaction in the solid state. The observation of such an interaction is consistent with the complexity of the low temperature spectrum of **23** and the broadening of the benzyl methylene signal in the low temperature spectra of

24 and **25** (*vide supra*). *Ipso*-interactions are relatively common and are evident in a number of similar compounds.[45-47]

Just as observed in the structures of the titanium and zirconium dimethyl complexes, **4** and **21**, there is little change in the internal amidinate bond distances on descending group 4. The N(1)-C(11) (1.295(3) Å (**23**), 1.297(5) Å (**24**), 1.286(9) Å (**25**)) and N(2)-C(11) (1.356(3) Å (**23**), 1.364(5) Å (**24**), 1.370(9) Å (**25**)) distances are within error for all three congeners and very similar to those seen in the dimethyl complexes, **4** and **21** and the N(1)-C(1) (1.2922(19) Å) and N(2)-C(1) (1.3627(17) Å) bond lengths of the protio-amidine. Some degree of π-bonding must persist in the dibenzyl complexes evidenced by the linearity of the M(1)-N(1)-C(11) bond angles (172.19(16)° (**23**), 168.7(3)° (**24**), 168.3(5) ° (**25**)).

3.5 Synthesis of zirconium diene complexes

In order to gain better understanding of the importance of activation on catalyst productivity, the diene chemistry for the cyclopentadienyl-amidinate titanium systems explored in Chaper 2 was extended to zirconium. It was also envisaged that structural characterisation of congeneric zirconium diene complexes may assist with understanding the bonding of such systems.

3.5.1 Synthesis of Cp*Zr{NC(Ph)N^{i}Pr$_2$}(η-2,3-C$_4$H$_4$Me$_2$) (26)

The zirconium diene complex, Cp*Zr{NC(Ph)N^{i}Pr$_2$}(η-2,3-C$_4$H$_4$Me$_2$) (**26**), was prepared in a similar manner to the titanium congener (**5)** by reduction with two equivalents of ^{n}BuLi in the presence of excess 2,3-dimethyl-1,3-butadiene although heating was required reflecting the enhanced stability of the group oxidation state for the heavier element (Equation 3.3). A single isomer of compound **26** was isolated as a dark red crystalline solid in moderate isolated yield following recrystallisation from pentane (35 %) and has been fully characterised by NMR and IR spectroscopy, EI mass spectrometry and elemental analysis. The room temperature ^{1}H NMR spectrum is shown in Figure 3.5.

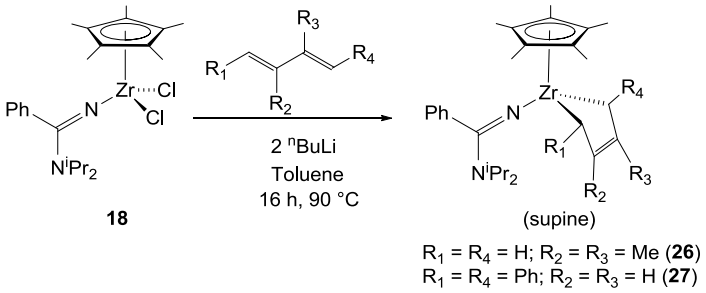

Equation 3.3

The room temperature ^{1}H NMR spectrum of **26** in C_6D_6 exhibits the expected signals corresponding to the Cp* (1.98 ppm) and aromatic amidinate protons (7.19-6.99 ppm). Fast rotation about the Zr-N bond results in time-averaged C_s symmetry of the molecule such that, in contrast to the room temperature spectrum of **5**, a single signal for the diene methyl groups (2.11 ppm) and two doublets corresponding to the *syn* (2.48 ppm) and *anti* (0.20 ppm) protons (^{2}J = 8.5 Hz) of the terminal diene carbons are observed. One doublet (1.03 ppm) and one septet (3.79 ppm) are observed for the methyl and methine amidinate *iso*-propyl protons. The peaks at 58.5 and 124.1 ppm in the room temperature ^{13}C NMR spectrum were assigned to the terminal and central diene carbons respectively using an HSQC two-dimensional experiment. The similarity of the ^{1}H and ^{13}C NMR spectra to those of **5** are suggestive of *cis* coordination of the diene in a supine conformation; this is supported by crystallographic characterisation of **26** (*vide infra*). The $^{1}J_{CH}$ coupling constant (ca. 140 Hz), measured using the proton-coupled ^{13}C spectrum of **26** (Figure 3.5, inset), is the same as that observed for $Cp_2Zr(\eta\text{-}2,3\text{-}C_4H_4Me_2)$[48] and smaller than that of the titanium congener (**4**) (145 Hz) suggesting a greater degree of reduction of the diene in **26** with the oxidation state of zirconium lying further towards the +4 limit.

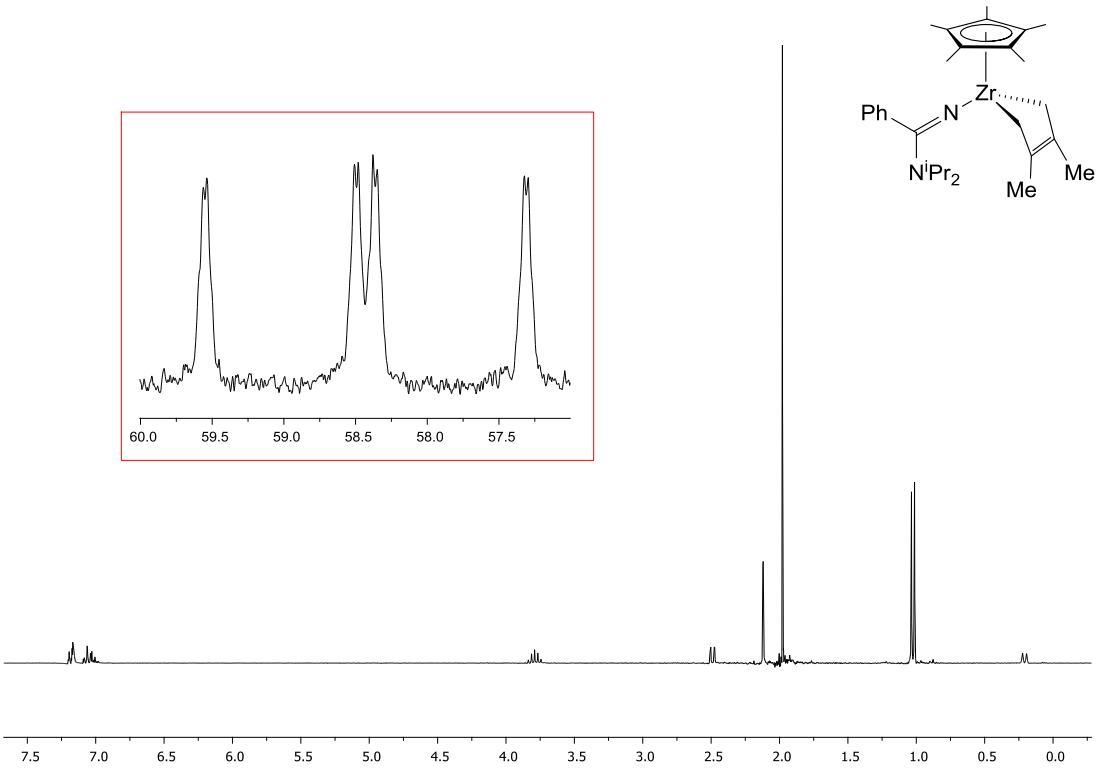

Figure 3.5. ^{1}H NMR spectrum (299.9 MHz, 293 K) of the (**26**) in C_6D_6. Residual protio-solvent, δ = 7.16 ppm. The inset illustrates the ^{13}C (proton-coupled) spectrum (125.7 MHz) between 57.0 and 60.0 ppm.

3.5.2 Synthesis of Cp*Zr{NC(Ph)N^{i}Pr$_2$}(η-1,4-C$_4$H$_4$Ph$_2$) (27)

Reduction of **18** with two equivalents of ^{n}BuLi in the presence of one equivalent of 1,4-diphenyl-1,3-butadiene gave a single isomer of Cp*Zr{NC(Ph)N^{i}Pr$_2$}(η-1,4-C$_4$H$_4$Ph$_2$) (**27**) (Equation 3.3). Similarly to the preparation of the titanium congener (**7**), unreacted free diene was removed by sublimation. Compound **27** has been fully characterised by NMR and IR spectroscopy, EI mass spectrometry and elemental analysis. The room temperature ^{1}H NMR spectrum in C_6D_6 shows important similarities with that of **26**: one isomer is observed (no minor peaks are located in the region of the Cp* singlet (1.85 ppm)) in which fast rotation about the Zr-N bond results in time-averaged C_s-symmetry such that the amidinate *iso*-propyl methyl and methine protons appear as one doublet (1.08 ppm) and one septet (3.79 ppm) respectively. Two signals corresponding to the terminal and central diene protons are observed at 2.01 and 6.22 ppm. The aromatic protons of the diene and amidinate ligands are observed as overlapping multiplets spanning the range 7.40-6.86 ppm. The similarity of the chemical shifts of the diene protons in **27** with the major (supine)

isomer of **7** suggests that the supine conformation of the coordinated diene is also adopted in the zirconium congener. Structural characterisation of **27** served to support this conclusion (*vide infra*).

3.5.3 X-ray structures of Cp*Zr{NC(Ph)N^{i}Pr$_2$}(η-2,3-C$_4$H$_4$Me$_2$) (26) and Cp*Zr{NC(Ph)N^{i}Pr$_2$}(η-1,4-C$_4$H$_4$Ph$_2$) (27)

Compounds **26** and **27** were further characterised by single crystal X-ray diffraction. Single crystals suitable for X-ray diffraction were grown from pentane solutions at -30 °C. The molecular structures of **26** and **27** are shown in Figure 3.6 and full crystallographic data can be found in the CD appendix. Selected bond lengths and angles of **26** and **27** are presented in Table 3.4.

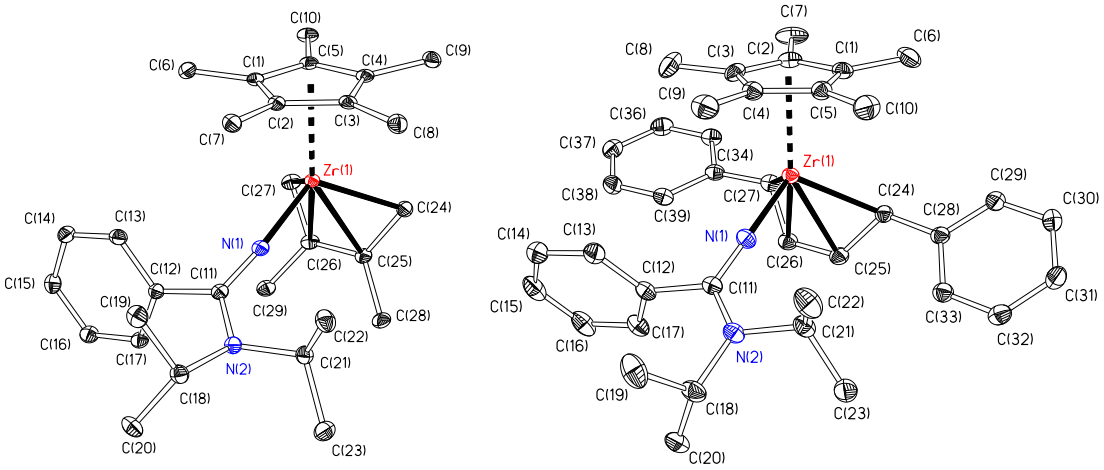

Figure 3.6. Displacement ellipsoid plots (20% probability) of Cp*Zr{NC(Ph)N^{i}Pr$_2$}(η-2,3-C$_4$H$_4$Me$_2$) (**26**) and Cp*Zr{NC(Ph)N^{i}Pr$_2$}(η-1,4-C$_4$H$_4$Ph$_2$) (**27**). H atoms omitted for clarity.

The molecular structures of **26** and **27** (which is isomorphous with the titanium congener, **7**) are consistent with the spectroscopic data which suggests *cis* coordination of the diene ligand with a supine conformation as in the cases of the titanium diene complexes **5**-**8**. Consistent with the trend observed for the congeneric dialkyl complexes, the Zr(1)-C(24) (2.301(4) Å (**26**), 2.342(3) Å (**27**)) and Zr(1)-C(27) (2.294(4) Å (**26**), 2.358(3) Å (**27**)) distances are longer than the Ti(1)-C(24) (2.1779(18) Å (**5**), 2.244(3) Å (**7**)) and Ti(1)-C(27) (2.1641(18) (**5**), 2.269(3) Å (**7**)) distances in the corresponding titanium diene complexes. As observed in the comparison of titanium diene complexes **5**-**8** with the dimethyl compound **4**, the Zr(1)-C(24) and Zr(1)-C(27) distances are only slightly longer than those of **21**

(2.263(3) and 2.259(3) Å). The longer Zr(1)-C(24) and Zr(1)-C(27) distances in **27** (2.342(3), 2.358(3) Å) than in **26** are attributed to the steric influence of the phenyl substituents of the diene. Metallocyclopentene character is clearly observed in the zirconium complexes from inspection of the diene carbon-carbon distances: similarly to **5** and **7** the central C-C bonds (1.378(6) Å (**26**), 1.385(4) Å (**27**)) are shorter than the peripheral C-C bonds (1.468(6), 1.463(6) Å (**26**) and 1.448(4), 1.438(4) Å (**27**)). These observations appear to support the oxidiation state of zirconium being better described as +4 just as discussed for the titanium diene complexes.

Consideration of the comparable internal diene C-C distances for the pairs of congeners independently of each other suggests that the extent of diene reduction is little affected on switching from titanium to zirconium. However, considering that the values for the terminal diene bond lengths of **5** (1.443(3), 1.447(2) Å) and **7** (1.435(4), 1.421(4) Å) are all smaller than those of the corresponding zirconium complexes, **26** and **27**, coinciding with similar central C-C bonds in the cases of **5** (1.387(3) Å) and **7** (1.385(4) Å) respectively, the dianionic, σ-bound character of the diene appears greater in the zirconium congeners consistent with the more reducing nature of the second row metal. This observation is also consistent with the related constrained geometry titanium and zirconium butadiene compounds (η^5, η^1-$C_5Me_4SiMe_2N^tBu$)M(η-C_4H_6); M = Ti, Zr) in which a more dramatic switch occurs from a predominantly π-bound prone diene in the titanium case to a supine metallocyclopentene-type coordination in the zirconium congener which is more closely related to the structures of the diene complexes presented in this Thesis.[49]

The Zr-Cp*$_{cent}$ distances (2.24 Å (**26**), 2.22 Å (**27**)) are very similar to that observed for the dimethyl complex, **21** (2.22 Å). The Zr(1)-N(1) bond length in **27** (1.994(2) Å) is also comparable to that of **21** (1.984(2) Å) and **26** (2.014(3) Å). The linear Zr(1)-N(1)-C(11) bond angle of the amidinate persists in **26** (170.2(3)°) and **27** (168.3(2)°) although the N(1)-C(11) (1.283(5) Å (**26**), 1.277(3) Å (**27**)) and C(11)-N(2) (1.385(5) Å (**26**), 1.376(4) Å (**27**)) internal amidinate bond lengths do not appear significantly different from the corresponding distances in **21** (1.287(3) Å and 1.373(3) Å) suggesting similar π-character of the amidinate-zirconium interaction in the diene complexes.

Table 3.4. Selected bond lengths (Å) and angles (°) for Cp*Zr{NC(Ph)N^{i}Pr$_2$}(η-2,3-C$_4$H$_4$Me$_2$) (**26**) and Cp*Zr{NC(Ph)N^{i}Pr$_2$}(η-1,4-C$_4$H$_4$Ph$_2$) (**27**). Cp$_{cent}$ is the computed Cp* ring carbon centroid.

Parameter	**26**	**27**
Zr(1)-Cp$_{cent}$	2.24	2.22
Zr(1)-N(1)	2.014(3)	1.994(2)
N(1)-C(11)	1.283(5)	1.277(3)
N(2)-C(11)	1.385(5)	1.376(4)
Zr(1)-C(24)	2.301(4)	2.342(3)
Zr(1)-C(27)	2.294(4)	2.358(3)
Zr(1)-C(25)	2.469(4)	2.424(3)
Zr(1)-C(26)	2.456(4)	2.439(3)
C(24)-C(25)	1.468(6)	1.448(4)
C(25)-C(26)	1.378(6)	1.385(4)
C(26)-C(27)	1.463(6)	1.438(4)
Cp$_{cent}$-Zr(1)-N(1)	113.8	113.3
Cp$_{cent}$-Zr(1)-C(24)	115.3	117.6
Cp$_{cent}$-Zr(1)-C(27)	116.1	114.3
Zr(1)-N(1)-C(11)	170.2(3)	168.3(2)
N(1)-Zr(1)-C(24)	117.76(15)	110.67(10)
N(1)-Zr(1)-C(27)	110.63(16)	116.13(10)
C(24)-Zr(1)-C(27)	78.57(18)	81.25(11)
Zr(1)-C(24)-C(25)	78.5(2)	75.44(16)
Zr(1)-C(27)-C(26)	78.2(2)	75.68(16)
C(24)-C(25)-C(26)	121.7(4)	126.2(3)
C(25)-C(26)-C(27)	121.2(4)	124.7(3)

3.5.4 Synthesis of Cp*Zr{NC(Ph)N^{i}Pr$_2$}{η^3-CH$_2$C(Me)C(Me)CH$_2$BAr$^{F}_3$} (28)

It was shown in Chapter Two that it is possible to 'activate' amidinate-supported titanium diene precatalysts with BAr$^{F}_3$ to generate well-defined zwitterionic half-sandwich allyl borate complexes. Stoichiometric reaction of **26** with BAr$^{F}_3$ in n-hexanes results in an immediate colour change from red to yellow with subsequent precipitation of the zwitterionic species, Cp*Zr{NC(Ph)N^{i}Pr$_2$}{η^3-CH$_2$C(Me)C(Me)CH$_2$BAr$^{F}_3$} (**28**) (84 %) in which, just as observed in formation of the titanium congener **9**, the borate moiety was found to be located on a terminal CH$_2$ of the diene with the other three diene carbons forming an allylic ligand (Equation 3.4).

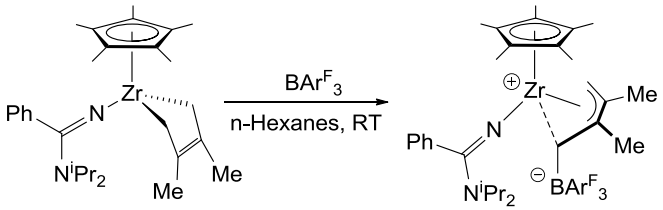

26 **28**

Equation 3.4

Compound **28** has been fully characterised by NMR and IR spectroscopy, EI mass spectrometry and elemental analysis. As with the titanium congener **9**, a broad room temperature ^{1}H NMR spectrum in toluene-d_8 required characterisation by NMR at low temperature (-20 °C) in the slow C-N^{i}Pr$_2$ bond rotation regime. The low temperature spectrum of **28** is similar to that of **9**: the expected Cp* (1.68 ppm) and amidinate aromatic protons (7.18-6.75 ppm) are observed at similar chemical shifts. The *iso*-propyl groups correspond to two septets at 4.25 and 3.20 ppm for the methine protons with resonances at 1.17 and 0.68 ppm for the methyl groups. Singlets at 1.62 and 1.25 ppm are assigned to the diene methyl groups with the terminal allylic protons appearing as two doublets at 2.30 and 0.81 ppm (^{2}J = 8.7 Hz). The methylene protons adjacent to BAr$^F_3$ appear as broad signals at 0.22 and -0.03 ppm. The appearance and chemical shifts of these broad signals are similar to those seen in **9** suggesting that **28** is also stabilised by agostic-type interactions between the CH$_2$BAr$^F_3$ hydrogens and zirconium. Again, further evidence for such interactions was garnered from structural characterisation of **28** (*vide infra*). Consistent with the close similarities between the low temperature spectra of **28** and **9**, a supine-type orientation of the allyl borate ligand also appears to be adopted in **28** evidenced by through-space correlations observed between the Cp* methyl protons with terminal allylic and CH$_2$-BAr$^F_3$ protons. This supine-type conformation of **28** was also observed in the solid state. Restricted rotation about the B-CH$_2$ bond at room temperature results in a broad and complicated ^{19}F NMR spectrum. The three signals for the *ortho*-, *para*- and *meta*-fluorines of the aryl rings of the borate are observed at -130.6, -160.6 and -165.1 ppm respectively in the ^{19}F NMR spectrum recorded at 70 °C in toluene-d_8. As with **9**, no high field (~ -200 ppm) resonance is observed supporting the supposed agostic-type stabilisation of **28** rather than that derived from interaction of an *ortho*-fluorine of the perfluorinated aryl rings with zirconium.[50] The room temperature ^{11}B NMR spectrum displays the expected sharp singlet at -12.0 ppm.

3.5.5 Attempted reaction of Cp*Zr{NC(Ph)N^{i}Pr$_2$}(η-1,4-C$_4$H$_4$Ph$_2$) (27) with BAr$^{F}_{3}$

Similarly to Cp*Ti{NC(Ph)N^{i}Pr$_2$}(η-1,4-C$_4$H$_4$Ph$_2$) (**7**), the zirconium congener **27** did not react immediately with BAr$^{F}_{3}$ at room temperature to form a well-defined zwitterionic species. Just as was observed with **7**, reaction of **27** with BAr$^{F}_{3}$ at room temperature for several days eventually afforded of a mixture of products from inspection of the ^{1}H, ^{19}F and ^{11}B NMR spectra. A similar mixture of products was observed from heating **27** with BAr$^{F}_{3}$ at 60 °C for 3 h. As with **7**, signals corresponding to the free diene are observed in the ^{1}H NMR spectrum. The phenyl substituents on the diene in **7** and **27** prevent formation of the allyl borate presumably due to their steric protection of the terminal diene carbons.

3.5.6 X-ray structure of Cp*Zr{NC(Ph)N^{i}Pr$_2$}{η^{3}-CH$_2$C(Me)C(Me)CH$_2$BAr$^{F}_{3}$} (28)

Compound **28** was further characterised by single crystal X-ray diffraction. Single crystals suitable for X-ray diffraction were grown at room temperature from a benzene solution. The molecular structure of **28** is shown in Figure 3.7 and full crystallographic data can be found in the CD appendix. Selected bond lengths and angles of **28** are presented in Table 3.5.

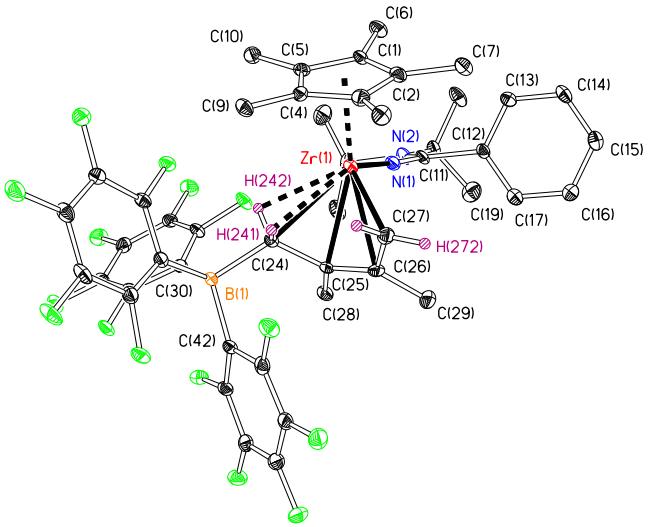

Figure 3.7. Displacement ellipsoid plots (20% probability) of Cp*Zr{NC(Ph)N^{i}Pr$_2$}{η^{3}-CH$_2$C(Me)C(Me)CH$_2$BAr$^{F}_{3}$} (**28**). H atoms omitted for clarity.

The molecular structure of **28** is consistent with the spectroscopic data and closely comparable to that of the titanium congener, **9**, with the supine conformation of the coordinated diene in **26** being maintained in **28**. As discussed for the titanium zwitterions in Chapter Two, the distances between the terminal η^3-allyl carbons (C(25) and (C(27)) and zirconium (2.487(5) and 2.306(6) Å) are shorter than the bond length observed between zirconium and the central allylic carbon (2.506(5) Å) which is commonly observed for allyl complexes of the early transition metals.[51] As expected, these distances are longer than the corresponding distances observed in **9** (2.330(3), 2.374(3), 2.201(3) Å). The internal C(25)-C(26) and C(26)-C(27) bond lengths of the allylic moiety (1.398(9) and 1.430(8) Å) are very similar to those in **9** (1.398(4) and 1.420(4) Å). The C(25)-C(26)-C(27) angle in **28** (123.3(6)º) is also similar to those of the titanium zwitterions (**9**-**12**) (121.1(3)-125.8(2)º) and published η^3-allyl complexes.[50, 52, 53]

Similarly to the molecular structure of **9**, the allyl moiety exhibits a *Z*-configuration with respect to the C(25)-C(26) π-bond bringing C(24) into a position facilitating agostic interactions between H(241) and H(242) and zirconium. These hydrogen atoms were located from a Fourier difference map and positionally and isotropically refined. The Zr(1)-H(241) and Zr(1)-H(242) bond lengths are relatively short (2.55(5) and 2.47(5) Å) but longer than in **9** (2.22(3) and 2.47(5) Å). In spite of these distances lying outside the range (*ca.* 1.8-2.3 Å)[54] expected for classical agostic interactions, combined with the linear Zr(1)-C(24)-B(1) bond angle (168.2(4)º) and similarities with the titanium zwitterions described in Chapter Two, the data are suggestive of the presence of agostic-type interactions between the $CH_2BAr^F{}_3$ hydrogens and the metal centre. The intramolecular π-stacking-type interaction between one of the perfluorinated ary rings and the allylic cation observed in the titanium zwitterionic species is less apparent in **28** due to the similarity of the three H_2C-B-C(Ar^F) bond angles (108.6(4)º, 114.6(4)º, 105.6(4)º) (*cf.* Chapter Two).

Table 3.5. Selected bond lengths (Å) and angles (°) for Cp*Zr{NC(Ph)N^{i}Pr$_2$}{η^3-CH$_2$C(Me)C(Me)CH$_2$BAr$^{F}_3$} (**28**). Cp$_{cent}$ is the computed Cp* ring carbon centroid.

Parameter		Parameter	
Zr(1)-Cp$_{cent}$	2.21	N(1)-Zr(1)-C(27)	113.8(2)
Zr(1)-N(1)	1.957(5)	C(24)-Zr(1)-C(27)	76.5(2)
N(1)-C(11)	1.307(7)	C(24)-Zr(1)-C(25)	35.58(17)
N(2)-C(11)	1.343(8)	C(24)-Zr(1)-C(26)	60.94(19)
Zr(1)-C(24)	2.529(5)	C(25)-Zr(1)-C(26)	32.5(2)
Zr(1)-H(241)	2.55(5)	C(25)-Zr(1)-C(27)	62.4(2)
Zr(1)-H(242)	2.47(5)	C(26)-Zr(1)-C(27)	34.3(2)
Zr(1)-C(27)	2.306(6)	Zr(1)-C(24)-C(25)	70.7(3)
Zr(1)-C(25)	2.487(5)	Zr(1)-C(25)-C(24)	73.7(3)
Zr(1)-C(26)	2.506(5)	Zr(1)-C(25)-C(26)	74.5(3)
C(24)-C(25)	1.533(8)	Zr(1)-C(26)-C(25)	73.0(3)
C(25)-C(26)	1.398(9)	Zr(1)-C(26)-C(27)	65.2(3)
C(26)-C(27)	1.430(8)	Zr(1)-C(27)-C(26)	80.5(4)
C(24)-B(1)	1.688(7)	C(24)-C(25)-C(26)	121.1(5)
Cp$_{cent}$-Zr(1)-N(1)	111.4	C(25)-C(26)-C(27)	123.3(6)
Cp$_{cent}$-Zr(1)-C(25)	156.9	Zr(1)-C(24)-B(1)	168.2(4)
Cp$_{cent}$-Zr(1)-C(26)	144.8	B(1)-C(24)-C(25)	116.9(4)
Cp$_{cent}$-Zr(1)-C(27)	110.5	C(24)-B(1)-C(30)	108.6(4)
Zr(1)-N(1)-C(11)	173.7(4)	C(24)-B(1)-C(36)	114.6(4)
N(1)-Zr(1)-C(24)	116.27(18)	C(24)-B(1)-C(42)	105.6(4)

As expected, the M(1)-Cp$_{cent}$ (2.21 Å (**28**), 2.06 Å (**9**)) and M(1)-N(1) (1.957(5) Å (**28**), 1.855(2) Å (**9**)) distances in **28** are longer than in the titanium congener **9**. The Zr(1)-Cp$_{cent}$ (2.24 Å) and Zr(1)-N(1) (2.014(3) Å) distances in the neutral diene complex **26** are clearly longer than those in **28** reflecting the stronger interactions expected with the cationic zirconium centre in the zwitterion. This effect is also evident for the titanium diene compounds and corresponding zwitterionic complexes. Compound **28** exhibits the familiar linear geometry about N(1) (173.7(4)°) but with a somewhat greater amidinate π-interaction with zirconium than in **26** judging from the internal amidinate bond lengths: the N(1)-C(11) (1.307(7) Å (**28**), 1.283(5) Å (**26**)) distances are broadly similar but the N(2)-C(11) (1.343(8) Å (**28**), 1.385(5) Å (**26**)) bond length is shorter in the zwitterion than in the diene complex. This trend is also observed in the congeneric titanium complexes **5** and **9** with the N(1)-C(11) (1.288(4) Å (**9**), 1.273(2) Å (**5**)) and N(2)-C(11) (1.374(4) Å (**9**), 1.389(2) Å (**5**)) distances

implying a slightly greater degree of dπ-pπ bonding between the amidinate and the metal centre in the zwiterionic species.

3.5.7 Zwitterion-diene cross-over reactions

In order to assess the reversibility of the diene 'activation' with BAr^F_3, similar cross-over experiments were devised to those described in Chapter Two. Mixing equimolar quantities of zirconium diene complex **26** and titanium zwitterionic compound **9** in C_6D_6 results in immediate quantitative formation of **28** and **5** (Equation 3.5). No reaction was observed mixing titaniun diene complex **5** with zirconium zwitterion **28**.

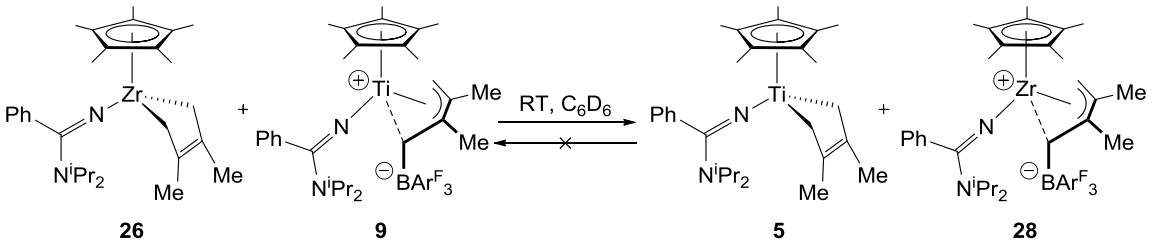

26 **9** **5** **28**

Equation 3.5

The driving force for this reaction is speculated to derive from the larger second row metal favouring higher coordination numbers and interacting more strongly with the allyl borate ligand. It was also found that heating the zirconium zwitterion **28** in C_6D_6 with Cp*Ti{NC(Ph)N^{i}Pr$_2$}(η-1,4-$C_4H_4Me_2$) (**6**) resulted in irreversible formation of **26** and the corresponding titanium zwitterion (**10**) (Equation 3.6). The rearrangement and conformational switch in formation of **10** appears to lend it greater stability with respect to dissociative reformation of diene complex and BAr^F_3 in comparison to the congeneric zwitterions, **9** and **28**.

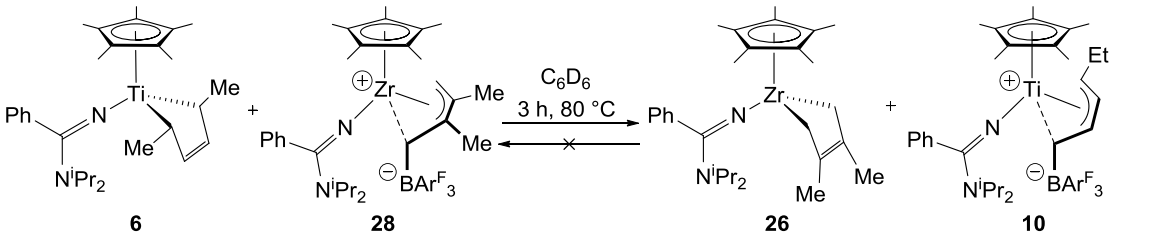

6 **28** **26** **10**

Equation 3.6

3.5.8 Variable temperature ^{19}F NMR experiments with 28

Comparison was made in Chapter Two between the stabilities of **9** and **10** with respect to diene reformation using variable temperature ^{19}F experiments whereby a zwitterion was heated with one equivalent of BAr^F_3; broadening of the borane ^{19}F

resonances was ascribed to exchange of free and associated borane. A similar experiment was performed with **28**: in contrast to the titanium congener **9**, no line broadening of the ^{19}F signals corresponding to the borane-borate exchange was observed even at 90 °C. This result is consistent with the observations for the cross-over reactions described above; the kinetic barrier to reformation of the diene complex appears higher for **28** compared to **9**. As discussed (*vide supra*) this may be explained by stronger bonding between the allyl borate ligand and zirconium combined with a less sterically congested metal centre.

3.5.9 Attempted reaction of Cp*Zr{NC(Ph)N^{i}Pr$_2$}(η-2,3-C$_4$H$_4$Me$_2$) (26) with [CPh$_3$][BAr$^{F}_4$]

Stoichiometric reaction of Cp*Zr{NC(Ph)N^{i}Pr$_2$}(η-2,3-$C_4H_4Me_2$) (**26**) with [CPh_3][BAr^{F}_4] in C_6D_6 at room temperature immediately resulted in a colour change from red to dark brown. The ^{1}H and ^{19}F NMR spectra showed quantitative reaction of **26** but the complexity of the spectra precluded identification of the product(s). Attempts to grow crystals of the products of a scaled-up reaction were unsuccessful due to the oily nature of the material. A small number of colourless crystals were recovered after two weeks but were found by X-ray diffraction to be triphenylmethane. This is likely to be a minor product since the characteristic signal in the ^{1}H NMR corresponding to the aliphatic methine proton was not observed in the NMR-scale reaction. However, the experiment did serve to suggest that **26** may be 'activated' with [CPh_3][BAr^{F}_4] consistent with the moderate productivity of the **26**/[CPh_3][BAr^{F}_4] system in polymerisation experiments (*vide infra*).

3.6 Density functional theory calculations

Density functional theory (DFT) calculations were performed by Dr Betty Coussens (DSM, The Netherlands) in order to enhance understanding of the amidinate-metal bonding in the neutral half-sandwich complexes described in this Thesis so far. It was hoped to probe the possible bonding analogy with group 4 terminal imido complexes; the Ti-N interaction in such complexes having being extensively studied.[55-63] Application of modern computational techniques to assist understanding of the bonding in group 4 diene complexes was also envisaged in order to understand more about the extent of reduction of the diene in these complexes and the relative importance of steric and electronic factors in determining diene ligand conformation.

Previous work in this area utilised extended Hückel calculations to calculate prone and supine conformations on Cp*TiCl(η-C_4H_8) which were found to be very close in energy with diene-metal bonding being better described as a σ^2,π-interaction.[64] Similar calculations described by Teuben and Hessen for (supine) CpZrCl(η-C_4H_8) also appear to support a σ^2,π-metallacyclopentene structure.[65]

3.6.1 Cp*M{NC(Ph)N^{i}Pr$_2$}Me$_2$ (M =Ti or Zr)

The putative isolobal relationship between the neutral half-sandwich amidinate complexes with metallocenes provided impetus to study computationally the amidinate-metal interaction in more detail. The degree of π-donation from the amidinate leads to limiting cases involving 14VE or 16VE metal centres; the latter being analagous to metallocenes (Figure 3.8). The parameters determined from the solid-state structures of **4** and **21** show good agreement with those of the corresponding energy-minimised structures, **I** (M = Ti) and **II** (M = Zr). A comparison of selected bond lengths is presented in Table 3.6.

Table 3.6. Selected bond lengths (Å) for Cp*M{NC(Ph)N^{i}Pr$_2$}Me$_2$ (M = Ti, (**4**) or Zr (**21**)) and corresponding calculated structures (M = Ti (**I**) or Zr (**II**)).

Parameter	**4**	**I**	**21**	**II**
M-N	1.8452(15)	1.860	1.984(2)	2.023
N=C	1.290(2)	1.288	1.287(3)	1.285
N-$C_{C=N}$	1.363(2)	1.377	1.373(3)	1.378
M-$C_{methyl\ 1}$	2.1227(18)	2.120	2.263(3)	2.284
M-$C_{methyl\ 2}$	2.1326(19)	2.128	2.259(3)	2.277

Compounds **I** and **II** were divided into neutral d^1 Cp*Mme$_2$ and NC(Ph)N^{i}Pr$_2$ (S = ½) fragments in order to make qualitative assessment of the contributions to the metal-amidinate interaction (Figure 3.8).

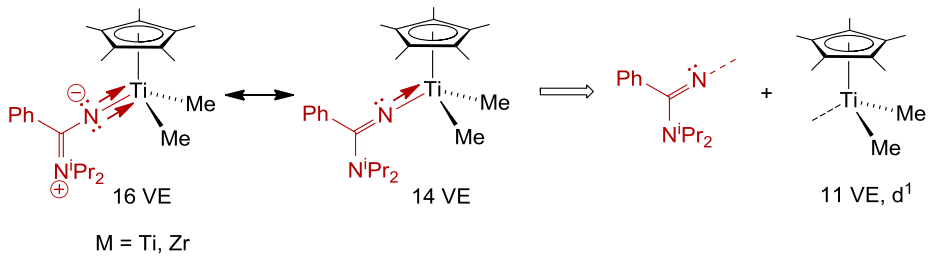

Figure 3.8.

The relevant Mos of the fragments for potential amidinate-metal bonding are shown in Figure 3.9 for the titanium case (**I**). The Cp^*TiMe_2 fragment has four metal-based orbitals which are available for bonding: the SHOMO can form a σ-bond while the LUMO and LUMO+1 are set up for π-overlap. Ligand interaction with the more asymmetric LUMO might be predicted to be somewhat less favourable than with the LUMO+1. The LUMO+2 of the Cp^*TiMe_2 fragment provides potential δ-overlap with a ligand MO but is expected to be non-bonding in the case of **I**.

The SHOMO and SHOMO-4 of the $NC(Ph)N^iPr_2$ fragment represent the non-bonding and bonding π-orbitals of the allylic-like amidinate π-system respectively. The unoccupied π*-antibonding orbital of the allylic system corresponds to the LUMO+3 of the amidine fragment. A second MO set up for a potential π-interaction with the metal lies orthogonal to the amidine allylic system: the SHOMO-1 consists largely of a lone pair 2p-type AO on the imine nitrogen. Thus from interactions involving the SHOMO and SHOMO-1, two possible π-interactions may be predicted with the metal centre. As may be expected, the MO set up for a σ-interaction with the Cp^*TiMe_2 fragment is observed lower in energy (SHOMO-5). This MO is mainly comprised of a orbital ressembling an sp-type σ-donor orbital on the imine nitrogen.

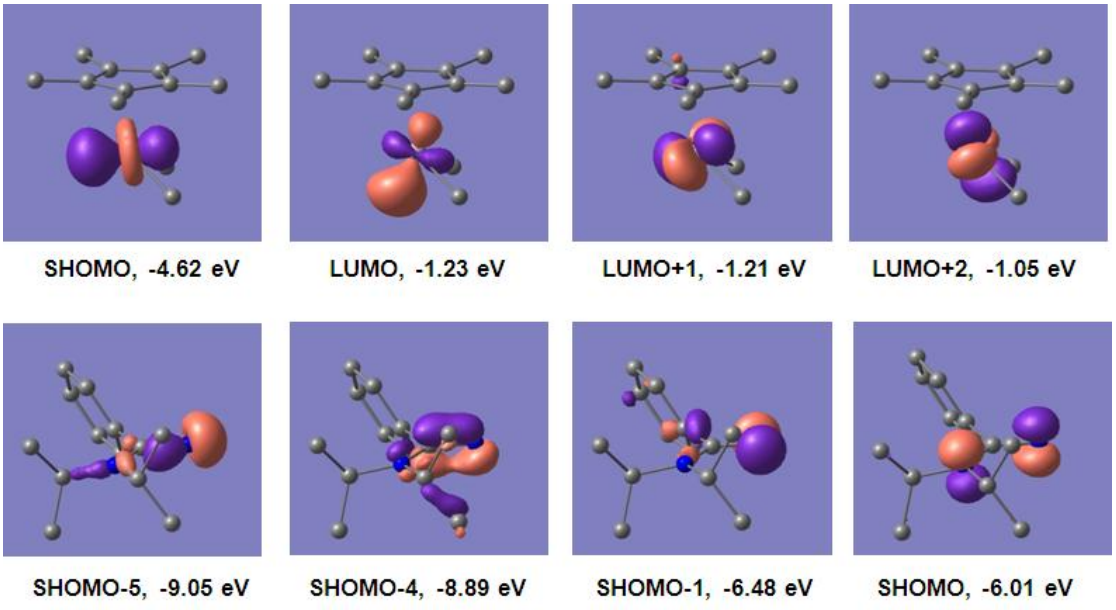

Figure 3.9. Selected Mos of Cp^*TiMe_2 (top) and $NC(Ph)N^iPr_2$ (bottom) fragments (S = ½ in each case). The value for the isosurfaces is 0.09 au. H atoms omitted.

The frontier molecular orbitals (FMOs) of **I** (Figure 3.10) comprise the π-bonding, non-bonding and π*-antibonding Mos with the Ti-N σ-bonding orbital formed from

contributions from the SHOMO and the SHOMO-5 of the respective Cp^*TiMe_2 and $NC(Ph)N^iPr_2$ fragments lying at lower energy. The π-bonding picture is complicated by partial mixing of the ligand Mos but a useful qualitative picture of the amidinate-metal bonding emerges from comparison of the Mos of the fragments (*vide supra*) with those of **I**. The HOMO-5 of **I** clearly shows a metal-amidinate π-interaction resulting from overlap of a metal-based orbital ressembling the LUMO of the Cp^*TiMe_2 fragment with an orbital ressembling the SHOMO (allylic non-bonding) of the $NC(Ph)N^iPr_2$ fragment. A second π-interaction comprising orbitals ressembling the LUMO+1 of the Cp^*TiMe_2 and the SHOMO-1 of the $NC(Ph)N^iPr_2$ fragment is also observed by inspection of the HOMO-2 of **I**. The HOMO-5 (-6.44 eV) is significantly lower in energy than the HOMO-2 (-5.93 eV) which may be explained, at least in part, by the significant contribution to the former by a 2p AO on the amine nitrogen resulting in overall stabilisation of the MO; the higher energy HOMO-2 has very little orbital coefficient on the amine nitrogen. The HOMO and HOMO-1 of **I** have much greater coefficients on the Cp* ligand: the latter is essentially non-bonding with titanium while the former corresponds mostly to a Cp*-metal interaction. The LUMO of **I** may also be considered non-bonding and involves an amidinate-based contribution ressembling the π*-antibonding orbital of the allylic system. Contrastingly, the LUMO+4 is much higher in energy (-0.04 eV) and may be considered the π*-antibonding partner of the HOMO-2 π-bonding MO. As predicted, the LUMO+1 is a non-bonding metal-based orbital (*cf.* the LUMO+2 of the Cp^*TiMe_2 fragment (*vide supra*)).

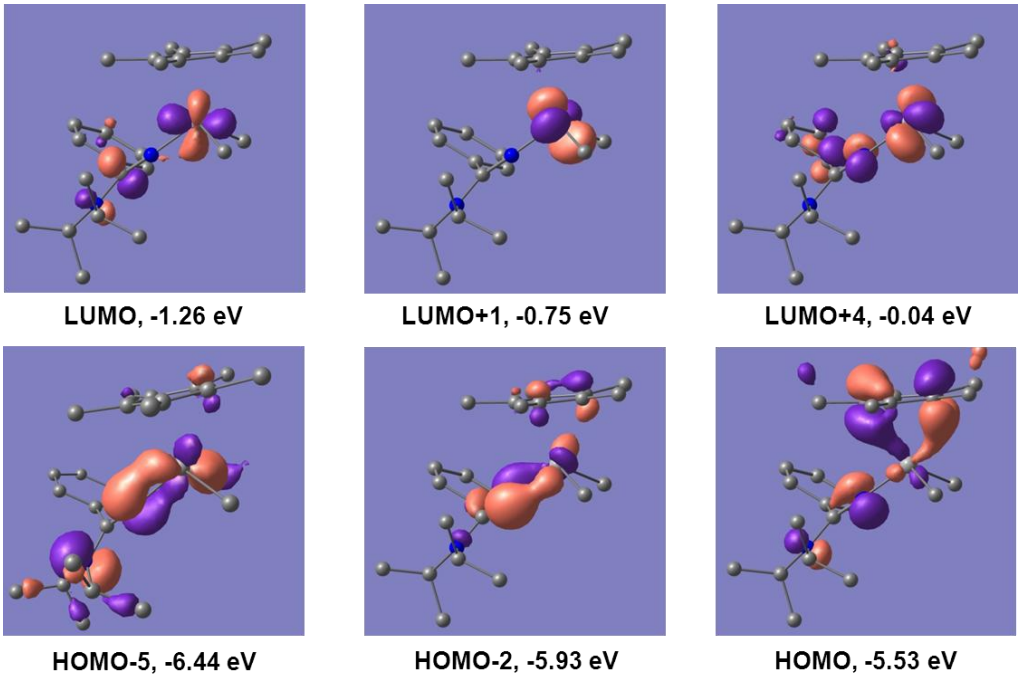

Figure 3.10. FMOs of Cp*Ti{NC(Ph)N^{i}Pr$_2$}Me$_2$ (**I**). The value for the isosurfaces is 0.06 au. H atoms omitted.

The molecular orbitals calculated for the zirconium congener **II** are qualitatively very similar to those of **I**. The HOMOs in **II** are very similar in energy (-6.44 eV (HOMO-5), -5.92 eV (HOMO-2), -5.52 eV (HOMO)) to those of **I** which may suggest that the destabilising effect associated with the poorer energy match with zirconium 4d orbitals is countered by enhanced overlap due to their greater radial extension. However, the higher energy metal orbitals does result in the LUMOs of **II** being slightly higher in energy in comparison to **I** with the non-bonding metal-based LUMO+3 (analogous to the LUMO+1 in **I**) being higher in energy than two antibonding π* Mos of the amidinate phenyl ring (LUMO+1 and LUMO+2). The atomic charges of the imine nitrogen (-0.429 (**I**), -0.478 (**II**)) and the metal (+0.651 (**I**), +1.041 (**II**)) reflect the greater degree of charge separation between the amidinate and metal in the zirconium congener.

3.6.2 Cp*M{NC(Ph)N^{i}Pr$_2$}(η-2,3-C$_4$H$_4$Me$_2$) (M =Ti or Zr)

Having examined the metal-amidinate bonding in the dimethyl complexes, DFT calculations were futher utilised to enhance understanding of the bonding in the half-sandwich amidinate diene complexes. The parameters determined from the solid-state structures of **4** and **26** show good agreement with those of the corresponding energy-

minimised structures for the supine conformers, **III** (M = Ti) and **IV** (M = Zr) (Table 3.7).

Table 3.7. Selected bond lengths (Å) for Cp*M{NC(Ph)N^{i}Pr$_2$}(η-2,3-C$_4$H$_4$Me$_2$) (M = Ti, (**4**) or Zr (**26**)) and corresponding calculated structures (M = Ti (**III**) or Zr (**IV**)).

Parameter	**5**	**III**	**26**	**IV**
M-N	1.8907(14)	1.896	2.014(3)	2.046
N=C	1.273(2)	1.278	1.283(5)	1.280
N-C$_{C=N}$	1.389(2)	1.402	1.385(5)	1.395
M-C$_1$	2.1779(18)	2.183	2.301(4)	2.325
M-C$_4$	2.1641(18)	2.178	2.294(4)	2.320
M-C$_2$	2.3530(17)	2.376	2.469(4)	2.525
M-C$_3$	2.3448(16)	2.372	2.456(4)	2.522
C$_1$-C$_2$	1.443(3)	1.454	1.468(6)	1.469
C$_2$-C$_3$	1.387(3)	1.403	1.378(6)	1.401
C$_3$-C$_4$	1.447(2)	1.455	1.463(6)	1.469

Consistent with the X-ray data, the internal diene bond lengths are indicative of greater reduction of the diene in the case of zirconium with longer C$_1$-C$_2$/C$_3$-C$_4$ and shorter C$_2$-C$_3$ bonds in **IV** compared to **III**. This is supported by the sum of the Mulliken charges of the atoms of the diene fragment: -0.13 (**III**) and -0.43 (**IV**).

Comparison was made between the FMOs calculated in **I** with those of **III** providing an insight into the metal-diene π-interaction (Figure 3.11). Interestingly, the titanium-based non-bonding LUMO and LUMO+1 orbitals observed in **I** appear somewhat mixed in **III** and become integral to a backbonding π-interaction between the π^3 diene MO and the metal centre in the HOMO of **III**. The corresponding MO in **I** (LUMO+4) is largely metal-amidinate π* antibonding in nature. This backbonding into the diene π^3 MO explains the overall negative Mulliken charge and the internal bond length alternation of the diene fragments in **III** and **IV**. The LUMO of **III** is metal-based and is non-bonding with both diene and amidinate ligands.

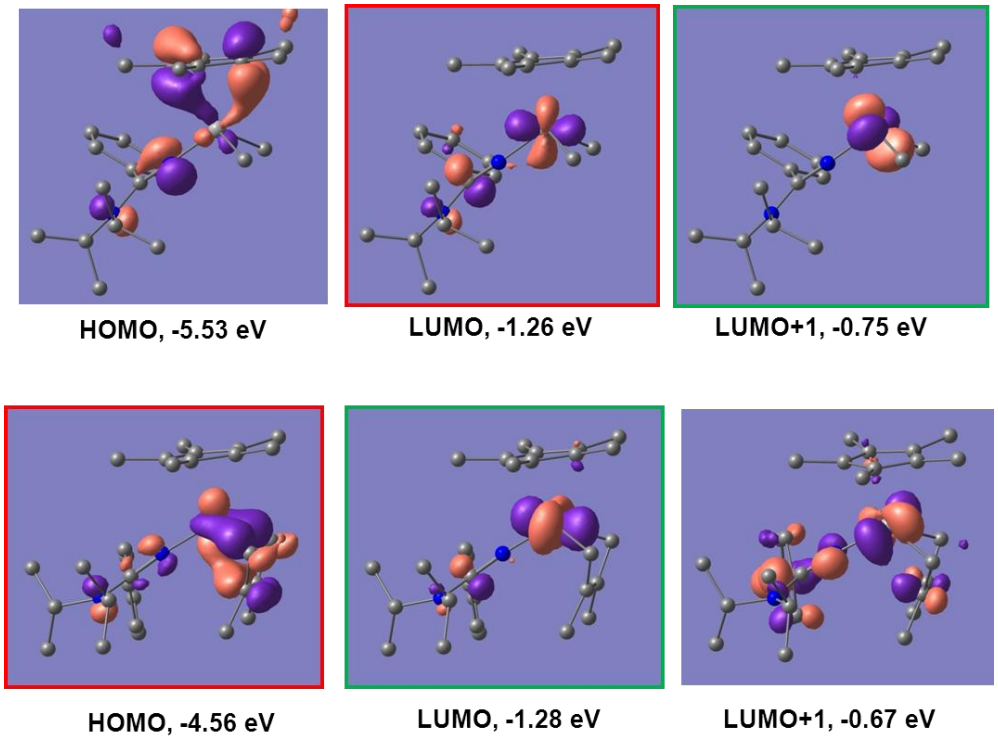

Figure 3.11. Comparison of FMOs of Cp*Ti{NC(Ph)N^{i}Pr$_2$}Me$_2$ (**I**, top) and Cp*Ti{NC(Ph)N^{i}Pr$_2$}(η-2,3-C$_4$H$_4$Me$_2$) (**III**, bottom). The value for the isosurfaces is 0.06 au. H atoms omitted.

3.6.3 Calculated supine and prone isomers of Cp*M{NC(Ph)N^{i}Pr$_2$}(η-2,3-C$_4$H$_4$Me$_2$) and CpM{NC(Ph)NMe$_2$}(η-C$_4$H$_6$) (M =Ti or Zr)

As discussed in Chapter Two, the prone constrained geometry diene complex, (η^5, η^1-C$_5$Me$_4$SiMe$_2$N^{t}Bu)Ti(η-1,4-C$_4$H$_4$Me$_2$), is described as predominantly π-bound.[66] In order to understand the effect of diene conformation on the extent of reduction, the prone conformers of Cp*M{NC(Ph)N^{i}Pr$_2$}(η-2,3-C$_4$H$_4$Me$_2$), **V** (M = Ti) and **VI** (M = Zr) were calculated (Figure 3.12). For better understanding of the relative influence of steric and electronic effects on conformation, optimised structures of both prone and supine conformers of the less sterically encumbered complex, CpM{NC(Ph)NMe$_2$}(η-C$_4$H$_6$) (**VII** (M = Ti; supine), **VIII** (M = Ti; prone), **IX** (M = Zr; supine) and **X** (M = Zr; prone)) were also calculated. The structures of the titanium congeners **V**, **VII** and **VIII** are shown in Figure 3.12. A comparison of the calculated conformers is presented in Table 3.8.

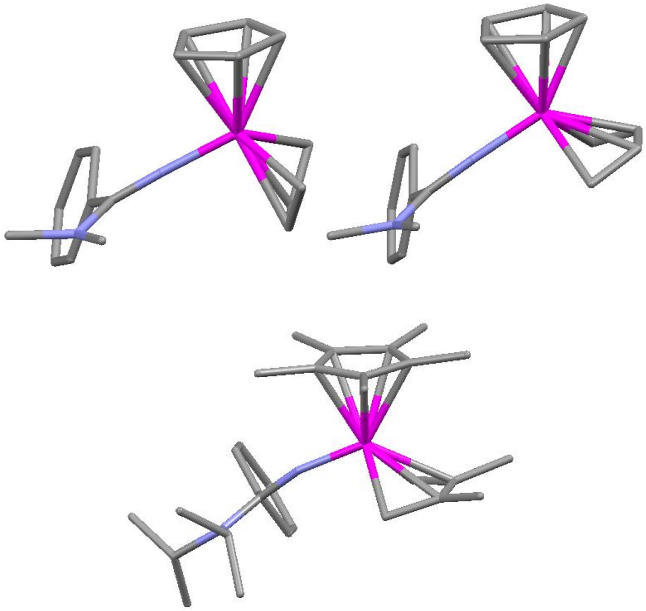

Figure 3.12. Calculated structures of supine (**VII**, top left) and prone (**VIII**, top right) conformers of CpTi{NC(Ph)NMe_2}(η-C_4H_6) and the prone conformer of Cp*Ti{NC(Ph)N^iPr_2}(η-2,3-$C_4H_4Me_2$) (**V**, bottom). H atoms omitted for clarity.

Consistent with experiment, the prone is higher in energy than the supine isomer by 27.7 and 29.7 kJ mol^{-1} for the titanium (**V**) and zirconium (**VI**) congeners respectively. In the cases of the models with less bulky ligand substituents, the supine conformer is preferred for titanium (**VII**) and zirconium (**IX**) by 11.6 kJ mol^{-1} and 15.4 kJ mol^{-1} respectively. It may therefore be concluded that the preference for the supine conformation is driven by both electronic and steric influences for these κ^1-amidinate-supported diene complexes.

Table 3.8. Selected bond lengths (Å) for calculated structures of supine (M = Ti (**III**) or Zr (**IV**)) and prone (M = Ti (**V**) or Zr (**VI**)) conformers of Cp*M{NC(Ph)N^{i}Pr$_2$}(η-2,3-$C_4H_4Me_2$) and supine (M = Ti (**VII**) or Zr (**IX**)) and prone (M = Ti (**VIII**) or Zr (**X**)) conformers of CpM{NC(Ph)NMe_2}(η-C_4H_6).

Parameter	**III**	**VII**	**V**	**VIII**	**IV**	**IX**	**VI**	**X**
M-N	1.896	1.872	1.882	1.869	2.046	2.025	2.030	2.026
N=C	1.278	1.275	1.282	1.280	1.280	1.278	1.283	1.281
N-$C_{C=N}$	1.402	1.398	1.390	1.392	1.395	1.390	1.387	1.387
M-C_1	2.183	2.203	2.178	2.230	2.325	2.335	2.322	2.339
M-C_4	2.178	2.203	2.174	2.225	2.320	2.335	2.316	2.343
M-C_2	2.376	2.313	2.417	2.316	2.525	2.474	2.555	2.481
M-C_3	2.372	2.314	2.417	2.311	2.522	2.475	2.559	2.484
C_1-C_2	1.454	1.437	1.455	1.430	1.469	1.453	1.467	1.452
C_2-C_3	1.403	1.399	1.408	1.407	1.401	1.395	1.402	1.397
C_3-C_4	1.455	1.439	1.457	1.432	1.469	1.455	1.469	1.451

The M-N distances are shorter for the less sterically encumbered titanium models **VII** and **VIII** compared to **III** and **V** reflecting the expected diminished steric interactions between the less bulky κ^1-amidinate, unsubstituted cyclopentadienyl and diene ligands. This also results in closer approach of the diene to the metal centre evidenced by smaller M-C_2/C_3 distances in **VII** and **VIII**. In contrast, the M-C_1/C_4 bond lengths appear slightly longer in **VII** and **VIII** compared to the more sterically encumbered **III** and **V** which may be due to slightly poorer donation from the less electron-rich unsubstituted diene. Similar trends are observed for the calculated zirconium complexes. In spite of the different conformations, the bond lengths of the supine (**IX**) and prone (**X**) isomers of CpM{NC(Ph)NMe_2}(η-C_4H_6) are very similar. The titanium congeners **VII** and **VIII** also display comparable bond lengths aside from the Ti-C_1/C_4 distances which are slightly shorter in the supine conformer **VII**. Comparing the calculated prone and supine structures for the bulkier structures, generally shorter M-N and longer M-C_2/C_3 distances are observed for the prone isomer but very similar internal diene bond distances indicate comparable reduction of the diene regardless of conformation. The Mulliken charges of the diene fragment in the titanium complexes suggest that the supine (-0.13 (**III**), -0.09 (**VII**)) and prone (-0.19 (**V**), -0.10 (**VIII**)) conformers are similarly reduced. The zirconium complexes show the expected greater reduction of the diene compared to the titanium congeners with the extent of

reduction being closely comparable for both supine (-0.43 (**IV**), -0.39 (**IX**)) and prone (-0.41 (**VI**), -0.39 (**X**)) isomers. Consistent with the trend in Mulliken charges, the extent of reduction of the butadiene ligand in the less bulky structures appears slightly diminished than in the more sterically encumbered models judging by the less pronounced alternation of the internal diene bond lengths. This is speculated to derive, at least in part, from poorer electron donation from the supporting ligands in **VII**-**X**.

3.6.4 Calculated supine and prone isomers of (η^5, η^1-$C_5Me_4SiMe_2N^tBu$)Ti(η-2,3-$C_4H_4Me_2$) and (η^5, η^1-$C_5H_4SiMe_2NMe$)Ti(η-C_4H_6)

Structures of constrained geometry complexes (η^5, η^1-$C_5Me_4SiMe_2N^tBu$)Ti(η-2,3-$C_4H_4Me_2$), **XI** (supine) and **XII** (prone), and (η^5, η^1-$C_5H_4SiMe_2NMe$)Ti(η-C_4H_6), **XIII** (supine) and **XIV** (prone), were calculated in order to understand further factors influencing the conformation and extent of diene reduction (Figure 3.13). Selected bond lengths of **XI**-**XIV** are presented in Table 3.9.

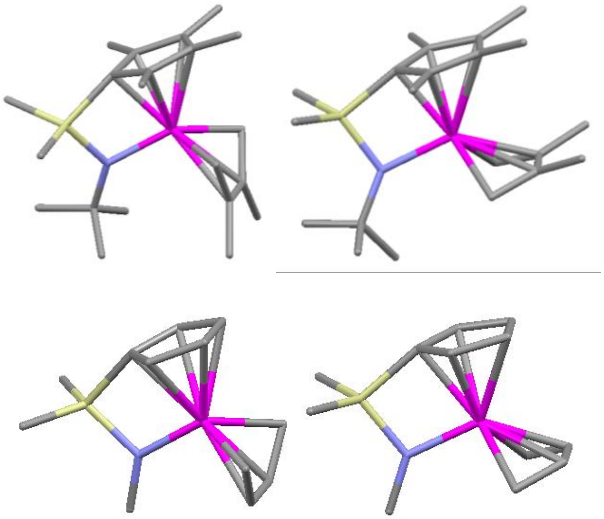

Figure 3.13. Calculated structures of supine (**XI**, top left) and prone (**XII**, top right) conformers of (η^5, η^1-$C_5Me_4SiMe_2N^tBu$)Ti(η-2,3-$C_4H_4Me_2$) and supine (**XIII**, bottom left) and prone (**XIV**, bottom right) conformers of (η^5, η^1-$C_5H_4SiMe_2NMe$)Ti(η-C_4H_6). H atoms omitted for clarity.

Similarly to the amidinate-supported systems there is an energetic preference for the supine conformer but the energy difference is much smaller in the case of (η^5, η^1-$C_5Me_4SiMe_2N^tBu$)Ti(η-2,3-$C_4H_4Me_2$) (3.9 kJ mol^{-1}) compared to Cp*Ti{NC(Ph)N^{i}Pr$_2$}(η-2,3-$C_4H_4Me_2$) (27.7 kJ mol^{-1}). With the less sterically encumbered model, (η^5, η^1-$C_5H_4SiMe_2NMe$)Ti(η-C_4H_6), the energetic preference for

the supine isomer (**XIII**) (7.0 kJ mol^{-1}) is similar to that observed for the κ^1-amidinate models **VII** and **VIII** (11.6 kJ mol^{-1}). The steric preference for the supine conformation in the constrained geometry complexes is therefore not as great as that observed for the κ^1-amidinate-supported systems. It may also be concluded that the supine conformation is preferred for larger and more reducing second and third row metals which concurs with the behaviour of (η^5, η^1-$C_5Me_4SiMe_2N^tBu$)M(η-C_4H_6) (M = Ti, Zr) for which, as discussed above, the prone titanium congener is predominantly π-bound while the zirconium complex adopts a supine metallocyclopentene-type structure.[49]

Table 3.9. Selected bond lengths (Å) for calculated structures of supine (**XI**) and prone (**XII**) conformers of (η^5, η^1-$C_5Me_4SiMe_2N^tBu$)Ti(η-2,3-$C_4H_4Me_2$) and supine (**XIII**) and prone (**XIV**) conformers of (η^5, η^1-$C_5H_4SiMe_2NMe$)Ti(η-C_4H_6).

Parameter	**XI**	**XIII**	**XII**	**XIV**
Ti-N	2.018	1.955	2.018	1.948
M-C_1	2.142	2.190	2.156	2.202
M-C_4	2.155	2.191	2.158	2.200
M-C_2	2.498	2.312	2.400	2.300
M-C_3	2.509	2.312	2.402	2.300
C_1-C_2	1.468	1.438	1.455	1.434
C_2-C_3	1.394	1.399	1.409	1.407
C_3-C_4	1.471	1.440	1.456	1.435

The less sterically encumbered systems **XIII** and **XIV** show shorter T-N and M-C_2/C_3 distances compared to **XI** and **XII** although as observed with the calculated amidinate complexes (*vide supra*) the Ti-C_1/C_4 bond lengths are actually slightly longer in **XIII** and **XIV** due to the poorer donating ability of the unsubstituted butadiene. The Ti-N and Ti-C_1/C_4 distances are similar for both sets of conformers but the Ti-C_2/C_3 bond lengths for (η^5, η^1-$C_5Me_4SiMe_2N^tBu$)Ti(η-2,3-$C_4H_4Me_2$) are signficantly shorter in the calculated prone isomer **XII**. This is thought to result from steric interactions between the methyl substituents on the central diene carbons and the ^{t}Bu group of the supporting ligand in the supine isomer. This is supported by the Ti-C_2/C_3 distances in the prone and supine conformers of the less bulky model (η^5, η^1-$C_5H_4SiMe_2NMe$)Ti(η-C_4H_6) being similar. In spite of similar Mulliken charges of the diene fragment in **XI** (-0.16) and **XII** (-0.14), a more pronounced short-long-short

bond length alternation is observed in **XI** indicating greater diene reduction in the supine isomer. As discussed for the κ^1-amidinate complexes above, the Mulliken charges of the unsubstituted butadiene complexes **XIII** (-0.09) and **XIV** (-0.08) reflect a smaller degree of reduction than in the bulkier models **XI** and **XII**. In spite of the similarity of the Mulliken charges, the internal diene bond lengths are consistent with apparently greater reduction of the diene ligand in the supine conformer. Overall, these considerations appear to be consistent with the experimental observations: predominant adoption of the prone conformation for constrained geometry titanium complexes with less reduction of the diene evident from experimentally determined internal diene bond lengths.[66]

3.7 Activation chemistry of dimethyl complexes 4 and 20-22 with $[CPh_3][BAr^F_4]$

As discussed in Chapter One, the active species for homogeneous Group 4 olefin polymerisation is formally a highly electron-deficient alkyl cation $[(L)M–R]^+$ (R = initiating group or polymeryl chain). The underlying chemistry of such cationic species has been the subject of intense investigation for a number of years.[42, 67-75] More recently, LANXESS Elastomers have investigated the activation chemistry of a closely related half-sandwich κ^1-amidinate dimethyl precatalyst, $Cp^*Ti\{NC(Ar^{F2})N^iPr_2\}Me_2$ (Ar^{F2} = 2,6-$C_6H_3F_2$), which included structural characterisation of a base-free dimeric dication bridged by two doubly α-agostic methyl groups.[76] Whilst a full investigation into the cation chemistry for the congeneric series of precatalysts is beyond the scope of this Thesis, preliminary reactions of the half-sandwich dimethyl complexes **4**, **20-22** with $[CPh_3][BAr^F_4]$ were carried out for comparison with $Cp^*Ti\{NC(Ar^{F2})N^iPr_2\}Me_2$ and to assist interpretation of polymerisation results (*vide infra*).

3.7.1 Reaction of $Cp^*Ti\{NC(Ph)N^iPr_2\}Me_2$ (4) with $[CPh_3][BAr^F_4]$

It was shown that stoichiometric reaction of $Cp^*Ti\{NC(Ar^{F2})N^iPr_2\}Me_2$ (Ar^{F2} = 2,6-$C_6H_3F_2$) with $[CPh_3][BAr^F_4]$ results in abstraction of a methyl ligand affording a cationic species which in the solid state adopts an unusual dimeric structure bridged by doubly α-agostic methyl groups (Equation 3.7).[76] Solution-phase characterisation is somewhat hampered by the irreversible crystallisation of the dimeric dication ($[Cp^*_2Ti_2\{NC(Ar^{F2})N^iPr_2\}_2(\mu\text{-}Me)_2]^{2+}$) providing a relatively short time window (*ca.*

1 h) in which to record solution NMR spectra. It may be speculated that the cation generated immediately in solution is monomeric since abstraction of the methyl ligand by the trityl cation occurs immediately with comcomitant formation of a soluble species which may be trapped with $POPh_3$ affording a cationic adduct or by another equivalent of $Cp^*Ti\{NC(Ar^{F2})N^iPr_2\}Me_2$ forming a methyl-bridged monocation.[76]

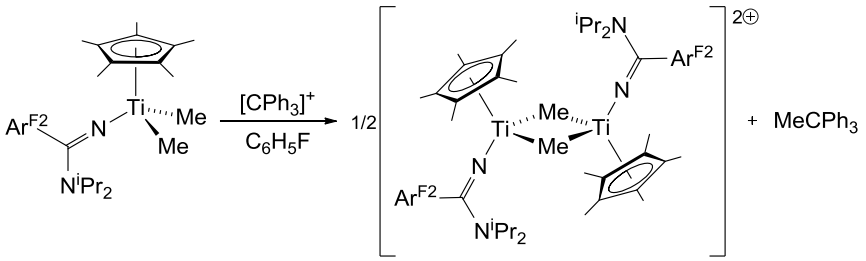

Equation 3.7 ($[BAr^F_4]^-$ anions omitted)

Similarly the reaction of **4** with $[CPh_3][BAr^F_4]$ in C_5D_5Cl immediately results in formation of a soluble cationic species, $[Cp^*Ti\{NC(Ph)N^iPr_2\}Me][BAr^F_4]$ (**29**). Although this reaction does not proceed as cleanly, evidenced by the presence of unidentifiable impurities in the ^1H NMR spectrum, the major signals corresponding to **29** bear close resemblance to those observed for the reaction of $Cp^*Ti\{NC(Ar^{F2})N^iPr_2\}Me_2$ with $[CPh_3][BAr^F_4]$.[76] The amidinate and $MeCPh_3$ aromatic protons are observed as a series of overlapping multiplets spanning the range 7.25-7.85 ppm. Two singlets observed at 1.50 and 0.81 ppm are assigned to the Cp* and Me ligand protons respectively. Restricted rotation about the C-N^iPr_2 bond results in observation of two septets (4.37 and 3.47 ppm) and two doublets (0.93 and 0.73 ppm) corresponding to the methine and methyl protons of the *iso*-propyl groups respectively. The resonance in the ^{13}C NMR spectrum assigned to the methyl ligand is observed at 68.0 ppm which compares closely to the corresponding signal observed for the related cationic species $[Cp^*Ti\{NC(Ar^{F2})N^iPr_2\}Me]^+$ (70.8 ppm).[76, 77] Unfortunately, in spite of repeated attempts to crystallise **29**, the cationic species invariably precipitates from solution as an oil which could not be redissolved. However, generation of the cation *in situ* also permitted characterisation by ESI^+ mass spectrometry: a peak was observed at *m/z* = 401.4 with the expected isotope distribution for the monomeric cation (calcd. *m/z* = 401.2).

3.7.2 Reaction of CpTi{NC(Ph)N^{i}Pr$_2$}Me$_2$ (20) with [CPh$_3$][BAr$^F{}_4$]

For comparison to the activation of **4** described above, a similar experiment was devised with the unsubstituted Cp analogue, **20**. Reaction of **20** with [CPh$_3$][BAr$^F{}_4$] in C_6H_5Cl immediately results in precipitation of a red oil which crystallises on standing for two hours affording the dimeric dication, [Cp$_2$Ti$_2${μ-NC(Ph)N^{i}Pr$_2$}$_2$Me$_2$][BAr$^F{}_4$] (**30**) (Equation 3.8).

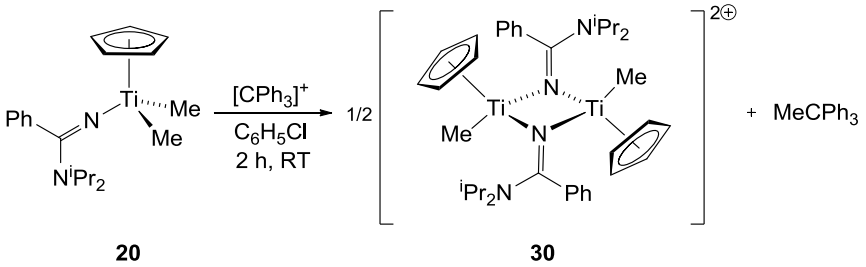

20 **30**

Equation 3.8 ([BAr$^F{}_4$]$^-$ anions omitted)

Compound **30** has been characterised by X-ray diffraction, IR spectroscopy, ESI$^+$ and EI mass spectrometry and elemental analysis. Unlike the case of **29**, the precipitation of insoluble **30** occurs too quickly for characterisation in solution by NMR. EI mass spectrometry results in significant fragmentation such that a peak corresponding to the dication is not observed. Similarly, the ESI$^+$ mass spectrum does not exhibit the expected peak for the dication (**30**$^{2+}$) at *m/z* = 331.2. However, a peak at *m/z* = 662.3 with the expected isotope distribution pattern for the dimeric monocation (calcd. *m/z* = 662.3) is observed suggesting reduction of the dimeric dication during the ionisation process has occurrred; such processes are not uncommon in ESI$^+$ mass spectrometry of cationic metal complexes. Fortunately growth of diffraction-quality crystals allowed structural characterisation of **30**. The molecular structure of the cation **30**$^{2+}$ is shown in Figure 3.14 and full crystallographic data can be found in the CD appendix. Selected bond lengths and angles of **30**$^{2+}$ are presented in Table 3.10.

The centrosymmetric molecular structure of **30**$^{2+}$ comprises pseudo-tetrahedral titanium centres surrounded by Cp* and methyl ligands and bridged by two nearly symmetrical μ-amidinate groups. This is clearly different to the structure of [Cp*$_2$Ti$_2${NC(Ar^{F2})N^{i}Pr$_2$}$_2$(μ-Me)$_2$]$^{2+}$ which is bridged by α-agostic methyl groups as discussed above; it may be conjectured that the greater steric demands of the Cp* ligand must disfavour the amidinate-bridging observed in **30**$^{2+}$. This is consistent with the previous work in the Mountford group concerning the cation chemistry of half-

sandwich TACN-supported imido cations: the formation of imido-bridged homo- or hetero-bimetallic species is encouraged by less sterically demanding imido ligand substituents.[75, 78, 79] Similar behaviour was also observed in Ti(III) phosphinimide systems: reduction of $CpTi(NP^tBu_3)Cl_2$ and $CpTi(NPR_3)Cl_2$ (R = Me, ^{i}Pr) with magnesium metal afforded $Cp_2Ti_2(NP^tBu_3)_2(\mu\text{-}Cl)_2$ and $Cp_2Ti_2(\mu\text{-}NPR_3)_2Cl_2$ dimers respectively.[80, 81]

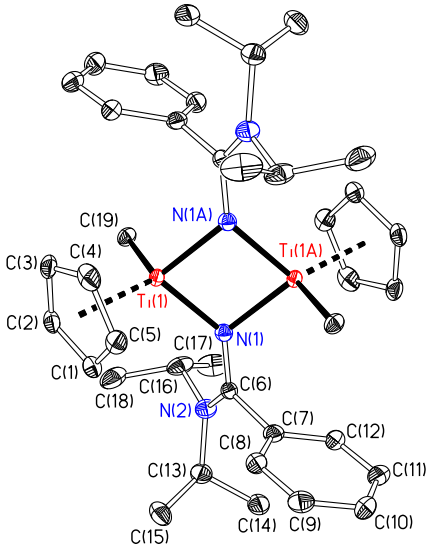

Figure 3.14. Displacement ellipsoid plot (20% probability) of $[Cp_2Ti_2\{\mu\text{-}NC(Ph)N^iPr_2\}_2Me_2]^{2+}$ (**30**$^{2+}$). H atoms, solvent of crystallisation and anions omitted for clarity. Atoms carrying the suffix 'A' are related to their counterparts by the symmetry operator [1-*x*, 1-*y*, 1-*z*].

The Ti(1)-N(1) (1.951(3) Å) and Ti(1)-N(1A) (2.016(3) Å) bond lengths are significantly longer than observed in the neutral titanium dimethyl complex **4** (1.8452(15) Å) and the cyclopentadienyl-supported zwitterion **12** (1.8499(19) Å) reflecting the bridging coordination mode of the amidinate as well as Coulombic repulsion between the formally cationic metal centres. The internal amidinate bond lengths are also altered dramatically: the N(1)-C(6) distance (1.343(4) Å) is now longer than the N(2)-C(6) bond length (1.303(5) Å). These structural observations appear indicative of the amidinate behaving like a bridging imido ligand facilitated by enhanced conjugation of the amine nitrogen lone pair towards the imine π-bond. The positive charge may therefore be considered to be distributed away from the metal centres onto the amidinate amine nitrogens permitting an analogy to be drawn between this dicationic amidinato-bridged complex and neutral imido-bridged

compounds. The Ti-N bond lengths in $Cp_2Ti_2(\mu\text{-}NPh)_2Cl_2$ (1.906(3)-1.920(4) Å)[82, 83] are broadly comparable to those observed in **30**$^{2+}$ in spite of the effect of the mutual electrostatic repulsion between the metal centres. The Ti(1)-Cp_{cent} (2.03 Å) distance is also the same as that observed for $Cp_2Ti_2(\mu\text{-}NPh)_2Cl_2$.[82] The Ti(1)-C(19) distance (2.097(4) Å) is slightly shorter than the Ti(1)-C_{methyl} bond lengths observed for the neutral titanium dimethyl complex **4** (2.1227(18) and 2.1326(19) Å) which is thought to reflect some degree of partial positive charge residing on titanium.

Table 3.10. Selected bond lengths (Å) and angles (°) for $[Cp_2Ti_2\{\mu\text{-}NC(Ph)N^iPr_2\}_2Me_2]^{2+}$ (**30**$^{2+}$). Cp_{cent} is the computed Cp ring carbon centroid.

Parameter		Parameter	
Ti(1)-Cp_{cent}	2.03	Cp_{cent}-Ti(1)-C(19)	110.2
Ti(1)-N(1)	1.951(3)	Ti(1)-N(1)-Ti(1A)	93.66(12)
Ti(1)-N(1A)	2.016(3)	N(1)-Ti(1)-N(1A)	86.34(12)
N(1)-C(6)	1.343(4)	Ti(1)-N(1)-C(6)	137.8(2)
N(2)-C(6)	1.303(5)	Ti(1A)-N(1)-C(6)	126.2(2)
Ti(1)-C(19)	2.097(4)	N(1)-Ti(1)-C(19)	103.25(13)
Cp_{cent}-Ti(1)-N(1)	125.5	N(1A)-Ti(1)-C(19)	108.12(14)
Cp_{cent}-Ti(1)-N(1A)	119.8		

3.7.3 Reaction of Cp*M{NC(Ph)N^{i}Pr$_2$}Me$_2$ (M = Zr (21) or Hf (22)) with [CPh$_3$][BAr$^F{}_4$]

Stoichiometric reaction of $[CPh_3][BAr^F{}_4]$ with $Cp^*M\{NC(Ph)N^iPr_2\}Me_2$ (M = Zr (**21**) or Hf (**22**)) in C_6H_5Cl also results in rapid crystallisation of an insoluble charge-separated species. Structural characterisation (*vide infra*) revealed that methyl abstraction had been followed by dimerisation affording a cationic amidinate-bridged dimer similar to the structure of **30**$^{2+}$ for both zirconium and hafnium (Equation 3.9). This activation behaviour is different to that of the titanium congener **4** which, as discussed above, on reaction with $[CPh_3][BAr^F{}_4]$ immediately forms a soluble cationic species which displays similar solution behaviour to that described for $[Cp^*{}_2Ti_2\{NC(Ar^{F2})N^iPr_2\}_2(\mu\text{-}Me)_2]^{2+}$.[76]

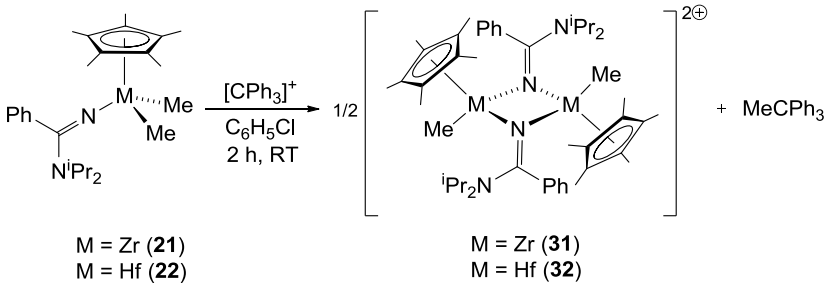

M = Zr (**21**)
M = Hf (**22**)

M = Zr (**31**)
M = Hf (**32**)

Equation 3.9 ([BAr$^F_4$]$^-$ anions omitted)

Compounds **31** and **32** have been characterised by X-ray diffraction, IR spectroscopy, EI mass spectrometry and elemental analysis. Irreversible crystallisation of insoluble **31** and **32** occurs too quickly for characterisation in solution by NMR. Unfortunately, a useful EI or ESI$^+$ mass spectrum could not be obtained; only peaks corresponding to fragments were observed in the EI spectrum. Fortunately growth of diffraction quality crystals allowed structural characterisation of both **31** and **32** which were found to be isomorphous. The molecular structure of the cation **32**$^{2+}$ is shown in Figure 3.15 and full crystallographic data can be found in the CD appendix. Selected bond lengths and angles of **31**$^{2+}$ and **32**$^{2+}$ are presented in Table 3.11.

As with **30**$^{2+}$, the centrosymmetric molecular structures of **31**$^{2+}$ and **32**$^{2+}$ comprise pseudo-tetrahedral metal centres coordinated by Cp*, methyl and two bridging almost symmetrical μ-amidinate groups. The more open metal centre in the zirconium and hafnium congeners is thought to encourage amidinate-bridging similarly to **30**$^{2+}$ in which the decreased steric bulk of unsubstituted Cp ligand is responsible for a more accessible titanium centre. Such effects have been observed notably for cyclooctatetraenyl-supported group 4 arylimido complexes: the titanium compounds either adopt fascinating monomeric one-legged piano stool or dimeric imido-bridged structures with the latter being favoured by less bulky ligand substituents.[63] The zirconium and hafnium congeners are thought to be exclusively bimetallic although they have not been structurally characterised.[84]

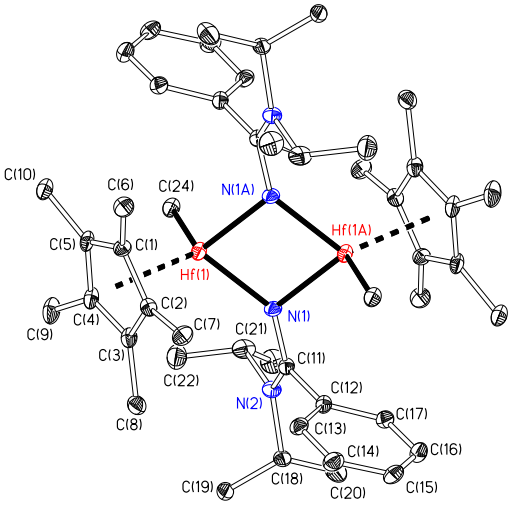

Figure 3.15. Displacement ellipsoid plot (20% probability) of $[Cp^*_2Hf_2\{\mu\text{-}NC(Ph)N^iPr_2\}_2Me_2]^{2+}$ (**32**$^{2+}$). H atoms and anion omitted for clarity. Atoms carrying the suffix 'A' are related to their counterparts by the symmetry operator [1–*x*, 1-*y*, 1-*z*]

As discussed for **30**$^{2+}$ significant donation of the amine N lone pair towards the imine π-bond results in much longer N(1)-C(11) (1.344(6) Å (**31**$^{2+}$), 1.353(7) Å (**32**$^{2+}$)) and shorter N(2)-C(11) (1.337(6) Å (**31**$^{2+}$), 1.300(8) Å (**32**$^{2+}$)) distances in the cationic species in comparison to those in the neutral zirconium and hafnium half-sandwich dialkyls in which the N(1)-C(11) (1.286(9)-1.297(5) Å) distance is significantly shorter than the N(2)-C(11) (1.364(5)-1.373(3) Å) bond. The effect lends bridging-imido character to the amidinate ligand resulting in M(1)-N(1) and M(1)-N(1A) (2.208(4), 2.097(4) Å (**31**$^{2+}$), 2.103(5), 2.186(5) Å (**32**$^{2+}$)) distances being comparable, if slightly longer due to Coulombic repulsion between the cations, to the Zr-N (1.951(9)-2.171(9) Å) and Hf-N_{imide} bond lengths (2.033(5)-2.117(5) Å) observed in related neutral imido-bridged dimeric species, $(\eta^5\text{-}C_5H_4Me)_2Zr_2(\mu\text{-}Nar)_2Cl_2$ (Ar = 2,6-$C_6H_3{}^iPr_2$)[84] and $Cp^*_2Hf_2(\mu\text{-}NPh)_2(NHPh)_2$[85] respectively. The positive charge must therefore be distributed between the metal centres and the amidinate amine nitrogens as concluded for **30**$^{2+}$. This is further demonstrated by the similarity of the M(1)-C(24) (2.244(6) Å (**31**$^{2+}$), 2.221(8) Å (**32**$^{2+}$)) distances with the Zr-C_{alkyl} (2.259(3)-2.307(4) Å) and Hf-C_{benzyl} (2.250(7), 2.289(6) Å) bond lengths observed in **21**, **24** and **25**. Furthermore, the M(1)-Cp^*_{cent} (2.23 Å (**31**$^{2+}$), 2.21 Å (**32**$^{2+}$)) distances are comparable to those of the neutral zirconium (2.22 Å (**21**), 2.23 Å (**24**)) and hafnium (2.21 Å (**25**) dialkyls as well as the related zirconium (2.237(1) Å)[84] and hafnium (2.21 Å)[85] μ-arylimido complexes discussed above.

Table 3.11. Selected bond lengths (Å) and angles (°) for $[Cp^*_2M_2\{\mu\text{-}NC(Ph)N^iPr_2\}_2Me_2]^{2+}$ (M = Zr (**31**$^{2+}$) or Hf (**32**$^{2+}$)). Cp_{cent} is the computed Cp* ring carbon centroid.

Parameter	**31**$^{2+}$	**32**$^{2+}$
M(1)-Cp_{cent}	2.23	2.21
M(1)-N(1)	2.208(4)	2.103(5)
M(1)-N(1A)	2.097(4)	2.186(5)
N(1)-C(11)	1.344(6)	1.353(7)
N(2)-C(11)	1.337(6)	1.300(8)
M(1)-C(24)	2.244(6)	2.221(8)
Cp_{cent}-M(1)-N(1)	130.6	121.9
Cp_{cent}-M(1)-N(1A)	117.0	126.3
Cp_{cent}-M(1)-C(24)	107.1	108.3
M(1)-N(1)-M(1A)	99.36(15)	97.33(19)
N(1)-M(1)-N(1A)	80.64(15)	82.67(19)
M(1)-N(1)-C(11)	148.0(3)	142.2(5)
M(1A)-N(1)-C(11)	110.2(3)	118.9(4)
N(1)-M(1)-C(24)	101.05(18)	105.5(2)
N(1A)-M(1)-C(24)	114.44(19)	108.9(3)

3.8 Polymerisation experiments

Small-scale ethylene homopolymerisation and ethylene-propylene copolymerisation testing was undertaken at LANXESS Elastomers, The Netherlands, in order to assess trends in productivity and polymer properties for the congeneric series of group 4 half-sandwich amidinate complexes. Full experimental details are given in Chapter Five. The molecular weight and polydispersity index (PDI) were obtained from GPC data with copolymer composition being measured using FT-IR. In each case, activation of the precatalysts was achieved with two equivalents of $[CPh_3][BAr^F_4]$; zirconium diene complexes **26**, **27** and zwitterion **28** were inactive with BAr^F_3. However, diene compound **26** was found to be active when used with $[CPh_3][BAr^F_4]$. The titanium dialkyl complex **20** was also inactive. The results for the active catalysts are summarised in Table 3.12.

3.8.1 Ethylene homopolymerisation

The titanium precatalysts are significantly more productive than both zirconium and hafnium congeners. The zirconium precatalysts are in turn more productive than the

hafnium dialkyls **22** and **25**. In order to ensure roughly isothermal conditions during polymerisation, the catalyst loading was lowered such that exotherms did not exceed 3 °C. Hence, in spite of the polymer yields being similar for titanium and hafnium, the productivities are much higher for the titanium precatalysts. The polymer samples from testing of the hafnium complexes could not be reliably analysed because of the high metal content derived from higher catalyst loading.

An apparent activator influence on productivity may be observed comparing the performance of the highly active titanium dimethyl (**4**) and dibenzyl (**23**) precatalysts: the productivity for **4** (62000 kg mol^{-1} h^{-1} bar^{-1}) is greater than observed for **23** (43000 kg mol^{-1} h^{-1} bar^{-1}) with lower molecular weight polyethylene exhibiting a higher PDI being produced by **23**. The origin of these differences remains unclear and the effect is not observed in the better controlled EP copolymerisation (*vide infra*) which does not reveal any differences to productivity or polymer properties associated with employment of the dimethyl (**4**) or dibenzyl (**23**) precatalyst.

Table 3.12. Polymerisation results[a]

Precatalyst	C3:C2	Cat. Loading[b] /µmol	Polymer Yield/g	Productivity/ kg mol^{-1} h^{-1} bar^{-1}	Polymer Analysis			
					C2/wt.%	C3/wt.%	M_n/ kg mol^{-1}	M_w/M_n
Cp*Ti{NC(Ph)N^{i}Pr$_2$}Me$_2$ (**4**)	0:100	0.02	1.44	62000	-	-	770	2.2
	80:40	0.14	10.55	65000	55.8	44.2	270	2.3
Cp*Ti{NC(Ph)N^{i}Pr$_2$}(CH$_2$Ph)$_2$ (**23**)	0:100	0.04	2.52	43000	-	-	470	4.3
	80:40	0.14	11.10	68000	55.1	44.9	270	2.4
Cp*Zr{NC(Ph)N^{i}Pr$_2$}Me$_2$ (**21**)	0:100	0.30	1.37	3900	-	-	13	8.7
	80:28	1.00	8.61	7400	56.1	43.9	2.2[c]	3.3
Cp*Zr{NC(Ph)N^{i}Pr$_2$}(CH$_2$Ph)$_2$ (**24**)	0:100	1.00	4.29	3700	-	-	12	12
	80:28	1.00	6.27	5400	60.0	39.4	2.0[c]	11
Cp*Zr{NC(Ph)N^{i}Pr$_2$}(η-2,3-C$_4$H$_4$Me$_2$) (**26**)	0:100	0.50	3.70	6300	-	-	13	8.0
	80:28	1.00	6.05	5200	57.6	41.7	2.2[c]	7.9
Cp*Hf{NC(Ph)N^{i}Pr$_2$}Me$_2$ (**22**)	0:100	1.00	1.53	1300	-	-	*d*	*d*
	80:28	1.00	1.41	1200	*d*	*d*	*d*	*d*
Cp*Hf{NC(Ph)N^{i}Pr$_2$}(CH$_2$Ph)$_2$ (**25**)	0:100	1.00	1.39	1200	-	-	*d*	*d*

[a]Conditions: T= 100 °C (E homopol.) or 90 °C (EP copol.), Pressure: 7 bar Scavenger: IBAO-65 ([Al] = 0.90 mM), 10 minute reaction time. Solvent pentamethylheptane (1L), 10 minute reaction time, Cocatalyst:[CPh$_3$][BAr$^F_4$] ([B]:[M] = 2). All polymer yields given are reproducible to within 10 % in duplicate runs. [b]Cat. Loading adjusted to limit exotherm to < 3 °C. [c]Molecular weight from conventional GPC calibration (too low for universal calibraton). [d]Polymer yield too low and cat. Loading too high for reliable polymer analysis.

The productivities observed with the borate-activated zirconium dimethyl (**21**), dibenzyl (**24**) and diene (**26**) precatalysts are similar (but considerably lower than those seen for the titanium compounds). The hafnium dialkyls are less productive than the zirconium congeners under these conditions consistent with smaller exotherms (1.4-1.6 ºC) observed for **22** and **25** compared to the **21** and **24** (1.9-2.0 ºC) for the same catalysts loading (1.0 μmol).

For the active zirconium precatalysts, the precise nature of the activator (dialkyl or diene) does not seem to exert a significant influence on productivity, M_n or molecular weight distribution. However, the η-1,4-$C_4H_4Ph_2$ diene complex (**27**) is inactive in combination with $[CPh_3][BAr^F_4]$ and both **26** and **27** are inactive when employed with BAr^F_3 as the cocatalyst. The latter is consistent with the inactivity of the zwitterionic species **28**; as discussed in Chapter Two, the productivity of the diene complex is closely related to that of the corresponding zwitterion. As discussed for the titanium congener of **27**, the phenyl diene substituents seem to prevent smooth activation with either borane or borate cocatalysts.

The lower productivity of the second and third row congeners, as well as the inactivity of the unsubstituted Cp precatalyst (**20**) are thought to be related to differences in the nature of the cationic species described above. In the light of the structures of cations $\mathbf{30}^{2+}$-$\mathbf{32}^{2+}$ it may be speculated that a more open metal centre results in greater propensity for formation of less active or inactive amidinate-bridged homo- or hetero-bimetallic species by reaction with aluminium alkyls. The greater steric protection of the smaller titanium centre in **4** is thought to preclude amidinate-bridging. The smaller productivity observed for hafnium compared to zirconium must be in part derived from the greater stability of Hf-C bonds with an associated increase of the barrier with respect to ethylene insertion.[8]

The GPC analysis of the homopolymers indicates that the zirconium precatalyst produces much lower molecular weight polymers (M_p = 18-23 kg mol^{-1}) than the titanium congeners (M_n = 440-770 kg mol^{-1}). Furthermore, the monomodal molecular weight distributions observed for the titanium precatalysts (M_w/M_n = 2.2-4.3) contrasts with the multimodal distributions observed for the zirconium congeners which result in larger PDIs (M_w/M_n = 8.0-12). The results are indicative of multi-site behaviour of the zirconium catalysts with competitive chain-transfer processes resulting in shorter, lower molecular weight polymers.[86, 87]

3.8.2 Ethylene-propylene copolymerisation

In order to make fair comparison of the productivities, the propylene:ethylene ratio of the feed was adjusted such that the propylene incorporation in the copolymer was similar (*ca.* 55 wt.% C2) for both titanium and zirconium precatalysts. This was achieved by increasing the C3:C2 ratio from 80:40 for the titanium precatalysts to 80:28 for the zirconium precatalysts. Clearly the more open metal centre in the zirconium catalyst does not enhance propylene incorporation but rather switching from titanium to zirconium appears to diminish propylene affinity.

The productivities for the titanium dialkyl precatalysts are very high (65000-68000 kg mol^{-1} h^{-1} bar^{-1}) on the Gibson scale[2] with the copolymers having identical molecular weight distributions (Figure 3.16) implying that the same active species results from the dimethyl (**4**) and dibenzyl (**23**) precatalysts. The productivites of the zirconium precatalysts (**21**, **24**, **26**) (5200-7400 kg mol^{-1} h^{-1} bar^{-1}) are very much lower and result in polymer with similar molecular weight distributions (*vide infra*). As discussed for the ethylene homopolymerisation data, the formation of homo- or hetero-bimetallic amidinate-bridged dormant species for zirconium and hafnium may account for the differences in performance with the titanium catalysts. The lower EP copolymerisation productivity observed for **22** (1200 kg mol^{-1} h^{-1} bar^{-1}) compared the zirconium precatalysts is thought to derive from greater stability of Hf-C bonds.

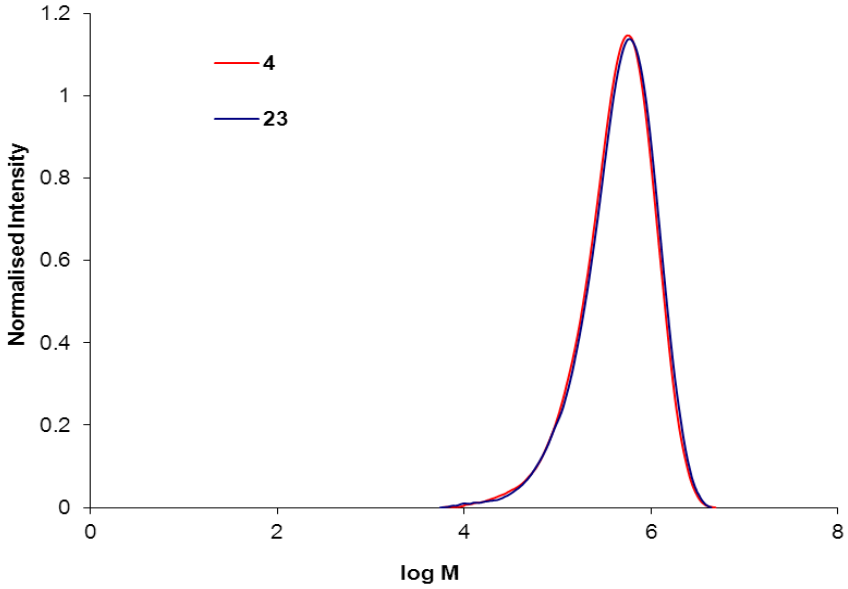

Figure 3.16. Molecular weight distribution determined by GPC for ethylene-propylene copolymer produced by Cp*Ti{NC(Ph)N^{i}Pr$_2$}Me$_2$ (**4**) and Cp*Ti{NC(Ph)N^{i}Pr$_2$}(CH$_2$Ph)$_2$ (**23**).

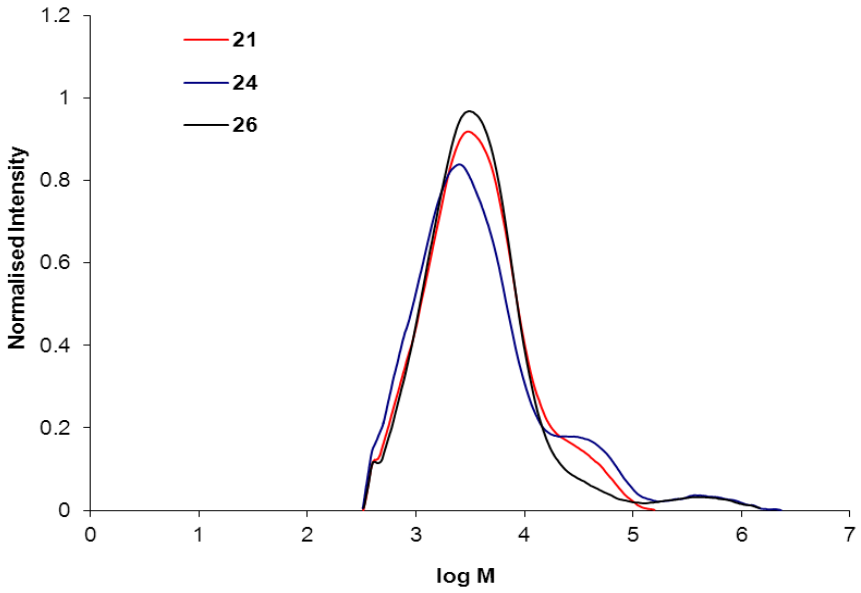

Figure 3.17. Molecular weight distribution determined by GPC for ethylene-propylene copolymer produced by Cp*Zr{NC(Ph)N^{i}Pr$_2$}Me$_2$ (**21**), Cp*Zr{NC(Ph)N^{i}Pr$_2$}(CH$_2$Ph)$_2$ (**24**), Cp*Zr{NC(Ph)N^{i}Pr$_2$}(η-2,3-C$_4$H$_4$Me$_2$) (**26**).

The temperature profiles for the titanium complexes indicate that the activated species is very active for approximately the first four minutes but subsequently deactivates over the subsequent six minutes of the run. In contrast, the zirconium and hafnium catalysts show a gradually inreasing exotherm which plateaus after approximately six minutes with the temperature remaining constant thereafter. It may therefore be speculated that longer runs may result in greater productivities being observed for the zirconium and hafnium catalysts.

As observed for the ethylene homopolymerisation, the dramatic decrease in productivities observed for the zirconium compared to the titanium precatalysts is combined with a switch from narrowly distributed (M_w/M_n = 2.3-2.4) monomodal, high molecular weight (M_n = 270 kg mol^{-1}) polymers (Figure 3.16) with the former to multimodal (M_w/M_n = 3.3-11) low molecular weight (M_p = 2.8-3.7 kg mol^{-1}) polymers (Figure 3.17) with the latter precatalysts. This behaviour for the zirconium catalysts is suggestive of involvement of more than one active site with low molecular weight polymers presumably resulting from rapid chain transfer processes.[86, 87] The FT-IR experiments served not only to estimate ethylene and propylene incorporation but also revealed the presence of vinylic end groups for the copolymers produced by the zirconium catalysts implying that β-hydrogen transfer is one such process competing with propagation (Figure 3.18). The number of vinyl end groups per chain was calculated from the FT-IR data to be 0.10-0.11 for the polymer produced by the zirconium catalysts **21**, **24** and **26**; no unsaturations were observed in the cases of the titanium catalysts **4** and **23**. These observations are consistent with the calculations of Ziegler *et al.* which suggest that the barrier to insertion, hence propagation, increases down group 4 with the barrier to β-hydrogen transfer remaining fairly constant resulting in greater propensity for β-hydrogen transfer descending the triad.[7] However, the significantly lower molecular weight polymer produced by the zirconium catalysts cannot be explained solely by β-hydrogen transfer given the relatively small number of unsaturations per polymer chain. It seems that chain transfer to aluminium is more prevalent for the zirconium than the titanium catalysts perhaps due to increased propensity to form hetero-bimetallic resting states for the former; the presence of such species has been correlated in the literature with chain transfer to aluminium.[75, 88]

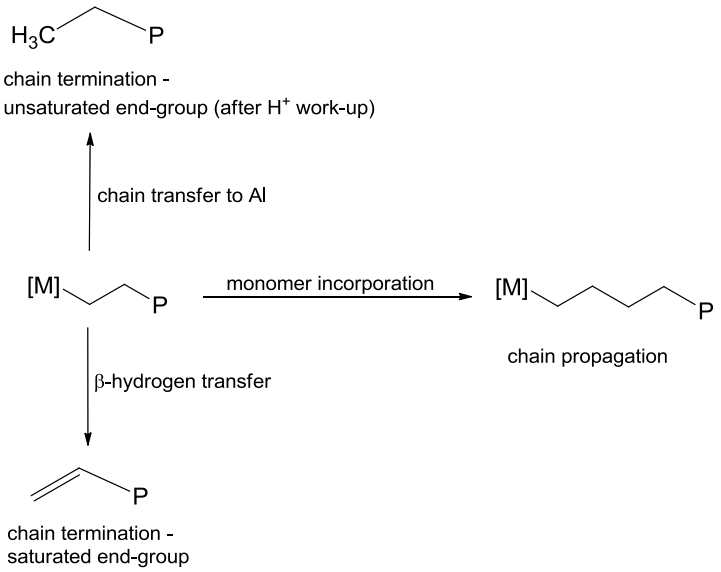

Figure 3.18. Competing chain transfer and propagation processes in ethylene polymerisation.

The similarities of the productivities and molecular weight distributions for **21**, **24** and **26** suggest that that same active species are formed under these polymerisation conditions. Consistent with the homopolymerisation results, the EP copolymerisation with the hafnium dimethyl complex **22** performed at C3:C2 ratio of 80:28 was less productive than the zirconium precatalyts; the combination of low polymer yield and high catalyst loading for the hafnium precatalysts meant that the polymer could not be reliably analysed.

The trends in productivity, polymer molecular weight and propylene affinity closely ressemble those seen for the MAO-activated half-sandwich aryl oxide complexes described in Section 3.2.[29, 30] As observed for the congeneric series described in this Chapter, the affinity for higher olefins (1-octene/2-methyl-1-pentene) decreases down the triad along with productivity and polymer molecular weight. The substituents of the phenoxy ligand are also critical to activity and incorporation of higher α-olefins since they determine the accessibility of the metal centre.[30] Comparison of titanium and zirconium constrained geometry systems has also shown the second row congener to be less active in ethylene-1-octene copolymerisations whilst apparently incorporating less of the higher α-olefin resulting in denser copolymers with higher melt indices.[89]

It may be that the productivity of zirconium and hafnium half-sandwich κ^1-amidinate-supported catalysts can be improved with bulkier ligand substituents which could act

to discourage formation of μ-amidinate dimers on activation which are speculated to be inactive dormant states. Additionally, more sterically demanding ligands are predicted similtaneously to lower insertion barriers and raise β-hydrogen transfer barriers which would increase polymer molecular weights.[7] Thus ligand optimisation for the second and third row metals may prove a fruitful avenue for future work.

3.9 Summary

This Chapter has described the preparation of a family of half-sandwich κ^1-amidinate complexes for olefin polymerisation. The half-sandwich group 4 dichloride complexes proved to be convenient precursors for dialkyl and, in the case of zirconium, diene precatalysts. Structural characterisation and use of DFT calculations provided a deeper insight into the metal-amidinate interaction and enhanced understanding of the bonding and conformational preference in the diene complexes. Preliminary experiments were undertaken into the activation chemistry of the diene and dialkyl precatalysts. Similarly to the observations described in Chapter Two, the zirconium diene complex **26**, formed a well-defined zwitterion (**28**) when reacted with one equivalent of BAr^F_3. Compound **28** could also be formed along with the titanium diene complex **5** by reaction of the titanium zwitterion **9** with the zirconium diene complex **26**. It was also found that heating **28** with Cp*Ti{NC(Ph)N^{i}Pr$_2$}(η-1,4-$C_4H_4Me_2$) (**6**) resulted in irreversible formation of **26** and the titanium zwitterion **10**.

The activation chemistry of the group 4 half-sandwich dimethyl complexes with $[CPh_3][BAr^F_4]$ demonstrated the influence of steric protection of the metal centre on the structure of the cationic species. Whilst the charge separated compound [Cp*Ti{NC(Ph)N^{i}Pr$_2$}Me][BAr^F_4] could not be crystallised, solution-phase spectroscopic similarities were observed with a closely related system which forms a methyl-bridged dimeric dication, $[Cp^*_2Ti_2\{NC(Ar^{F2})N^iPr_2\}_2(\mu\text{-}Me)_2]^{2+}$, in the solid state. In contrast, the more open zirconium and hafnium metal centres resulted in formation of structurally characterised amidinate-bridged dimeric dications. A similar μ-amidinate dicationic species was observed from reaction of CpTi{NC(Ph)N^{i}Pr$_2$}Me_2 (**20**) with $[CPh_3][BAr^F_4]$.

The homo- and copolymerisation experiments showed very high productivities with Cp*-supported titanium precatalysts but much poorer productivites with zirconium. The hafnium dialkyl precatalysts were less active than the zirconium complexes;

compound **20** was also shown to be inactive. It may be speculated in the light of the activation experiments with $[CPh_3][BAr^F_4]$ that formation of μ-amidinate homo- or hetero-bimetallic dormant species may be a likely deactivation pathway. Future research into the fundamental activation chemistry of the zirconium and hafnium dialkyl complexes described in this Chapter will include studying the reactivity of the cationic species with aluminium alkyls.

The polymer properties observed with zirconium compared to titanium catalysts are also markedly different: the titanium catalysts display single-site behaviour leading to monomodal, high molecular weight polymers with saturated chain ends whereas the zirconium congeners give multimodal, low molecular weight polymers with less propylene incorporation in copolymerisation experiments. The presence of vinylic end groups suggests that β-hydrogen transfer is one competing chain transfer mechanism although chain transfer to aluminium is thought to predominate.

3.10 References for Chapter Three

1. R. T. W. Scott, Part II Thesis, University of Oxford, 2009.
2. G. J. P. Britovsek, V. C. Gibson and D. F. Wass, *Angew. Chem., Int. Ed. Engl.*, 1999, **38**, 428-447.
3. G. W. Coates, *J. Chem. Soc., Dalton Trans.*, 2002, 467-475.
4. V. C. Gibson and S. K. Spitzmesser, *Chem. Rev.*, 2003, **103**, 283-315.
5. A. L. McKnight and R. M. Waymouth, *Chem. Rev.*, 1998, **98**, 2587-2598.
6. L. Resconi, L. Cavallo, A. Fait and F. Piemontesi, *Chem. Rev.*, 2000, **100**, 1253-1346.
7. P. Margl, L. Deng and T. Ziegler, *Top. Catal.*, 1999, **7**, 187-208.
8. L. Fan, D. Harrison, T. K. Woo and T. Ziegler, *Organometallics*, 1995, **14**, 2018-2026.
9. H. Makio and T. Fujita, *Bull. Chem. Soc. Jpn.*, 2005, **78**, 52-66.
10. H. Makio, Y. Tohi, J. Saito, M. Onda and T. Fujita, *Macromol. Rapid Commun.*, 2003, **24**, 894-899.
11. S.-i. Ishii, R. Furuyama, N. Matsukawa, J. Saito, M. Mitani, H. Tanaka and T. Fujita, *Macromol. Rapid Commun.*, 2003, **24**, 452-456.
12. K. V. Axenov, M. Klinga, O. Lehtonen, H. T. Koskela, M. Leskela and T. Repo, *Organometallics*, 2007, **26**, 1444-1460.

13. G. J. Domski, E. B. Lobkovsky and G. W. Coates, *Macromolecules*, 2007, **40**, 3510-3513.
14. T. R. Boussie, G. M. Diamond, C. Goh, K. A. Hall, A. M. LaPointe, M. K. Leclerc, V. Murphy, J. A. W. Shoemaker, H. Turner, R. K. Rosen, J. C. Stevens, F. Alfano, V. Busico, R. Cipullo and G. Talarico, *Angew. Chem., Int. Ed. Engl.*, 2006, **45**, 3278-3283.
15. C. Zuccaccia, A. Macchioni, V. Busico, R. Cipullo, G. Talarico, F. Alfano, H. W. Boone, K. A. Frazier, P. D. Hustad, J. C. Stevens, P. C. Vosejpka and K. A. Abboud, *J. Am. Chem. Soc.*, 2008, **130**, 10354-10368.
16. T. H. Warren, R. R. Schrock and W. M. Davis, *Organometallics*, 1996, **15**, 562-569.
17. R. Baumann, W. M. Davis and R. R. Schrock, *J. Am. Chem. Soc.*, 1997, **119**, 3830-3831.
18. R. R. Schrock, L.-C. Liang, R. Baumann and W. M. Davis, *J. Organomet. Chem.*, 1999, **591**, 163-173.
19. R. R. Schrock, R. Baumann, S. M. Reid, J. T. Goodman, R. Stumpf and W. M. Davis, *Organometallics*, 1999, **18**, 3649-3670.
20. L.-C. Liang, R. R. Schrock and W. M. Davis, *Organometallics*, 2000, **19**, 2526-2531.
21. P. Mehrkhodavandi, P. J. Bonitatebus and R. R. Schrock, *J. Am. Chem. Soc.*, 2000, **122**, 7841-7842.
22. P. Mehrkhodavandi and R. R. Schrock, *J. Am. Chem. Soc.*, 2001, **123**, 10746-10747.
23. P. Mehrkhodavandi, R. R. Schrock and P. J. Bonitatebus, *Organometallics*, 2002, **21**, 5785-5798.
24. P. Mehrkhodavandi, R. R. Schrock and L. L. Pryor, *Organometallics*, 2003, **22**, 4569-4583.
25. R. R. Schrock, J. Adamchuk, K. Ruhland and L. P. H. Lopez, *Organometallics*, 2003, **22**, 5079-5091.
26. Z. J. Tonzetich, C. C. Lu, R. R. Schrock, A. S. Hock and P. J. Bonitatebus, *Organometallics*, 2004, **23**, 4362-4372.
27. R. R. Schrock, J. Adamchuk, K. Ruhland and L. P. H. Lopez, *Organometallics*, 2005, **24**, 857-866.

28. Z. J. Tonzetich, R. R. Schrock, A. S. Hock and P. Müller, *Organometallics*, 2005, **24**, 3335-3342.
29. K. Nomura, *Dalton Trans.*, 2009, **0**, 8811-8823.
30. K. Itagaki, S. Hasumi, M. Fujiki and K. Nomura, *J. Mol. Catal. A: Chem.*, 2009, **303**, 102-109.
31. O. Alhomaidan, G. C. Welch, G. Bai and D. W. Stephan, *Can. J. Chem.*, 2009, **87**, 1163-1172.
32. D. W. Stephan, F. Guérin, R. E. v. H. Spence, L. Koch, X. Gao, S. J. Brown, J. W. Swabey, Q. Wang, W. Xu, P. Zoricak and D. G. Harrison, *Organometallics*, 1999, **18**, 2046-2048.
33. D. W. Stephan, J. C. Stewart and D. G. Harrison, *NOVA Chemicals International, EP 890581 A1*, 1999.
34. D. W. Stephan, J. C. Stewart, F. Guérin, R. E. v. H. Spence, W. Xu and D. G. Harrison, *Organometallics*, 1999, **18**, 1116-1118.
35. K. Dehnicke, M. Krieger and W. Massa, *Coord. Chem. Rev.*, 1999, **182**, 19-65.
36. C. K. Broder, A. E. Goeta, J. A. K. Howard, A. K. Hughes, A. L. Johnson, J. M. Malget and K. Wade, *J. Chem. Soc., Dalton Trans.*, 2000, 3526-3533.
37. A. E. Goeta, A. K. Hughes and J. M. Malget, *Acta Crystallogr., Sect. C*, 2001, **57**, 702-703.
38. M.-M. Sit, H.-S. Chan and Z. Xie, *Dalton Trans.*, 2008, 1454-1464.
39. H. Wang, H.-W. Li and Z. Xie, *Organometallics*, 2003, **22**, 4522-4531.
40. J. R. Hagadorn and J. Arnold, *Inorg. Chem.*, 1997, **36**, 2928-2929.
41. J. R. Hagadorn and J. Arnold, *Organometallics*, 1998, **17**, 1355-1368.
42. E. Y. X. Chen and T. J. Marks, *Chem. Rev.*, 2000, **100**, 1391-1434.
43. H. A. Bent, *Chem. Rev.*, 1961, **61**, 275-311.
44. E. G. Ijpeij, P. J. H. Windmuller, H. J. Arts, F. van der Burgt, G. H. J. van Doremaele and M. A. Zuideveld, *LANXESS ELASTOMERS, WO/2005/090418*, 2005.
45. E. Kirillov, L. Lavanant, C. Thomas, T. Roisnel, Y. Chi and J.-F. Carpentier, *Chem. Eur. J.*, 2007, **13**, 923-935.
46. M. Bochmann and S. J. Lancaster, *Organometallics*, 1993, **12**, 633-640.
47. R. F. Jordan, R. E. LaPointe, N. Baenziger and G. D. Hinch, *Organometallics*, 1990, **9**, 1539-1545.

48. C. Krueger, G. Mueller, G. Erker, U. Dorf and K. Engel, *Organometallics*, 1985, **4**, 215-223.
49. M. Dahlmann, J. Schottek, R. Fröhlich, D. Kunz, M. Nissinen, G. Erker, G. Fink and R. Kleinschmidt, *J. Chem. Soc., Dalton Trans.*, 2000, 1881-1886.
50. B. Temme, G. Erker, J. Karl, H. Luftmann, R. Fröhlich and S. Kotila, *Angew. Chem., Int. Ed. Engl.*, 1995, **34**, 1755-1757.
51. H. Yasuda and A. Nakamura, *Angew. Chem., Int. Ed. Engl.*, 1987, **26**, 723-742.
52. A. H. Cowley, G. S. Hair, B. G. McBurnett and R. A. Jones, *Chem. Commun.*, 1999, 437-438.
53. G. S. Hair, R. A. Jones, A. H. Cowley and V. Lynch, *Inorg. Chem.*, 2001, **40**, 1014-1019.
54. M. Brookhart, M. L. H. Green and G. Parkin, *Proceedings of the National Academy of Sciences*, 2007, **104**, 6908-6914.
55. T. R. Cundari, *Organometallics*, 1993, **12**, 4971-4978.
56. C. H. Zambrano, R. D. Profilet, J. E. Hill, P. E. Fanwick and I. P. Rothwell, *Polyhedron*, 1993, **12**, 689-708.
57. P. Mountford and D. Swallow, *J. Chem. Soc., Chem. Commun.*, 1995, 2357-2359.
58. N. Kaltsoyannis and P. Mountford, *J. Chem. Soc., Dalton Trans.*, 1999, 781-790.
59. T. R. Cundari, *Chem. Rev.*, 2000, **100**, 807-818.
60. S. C. Lawrence, M. E. G. Skinner, J. C. Green and P. Mountford, *Chem. Commun.*, 2001, 705-706.
61. P. D. Bolton, E. Clot, A. R. Cowley and P. Mountford, *Chem. Commun.*, 2005, 3313-3315.
62. C. L. Boyd, E. Clot, A. E. Guiducci and P. Mountford, *Organometallics*, 2005, **24**, 2347-2367.
63. S. C. Dunn, N. Hazari, N. M. Jones, A. G. Moody, A. J. Blake, A. R. Cowley, J. C. Green and P. Mountford, *Chem. Eur. J.*, 2005, **11**, 2111-2124.
64. H. Yamamoto, H. Yasuda, K. Tatsumi, K. Lee, A. Nakamura, J. Chen, Y. Kai and N. Kasai, *Organometallics*, 1989, **8**, 105-119.
65. J. Blenkers, B. Hessen, F. Van Bolhuis, A. J. Wagner and J. H. Teuben, *Organometallics*, 1987, **6**, 459-469.

66. D. D. Devore, F. J. Timmers, D. L. Hasha, R. K. Rosen, T. J. Marks, P. A. Deck and C. L. Stern, *Organometallics*, 1995, **14**, 3132-3134.
67. T. Cuenca, eds. D. M. P. Mingos and R. H. Crabtree, Elsevier, Amsterdam and Boston, 2007, pp. 323-695.
68. R. F. Jordan, F. G. A. Stone and W. Robert, in *Adv. Organomet. Chem.*, Academic Press, 1991, pp. 325-387.
69. M. Bochmann, *J. Chem. Soc., Dalton Trans.*, 1996, 255-270.
70. M. Bochmann and S. J. Lancaster, *Angew. Chem., Int. Ed. Engl.*, 1994, **33**, 1634-1637.
71. R. Vollmerhaus, M. Rahim, R. Tomaszewski, S. Xin, N. J. Taylor and S. Collins, *Organometallics*, 2000, **19**, 2161-2169.
72. C. L. Beswick and T. J. Marks, *J. Am. Chem. Soc.*, 2000, **122**, 10358-10370.
73. F. Song, S. J. Lancaster, R. D. Cannon, M. Schormann, S. M. Humphrey, C. Zuccaccia, A. Macchioni and M. Bochmann, *Organometallics*, 2005, **24**, 1315-1328.
74. P. D. Bolton, E. Clot, N. Adams, S. R. Dubberley, A. R. Cowley and P. Mountford, *Organometallics*, 2006, **25**, 2806-2825.
75. P. D. Bolton, E. Clot, A. R. Cowley and P. Mountford, *J. Am. Chem. Soc.*, 2006, **128**, 15005-15018.
76. E. G. Ijpeij, B. Coussens, M. A. Zuideveld, G. H. J. van Doremaele, P. Mountford, M. Lutz and A. L. Spek, *Chem. Commun.*, 2010, **46**, 3339-3341.
77. A. F. Russell and P. Mountford, in *Unpublished Results*, 2012.
78. C. T. Owen, P. D. Bolton, A. R. Cowley and P. Mountford, *Organometallics*, 2007, **26**, 83-92.
79. P. D. Bolton, N. Adams, E. Clot, A. R. Cowley, P. J. Wilson, M. Schröder and P. Mountford, *Organometallics*, 2006, **25**, 5549-5565.
80. D. W. Stephan, J. C. Stewart, F. Guérin, S. Courtenay, J. Kickham, E. Hollink, C. Beddie, A. Hoskin, T. Graham, P. Wei, R. E. v. H. Spence, W. Xu, L. Koch, X. Gao and D. G. Harrison, *Organometallics*, 2003, **22**, 1937-1947.
81. T. W. Graham, J. Kickham, S. Courtenay, P. Wei and D. W. Stephan, *Organometallics*, 2004, **23**, 3309-3318.
82. C. T. Vroegop, J. H. Teuben, F. van Bolhuis and J. G. M. van der Linden, *J. Chem. Soc., Chem. Commun.*, 1983, 550-552.

83. W. J. Grigsby, M. M. Olmstead and P. P. Power, *J. Organomet. Chem.*, 1996, **513**, 173-180.
84. D. J. Arney, M. A. Bruck, S. R. Huber and D. E. Wigley, *Inorg. Chem.*, 1992, **31**, 3749-3755.
85. Y. Bai, H. W. Roesky, M. Noltemeyer and M. Witt, *Chem. Ber.*, 1992, **125**, 825-831.
86. P. J. Flory, *Principles of Polymer Chemistry*, Cornell University Press, 1992.
87. G. Odian, *Principles of Polymerisation*, Wiley-Interscience, 1992.
88. G. J. P. Britovsek, S. A. Cohen, V. C. Gibson and M. van Meurs, *J. Am. Chem. Soc.*, 2004, **126**, 10701-10712.
89. J. C. Stevens and T. Kazuo Soga and Minoru, in *Stud. Surf. Sci. Catal.*, Elsevier, 1994, pp. 277-284.

Chapter Four

Chelated cyclopentadienyl-amidinate titanium complexes for olefin copolymerisation

4.1 Overview

This Chapter describes the syntheses, structures, EP and EPDM copolymerisation capability of a series of chelated cyclopentadienyl-amidinate titanium complexes. By tethering the cyclopentadienyl and amidinate ligands it was hoped to achieve better catalyst stability at higher temperatures whilst offering the possibility of greater propylene and diene comonomer incorporation. An effective synthetic route to bifunctional cyclopentadiene-benzamidine ligands is described; subsequent successful complexation to titanium allowing preparation of a series of half-sandwich dichloride and dimethyl precatalysts. Combined crystallographic and DFT studies of the chelated compounds suggest close electronic similarities with the related non-*ansa* titanium dichloride and dialkyl complexes previously described in this Thesis. Importantly, steric constraints imposed by the chelate bridge result a more open metal centre in the *ansa* compounds. Polymerisation experiments designed to test any advantage offered by the chelated complexes in terms of productivity, temperature stability and comonomer incorporation to the existing non-*ansa* precatalyts are described. A patent application covering some of the work in this Chapter is currently being drafted.

4.2 Synthesis and characterisation of *o*-aryl-bridged cyclopentadiene-amidine ligands

Selecting of a bridge of appropriate length is key in consideration of the design of chelated cyclopentadienyl-amidinate complexes: too short and the metal-amidinate π-interaction and steric protection of the metal centre will be compromised, too long and any advantage to be gained from ligand constraints leading to a more open metal centre will be negated. Indeed, the former consideration is exemplified by serendipitious discovery of a methylene-bridged cyclopentadienyl-amidinate titanium complex $\{\eta^5, \eta^1\text{-}C_5Me_4\text{-}CH_2\text{-}C(NMe_2)N\}TiCl_2$ in which structural characterisation reveals minimal steric protection for titanium resulting from the short linker and small amidinate substituents.[1] An *o*-aryl bridge was considered an appropriate compromise in terms of length whilst offering advantages of simplicity and flexibility of ligand synthesis (*vide infra*). A summary of constrained geometry-type systems employing a variety of linkers and donor moieties is given in Chapter One. The tethering of cyclopentadienyl groups to heteroatom donor moieties *via* aryl groups has also been exploited in a variety of catalyst systems.[2-14] Complexes of group 4 metals supported by bifunctional cyclopentadienyl-phenolate,[2-6] and –arylamide[7-13] ligands have been

described in the academic literature while similarly bridged cyclopentadienyl-ketimide complexes have been disclosed in the patent literature.[14] Previous related work in the Mountford group involved preparation of indium, aluminium and scandium alkyl complexes supported by *o*-phenoxy-functionalised triazacyclononane chelating ligands.[15-17] Group 4 complexes supported by *o*-arylimido-triazacyclononane ligands were also prepared[18] but displayed much poorer productivities in ethylene homopolymerisation than the related non-*ansa* arylimido sytems.[19] This section describes the preparation of the first series of cyclopentadienyl-benzamidine ligands with the subsequent two sections (4.3 and 4.4) detailing efforts to extend the scope of the synthesis.

4.2.1 Synthetic strategy for ligand synthesis

The synthetic strategy for synthesis of such *o*-aryl-bridged ligands is shown in Scheme 4.1. It employs the commercially available starting materials: 2,3,4,5-tetramethylcyclopent-2-enone and 2-(2-bromophenyl)-1,3-dioxolane. The first step affording C_5Me_4H-2-C_6H_4CHO was performed using a method adapted from the preparation described by Wills *et al.*[20] Lithium-bromine exchange of 2-(2-bromophenyl)-1,3-dioxolane at -78 °C with ^{n}BuLi followed by 1,2-nucleophilic addition to the cyclic enone and subsequent quenching with water affords the desired allylic alcohol. Subsequent acidic work-up results in deprotection of the acetal-protected benzaldehyde and dehydration of the allylic alcohol to give C_5Me_4H-2-C_6H_4CHO as a mixture of three double-bond isomers of the cyclopentadiene ring. The second step involves transformation of the aldehyde to the *O*-methyl oxime with the subsequent oxidation step to the nitrile proceeding *via* deprotonation of the aldehydic hydrogen with LDA. Such a transformation is exemplified in the patent literature as key steps in the synthesis of bifunctional cyclopentadienyl-ketimide ligands although the oxime and nitrile intermediates are not fully characterised.[14] The final step involves nucleophilic attack of the nitrile with a magnesium amide as described for the preparation of $HNC(Ph)N^{i}Pr_2$ (**1**) in Chapter Two.

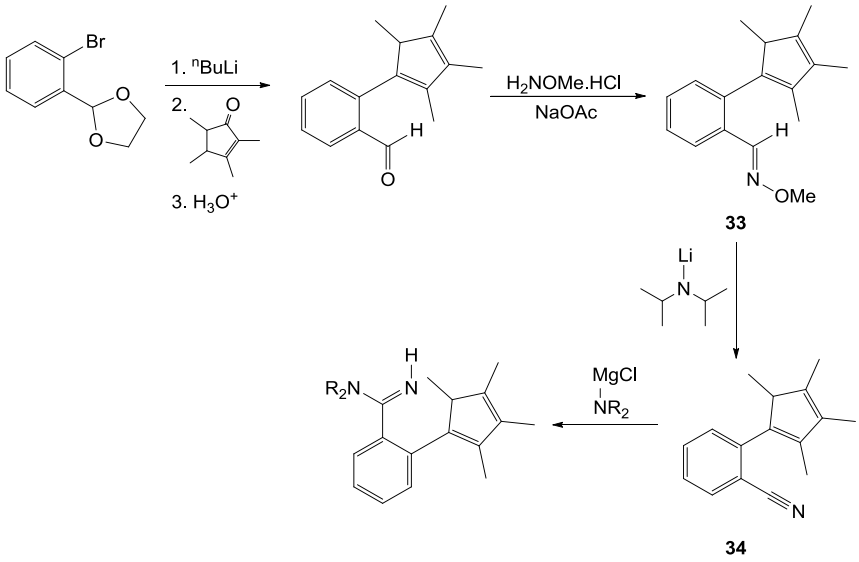

Scheme 4.1. Proposed route to *o*-aryl-bridged cyclopentadiene-amidine ligands.

4.2.2 Synthesis of ligand precursors: C_5Me_4H-2-$C_6H_4C(H)N(OMe)$ (33) and C_5Me_4H-2-C_6H_4CN (34)

Reaction of C_5Me_4H-2-C_6H_4CHO with a slight excess of $H_2NOMe{\cdot}HCl$ and NaOAc results in formation of C_5Me_4H-2-$C_6H_4C(H)N(OMe)$ (**33**) in reasonable isolated yield (77 %) after 30 minutes (Scheme 4.2) and may be accomplished on a multigram scale. As with the aldehyde, the compound exists as a mixture of the three possible double-bond isomers (Figure 4.1) although one (**33A**) is observed to predominate (80 %).

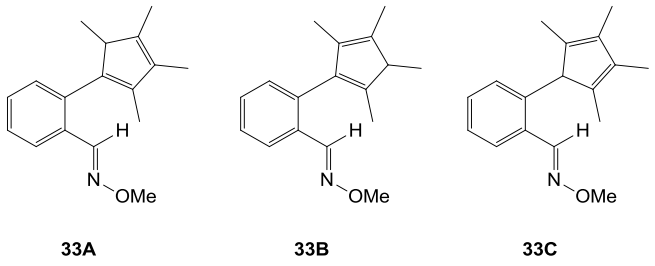

Figure 4.1

Compound **33** has been fully characterised by NMR and IR spectroscopy and high resolution FI mass spectrometry. The room temperature ^1H NMR spectrum of **33** in $CDCl_3$ reveals the presence of major (**33A**) and minor (**33B** and **33C**) isomers. Examination of the cyclopentadiene ring methyl and methine resonances allowed identification of the major isomer: a broad quartet (3.07 ppm) was observed corresponding to the methine proton which was shown in the two-dimensional COSY spectrum to couple to two methyl groups. Stronger scalar coupling (^3J = 7.5 Hz) is

observed to an immediately adjacent methyl group (0.88 ppm) with a weaker, longer range coupling (^4J = 1.8 Hz) to a methyl group on an adjacent ring carbon (1.67 ppm). No coupling is observed to the other two methyl groups which correspond to singlets at 1.89 and 1.83 ppm. The combined observations support assignment of the major isomer as **33A**; no ^3J coupling would be observed in the symmetrical double-bond isomer **33C** and two ^4J scalar coupling interactions would be expected in **33B**. The ^1H NMR spectrum of the major isomer comprises the expected singlets at 7.96 and 3.94 ppm corresponding to the aldehydic and oxime methyl protons respectively; the aromatic protons appearing as a series of overlapping multiplets spanning the range 7.93-7.08 ppm.

Subsequent reaction of **33** with three equivalents of LDA at -78 °C, slow warming to room temperature followed by quenching with water affords C_5Me_4H-2-C_6H_4CN (**34**) in good yield (92 %) (Scheme 4.2). An excess of the base is used due to the acidity of the methine proton of the cyclopentadiene ring.

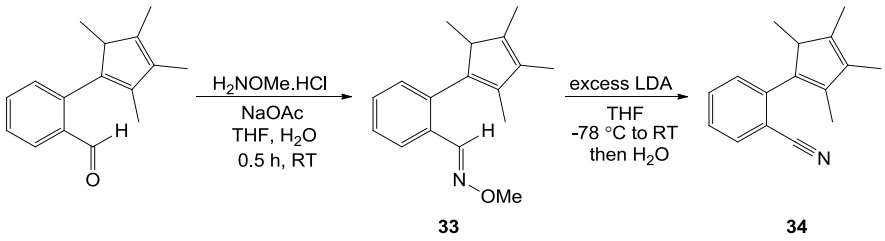

33 **34**

Scheme 4.2. Synthesis of C_5Me_4H-2-$C_6H_4C(H)N(OMe)$ (**33**) and C_5Me_4H-2-C_6H_4CN (**34**).

Compound **34** has been fully characterised by NMR and IR spectroscopy and high resolution FI mass spectrometry. Similarly to **33**, compound **34** exists as a mixture of three double bond isomers (Figure 4.2) but with predominance of one (70 %).

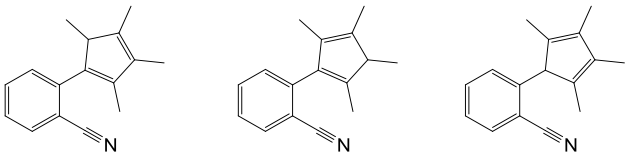

34A **34B** **34C**

Figure 4.2

The room temperature ^1H NMR spectrum of **34** in $CDCl_3$ exhibits a broad quartet corresponding to the methine proton (3.38 ppm) of the cyclopentadiene ring with strong coupling (^3J = 7.5 Hz) to the protons of an immediately adjacent methyl group

(0.92 ppm) and weaker coupling (^4J = 1.2 Hz) to two methyl groups on adjacent ring carbons. In contrast to the case in compound **33**, these observations are consistent with assigment of **34B** as the major isomer. A series of overlapping multiplets (7.70-7.22 ppm) correspond to the aromatic protons. The signal at 112.2 ppm in the ^{13}C NMR spectrum is assigned to the nitrile carbon whilst the peak in the IR spectrum at 2223 cm^{-1} corresponds to υ(C≡N).

4.2.3 Synthesis of C_5Me_4H-2-$C_6H_4C(NMe_2)NH$ (35)

Employing a method developed by Sanger,[21] the nitrile **34** was reacted with a large excess (six equivalents) of $LiNMe_2$ affording the protio-amidine, C_5Me_4H-2-$C_6H_4C(NMe_2)NH$ (**35**) in good isolated yield (95 %) (Scheme 4.3) following aqueous work-up. Unlike the reaction described in Chapter Two for the synthesis of N,N-diisopropylbenzamidine, the reaction does not proceed in toluene which is thought to result in large part from the insolubility of the conjugate base of **34** formed from deprotonation of the methine proton of the cyclopentadiene ring by the first equivalent of $LiNMe_2$. An excess of the lithium amide is required for efficient nucleophilic addition to the nitrile of the resulting anionic species. However, the reaction is successful in THF and may be performed on a multigram scale. Similarly to **33** and **34**, compound **35** exists as a mixture of three double-bond isomers (Figure 4.3) with preponderance of one (80 %).

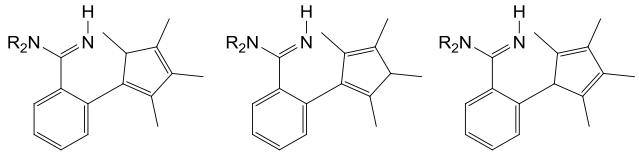

Figure 4.3

Compound **35** has been fully characterised by NMR and IR spectroscopy and high resolution FI mass spectrometry. The methyl signals (major isomer) of the amidine moiety are broad in the room temperature ^1H NMR spectrum in CD_2Cl_2 presumably due to restricted rotation about the C-NMe_2 bond but sharpen considerably to two singlets (3.16 and 2.54 ppm) on cooling to -30 °C. A series of overlapping multiplets (7.50-7.16 ppm) correspond to the four aromatic protons. The weak ^4J coupling between the methine proton of the cyclopentadiene, which itself appears as the

familiar broad quartet at 2.87 ppm, and the methyl protons attached to adjacent ring carbons is less obvious than in the case of **33** and **34** although stronger coupling (^3J = 7.1 Hz) to an immediately adjacent methyl group (0.79 ppm) is observed. The slightly broader appearance of the singlets at 1.88 and 1.84 ppm compared to that at 1.38 ppm suggests that the dominant isomer is **35B** (Figure 4.3). The imine carbon signal is observed at 166.3 ppm in the low temperature (-30 °C) ^{13}C NMR spectrum.

4.2.4 Synthesis of C_5Me_4H-2-$C_6H_4C(N^iPr_2)NH$ (36) and C_5Me_4H-2-$C_6H_4C(NCy_2)NH$ (37)

The work described in Chapter Three emphasises the importance of steric considerations in determining catalyst productivity with more open, less sterically protected metal centres (and imine nitrogens) leading to possible formation of inactive homo- or hetero-bimetallic species during catalysis. Fortunately this route *via* compound **34** provides a degree of flexibility in terms of substitution of the amine nitrogen such that more steric encumbrance may be introduced by nucleophilic addition of bulkier secondary amines to the nitrile. Similarly to the preparation of **1** described in Chapter Two, deprotonation of diisopropylamine or dicyclohexylamine with MeMgBr followed by reaction with **34** gives, after aqueous work-up, the desired bulkier protio-amidines **36** and **37** respectively (Scheme 4.3). As in the preparation of **35**, the reaction fails in toluene but proceeds in THF due to the solubility of the conjugate base of **34**. Also noteworthy is that the lithiated secondary amines are not sufficiently nucleophilic to react with the nitrile (excess LDA was used to prepare **34** without resulting in further reaction to give **36**). The isolated yields (34-51 %) following purification by flash column chromatography reflect the increased difficulty of addition to a nitrile by more bulky nucleophiles. However, multigram quantities of **36** and **37** can be prepared using this route.

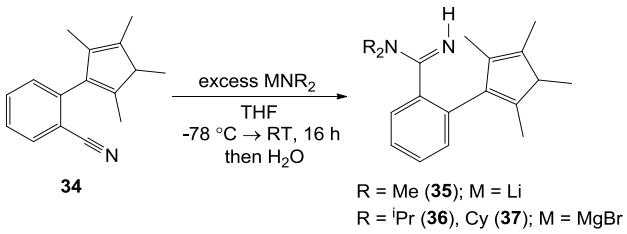

Scheme 4.3. Synthesis of *o*-aryl-bridged cyclopentadiene-amidines **35-37** from the nitrile **34**.

Compounds **36** and **37** have been fully characterised by NMR and IR spectroscopy and high resolution ESI^+ mass spectrometry. Similarly to compounds **33**-**35**, compounds **36** and **37** exist as mixture of three double bond isomers (Figure 4.3). In both the major isomer (70 %) was spectroscopically characterised by ^1H and ^{13}C NMR. The room temperature ^1H NMR spectrum in $CDCl_3$ of **36** reveals the expected signals corresponding the aromatic protons spanning the range 7.34-7.08 ppm. Restricted rotation about the C-N^{i}Pr$_2$ bond results in observation of two methine septets (3.62 and 3.44 ppm) and two doublets (1.08 and 0.74 ppm) corresponding to the *iso*-propyl groups. This is consistent with the behaviour of **35** in which the slow C-NMe_2 bond rotation regime lies at lower temperature (-30 °C) presumably due to the smaller amidine methyl substituents leading to a lower barrier to rotation. Similarly to **33**-**35**, a broad quartet (3.44 ppm) corresponds to the methine proton of the cyclopentadiene which exhibits coupling (^3J = 7.5 Hz) to an adjacent methyl group (0.87 ppm). Whilst the weaker ^4J coupling to methyl protons on adjacent ring carbons cannot be observed in the COSY spectrum, two of the remaining methyl signals are sharp (1.85 and 1.83 ppm) with a broader singlet being observed at slightly higher field (1.67 ppm). Broadening of the latter is thought to result from weak ^4J coupling with cyclopentadiene methine proton suggesting that the major isomer is **36A** (Figure 4.3). The room temperature ^{13}C NMR spectrum exhibits a peak at 158.8 ppm expected for the imine carbon of the major isomer.

The room temperature ^1H NMR spectrum in $CDCl_3$ of **37** is similar to that of **36** aside from the differences in substitution of the amine nitrogen: the cyclohexyl methine signals are observed at 3.46 and 2.99 ppm with the other ring protons appearing as a series of overlapping multiplets spanning the range 1.74-0.91 ppm. A series of multiplets (7.31-7.08 ppm) account for the four aromatic protons. Similarly to **36**, the major isomer is assigned as **37A** (Figure 4.3): the cyclopentadiene methine proton (3.44 ppm) is coupled (^3J = 7.5 Hz) to the highest field methyl group (0.86 ppm) with the other methyls corresponding to two sharp singlets (1.85 and 1.82 ppm) and a broader peak (1.60 ppm). A broad signal at 5.78 ppm is thought to correspond to the imine nitrogen proton. As observed for compounds **35** and **36** the lowest field peak in the ^{13}C NMR spectrum is assigned to the imine carbon (168.3 ppm).

4.3 Extension to indene derivatives

It was hoped to extend the scope of the synthetic strategy in order to prepare *o*-aryl-bridged indene-amidine ligands. A similar modular synthesis to that described for the cyclopentadiene-type derivatives beginning with the commercially available and inexpensive 1-indenone was envisaged. This precursor was employed successfully for preparation of group 4 complexes supported by indenyl-phenolate[3, 4] and indenyl-arylamide[13] chelating ligands.

4.3.1 Synthesis of (1-C_9H_8OH)-2-$C_6H_4CH(C_2H_4O_2)$ (38)

Using similar methodology to that described by Wills (*vide supra*),[20] *ortho*-lithiation of 2-(2-bromophenyl)-1,3-dioxolane at -78 °C with subsequent 1,2-nucleophilic addition to the 1-indenone and subsequent quenching with water (Scheme 4.4) affords the desired indenol **38** in reasonable isolated yield following crystallisation (59 %).

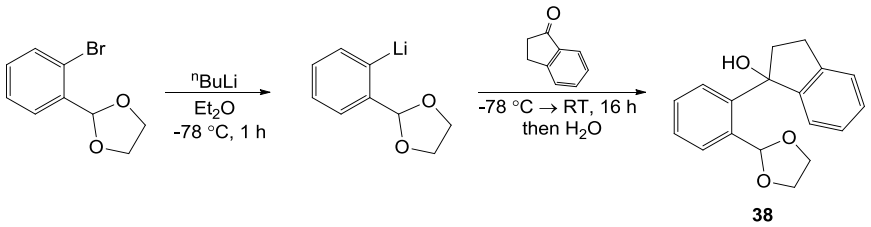

Scheme 4.4. Synthesis of (1-C_9H_8OH)-2-$C_6H_4CH(C_2H_4O_2)$ (**38**).

Compound **38** has been fully characterised by NMR and IR spectroscopy and high resolution ESI^+ mass spectrometry. The room temperature ^1H NMR spectrum in $CDCl_3$ exhibits the expected signals corresponding to the eight aromatic protons in the region 7.72-6.76 ppm. The indenol ring methylene protons adjacent to the aryl ring and adjacent to the hydroxyl-bearing ring carbon are observed at 2.91 and 2.55 ppm respectively. The hydroxyl proton itself corresponds to a fairly broad signal at 3.21 ppm. The acetal methylene resonances occur at 4.14 and 3.96 ppm with the aldehydic proton corresponding to a singlet at 6.41 ppm. The connectivity was confirmed by structural characterisation of **38** (*vide infra*).

4.3.2 Synthesis of (1-C_9H_7)-2-C_6H_4CHO (39)

Whilst acetal-deprotection proved straightforward in aqueous acid, dehydration of the indenol could not be accomplished so easily. Screening of a variety of conditions, including use of concentrated acid and Dean-Stark apparatus as well as acidic ion-exchange resins, did not provide an effective path to the indene. Following

deprotection of the acetal under mildly acidic conditions and purification by flash column chromatography, a colourless solid was isolated which was speculated to be an intramolecular hemiacetal from reaction of the deprotected benzaldehyde with the proximal hydroxyl group of the indenol (Scheme 4.5). This was supported by the ^{1}H NMR spectrum of the material in which four inequivalent methylene protons of the indenol ring were observed with notable absence of the characteristic low field aldehydic proton resonance. Furthermore, the high resolution FI mass spectrum of the material exhibits a peak at *m/z* = 238.0997 with the expected isotope distribution pattern for the intramolecular hemiacetal (calcd. *m/z* = 238.0994).

Fortunately, dehydration to the desired indene was accomplished by short path Kuglerohr) distillation of the acetal-deprotected material resulting in isolation of a single double-bond isomer of (1-C_9H_7)-2-C_6H_4CHO (**39**) as a yellow oil (47 %) (Scheme 4.5).

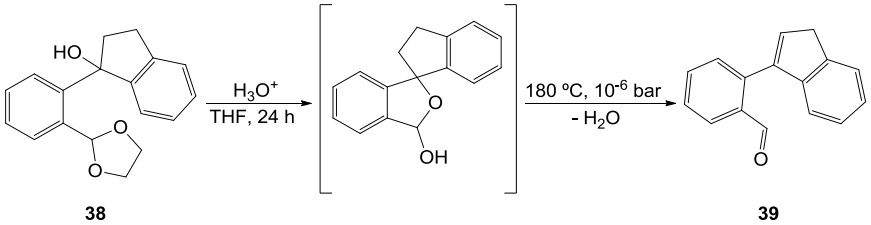

38 **39**

Scheme 4.5. Synthesis of (1-C_9H_7)-2-C_6H_4CHO (**39**) by deprotection and dehydration of (1-C_9H_8OH)-2-C_6H_4CH($C_2H_4O_2$) (**38**).

Compound **39** has been fully characterised by NMR and IR spectroscopy and high resolution ESI^{+} mass spectrometry. The room temperature ^{1}H NMR spectrum in $CDCl_3$ displays a series of aromatic resonances (8.04-7.17 ppm) corresponding to the eight aryl protons. The assignment of the double bond isomer stems from observation of a higher field doublet (3.58 ppm) coupled to a lower field triplet (6.52 ppm) corresponding to methylene and vinylic methine indene protons respectively. The origin of the preference for this isomer presumably lies in conjugation of the indene moiety with the benzaldehyde ring. The aldehydic proton resonance is observed at 10.04 ppm with the carbonyl carbon signal appearing at 192.3 ppm in the ^{13}C NMR spectrum. The expected υ(C=O) is observed as an intense IR band at 1691 cm^{-1}.

4.3.3 Synthesis of (1-C_9H_7)-2-C_6H_4C(H)N(OMe) (40)

Similarly to the preparation of **33**, (1-C_9H_7)-2-C_6H_4C(H)N(OMe) (**40**) could be prepared efficiently from **39** by reaction with a slight excess of H_2NOMe·HCl in the presence of NaOAc (Scheme 4.6). Thus compound **40** was isolated as a single double-bond isomer in good isolated yield (90 %) without further purification.

Compound **40** has been fully characterised by NMR and IR spectroscopy and high resolution ESI^+ mass spectrometry. The room temperature ^{1}H NMR spectrum of **40** is shown in Figure 4.4. The eight aryl protons are observed in the range 8.04-7.16 ppm with the aldehydic and oxime methyl protons appearing as singlets at 8.11 and 3.92 ppm respectively. Similarly to the aldehyde (**39**), a doublet (3.55 ppm) and a triplet (6.46 ppm) account for the methylene and vinylic methine indene protons and permit assignment of the double-bond isomer. This was confirmed by structrual characterisation of **40** (*vide infra*).

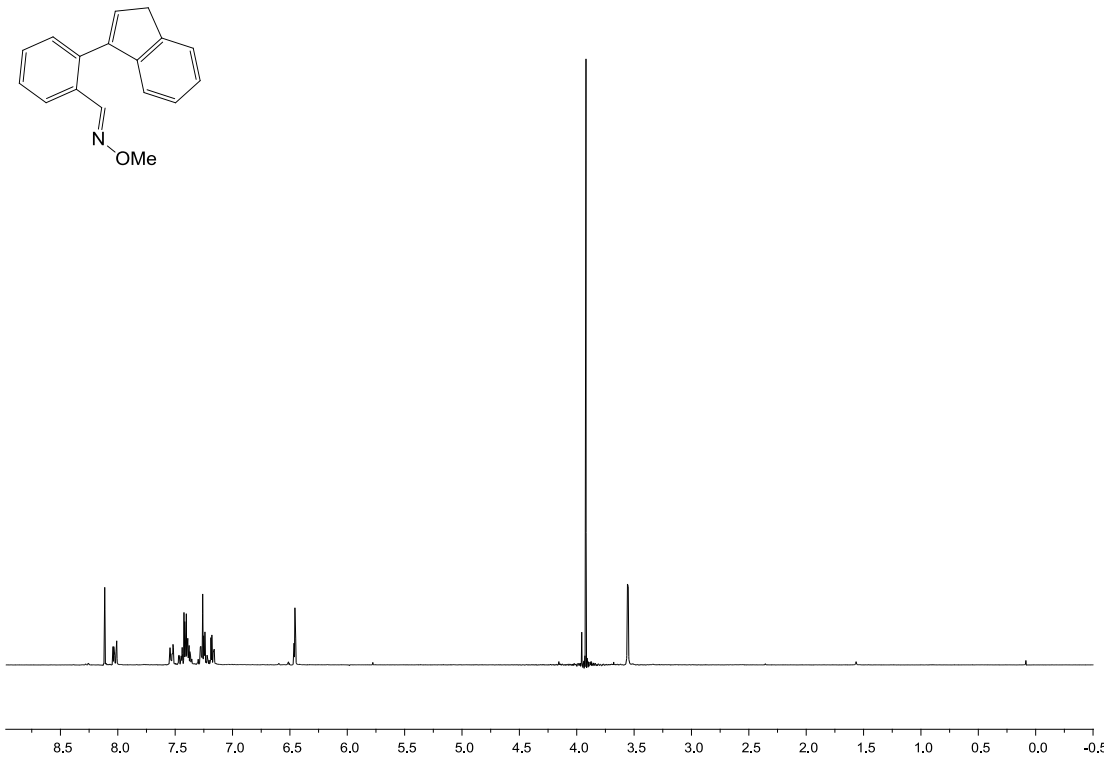

Figure 4.4. ^{1}H NMR spectrum (299.9 MHz, 293 K) of O-methyl-2-(1H-inden-3-yl)benzaldehyde oxime (**40**) in $CDCl_3$. Residual protio-solvent, δ = 7.24 ppm.

4.3.4 X-ray structures of (1-C_9H_8OH)-2-$C_6H_4CH(C_2H_4O_2)$ (38) and (1-C_9H_7)-2-$C_6H_4C(H)N(OMe)$ (40)

Compounds **38** and **40** were further characterised by single crystal X-ray diffraction. Single crystals suitable for X-ray diffraction were grown at room temperature by slow evaporation of acetonitrile solutions. The molecular structures of **38** and **40** are shown in Figure 4.5 and full crystallographic data can be found in the CD appendix. The connectivity observed in the molecular structures of **38** and **40** is consistent with the spectroscopic data. Furthermore, the C(7)-C(8) bond length (1.501(2) Å) is significantly longer than the C(8)-C(9) distance (1.345(2) Å) in **40** in agreement with assignment of the double-bond isomer from ^{1}H and ^{13}C NMR spectra.

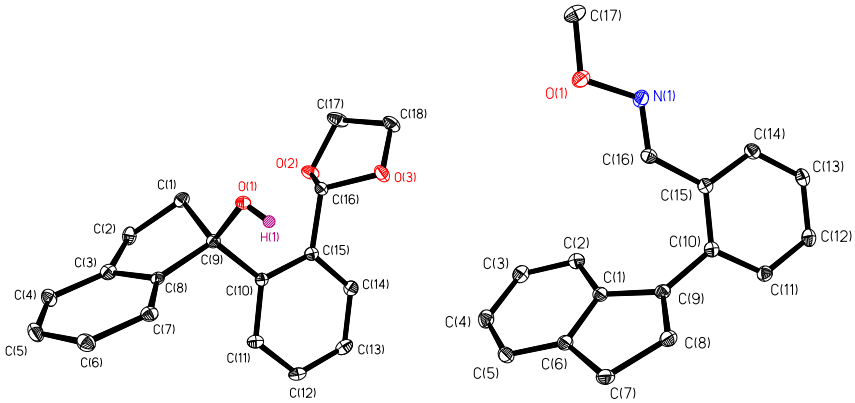

Figure 4.5. Displacement ellipsoid plots (20% probability) of (1-C_9H_8OH)-2-$C_6H_4CH(C_2H_4O_2)$ (**38**) (other crystallographically independent molecules omitted) and (1-C_9H_7)-2-$C_6H_4C(H)N(OMe)$ (**40**). H(1) in **38** drawn as a sphere of arbitrary radius. Other H atoms omitted for clarity.

4.3.5 Synthesis of (1-C_9H_7)-2-C_6H_4CN (41)

Employing similar conditions used in the preparation of **34**, reaction of the oxime **40** with excess LDA followed by aqueous work-up afforded (1-C_9H_7)-2-C_6H_4CN (**41**) (Scheme 4.6) in good isolated yield (85 %) without requirement for further purification.

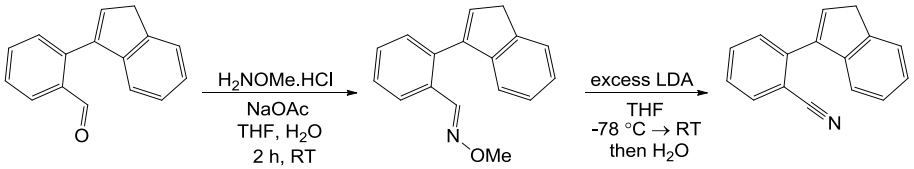

39 **40** **41**

Scheme 4.6. Synthesis of (1-C_9H_7)-2-$C_6H_4C(H)N(OMe)$ (**40**) and (1-C_9H_7)-2-C_6H_4CN (**41**).

Compound **41** has been fully characterised by NMR and IR spectroscopy and high resolution ESI^+ mass spectrometry. The room temperature ^1H NMR spectrum of **41** in $CDCl_3$ reveals the expected preference for the double-bond isomer in which the indene and benzonitrile rings are conjugated. The indene methylene and vinylic protons correspond to a doublet (6.46 ppm) and triplet (3.22 ppm) respectively. The aromatic signals are observed as a series of overlapping multiplets (7.40-6.84 ppm). The expected peak corresponding to the nitrile carbon is observed at 112.0 ppm in the ^{13}C NMR spectrum whilst an IR band at 2226 cm^{-1} is assigned to υ(C≡N).

4.3.6 Attempted synthesis of (1-C_9H_7)-2-$C_6H_4C(NMe_2)NH$ and (1-C_9H_7)-2-$C_6H_4C(N^iPr_2)NH$

A variety of conditions were employed for attempted reactions of **41** with secondary amine-derived nucleophiles. Reactions with $LiNMe_2$ or $BrMgN^iPr_2$ at room temperature resulted in quantitative recovery of **41**; heating these reaction mixtures results in decomposition to intractable mixtures of tar-like compounds. It may be speculated that initial deprotonation of the acidic indene proton by the first equivalent of the nucleophile may lead to diminished electrophilicity of the nitrile and unwanted decomposition *via* reactions involving the indenyl anion when heated; the anion being less well sterically protected compared to the tetramethylcyclopentadienyl case. Milder routes employing copper[22] or lanthanide[23] activation of the nitrile also proved to be ineffective. Reaction of **41** with $Ti(NMe_2)_4$ whereby the envisaged complexation of the indenyl ring by protonolysis may be followed by insertion of RC≡N into a Ti-NMe_2 bond was attempted but also led to a mixture of products. [24-27]

4.4 Attempted elongation of the aryl bridge

An intermediate methylene group between the aryl and tetramethylcyclopentadienyl groups would change the steric requirements of the ligand resulting in an increased bite angle in the complex. A potential route to such a ligand is shown in Scheme 4.7.

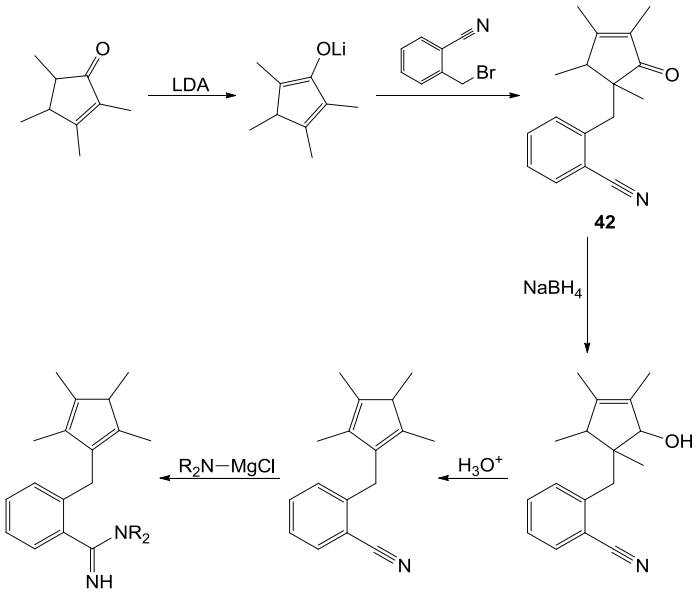

Scheme 4.7. Proposed route to C_5Me_4H-CH_2-2-$C_6H_4C(NR_2)NH$.

The key steps are selective 1,2-reduction of the enone in the presence of the nitrile and dehydration of the resulting allylic alcohol incorporating a Wagner-Meerwein 1,2-rearrangement. A similar route has been demonstrated by Mintz for preparation of l-benzyl-2,3,4,5-tetramethylcyclopentadiene.[28]

4.4.1 Synthesis of ±2-(((1R,2S)-1,2,3,4-tetramethyl-5-oxocyclopent-3-en-1-yl)methyl)benzonitrile (42)

Reaction of 2,3,4,5-tetramethylcyclopent-2-enone (mixture of *cis* and *trans* isomers) with a slight excess of LDA generates the corresponding enolate. Stoichiometric reaction of the enolate with 2-(bromomethyl)benzonitrile affords exclusively ±2-(((1R,2S)-1,2,3,4-tetramethyl-5-oxocyclopent-3-en-1-yl)methyl)-benzonitrile (**42**) from reaction on the less hindered face of the enolate (Scheme 4.8). The reaction may be peformed on a multigram scale with isolation of **42** in reasonable yield (71 %).

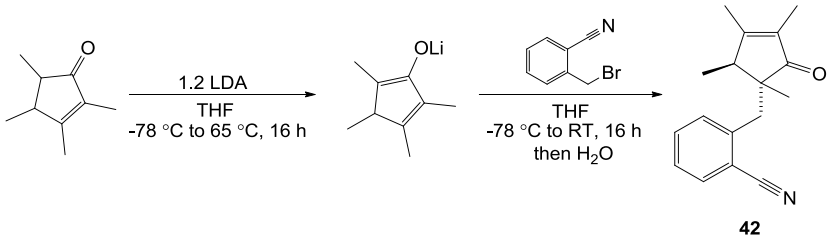

Scheme 4.8. Synthesis of ±2-(((1R,2S)-1,2,3,4-tetramethyl-5-oxocyclopent-3-en-1-yl)methyl)benzonitrile (**42**).

Compound **42** has been fully characterised by NMR and IR spectroscopy and high resolution ESI^+ mass spectrometry. The room temperature ^1H NMR spectum in $CDCl_3$ reveals signals expected for the four aromatic protons as a series of multiplets (7.15-6.81 ppm); the two methyl groups attached to the vinylic enone carbons are observed as singlets at 1.44 (closer to CHMe) and 1.21 (closer to C=O) ppm. The enone ring proton is observed as a quartet (2.14 ppm) coupled to the adjacent methyl group (0.62 ppm) with the remaining methyl group corresponding to a singlet at 0.64 ppm. Two doublets (2.70 and 2.57 ppm) account for the methylene protons between the enone and benzonitrile rings. A through-space correlation is observed in the two-diemsional ROESY NMR spectrum between the methine proton of the cyclic enone and the protons of the methylene linker; no such correlation is observed between these protons and either of the two higher field methyl signals. This suggests that the benzonitrile moiety is located on the opposite face of the enone ring to these methyl groups; this observation is confirmed by structural characterisation of **42** (*vide infra*). Peaks at 211.9 and 113.8 ppm in the ^{13}C NMR spectrum correspond to the C=O and C≡N carbons with the corresponding stretches being observed at 1687 and 2219 cm^{-1} respectively in the IR spectrum.

Compound **42** was further characterised by single crystal X-ray diffraction in order to confirm the connectivity and assign the single diastereomer. Single crystals suitable for X-ray diffraction were grown at room temperature by slow evaporation of a dilute methanol solution. The molecular structure of **42** are shown in Figure 4.6 and full crystallographic data can be found in the CD appendix.

Whilst confirming the desired connectivity, the molecular structure of **42** also serves to support the assignment of the diastereomer derived from spectroscopic data. Methyl carbons C(8) and C(9) occupy the opposite face of the cyclic enone ring to the benzonitrile ring. This diastereoselectivity may be explained by one of the faces of the

planar 2,3,4,5-tetramethylcyclopent-2-enone enolate being protected by a methyl group resulting in reaction with the electrophile on the opposite face.

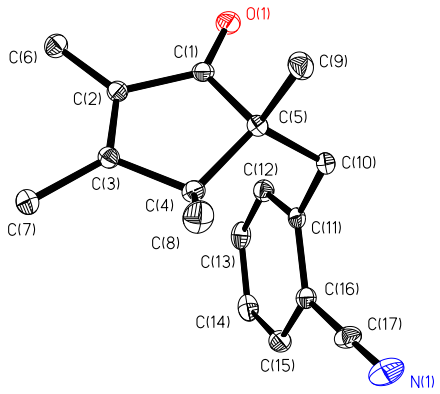

Figure 4.6. Displacement ellipsoid plots (20% probability) of ±2-(((1R,2S)-1,2,3,4-tetramethyl-5-oxocyclopent-3-en-1-yl)methyl)benzonitrile (**42**). H atoms omitted for clarity.

4.4.2 Attempted reduction of 42

A variety of reagents and conditions were screened to effect selective 1,2-reduction of the enone in the presence of the nitrile; the lithium aluminiumhydride reduction described in the preparation of l-benzyl-2,3,4,5-tetramethylcyclopentadiene[28] would also reduce the nitrile. Reaction of **42** with sodium borohydride in methanol or ethanol did not reduce the enone with work-up resulting in near quantatitive recovery of **42**. However, reduction with $LiBH_4$ or $Ca(BH_4)_2$ employing a variety of solvents and conditions was shown by NMR and mass spectrometry to overreduce the enone to the saturated alcohol in each case. The conditions descibed by Luche[29] for selective borohydride reduction of enones with assistance from lanthanoid chlorides were too mild to reduce **42**.

In order to introduce such a methylene spacer, it seems an alternative route must be sought. However, the remainder of this Chapter will focus largely on the complexes derived from the successfully prepared cyclopentadiene-amidine ligands **35**-**37** (*vide supra*).

4.5 Synthesis and characterisation of titanium *o*-aryl-bridged cyclopentadienyl-amidinate dichloride complexes

4.5.1 Synthesis of $\{\eta^5, \eta^1\text{-}C_5Me_4\text{-}2\text{-}C_6H_4C(NMe_2)N\}TiCl_2$ (43)

Addition of a toluene solution of N,N-dimethyl-2-(2,3,4,5-tetramethylcyclopentadienyl)benzamidine (**35**) to a toluene solution of a stoichiometric quantity of $Ti(NMe_2)_4$ results in an immediate colour change from orange to dark red . The resulting half-sandwich diamide is not isolated due to its oily nature but reacted *in situ* with trimethylsilyl chloride affording $\{\eta^5, \eta^1\text{-}C_5Me_4\text{-}2\text{-}C_6H_4C(NMe_2)N\}TiCl_2$ (**43**) (Scheme 4.9) as an orange microcrystalline powder in moderate isolated yield (45 %) following recrystallisation from toluene.

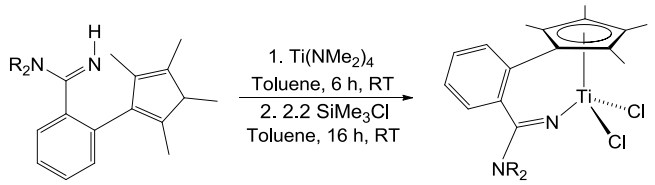

R = Me (**35**)
R = ^{i}Pr (**36**)
R = Cy (**37**)

R = Me (**43**)
R = ^{i}Pr (**44**)
R = Cy (**45**)

Scheme 4.9. Synthesis of titanium *o*-aryl-bridged cyclopentadienyl-amidinate dichloride complexes **43**-**45**.

Compound **43** has been fully characterised by NMR and IR spectroscopy, EI mass spectrometry and elemental analysis. The room temperature ^{1}H NMR spectrum of **43** in CD_2Cl_2 is shown in Figure 4.7. The spectrum reveals a time-averaged C_s-symmetric structure in solution: two singlets at 3.34 and 3.14 ppm are observed for the twelve cyclopentadienyl methyl protons with two signals at 2.19 and 1.73 ppm corresponding to the amidinate methyl groups. The four aromatic protons of the aryl bridge correspond to a series of multiplets spanning the range 7.64-7.46 ppm.

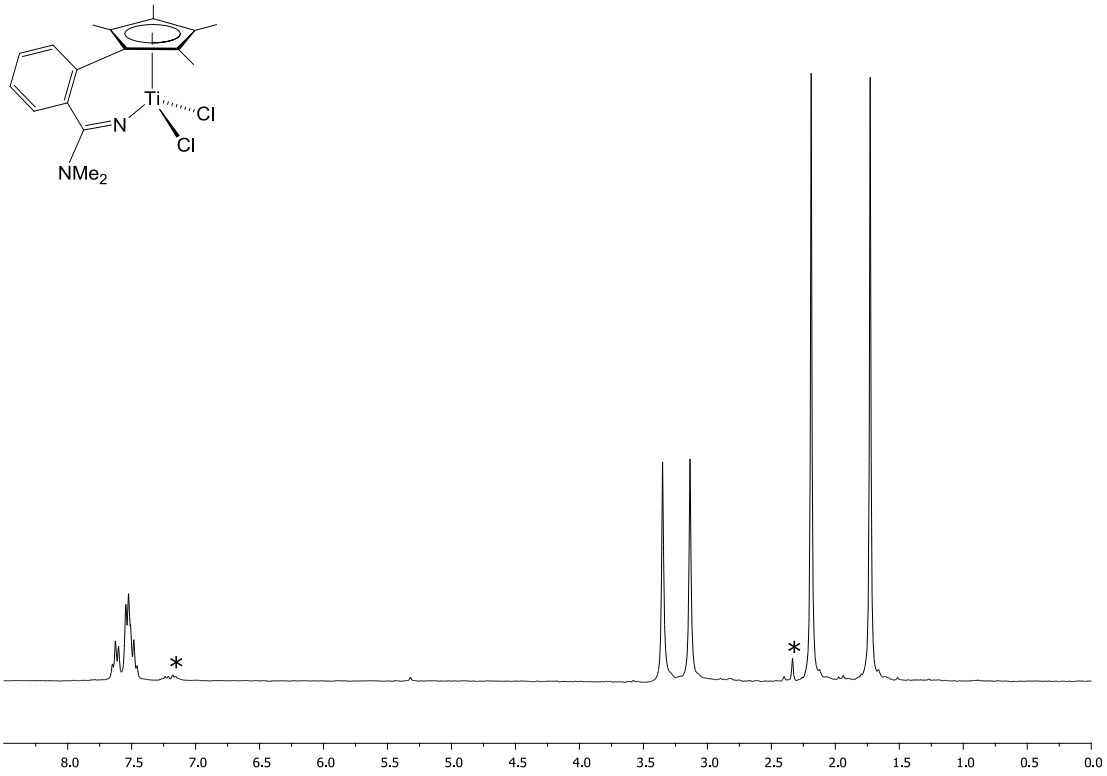

Figure 4.7. ^{1}H NMR spectrum (299.9 MHz, 293 K) of {η^5, η^1-C_5Me_4-2-$C_6H_4C(NMe_2)N$}$TiCl_2$ (**43**) in CD_2Cl_2. Residual protio-solvent, δ = 5.32 ppm. ('*' denotes peaks corresponding to residual toluene of crystallisation)

The room temperature ^{13}C spectrum in CD_2Cl_2 exhibits a signal at 168.8 ppm corresponding to the imine carbon of the amidinate. Correlations involving the cyclopentadienyl methyl protons in the $^{n}J_{CH}$ HMBC spectrum permit assignment of signals at 130.7, 128.7 and 125.1 ppm to cyclopentadienyl ring carbons further from, nearer and adjacent to the aryl bridge respectively. This experiment also allows assignment of the singlet at 2.19 ppm to the two cyclopentadienyl methyl groups lying further from the aryl ring with the resonance at 1.73 ppm corresponding to the methyl groups located closer to the aryl bridge. Furthermore, a two-dimensional $^{1}J_{CH}$ HSQC experiment was utilised for assignment of signals at 13.1 and 12.4 ppm to the respective cyclopentadienyl methyl carbons closer to and further from the aryl linker. The amidinate methyl carbons correspond to resonances at 41.7 and 40.1 ppm.

4.5.2 Synthesis of {η^5, η^1-C_5Me_4-2-$C_6H_4C(N^iPr_2)N$}$TiCl_2$ (44)

As described for the preparation of **43**, the oily half-sandwich diamide formed initially from the protonolysis reaction of $Ti(NMe_2)_4$ with **36** was not isolated but reacted with trimethylsilyl chloride *in situ* affording {η^5, η^1-C_5Me_4-2-$C_6H_4C(N^iPr_2)N$}$TiCl_2$ (**44**)

(Scheme 4.9) in reasonable isolated yield (61 %) following recrystallisation from benzene. Compound **44** has been fully characterised by NMR and IR spectroscopy, EI mass spectrometry and elemental analysis. The room temperature and low temperature (-60 °C) ^{1}H NMR spectra of **44** is shown in Figure 4.8.

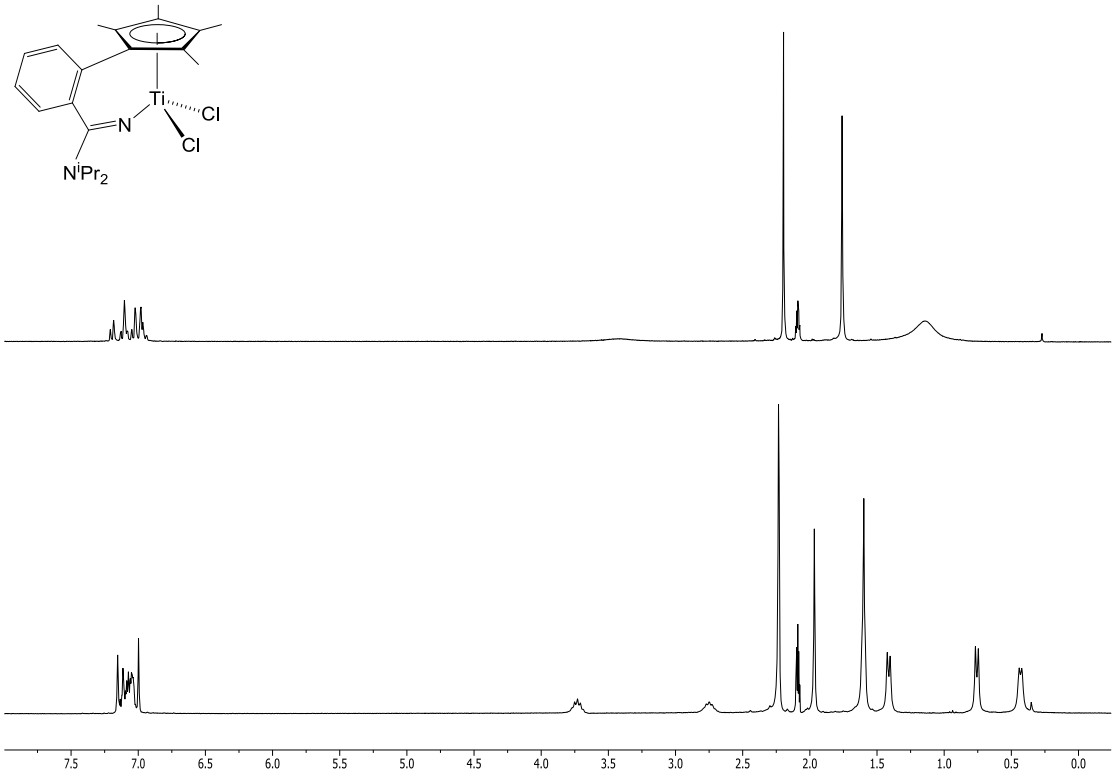

Figure 4.8. ^{1}H NMR spectra (299.9 MHz) of {η^5, η^1-C_5Me_4-2-$C_6H_4C(N^iPr_2)N$}$TiCl_2$ (**44**) in toluene-d_8. Top: 293 K; bottom: 213 K. Residual protio-solvent shifts: δ = 7.09, 7.00, 6.98, 2.09 ppm.

As observed in **43**, the room temperature spectrum of **44** in toluene-d_8 indicates a C_s-symmetric structure with two singlets (2.20 and 1.76 ppm) accounting for the twelve methyl protons of the cyclopentadienyl ring. Similarly to the solution behaviour of $(C_5R_5)Ti\{NC(Ph)N^iPr_2\}Cl_2$ (R = H (**2**), Me (**3**)), restricted rotation about the C-N^{i}Pr$_2$ bond results in broad signals at 3.42 and 1.14 ppm corresponding to the methine and methyl protons of the amidinate *iso*-propyl groups. The four aromatic protons appear as a series of multiplets in the range 7.21-6.94 ppm.

Cooling to -60 °C reveals a lower symmetry structure of **44** indicating that the C_s-symmetry observed at room temperature is time-averaged. Three signals at 2.23, 1.97 and 1.60 ppm are observed in the low temperature spectrum corresponding to the cyclopentadienyl methyl groups. The ratio of the peaks is 2:1:2 but examination of the

COSY spectrum reveals that the signal at 1.60 ppm is overlapping with a doublet corresponding to an *iso*-propyl methyl group; the ratio of cyclopentadienyl methyl protons is therefore 2:1:1. A ROESY spectrum was used to assign these peaks with respect to their proximity to the aryl ring: a through-space correlation was observed between the methyl protons at 1.97 ppm with an aromatic resonance presumably corresponding to the aryl proton *ortho* to the cyclpentadienyl ring. No such correlations were observed for the methyl protons at 2.23 and 1.60 ppm. These observations indicate that the aryl ring is tilted towards one of the methyl groups (1.97 ppm) and away from the other (1.60 ppm); the signal at 2.23 ppm corresponds to the two methyl groups furthest from the aryl ring. It may also be suggested that the time-averaged C_s-symmetry of the molecule at higher temperature derives from a 'wagging' of the bridging aryl group in the plane perpendicular to that of the cyclopentadienyl ring.

Slow rotation about the C-N^{i}Pr$_2$ bond is also observed at low temperature such that signals are observed corresponding to *cis* and *trans iso*-propyl groups with respect to the aryl ring. Through-space correlations are observed between the *cis* methine (3.73 ppm) and methyl (0.76 ppm) *iso*-propyl protons and the aryl proton *ortho* to the amidinate moiety; a correlation with the methyl signal of the same *iso*-propyl group (0.43 ppm) is not observed due to a greater distance between the protons resulting from the tilt of the aryl ring. The *trans iso*-propyl protons correspond to a broad septet at 2.75 ppm (methine) with two doublets at 1.60 and 1.41 ppm (methyls); the signal at 1.60 ppm overlapping with a cyclopentadienyl methyl signal as discussed above.

4.5.3 Synthesis of {η^5, η^1-C_5Me_4-2-$C_6H_4C(NCy_2)N$}$TiCl_2$ (45)

Similarly to the synthesis of **43** and **44**, protonolysis of $Ti(NMe_2)_4$ with **37** followed by reaction with trimethylsilyl chloride affords {η^5, η^1-C_5Me_4-2-$C_6H_4C(NCy_2)N$}$TiCl_2$ (**45**) (Scheme 4.9) in modest isolated yield (32 %) following recrystallisation from toluene. Compound **45** has been fully characterised by NMR and IR spectroscopy, EI mass spectrometry and elemental analysis. The room temperature ^{1}H NMR spectrum of **45** in CD_2Cl_2 reveals a time-averaged C_s-symmetric structure consistent with the ambient temperature spectra of **43** and **44**. By analogy with the assignment described for **43**, the two singlets at 2.16 and 1.81 ppm correspond to the cyclopentadienyl methyl groups further from and closer to the bridging aryl ring respectively. The expected signals for the four aromatic protons

correspond to a series of multiplets in the range 7.60-7.39 ppm. Two broad signals at 3.92 and 2.98 ppm are assigned to the methine protons of the cyclohexyl rings with the remaining protons being observed as a series of overlapping multiplets spanning the region 1.91-1.10 ppm.

4.5.4 X-ray structures of {η^5, η^1-C_5Me_4-2-$C_6H_4C(NR_2)N$}$TiCl_2$ (R = Me (43), ^{i}Pr (44), Cy (45))

Compounds **43**-**45** were further characterised by single crystal X-ray diffraction. Single crystals suitable for X-ray diffraction analysis were grown from concentrated benzene solutions at room temperature. The molecular structures of **43**-**45** are shown in Figure 4.9 and full crystallographic data can be found in the CD appendix. Selected distances and angles are listed in Table 4.1.

The molecular structures of **43**-**45** show the expected *pseudo*-tetrahedral titanium centre coordinated by the η^5-cyclopentadienyl ring and κ^1-amidinate of the chelating ligand with the remaining sites occupied by two chloride ligands. The C_1-symmetric structures are consistent with the low temperature spectroscopic data described for **44** in which the bridging aryl ring is observed to be tilting from the plane perpendicular to the cyclopentadienyl ring. Also in agreement with solution phase observations described for **44**, *cis* and *trans* amine nitrogen alkyl groups with respect to the phenyl ring are clearly evident in the solid state.

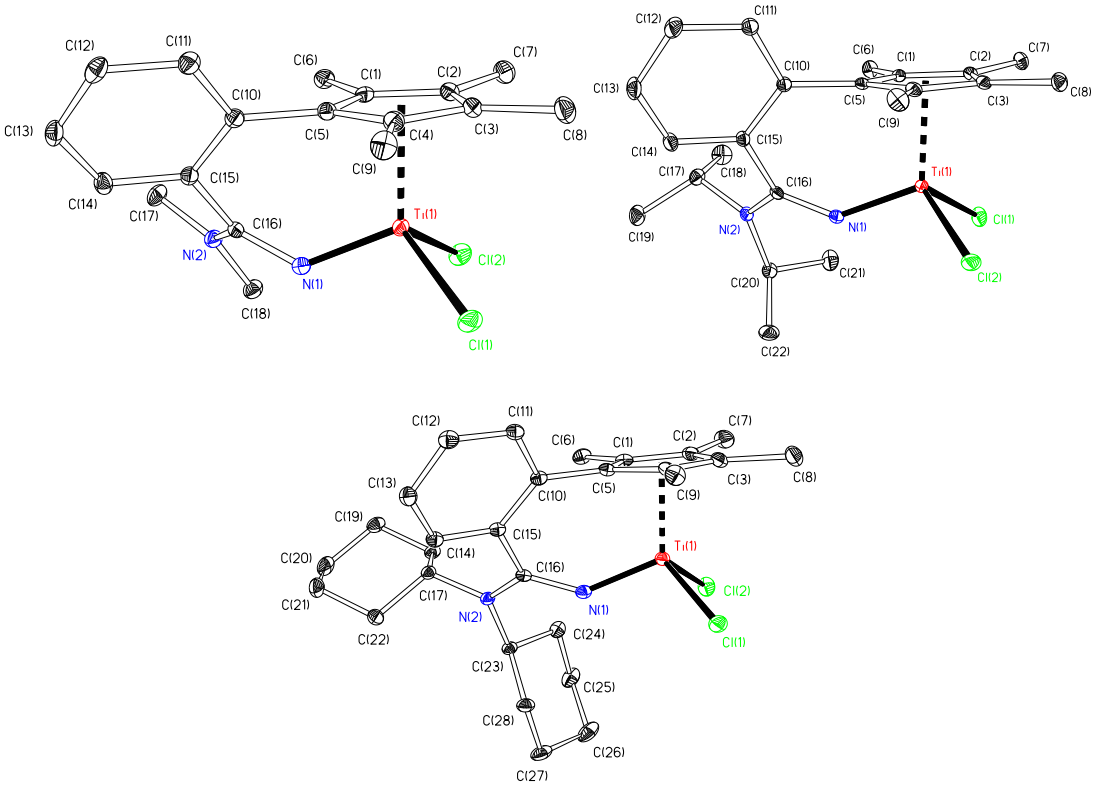

Figure 4.9. Displacement ellipsoid plots (20% probability) of {η^5, η^1-C_5Me_4-2-$C_6H_4C(NR_2)N$}$TiCl_2$ (R = Me (**43**; top left), ^{i}Pr (**44**; top right), Cy (**45**; bottom)). Other crystallographically independent molecule omitted in the case of **44**. H atoms omitted for clarity.

The constraints imposed by the aryl tether result in significant deviation from the linear Ti(1)-N(1)-$C_{C=N}$ bond angle observed in **3** (165.2(3)°). This effect is particularly noticeable in **43** (131.7(3) °) but the larger amidine substituents in **44** and **45** appear to assist widening of the Ti(1)-N(1)-$C_{C=N}$ bond angle (140.19(12)° and 140.64(12)° (**44**), 141.63(14)° (**45**)) although these angles are still significantly smaller than that observed in **3**. The aryl bridge also serves to shorten the Ti(1)-Cp_{cent} distances in the chelated complexes (2.04 Å (**43**), 2.03 Å (**44**), 2.03 Å (**45**)) in comparison to **3** (2.05 Å) with associated narrowing of the Cp_{cent}-Ti(1)-N(1) angles (113.2° (**43**), 113.3° and 112.9° (**44**), 112.3° (**44**)) relative to **3** (118.0 °).

Table 4.1. Selected bond lengths (Å) and angles (°) for Cp*Ti{NC(Ph)N^{i}Pr$_2$}Cl$_2$ (**3**) and {η^5, η^1-C$_5$Me$_4$-2-C$_6$H$_4$C(NR$_2$)N}TiCl$_2$ (R = Me (**43**), ^{i}Pr (**44**), Cy (**45**)). Cp$_{cent}$ is the computed cyclopentadienyl ring carbon centroid.

Parameter	**3**	**43**	**44**[†]	**45**
Ti(1)-Cp$_{cent}$	2.05	2.04	2.03, 2.03	2.03
Ti(1)-Cl(1)	2.3137(11)	2.2930(7)	2.3154(6), 2.2995(5)	2.2880(6)
Ti(1)-Cl(2)	2.3051(11)	2.3155(8)	2.2978(5), 2.3186(5)	2.3071(7)
Ti(1)-N(1)	1.800(3)	1.797(2)	1.8086(14), 1.8058(14)	1.8015(17)
N(1)-C$_{C=N}$	1.310(4)	1.325(3)	1.317(2), 1.314(2)	1.318(3)
N(2)-C$_{C=N}$	1.340(4)	1.325(3)	1.347(2), 1.349(2)	1.345(2)
Cp$_{cent}$-Ti(1)-N(1)	118.0	113.2	113.3, 112.9	112.3
Cp$_{cent}$-Ti(1)-Cl(1)	113.5	114.9	114.8, 114.7	115.8
Cp$_{cent}$-Ti(1)-Cl(2)	115.0	116.1	114.5, 114.6	115.6
Ti(1)-N(1)-C$_{C=N}$	165.2(3)	131.7(3)	140.19(12), 140.64(12)	141.63(14)
N(1)-Ti(1)-Cl(1)	102.93(10)	107.32(7)	103.77(5), 106.52(5)	104.26(6)
N(1)-Ti(1)-Cl(2)	104.21(10)	102.02(7)	107.04(5), 104.74(5)	104.79(6)
Cl(1)-Ti(1)-Cl(2)	101.24(4)	101.82(3)	102.30(2), 102.25(2)	102.75(3)

[†] Two molecules in the asymmetric unit.

The Ti(1)-N(1) bond length observed in all three tethered complexes (1.797(2)-1.8086(14) Å) are comparable to that observed in **3** (1.800(3) Å) with similar N(1)-C$_{C=N}$ (1.314(2)-1.318(3) Å) and N(2)-C$_{C=N}$ (1.345(2)-1.349(2) Å) distances observed in **44** and **45** compared to **3** (1.310(4) Å; 1.340(4) Å) implying a similar degree of π-donation in spite of the influence of the aryl linker on alignment of the amidinate with respect to the metal. The N(1)-C$_{C=N}$ (1.325(3) Å) and N(2)-C$_{C=N}$ (1.325(3) Å) distances in **43** actually imply an enhanced π-interaction with titanium in spite of the significant deviation of the Ti(1)-N(1)-C$_{C=N}$ angle from linearity. Overall, the chelated complexes bear close resemblance to the non-*ansa* compound **3** in spite of the influence of the tether restricting the amidinate ligand from adopting its preferred conformation with respect to the metal centre.

4.6 Synthesis and characterisation of titanium *o*-aryl-bridged cyclopentadienyl-amidinate dimethyl complexes

As described in Chapter Three, dialkyl complexes are often employed as precatalysts in combination with [CPh$_3$][BAr$^{F}_4$] and related activators.[30] As well as polymerisation testing of **43-45**, it was deemed necessary to prepare the corresponding half-sandwich dimethyl complexes for thorough assessment of the polymerisation capability of the

series of chelated compounds and direct comparison with Cp*Ti{NC(Ph)N^{i}Pr$_2$}Me$_2$ (**4**).

4.6.1 Synthesis of {η^5, η^1-C$_5$Me$_4$-2-C$_6$H$_4$C(NR$_2$)N}TiMe$_2$ (R = Me (46), ^{i}Pr (47), Cy (48))

Reaction of half-sandwich dichloride complexes **43-45** with two equivalents of MeMgCl or MeLi (Equation 4.1) affords the corresponding dimethyl complexes, {η^5, η^1-C$_5$Me$_4$-2-C$_6$H$_4$C(NR$_2$)N}TiMe$_2$ (R = Me (**46**), ^{i}Pr (**47**), Cy (**48**)) in moderate yield (30-40 %) following recrystallisation from pentane or n-hexanes. Conversion to the dimethyl compounds appears quantitative when tested in NMR tube-scale reactions; the isolated yields are lower due to the highly soluble nature of **46**-**48**.

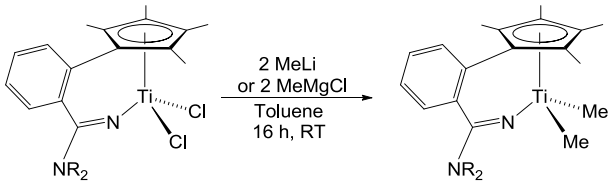

R = Me (**43**)
R = ^{i}Pr (**44**)
R = Cy (**45**)

R = Me (**46**)
R = ^{i}Pr (**47**)
R = Cy (**48**)

Equation 4.1

Compounds **46-48** have been fully characterised by NMR and IR spectroscopy, EI mass spectrometry and elemental analysis. The room temperature ^{1}H NMR spectrum of **46** is shown in Figure 4.10 as an example. Similarly to **43-45**, the room temperature spectrum of **46** in C$_6$D$_6$ exhibits two singlets at 2.19 and 1.51 ppm corresponding to the cyclopentadienyl methyl protons suggesting time-averaged C$_s$-symmetry. A single peak is also observed for the methyl ligands at 0.60 ppm. Faster rotation about the C-NMe$_2$ bond than observed in **43** results in the amidine methyl protons in **46** appearing as one fairly broad singlet (2.65 ppm). Four separate multiplets (7.29, 7.09, 6.95 and 6.91 ppm) corresponding to the protons of the aryl linker were assigned relative to the amidine and cyclopentadienyl ring moieties using various two-dimensional NMR experiments.

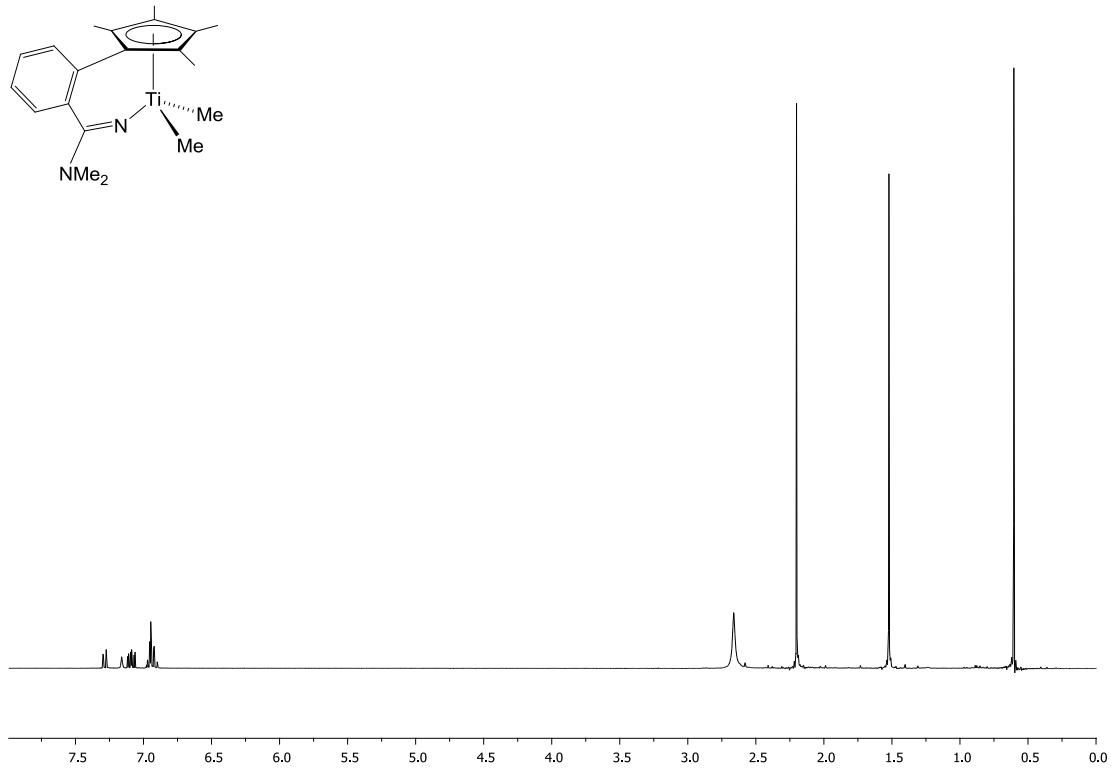

Figure 4.10. ^{1}H NMR spectrum (299.9 MHz, 293 K) of {η^5, η^1-C_5Me_4-2-$C_6H_4C(NMe_2)N$}$TiMe_2$ (**46**) in C_6D_6. Residual protio-solvent, δ = 7.16 ppm.

Assignment of signals at 123.8, 120.5 and 119.0 ppm in the room temperature ^{13}C spectrum in C_6D_6 to the respective cyclopentadienyl ring carbons further from, nearer and adjacent to the aryl bridge was assisted using a $^{n}J_{CH}$ HMBC spectrum as described in the case of **43**. Similarly, the singlets at 2.19 and 1.51 ppm in the ^{1}H NMR spectrum were assigned to the cyclopentadienyl methyl groups lying further from and closer to the aryl ring respectively.

The room temperature ^{1}H NMR spectra of **47** and **48** in C_6D_6 are similar aside from differences associated with the alkyl substituents on the amine nitrogen. In both cases three singlets of equal intensity are observed corresponding to the methyl substituents of the cyclopentadienyl ring (2.20 and 1.64 ppm (**47**), 2.21 and 1,69 ppm (**48**)) and the methyl ligands (0.52 ppm (**47**), 0.53 ppm (**48**)). The assignment of the cyclopentadienyl methyl groups by their proximity to the aryl linker was done in the same way as described for **43**. Similarly to **46**, the aromatic protons in **47** and **48** correspond to four separate multiplets which were assigned by their proximity to the amidine and cyclopentadienyl substituents on the aryl ring. Apparently faster rotation about the C-NR_2 bond in **47** and **48** than observed in the half-sandwich dichloride

precursor complexes **44** and **45** results in observation of a single methine resonance (3.47 ppm (**47**), 3.30 ppm (**48**)) with one signal corresponding to the *iso*-propyl methyl groups (1.28 ppm) in **47**; the remaining cyclohexyl protons in **48** appearing as a series of overlapping multiplets spanning the range 1.65-0.85 ppm. Structural characterisation of **46**-**48** (*vide infra*) reveals slightly longer C-NR_2 bonds than in the corresponding dichloride complexes (**43**-**45**) suggesting that enhanced σ-donation from the methyl ligands results in a slightly diminished amidinate-metal π-interaction (*cf.* Chapters Two and Three). Consequently, faster rotation about the C-NR_2 bond is thought to stem from an associated decrease in its double-bond character.

4.6.2 X-ray structures of {η^5, η^1-C_5Me_4-2-$C_6H_4C(NR_2)N$}$TiMe_2$ (R = Me (46), ^{i}Pr (47), Cy (48))

Compounds **46**-**48** were further characterised by single crystal X-ray diffraction. Single crystals suitable for X-ray diffraction analysis were grown from concentrated benzene solutions at room temperature. The molecular structures of **46**-**48** are shown in Figure 4.11 and full crystallographic data can be found in the CD appendix. Selected distances and angles are listed in Table 4.2.

As expected from the molecular structures of the half-sandwich dichloride complexes **43**-**45**, the corresponding dimethyl compounds **46**-**48** exhibit a *pseudo*-tetrahedral three-legged piano stool titanium centre surrounded by the η^5-cyclopentadienyl ring and κ^1-amidinate of the chelating ligand with two methyl ligands occupying the remaining coordination sites. As observed for **43**-**45**, the aryl bridged is tilting from the plane perpendicular to the cyclopentadienyl ring resulting in C_1-symmetry in the solid state. As discussed above, a 'wagging' of the aryl ring results in compounds **46**-**48** possessing time-averaged C_s-symmetry in solution at room temperature.

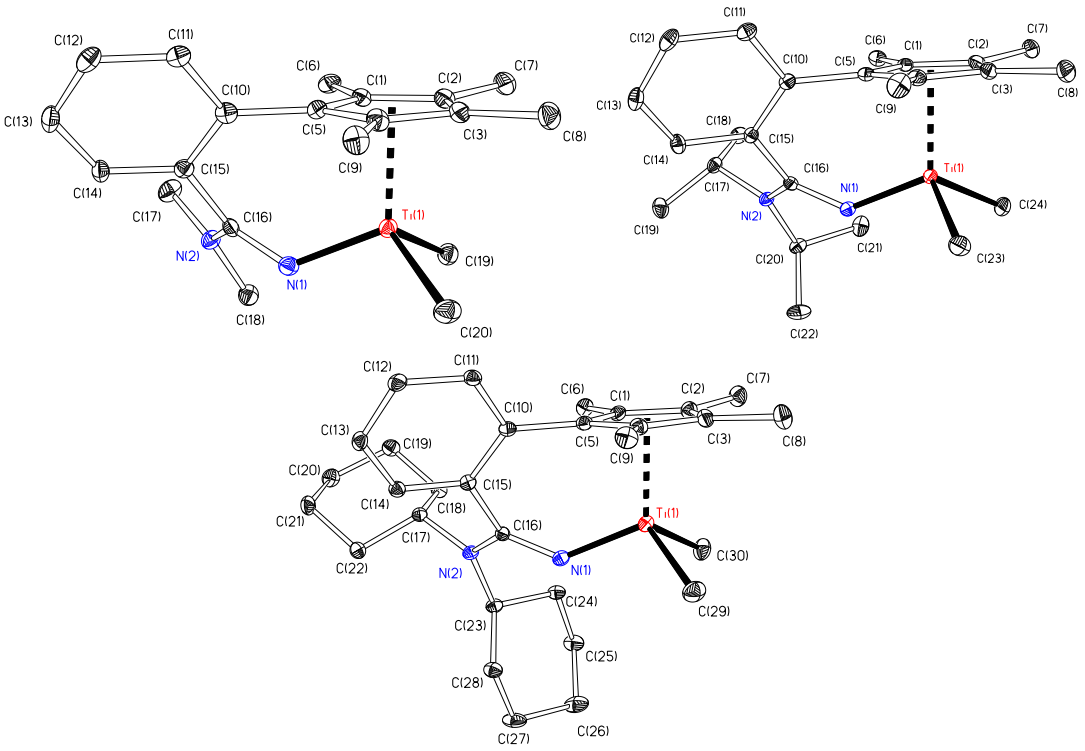

Figure 4.11. Displacement ellipsoid plots (20% probability) of $\{\eta^5, \eta^1\text{-}C_5Me_4\text{-}2\text{-}C_6H_4C(NR_2)N\}TiMe_2$ (R = Me (**46**; top left), ^{i}Pr (**47**; top right), Cy (**48**; bottom)). Other crystallographically independent molecule omitted in the case of **48**. H atoms omitted for clarity.

Similar trends relating to the constraints imposed by the bridging aryl group noted in comparison of **43**-**45** with **3** (*vide supra*) are also observed in the corresponding dimethyl complexes **46**-**48** and **4**. Immediately noticeable is significant deviation from the linear Ti(1)-N(1)-$C_{C=N}$ bond angle in **4** (163.00(13)°) in **46**-**48** (127.6(2)-138.24(16)°). As seen in the chelated dichloride complexes, the larger amidine substituents in **47** and **48** appear to assist a degree widening of the Ti(1)-N(1)-$C_{C=N}$ angle (136.64(11)° (**47**), 136.58(16)° and 138.24(16)° (**48**)) in comparison to **46** (127.6(2)°).

Consistent with comparison of the non-*ansa* group 4 dichloride and dimethyl complexes described in Chapters Two and Three, the enhanced σ-donating properties of the methyl ligands result in slightly longer Ti(1)-Cp_{cent} and Ti(1)-N(1) distances in in **46**-**48** (2.05-2.06 Å; 1.834(3)-1.843(2) Å) than observed for **43**-**45** (2.03-2.04 Å; 1.797(2)-1.8086(14) Å). As discussed for the dichloride complexes (*vide supra*), the aryl bridge results in shortening of the Ti(1)-Cp_{cent} distances in **46**-**48** in comparison to the non-*ansa* dimethyl complex **4** (2.07 Å); an associated narrowing of the Cp_{cent}-

Ti(1)-N(1) angles in the tethered complexes (115.1° (**46**), 114.3° (**47**), 114.0° and 113.8° (**48**)) relative to **4** (120.8°) is also observed.

The definition of a constrained geometry complex given by Stevens *et al.* describes the linking of some π-bonded moiety, such as a cyclopentadienyl-type ligand, to another ligand coordinated to the same metal centre resulting in a smaller angle between the centroid of the π-system, the metal and the additional ligand than in comparable non-*ansa* complexes.[31] From comparison of the molecular structures of **3** and **4** with **43**-**48**, it seems that these *o*-aryl-bridged compounds may be correctly described as constrained geometry complexes.

Table 4.2. Selected bond lengths (Å) and angles (°) for Cp*Ti{NC(Ph)N^{i}Pr$_2$}Me$_2$ (**4**) and {η^5, η^1-C$_5$Me$_4$-2-C$_6$H$_4$C(NR$_2$)N}TiMe$_2$ (R = Me (**46**), ^{i}Pr (**47**), Cy (**48**)). Cp$_{cent}$ is the computed Cp* ring carbon centroid.

Parameter	**4**	**46**	**47**	**48**[†]
Ti(1)-Cp$_{cent}$	2.07	2.06	2.05	2.06, 2.05
Ti(1)-N(1)	1.8452(15)	1.834(3)	1.8368(14)	1.843(2), 1.840(2)
N(1)-C$_{C=N}$	1.290(2)	1.303(4)	1.304(2)	1.304(3), 1.303(3)
N(2)-C$_{C=N}$	1.363(2)	1.353(4)	1.359(2)	1.365(3), 1.358(3)
Ti(1)-C$_{methyl\ 1}$	2.1227(18)	2.142(4)	2.137(2)	2.115(3), 2.137(3)
Ti(1)-C$_{methyl\ 2}$	2.1326(19)	2.116(4)	2.1182(19)	2.144(3), 2.118(3)
Cp$_{cent}$-Ti(1)-N(1)	120.8	115.1	114.3	114.0, 113.8
Cp$_{cent}$-Ti(1)-C$_{methyl\ 1}$	113.9	114.2	114.3	115.3, 114.2
Cp$_{cent}$-Ti(1)-C$_{methyl\ 2}$	113.9	115.0	114.6	113.8, 114.8
Ti(1)-N(1)-C$_{C=N}$	163.00(13)	127.6(2)	136.64(11)	136.58(16), 138.24(16)
N(1)-Ti(1)-C$_{methyl\ 1}$	104.21(7)	101.92(15)	105.79(7)	107.03(10), 104.96(10)
N(1)-Ti(1)-C$_{methyl\ 2}$	104.04(7)	107.63(15)	105.28(7)	104.61(10), 106.10(10)
C$_{methyl\ 1}$-Ti(1)-C$_{methyl\ 2}$	96.93(8)	101.48(16)	101.16(9)	100.65(12), 101.80(12)

[†] Two molecules in the asymmetric unit.

In spite of the influence of the aryl linker on the Ti(1)-N(1)-C$_{C=N}$ angle, the Ti(1)-N(1) distances in **46**-**48** are similar to that observed in **4**. Comparable N(1)-C$_{C=N}$ and N(2)-C$_{C=N}$ distances in **4** (1.290(2) Å; 1.363(2) Å) and **46**-**48** (1.303(4)-1.304(3) Å; 1.353(4)-1.365(3) Å) suggest a similar degree of amidinate-metal π-donation. Comparison of the dichloride (**43**-**45**) and dimethyl (**44**-**46**) complexes appears to suggest a slightly diminished amidinate-metal π-interaction in the latter by virtue of somewhat shorter N(1)-C(16) and longer C(16)-N(2) bonds than observed in **43**-**45** (1.314(2)-1.325(3) Å; 1.325(3)-1.349(2) Å). This is consistent with the solution

behaviour of **44-46** (*vide supra*) and the solid-state and solution behaviour of the related non-*ansa* complexes described in Chapter Two: apparently faster rotation about the C-NR_2 bond is observed for the dimethyl compared to the corresponding dichloride compounds. As concluded for the dichloride complexes **43**-**45**, the chelated half-sandwich dimethyl complexes appear to bear close ressemblance to the non-*ansa* compound **4** suggesting that the coordination and π-donating ability of the amidinate is not significantly influenced by the geometric constraints imposed by the aryl bridge.

4.7 Density functional theory calculations

Density functional theory (DFT) calculations were performed by Dr Betty Coussens (DSM, The Netherlands) in order to compare steric and electronic properties of the chelated half-sandwich dimethyl complexes and the related non-*ansa* complex **4**.

4.7.1 $\{\eta^5, \eta^1\text{-}C_5Me_4\text{-}2\text{-}C_6H_4C(N^iPr_2)N\}TiMe_2$

Compound **47** was selected as a representative example of the bridged cyclopentadienyl-amidinate complexes; the *iso*-propyl amidinate substituents making for a fairer comparison with the non-*ansa* complex **4**. The parameters determined from the solid-state structure of **47** show good agreement with those of the corresponding energy-minimised structure, **XV**. A comparison of selected bond lengths is presented in Table 4.3.

Table 4.3. Selected bond lengths (Å) and angle (°) for $\{\eta^5, \eta^1\text{-}C_5Me_4\text{-}2\text{-}C_6H_4C(N^iPr_2)N\}TiMe_2$ (**47**) and calculated structure (**XV**).

Parameter	**47**	**XV**
Ti-N	1.8368(14)	1.852
N=C	1.304(2)	1.293
$N\text{-}C_{C=N}$	1.359(2)	1.381
$Ti\text{-}C_{methyl\ 1}$	2.137(2)	2.126
$Ti\text{-}C_{methyl\ 2}$	2.1182(19)	2.114
$Ti\text{-}N\text{-}C_{C=N}$	136.64(11)	138.0

Selected FMOs of **XV** corresponding to π-bonding, non-bonding and π*-antibonding MOs are shown in Figure 4.12. These appear qualitatively similar to those for the related non-*ansa* titanium complex **I** described in Chapter Three. The HOMO-5 of

XV shows an amidinate-metal π-bonding interaction involving the allylic non-bonding MO of the amidine moiety. The constraints imposed by the aryl bridge result in twisting of the amidinate such that poorer orbital overlap seems apparent between the imine nitrogen and titanium than observed in the HOMO-5 of **I**. The second π-interaction observed in the HOMO-2 appears unaffected by the aryl linker and closely ressembles that of **I**. The HOMO represents mostly a Cp*-metal interaction with some π-contribution from the amidinate; the non-bonding LUMO involves an amidinate-based contribution from the π*-antibonding orbital of the allylic system. Similarly to **I**, the LUMO+1 and LUMO+4 are metal-based non-bonding and π*-antibonding orbitals respectively.

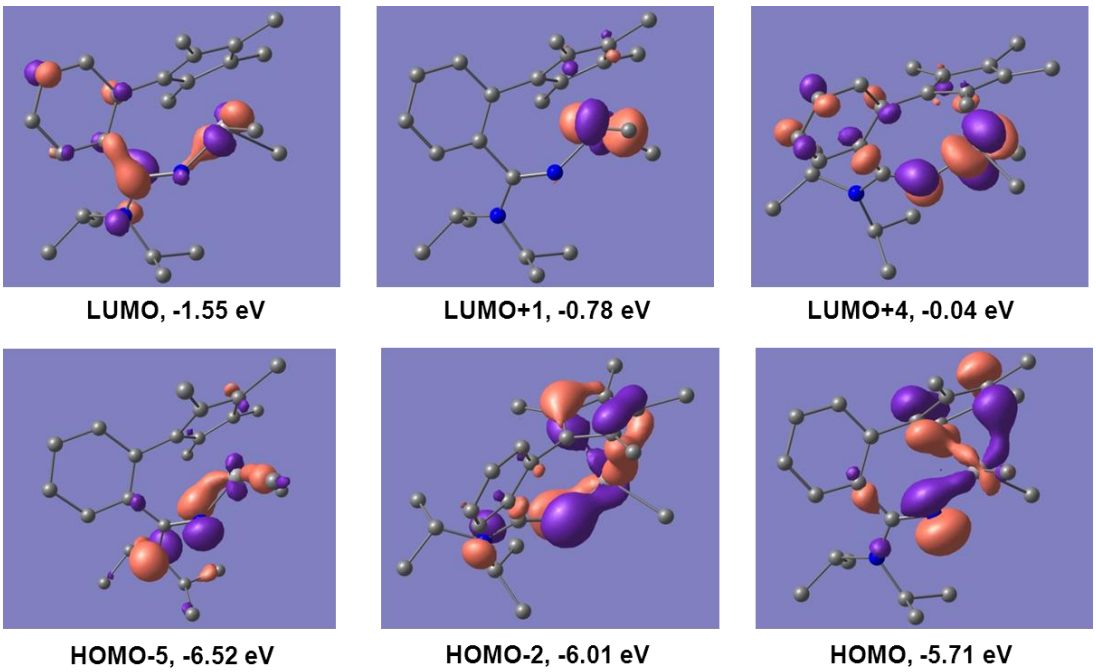

Figure 4.12. FMOs of {η^5, η^1-C_5Me_4-2-$C_6H_4C(N^iPr_2)N$}$TiMe_2$ (**XV**). The value for the isosurfaces is 0.06 au. H atoms omitted.

The energies of the FMOs in **XV** are very close to those of **I** presented in Chapter Three. In spite of the degree of amidinate-metal π-overlap in the HOMO-5 of **XV** (-6.52 eV) not appearing as extensive as in the HOMO-5 of **I** (-6.44 eV) the energies are very similar. The HOMO-LUMO gap in **XV** (4.16 eV) is also very close to that of **I** (4.27 eV). The atomic charges of the titanium (+0.651 (**I**), +0.643 (**XV**)) and imine nitrogens (-0.429 (**I**), -0.435 (**XV**)) further exemplify the electronic similarities between the chelated and non-*ansa* complexes.

4.7.2 Steric factor calculations

Cone angles were introduced by Tolman in order to quantify the steric bulk of ligands around a metal centre.[32] More recently, an approach which accounts for ligands which are not adequately approximated by a cone has been developed by Taverner.[33] Projection of the ligand atoms onto the surface of a sphere centred at the metal permits definition of the solid angle as the area covered by the projected atoms divided by the radius of the sphere (Figure 4.13). The dimensionless steric factor is then calculated by dividing the solid angle by the total surface area of the sphere.

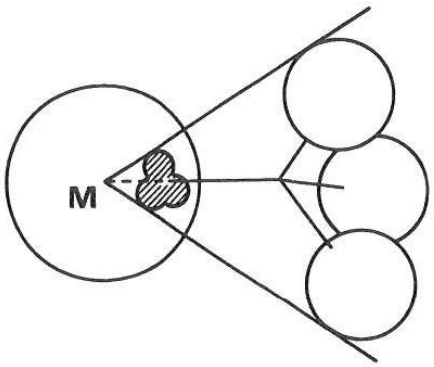

Figure 4.13. Projection of ligand atoms onto surface of a sphere.

Calculated structures of the monomeric cations (Figure 4.14) are used for the steric factor analysis since the spatial arrangement of ligands of the activated species will provide a more direct relationship with catalyst behaviour than could be achieved from similar treatment with the neutral dimethyl precatalysts. This simple treatment does however neglect possible stabilisation of the cationic species *via* α-agostic interactions.[34-37] Calculation of the non-*ansa* cation **[**Cp*Ti{NC(Ph)N^{i}Pr$_2$}Me]$^+$ (**XVI**$^+$) allowed comparison with the bridged systems: [{η^5, η^1-C$_5$Me$_4$-2-C$_6$H$_4$C(NR$_2$)N}TiMe]$^+$ (R = Me (**XVII**$^+$), ^{i}Pr (**XVIII**$^+$), Cy (**XIX**$^+$)).

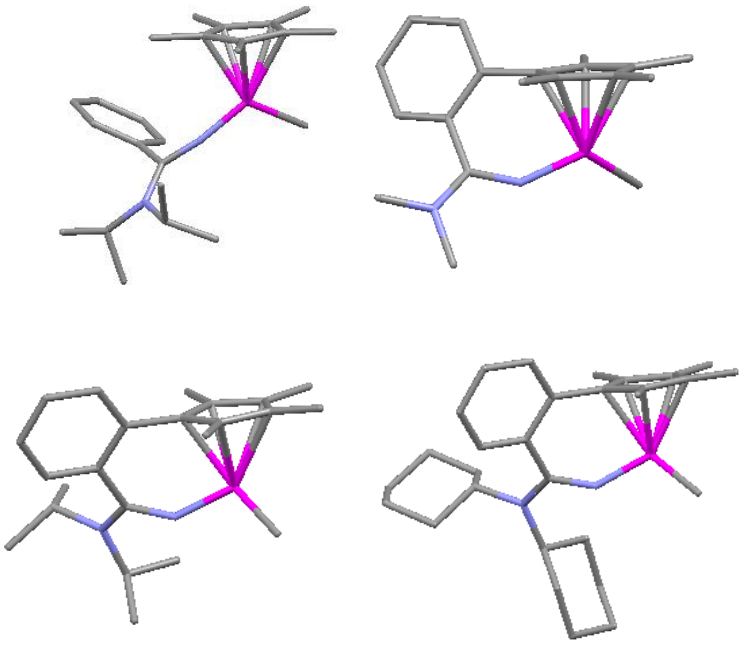

Figure 4.14. Calculated structures of **[**Cp*Ti{NC(Ph)N^{i}Pr$_2$}Me]$^+$ (**XVI**$^+$; top left), [{η^5, η^1-C_5Me_4-2-$C_6H_4C(NR_2)N$}TiMe]$^+$ (R = Me (**XVII**$^+$; top right), ^{i}Pr (**XVIII**$^+$); bottom left), Cy (**XIX**$^+$; bottom right)). H atoms omitted.

The cations were optimised at the B3LYP/3-21G* and B3-LYP/def-SV(P) level of theory using *Gaussian 03* and *Turbomole* programs respectively. The solid angles for the cations were obtained using the program *Steric* by Taverner.[33] The steric factors for the non-*ansa* and *o*-aryl-bridged cations are presented in Table 4.4.

Table 4.4. Steric factors calculated for **[**Cp*Ti{NC(Ph)N^{i}Pr$_2$}Me]$^+$ (**XVI**$^+$), [{η^5, η^1-C_5Me_4-2-$C_6H_4C(NR_2)N$}TiMe]$^+$ (R = Me (**XVII**$^+$), ^{i}Pr (**XVIII**$^+$)), Cy (**XIX**$^+$)).

	XVI$^{+\dagger}$	**XVII**$^+$	**XVIII**$^+$	**XIX**$^+$
Steric Factor (B3-LYP/def-SV(P))	0.654, 0.664	0.556	0.614	0.623
Steric Factor (B3LYP/3-21G*)	0.659, 0.665	0.540	0.601	0.630

† Two conformations calculated.

The structures optimised with *Gaussian 03* and *Turbomole* result in reassuringly similar steric factors for each cation. Two low-energy conformations of the non-*ansa* cation **X**$^+$ corresponding to two N-CHMe$_2$ bond rotamers were calculated but gave similar steric factors demonstrating the robust nature of the technique with respect to small conformational changes of the ligands. The steric factors of the non-*ansa* cation **XVI**$^+$ are higher than the bridged cations **XVII**$^+$-**XIX**$^+$ reflecting the more open metal

centre resulting from constraints imposed by the aryl linker. The trend in steric factors in the *ansa* complexes reflects the size of the amidinate substituents.

The steric factors provide a quantitative measure of the effect of the chelate bridge on the steric environment around the metal centre. Combined with the electronic similarities observed between the the non-*ansa* and *o*-aryl-bridged complexes it may be tentatively speculated that any differences in polymerisation behaviour may to a greater extent be ascribed to the differing steric characteristics of the chelated compared to the non-bridged complexes.

4.8 Attempted synthesis of an unconstrained chelated complex

The importance of the degree of strain induced by the tether was emphasised by Stevens *et al.* using examples of the relative performance of silanediyl- and disilanediyl-bridged cyclpentadienyl-amido complexes to claim that the shorter linker leads to a more constrained yet better performing catalyst.[31] It was decided to attempt a similar evaluation by synthesis of a less constrained chelated complex with a longer, less rigid bridge for comparison with the constrained complexes **43**-**48** and the non-bridged amidinate-supported precatalyst **4**. Furthermore, it was anticipated that a longer and more flexible linker might assist understanding of the influence of the amidinate-metal π-bonding interaction on ligand conformation and orientation with respect to the metal centre.

4.8.1 Synthesis of 2-(2-(2,3,4,5-tetramethylcyclopentadienyl)ethyl)isoindolin-1-imine (49)

Previous work in the Mountford group in collaboration with DSM Research involved preparation of cyclic amidines exemplified by the reaction of 2,6-dimethylaniline with 2-(bromomethyl)benzonitrile forming the hydrobromide salt of 2-(2,6-dimethylphenyl)isoindolin-1-imine (Equation 4.2).[38] This reaction is convenient due to straightforward isolation and purification of the product which crystallises from the toluene solution.

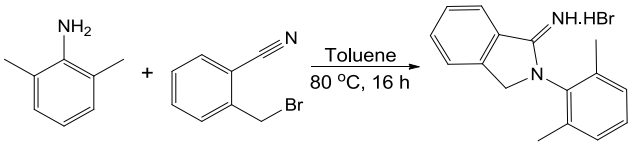

Equation 4.2

It was considered that such a reaction may be employed to synthesise a chelating cyclopentadiene-amidine ligand with the desired longer, less rigid bridge by reaction of 2-(2,3,4,5-tetramethylcyclopentadienyl)ethanamine, prepared using the convenient method of Hessen *et al.*,[39] with 2-(bromomethyl)benzonitrile (Scheme 4.10). Following refluxing the reactants in toluene, the hydrobromide salt was collected as a colourless precipitate. Neutralisation with sodium hydroxide solution afforded the desired protio-ligand in moderate overall yield (53 %) as a mixture of endocyclic double-bond isomers.

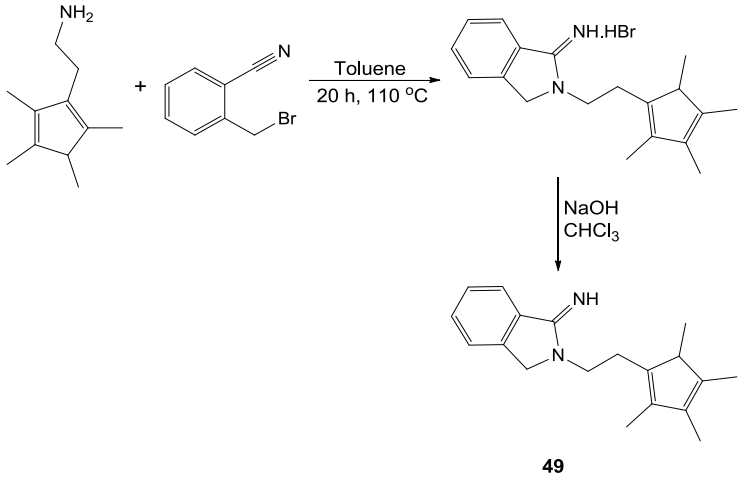

Scheme 4.10. Synthesis of 2-(2-(2,3,4,5-tetramethylcyclopentadienyl)ethyl)isoindolin-1-imine (**49**)

Compound **49** has been fully characterised by NMR and IR spectroscopy and high resolution ESI^+ mass spectrometry. The room temperature ^1H NMR spectrum of **49** in C_6D_6 reveals a mixture of double-bond isomers as observed in **33**-**37**. Unlike 2-(2,3,4,5-tetramethylcyclopentadienyl)ethanamine, in which an exocyclic double-bond isomer is observed, the absence of a lower field vinylic proton signal in **49** suggests the exclusive presence of endocyclic double-bond isomers (Figure 4.15).

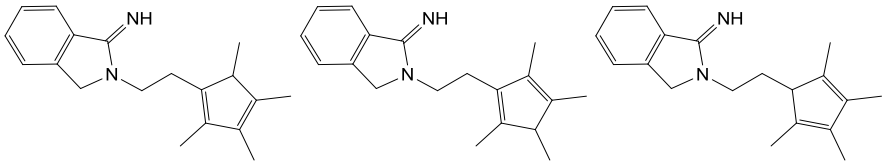

49A **49B** **49C**

Figure 4.15

The major isomers are assigned to **49A** and **49B** with preponderance of the former (60 %). Signals in the ^{1}H and ^{13}C NMR spectra corresponding to the major isomer are detailed in Chapter Five. The methine proton of the cyclopentadienyl ring corresponds to the familiar broad quartet (2.79 ppm) with stronger (^{3}J = 7.5 Hz) and weaker (^{4}J = 1.7 Hz) coupling respectively to protons of methyl groups immediately adjacent (1.08 ppm) and attached to an adjacent ring carbon (1.68 ppm). Two singlets (1.78 and 1.77 ppm) correspond to the remaining cyclopentadienyl methyl groups. These observations support assignment of **49A** as the major isomer since longer range coupling is observed to one methyl group rather than to two as would be expected in **49B**. The ethylene protons adjacent to the cyclopentdienyl and isoindolin-1-imine rings correspond to multiplets at 3.59 and 2.67 ppm respectively. A singlet at 3.83 ppm is observed for the methylene protons adjacent to the ring nitrogen with a series of overlapping multiplets spanning the range 7.12-6.88 ppm accounting for the four aromatic protons. A broad signal at 7.32 ppm is assigned to the NH proton. The imine carbon of the isoindolin-1-imine ring corresponds to an expected low field resonance (163.8 ppm) in the ^{13}C NMR spectrum.

4.8.2 Attempted synthesis of {η^5, η^1-C_5Me_4-C_2H_4-$C_8H_7N_2$}$TiCl_2$ (50)

Protonolysis of $Ti(NMe_2)_4$ with **49** as described in the synthesis of **43-45** proved unsuccessful; heating resulted in intractable mixtures of products. Similarly attempted protonolysis routes using a variety of titanium and zirconium precursors including $Ti(NMe_2)_2Cl_2$, $Ti(O^iPr)_4$, $Zr(NMe_2)_4$ and $Zr(CH_2Ph)_4$ did not appear viable routes when tested in NMR tube-scale reactions. The presence of high field doublets in the ^{1}H NMR spectra corresponding to the methyl groups immediately adjacent to the cyclopentadienyl methine indicates that the cyclopentadienyl ring remains protonated in spite of apparent coordination of the cyclic amidine. Metathesis reactions of the lithiated, sodiated or potassiated ligand with $TiCl_4$ or $Ti(NMe_2)_2Cl_2$ result in apparent

reduction to Ti(+3) species with immediate precipitation of brown-green insoluble material.

An alternative dehalosilylation reaction was devised whereby double deprotonation of **49** with NaH followed by reaction with two equivalents of trimethylsilyl chloride first generated the disilylated ligand which was subsequently reacted with $TiCl_4$ (Scheme 4.11).

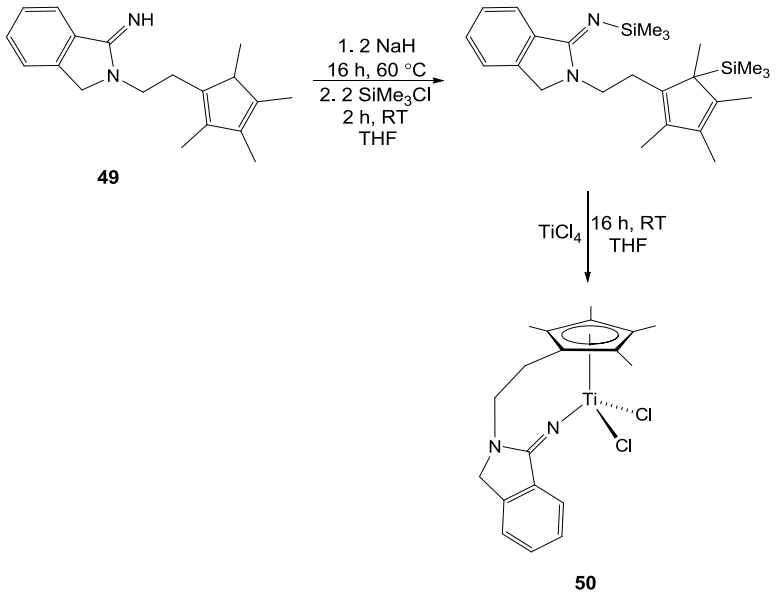

Scheme 4.11. Attempted synthesis of $\{\eta^5, \eta^1\text{-}C_5Me_4\text{-}C_2H_4\text{-}C_8H_7N_2\}TiCl_2$ (**50**) by reaction of silylated **49** with $TiCl_4$.

Following the reaction by NMR reveals that the double deprotonation and silylation steps proceed quantitatively. Subsequent reaction with $TiCl_4$ results in replacement of the characteristic high field signals corresponding to the silyl methyl protons with the expected trimethylsilyl chloride signal. The ^{1}H NMR spectrum of the crude product isolated by removal of the volatiles *in vacuo* and washing of the resulting dark solid with n-hexanes is complicated and reveals the apparent presence of more than one species. However, in spite of its complexity, the spectrum appears to show the signals expected for a C_1-symmetric complex: four singlets are observed (1.85, 1.77, 1.72 and 1.63 ppm) corresponding the cyclopentadienyl methyl groups. The methylene protons adjacent to the cyclopentadienyl ring are observed as two multiplets at 1.09 and 0.77 ppm. The methylene protons next to the amine nitrogen of the isoindolin-1-imine ring are assigned to multiplets at 2.74 and 2.55 ppm. The methylene ring protons adjacent to the amine nitrogen correspond to signals at 3.91 ppm and 3.85 ppm with the four

aromatic protons appearing a series of overlapping multiplets in the range 7.14-6.89 ppm. The EI mass spectrum exhibits a peak at *m/z* = 396.06 with the expected isotope distribution for $\{\eta^5, \eta^1\text{-}C_5Me_4\text{-}C_2H_4\text{-}C_8H_7N_2\}TiCl_2$ (**50**) (calcd. *m/z* = 396.06).

Unfortunately attempts to obtain a pure sample of **50** by crystallisation and sublimation techniques proved unsuccessful. It was decided to attempt an alternative synthetic route to **50**.

Whilst metathesis routes involving $TiCl_4$ and $Ti(NMe_2)_2Cl_2$ failed due to postulated reduction to Ti(+3) compounds (*vide supra*), a common synthetic strategy employed in complexation of bifunctional cyclopentadienyl chelating ligands to titanium involves an initial salt elimination reaction of the metal salt of the ligand with $TiCl_3(THF)_3$ with subsequent oxidation to the desired Ti(+4) complex which may be achieved with a variety of oxidising agents including AgCl, $PbCl_2$ and CH_2Cl_2.[40-44] Such a route was devised involving deprotonation of **49** with two equivalents of ^{n}BuLi, reaction of the dilithium salt with $TiCl_3(THF)_3$ followed by oxidation with $PbCl_2$. (Scheme 4.12).

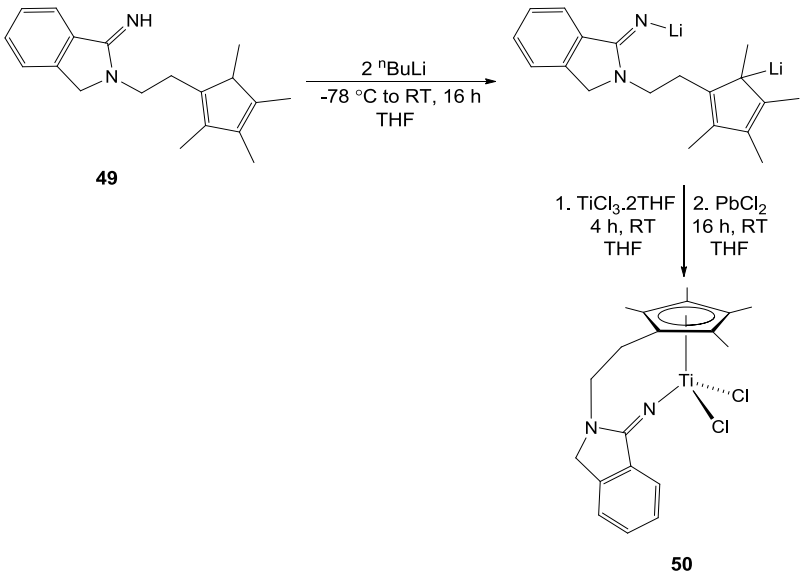

Scheme 4.12. Attempted synthesis of $\{\eta^5, \eta^1\text{-}C_5Me_4\text{-}C_2H_4\text{-}C_8H_7N_2\}TiCl_2$ by salt metathesis of lithiated **49** with $TiCl_3(THF)_3$ followed by oxidation with $PbCl_2$.

Unfortunately in spite of attempting this reaction under a variety of conditions and employing several different oxidising agents, an intractable dark green insoluble material is invariably recovered. The nature of this product is as yet unknown. Fortunately, repeated recrystallisations eventually resulted in growth of a small

number of orange crystals which were characterised by single crystal X-ray diffraction serving unambiguously to confirm the desired connectivity of **50**. The very low yield and air-sensitivity of the crystals precluded further spectroscopic characterisation. The molecular structure of **50** is shown in Figure 4.16 and full crystallographic data can be found in the CD appendix. Selected distances and angles are listed in Table 4.5.

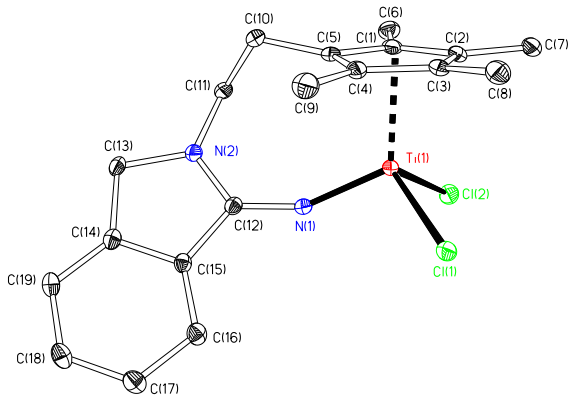

Figure 4.16. Displacement ellipsoid plots (20% probability) of $\{\eta^5, \eta^1\text{-}C_5Me_4\text{-}C_2H_4\text{-}C_8H_7N_2\}TiCl_2$ (**50**). H atoms omitted for clarity.

The molecular structure of **50** reveals the expected pseudo-tetrahedral, three-legged piano stool complex coordinated by the tethered η^5-cyclopentadienyl and κ^1-amidinate ligands with two chlorides occupying the remaining coordination sites. The C_1-symmetric structure is consistent with spectroscopic data described for the crude product from reaction of $TiCl_4$ with the disilylated ligand (*vide supra*). The isoindolin-1-iminate ring is twisted from the plane perpendicular to that of the cyclopentadienyl ring such that the lone pair atomic orbital on the amine nitrogen may become involved in the C=N-Ti π-system. Consequently the N(2)-C(12) distance (1.346(4) Å) is shorter than the N(2)-C(13) bond length (1.464(4) Å).

The feebler steric constraints imposed by the longer, more flexible ethylene tether result in much less significant deviation from the linear Ti(1)-N(1)-$C_{C=N}$ bond angle observed in **3** (165.2(3)°) than in the *o*-aryl-bridged complexes **43**-**48** (127.6(2)°-141.63(14)°). The Ti(1)-N(1)-$C(12)_{(C=N)}$ angle (151.7(2)°) in **50** is intermediate between the angles observed for the more constrained aryl-linked complexes and the completely unconstrained non-*ansa* compounds. The longer and more flexible bridge

further results in the same Ti(1)-Cp_{cent} distances (2.05 Å) and similar Cp_{cent}-Ti(1)-N(1) angles (117.3° (**50**), 118.0° (**3**)) being observed in **50** and **3**.

Table 4.5. Selected bond lengths (Å) and angles (°) for $\{\eta^5, \eta^1\text{-}C_5Me_4\text{-}C_2H_4\text{-}C_8H_7N_2\}TiCl_2$ (**50**). Cp_{cent} is the computed cyclopentadienyl ring carbon centroid.

Ti(1)-Cp_{cent}	2.05	Cp_{cent}-Ti(1)-Cl(1)	114.2
Ti(1)-Cl(1)	2.3244(10)	Cp_{cent}-Ti(1)-Cl(2)	114.6
Ti(1)-Cl(2)	2.3017(9)	Cp_{cent}-Ti(1)-N(1)	117.3
Ti(1)-N(1)	1.797(3)	Ti(1)-N(1)-C(12)	151.7(2)
N(1)-C(12)	1.306(4)	N(1)-Ti(1)-Cl(1)	101.97(9)
N(2)-C(12)	1.346(4)	N(1)-Ti(1)-Cl(2)	105.05(9)
N(2)-C(13)	1.464(4)	Cl(1)-Ti(1)-Cl(2)	101.79(4)

The Ti(1)-N(1) bond length observed in **50** (1.797(3) Å) is very close to that in **3** (1.802(4) Å) with similar N(1)-$C_{C=N}$ (1.306(4) Å (**50**), 1.310(4) Å (**3**)) and N(2)-$C_{C=N}$ (1.346(4) Å (**50**), 1.340(4) Å (**3**)) distances implying a very similar degree of π-donation resulting from the favourable orientation of the amidinate with respect to the metal facilitated by the longer and more flexible bridge. However, in spite of the apparent enhanced π-interaction in **50**, the molecular structure reveals that the imine carbon and titanium centre are not well sterically protected making deactivation pathways involving reactivity of the Ti-N bond more likely (*cf.* Chapter Three). Substitution of a bulky group on C(16), as well as realisation of an effective synthetic route to the precatalyst, would be necessary to explore the true scope of such an *ansa* complex as a viable precatalyst for olefin polymerisation.

4.9 Polymerisation experiments

Small-scale EP and EPDM copolymerisation testing of the *o*-aryl-bridged cyclopentadienyl-amidinate complexes **43-48** was undertaken at LANXESS Elastomers, The Netherlands, in order to develop an understanding of the relationship between the small changes in structure associated with different amidinate substituents on productivity and resulting polymer properties. Importantly, it was hoped to make comparisons with the polymerisation behaviour of the non-*ansa* precatalyst **4** in order to assess the influence of the aryl tether on various aspects of catalyst performance. Experiments were designed in order to examine productivity, temperature stability and comonomer affinity of the chelated complexes and **4** under comparable conditions. In each case, activation of the precatalysts was achieved with

two equivalents of $[CPh_3][BAr^F_4]$ in the presence of an MAO scavenger. Isothermal conditions were achieved by adjustment of the catalyst loading. The molecular weight and polydispersity index (PDI) were obtained from GPC data with copolymer composition being measured using FT-IR. Full experimental details are given in Chapter Five. The bridged complexes **43** and **46** were inactive under these conditions. The results for the active catalysts are summarised in Tables 4.6-4.8.

4.9.1 Productivity comparison: EP and EPDM copolymerisations

For fair comparison of productivity (Table 4.6), adjustment of the the C3:C2 ratio of the feed gases was necessary such that the incorporation of propylene into the polymer chain is held at approximately 45-47 wt.%; enhanced incorporation of ethylene usually results in inflated productivities. It was necessary to decrease the ratio of propylene in the feed gas from a C3:C2 ratio of 80:40 for the non-*ansa* compound **4** to 50:50 for the bridged complexes suggesting enhanced propylene affinity for the constrained complexes. The diene (ENB and VNB) concentration was not adjusted in the same way due to the incorporation (~1 wt.%) being too low to influence productivity. Nonetheless, the *ansa* catalysts appear to incorporate more of the diene comonomers (1.59-1.64 wt.% ENB, 1.01-1.09 wt.% VNB) compared to **4** (1.10 wt.% ENB, 0.72 wt.% VNB). This is further explored in experiments designed primarily to compare comonomer incorporation (*vide infra*).

Freshly prepared catalyst samples and solutions were used for this comparison of productivities. A degree of catalyst ageing was observed in subsequent experiments resulting in slightly diminished productivities but properties of the resulting polymers appeared unaffected. The productivities observed for $\{\eta^5, \eta^1\text{-}C_5Me_4\text{-}2\text{-}C_6H_4C(NMe_2)N\}TiCl_2$ (**43**) and the corresponding dimethyl complex **46** are negligible suggesting that steric protection of the imine nitrogen and titanium centre by the amidinate methyl substituents is insufficient consistent with previous trends. It is speculated that unwanted reactivity of the exposed Ti-N bond with aluminium alkyl species may be responsible for the inactivity (*cf.* Chapter Three). The productivities of the bridged complexes bearing the more bulky *iso*-propyl (**47**) and cyclohexyl (**45**, **48**) amidinate substituents are very high (12000-16000 kg mol^{-1} h^{-1} bar^{-1} (EP), 11000-15000 kg mol^{-1} h^{-1} bar^{-1} (EPDM)) but still not as high as the non-*ansa* precatalyst **4** (139000 kg mol^{-1} h^{-1} bar^{-1} (EP), 81000 kg mol^{-1} h^{-1} bar^{-1} (EPDM)). The lower productivity is suggested to stem from poorer steric protection of the more open metal

centre in the constrained systems although the data as a whole show similar productivities for the *iso*-propyl- (**44**/**47**) and cyclohexyl-substituted (**45**/**48**) precatalysts in spite of the slightly larger steric factors of the latter (*vide supra*).

As mentioned in Chapter Two, hydrogen is added to the feed gases for EPDM copolymerisation reactions in order to minimise formation of very high molecular weight polymers and associated fouling of the reactor.[45-47] Hydrogen has a significant effect on both productivity and polymer molecular weight in the case of **4**: productivity drops from 139000 to 81000 kg mol^{-1} h^{-1} bar^{-1} on switching from EP to EPDM copolymerisation in which hydrogen is introduced to the feed gas mixture. The molecular weight of the polymer also drops significantly from 330 to 95 kg mol^{-1}. In contrast no real drop in productivity is observed with the *ansa* complexes and the molecular weight remains largely constant (150 kg mol^{-1} (EP), 155 kg mol^{-1} (EPDM) for **47**; 130 kg mol^{-1} (EP), 115 kg mol^{-1} (EPDM) for **48**) in spite of addition of hydrogen. Interestingly, it may be surmised that the barrier for chain transfer to hydrogen is raised in the bridged complexes in comparison to the non-*ansa* systems which may be related to enhanced anion association to the more open metal centre in the chelated catalyst species. Alternatively, the difference may be ascribed to hydrogen regenerating dormant states resulting from 2,1-insertion of propylene in the case of the unchelated catalyst,[45] the more open active site of the *ansa* species being much less sensitive to the steric impact of such regioerrors on subsequent insertions. This explanation is also consistent with an increased number of polymer chains per titanium centre (assuming all titanium species are active) when hydrogen is added to the non-*ansa* system; no change is observed for the bridged catalysts. In any case, further experiments are required including NMR polymer characterisation in order to ascertain any differences relating to the regiochemistry of propylene enchainment.[48, 49]

In spite of the molecular weight of the EP copolymer produced by the bridged catalysts being lower to that obtained using **4**, the EPDM copolymer produced by **48** has a comparable molecular weight to that of the unconstrained precatalyst **4**; the *ansa* precatalyst **47** results in a higher M_n EPDM copolymer than **4**. In all cases the fairly narrow, monomodal molecular weight distributions (PDI: 2.4-2.7) are indicative of single-site behaviour undergoing fast chain transfer.[50, 51]

4.9.2 Temperature stability comparison: EP copolymerisation

To determine the influence of the chelate bridge on the temperature stability of catalysts derived from borate activation of **47** and **48** in comparison to unchelated **4**, EP copolymerisations were performed at both 90 ºC and 120 ºC (Table 4.7). Adjustment of the pressure and C3:C2 ratio are required in order to account for the different solubilities of the reactant gases at the two temperatures. For comparison to an EP polymerisation experiment performed at 120 ºC, 7 bar pressure and a C3:C2 ratio of 80:28, the pressure and C3:C2 must be decreased to 5 bar and 80:31 respectively for a comparable polymerisation at 90 ºC.

The overall trends observed in the EP and EPDM copolymerisations described in the comparison of productivities (*vide supra*) are observed in these experiments. Productivities and molecular weights are significantly higher for the non-*ansa* precatalyst **4**; the productivities are fairly similar for **47** and **48** although the molecular weight of the polymer produced by **47** is slightly higher than that of **48**. In all cases the increase in temperature from 90 ºC to 120 ºC is accompanied by a marked decrease in productivity to between half and a third of that observed at 90 ºC. This is accompanied for each of the precatalysts by a decrease in propylene incorporation at the higher temperature.

A decrease in the M_n of the polymer as a result of the increase in temperature is consistently observed for all three precatalysts (**4**, **47** and **48**) but interestingly this does not occur to the same extent for both bridged and non-*ansa* catalysts. A much larger decrease is observed for **4** (290 kg mol^{-1} (90 ºC), 65 kg mol^{-1} (120 ºC)) compared to **47** (135 kg mol^{-1} (90 ºC), 90 kg mol^{-1} (120 ºC)) and **48** (85 kg mol^{-1} (90 ºC), 55 kg mol^{-1} (120 ºC)). Indeed, the high temperature polymer molecular weights are similar to (**48**) or even exceed (**47**) those produced by **4**.

Table 4.6. Polymerisation results: productivity comparison[a]

Precatalyst	Copolymer	C3:C2	Cat. Loading[b]/µmol	Polymer Yield/g	Productivity/ kg mol^{-1} h^{-1} bar^{-1}	Polymer Properties C2/wt. %	C3/wt. %	ENB/wt. %	VNB/wt. %	M_n/ kg mol^{-1}	M_w/M_n
4	EP	80:40	0.03	4.88	139000	52.3	47.8	-	-	330	2.6
	EPDM[c]	80:40	0.07	6.62	81000	50.7	47.5	1.10	0.72	95	2.4
47	EP	50:50	0.50	9.41	16000	55.5	45.5	-	-	150	2.4
	EPDM[c]	50:50	0.50	8.61	15000	51.8	45.6	1.59	1.01	155	2.7
45	EP	50:50	0.50	7.72	13000	55.1	44.9	-	-	130	2.4
48	EP	50:50	0.50	6.83	12000	54.3	45.7	-	-	115	2.4
	EPDM[c]	50:50	0.50	6.66	11000	52.6	44.7	1.64	1.09	115	2.5

[a]Conditions: T= 90 °C, Pressure: 7 bar, Scavenger: MAO-10T ([Al] = 0.45-0.50 mM), 10 minute reaction time. Solvent pentamethylheptane (1L), Cocatalyst:[CPh_3][$BAr^F{}_4$] ([B]:[Ti] = 2). [b]Cat. Loading adjusted to limit exotherm to < 3 °C. [c]EPDM copol: H_2 flow: 3.5 NL/h, ENB: 0.7 mL, VNB: 0.7 mL.

Table 4.7. Polymerisation results: temperature stability comparison[d]

Precatalyst	Temp./°C	P/bar	C3:C2	Cat. Loading[e]/µmol	Polymer Yield/g	Productivity/ kg mol^{-1} h^{-1} bar^{-1}	Polymer Properties C2/wt. %	C3/wt. %	M_n/ kg mol^{-1}	M_w/M_n
4	90	5	80:31	0.14	7.96	136000	45.4	54.7	290	3.4
	120	7	80:28	0.40	11.51	49000	52.6	47.3	65	2.7
47	90	5	80:31	0.50	1.78	4000	33.3	66.7	135	2.3
	120	7	80:28	0.50	0.90	1500	41.9	58.2	90	2.2
48	90	5	80:31	0.50	3.75	9000	33.7	66.3	85	2.3
	120	7	80:28	0.70	3.61	4500	40.5	59.3	55	2.4

[d]Conditions: Scavenger: MAO-10T ([Al] = 0.45-0.50 mM), 10 minute reaction time. Solvent pentamethylheptane (1L), Cocatalyst:[CPh_3][$BAr^F{}_4$] ([B]:[Ti] = 2).[e]Cat. loading adjusted to limit exotherm to < 3 °C.

Table 4.8. Polymerisation results: comonomer incorporation comparison[f]

Precatalyst	Copolymer	Cat. Loading[g]/µmol	Polymer Yield/g	Productivity/ kg mol^{-1} h^{-1} bar^{-1}	Polymer Properties					
					C2/wt. %	C3/wt. %	ENB/wt. %	VNB/wt. %	M_n/ kg mol^{-1}	M_w/M_n
4	EP	0.03	4.88	139000	52.3	47.8	-	-	330	2.6
	EPDM[h]	0.07	6.62	81000	50.7	47.5	1.10	0.72	95	2.4
44	EP	0.50	8.68	15000	39.8	60.2	-	-	120	2.5
47	EP	0.25	5.89	20000	40.4	59.6	-	-	120	2.5
	EPDM[h]	0.50	1.98	3500	38.8	59.6	1.61	0.93	130	2.2
45	EP	0.50	7.22	12000	41.1	58.9	-	-	110	2.1
48	EP	0.50	9.76	17000	38.8	61.2	-	-	95	2.2
	EPDM[h]	0.50	4.67	8000	38.0	59.5	1.51	0.98	80	2.6

[f]Conditions: T= 90 °C, Pressure: 7 bar, Scavenger: MAO-10T ([Al] = 0.45-0.50 mM), 10 minute reaction time. Solvent pentamethylheptane (1L), Cocatalyst:[CPh_3][$BAr^F{}_4$] ([B]:[Ti] = 2). [g]Cat. Loading adjusted to limit exotherm to < 3 °C. C_3:C_2 = 80/40. [h]EPDM copol: H_2 flow: 3.5 NL/h, ENB: 0.7 mL, VNB: 0.7 mL.

It seems that, judging from the productivities, the high temperature stability of the active species derived from the chelated complexes is no better than the non-*ansa* system. However, the decreased detrimental influence of higher temperature on polymer molecular weight for the *ansa* systems represents an advantage over the non-*ansa* catalyst. Furthermore, this observation is demonstrative of the surprising effects which may be observed from fairly small ligand modifications on the relative preponderance of chain tranfer and propagation mechanisms.

4.9.3 Comonomer incorporation comparison: EP and EPDM copolymerisations

Adjustment of the C3:C2 ratio from 80:40 for **4** to 50:50 for the bridged precatalysts was required for fair assessment of differences in productivity (*vide supra*) reflecting an enhanced propylene affinity of the constrained systems. In order to make more rigorous comparison of the relative propylene and diene affinities it was necessary to test the precatalysts under the same conditions with the same monomer feed ratios (Table 4.8). Both EP and EPDM copolymers exhibit fairly narrow, monomodal molecular weight distributions indicative of single-site catalyst behaviour (Figures 4.17 and 4.18). The trend in molecular weights for the polymers in this experiment performed at 90 ºC is consistent with those observed in Section 4.9.1 although the M_n values are slightly smaller in this case perhaps resulting from greater incorporation of propylene under these conditions.

The non-*ansa* precatalyst **4** gives a polymer with approximately equal (50:50) uptake of propylene and ethylene under these conditions. The EPDM copolymer has a similar ethylene:propylene ratio but incorporates 1.10 wt.% ENB and 0.72 wt.% VNB. These monomer incorporations are very similar to those discussed in Chapter Two for EPDM polymerisations involving borane activation of **4** and the diene precatalysts. Employing MAO as a scavenger and in conjunction with the $[CPh_3][BAr^F{}_4]$ cocatalyst, the dichloride complexes (**44** and **45**) display comparable performance to the dimethyl compounds (**47** and **48**).[52] More importantly, the bridged precatalysts **44**, **45**, **47** and **48** result in EP and EPDM copolymers with 60 % propylene uptake. Furthermore, the EPDM copolymers incorporate approximately 30-40 % more ENB (1.51-1.61 wt.%) and VNB (0.93-0.98 wt.%) than the non-*ansa* system. The enhanced uptake of the most costly reactants in the process represents a clear commercial advantage of the cheltated systems.

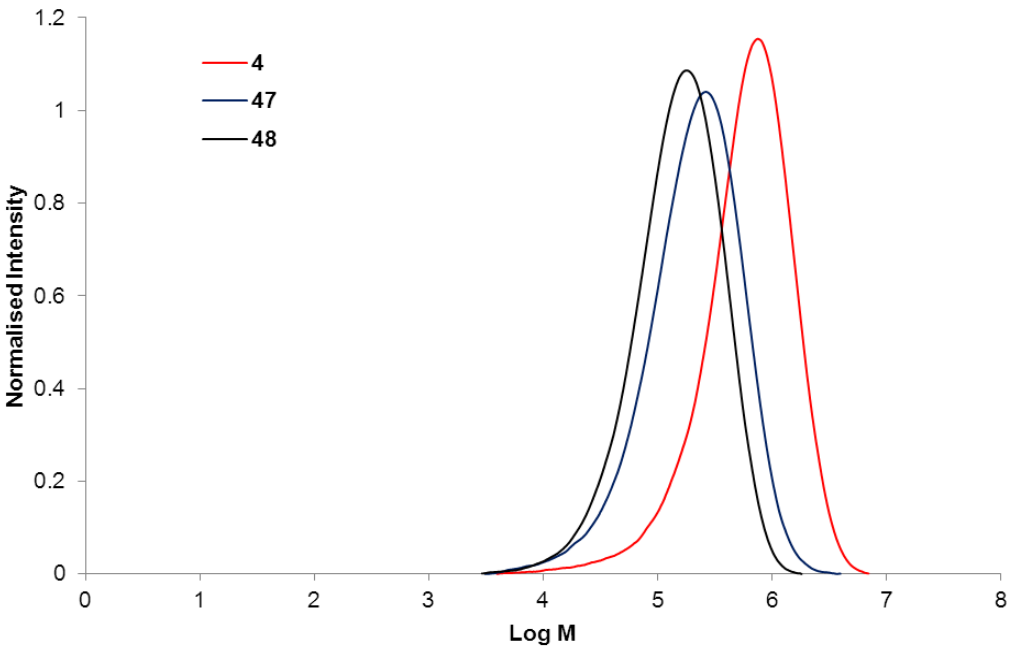

Figure 4.17. Molecular weight distribution determined by GPC for EP copolymer produced by Cp*Ti{NC(Ph)N^{i}Pr$_2$}Me$_2$ (**4**), {η^5, η^1-C$_5$Me$_4$-2-C$_6$H$_4$C(N^{i}Pr$_2$)N}TiMe$_2$ (R = ^{i}Pr (**47**), Cy (**48**))

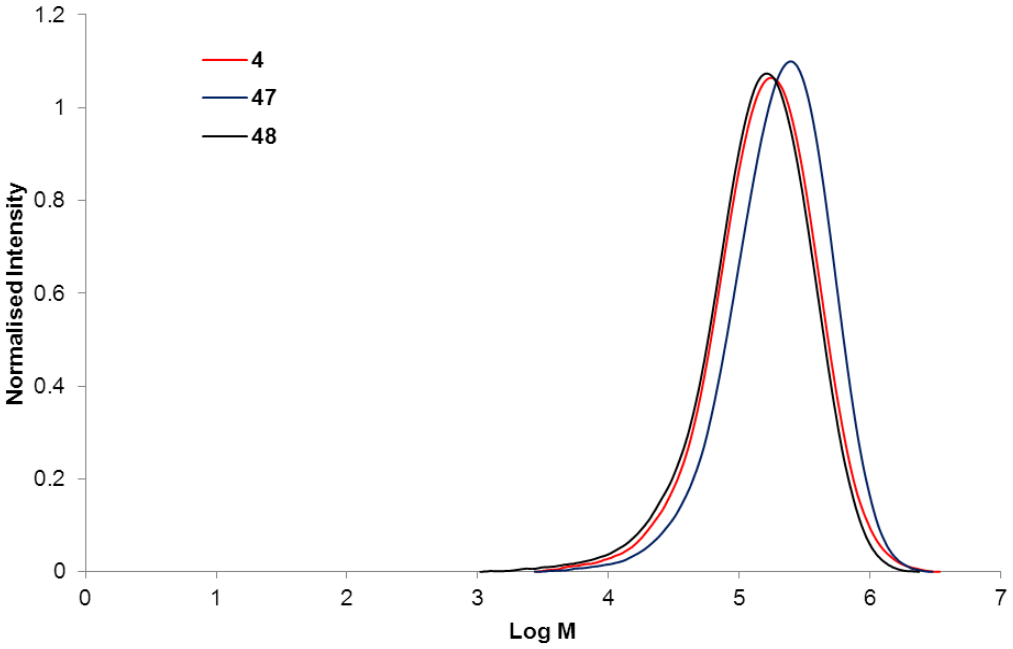

Figure 4.18. Molecular weight distribution determined by GPC for EPDM copolymer produced by Cp*Ti{NC(Ph)N^{i}Pr$_2$}Me$_2$ (**4**), {η^5, η^1-C$_5$Me$_4$-2-C$_6$H$_4$C(N^{i}Pr$_2$)N}TiMe$_2$ (R = ^{i}Pr (**47**), Cy (**48**))

4.10 Summary

This Chapter has described various synthetic attempts to synthesise chelating cyclopentadiene-amidine ligands. In spite of difficulties encountered in preparation of indenyl and homologated variants, successful synthesis of the *o*-aryl-bridged ligands **35-37** provides straightforward access to a family of constrained half-sandwich titanium complexes **43-48**. Combined crystallographic and DFT studies of these chelated complexes suggest similar electronic similarities but a more sterically exposed metal centre compared to the non-*ansa* systems. In spite of difficulties encountered in isolation of the complex, the longer and more flexible chelate bridge observed in **50** demonstrates the potential for optimisation of the amidinate-metal bonding interaction whilst retaining potential benefits derived from covelent tethering of the cyclopentadienyl and amidinate ligands. This offers scope for potential future work associated with this topic.

A series of copolymerisation experiments under industrially relevant conditions were undertaken in order to assess the performance of the chelated complexes and to compare to the non-*ansa* precatalyst **4**. The testing reveals very high productivities for **44**, **45**, **47** and **48** but these are not as productive as **4**; the more exposed metal centre in the *ansa* species being suggested to result in lower productivities for the bridged complexes. The temperature stability of the bridged catalysts is also similar to that of the non-*ansa* system. However, important advantages associated with the chelated catalysts are observed in terms of their capability of producing higher molecular weight EPDM than **4** at 90 ºC and 120 ºC combined with enhanced affinity for propylene and non-conjugated diene (ENB and VNB) comonomers.

4.11 References for Chapter Four

1. D. Guo, H.-B. Tong and M. Zhou, *Acta Crystallogr., Sect. E*, 2009, **65**, m611.
2. Y.-X. Chen, P.-F. Fu, C. L. Stern and T. J. Marks, *Organometallics*, 1997, **16**, 5958-5963.
3. M. G. Thorn, P. E. Fanwick, I. P. Rothwell and R. W. Chesnut, *Chem. Commun.*, 1999, 2543-2544.
4. L. E. Turner, M. G. Thorn, P. E. Fanwick and I. P. Rothwell, *Chem. Commun.*, 2003, 1034-1035.
5. Y. Zhang, Y. Mu, C. Lue, G. Li, J. Xu, Y. Zhang, D. Zhu and S. Feng, *Organometallics*, 2004, **23**, 540-546.
6. Y. Zhang and Y. Mu, *Organometallics*, 2006, **25**, 631-634.
7. D. J. Cho, C. J. Wu, S. S, W.-S. Han, S. O. Kang and B. Y. Lee, *Organometallics*, 2006, **25**, 2133-2134.
8. D. J. Joe, C. J. Wu, T. Bok, E. J. Lee, C. H. Lee, W.-S. Han, S. O. Kang and B. Y. Lee, *Dalton Trans.*, 2006, 4056-4062.
9. U. G. Joung, C. J. Wu, S. H. Lee, C. H. Lee, E. J. Lee, W.-S. Han, S. O. Kang and B. Y. Lee, *Organometallics*, 2006, **25**, 5122-5130.
10. S. H. Lee, C. J. Wu, U. G. Joung, B. Y. Lee and J. Park, *Dalton Trans.*, 2007, 4608-4614.
11. C. Ji Wu, S. Hoon Lee, H. Yun and B. Yeoul Lee, *J. Organomet. Chem.*, 2006, **691**, 5626-5634.
12. S. H. Lee, C. J. Wu, J. Yoo, J.-e. Kwak, H. Yun and B. Y. Lee, *J. Organomet. Chem.*, 2008, **693**, 457-467.
13. C. J. Wu, S. H. Lee, S. T. Yu, S. J. Na, H. Yun and B. Y. Lee, *Organometallics*, 2008, **27**, 3907-3917.
14. H. Hanaoka, E. Yoshikawa and Y. Imamoto, *Sumitomo Chemical Co., WO2003024983A1*, 2003.
15. C. S. Tredget, S. C. Lawrence, B. D. Ward, R. G. Howe, A. R. Cowley and P. Mountford, *Organometallics*, 2005, **24**, 3136-3148.
16. D. A. Robson, S. Y. Bylikin, M. Cantuel, N. A. H. Male, L. H. Rees, P. Mountford and M. Schröder, *J. Chem. Soc., Dalton Trans.*, 2001, 157-169.
17. M. E. G. Skinner, B. R. Tyrrell, B. D. Ward and P. Mountford, *J. Organomet. Chem.*, 2002, **647**, 145-150.

18. N. A. H. Male, M. E. G. Skinner, S. Y. Bylikin, P. J. Wilson, P. Mountford and M. Schröder, *Inorg. Chem.*, 2000, **39**, 5483-5491.
19. N. Adams, H. J. Arts, P. D. Bolton, D. Cowell, S. R. Dubberley, N. Friederichs, C. M. Grant, M. Kranenburg, A. J. Sealey, B. Wang, P. J. Wilson, M. Zuideveld, A. J. Blake, M. Schröder and P. Mountford, *Organometallics*, 2006, **25**, 3888-3903.
20. D. S. Matharu, D. J. Morris, A. M. Kawamoto, G. J. Clarkson and M. Wills, *Org. Lett.*, 2005, **7**, 5489-5491.
21. A. R. Sanger, *Inorg. Nucl. Chem. Lett.*, 1973, **9**, 351-354.
22. G. Rousselet, P. Capdevielle and M. Maumy, *Tetrahedron Lett.*, 1993, **34**, 6395-6398.
23. J. H. Forsberg, V. T. Spaziano, T. M. Balasubramanian, G. K. Liu, S. A. Kinsley, C. A. Duckworth, J. J. Poteruca, P. S. Brown and J. L. Miller, *J. Org. Chem.*, 1987, **52**, 1017-1021.
24. C. K. Broder, A. E. Goeta, J. A. K. Howard, A. K. Hughes, A. L. Johnson, J. M. Malget and K. Wade, *J. Chem. Soc., Dalton Trans.*, 2000, 3526-3533.
25. A. E. Goeta, A. K. Hughes and J. M. Malget, *Acta Crystallogr., Sect. C*, 2001, **57**, 702-703.
26. H. Wang, H.-W. Li and Z. Xie, *Organometallics*, 2003, **22**, 4522-4531.
27. M.-M. Sit, H.-S. Chan and Z. Xie, *Dalton Trans.*, 2008, 1454-1464.
28. E. A. Mintz, J. C. Pando and I. Zervos, *J. Org. Chem.*, 1987, **52**, 2948-2950.
29. J. L. Luche, *J. Am. Chem. Soc.*, 1978, **100**, 2226-2227.
30. E. Y. X. Chen and T. J. Marks, *Chem. Rev.*, 2000, **100**, 1391-1434.
31. J. C. Stevens, F. J. Timmers, D. R. Wilson, G. F. Schmidt, P. N. Nickias, R. K. Rosen, G. W. Knight and S. Y. Lai, *Dow Chemical Co., EP416815A2*, 1991.
32. C. A. Tolman, *Chem. Rev.*, 1977, **77**, 313-348.
33. B. C. Taverner, *J. Comput. Chem.*, 1996, **17**, 1612-1623.
34. W. Scherer and G. S. McGrady, *Angew. Chem., Int. Ed. Engl.*, 2004, **43**, 1782-1806.
35. E. Clot and O. Eisenstein, in *Principles and Applications of Density Functional Theory in Inorganic Chemistry II*, Springer Berlin Heidelberg, 2004.
36. P. D. Bolton, E. Clot, N. Adams, S. R. Dubberley, A. R. Cowley and P. Mountford, *Organometallics*, 2006, **25**, 2806-2825.

37. M. Feliz, P. D. Bolton, P. Mountford and E. Clot, *Organometallics*, 2008, **27**, 6111-6122.
38. H. Bigmore, DPhil Thesis, University of Oxford, 2007.
39. D. van Leusen, D. J. Beetstra, B. Hessen and J. H. Teuben, *Organometallics*, 2000, **19**, 4084-4089.
40. G. A. Luinstra and J. H. Teuben, *J. Chem. Soc., Chem. Commun.*, 1990, 1470-1471.
41. J. A. M. Canich, *Exxon Chemical Patents Inc., US5096867A*, 1992.
42. D. D. Devore, *Dow Chemical Co., EP514828A1*, 1992.
43. A. L. McKnight, M. A. Masood, R. M. Waymouth and D. A. Straus, *Organometallics*, 1997, **16**, 2879-2885.
44. P. N. Nickias, M. H. McAdon, J. T. Patton, B. P. Friedrichsen, J. Soto, J. C. Stevens and D. D. Vanderlende, *Dow Chemical Co., WO9715583A1*, 1997, .
45. S. W. Ewart, M. A. Parent and M. C. Baird, *J. Polym. Sci., Part A: Polym. Chem.*, 1999, **37**, 4386-4389.
46. Y. V. Kissin, R. I. Mink, T. E. Nowlin and A. J. Brandolini, *J. Polym. Sci., Part A: Polym. Chem.*, 1999, **37**, 4281-4294.
47. H. Mori, M. Endo and M. Terano, *J. Mol. Catal. A: Chem.*, 1999, **145**, 211-220.
48. H. N. Cheng, *Chem. Anal.* , 1991, **113**, 409-493.
49. F. A. Bovey and P. A. Mirau, *NMR of Polymers*, Academic, 1996.
50. G. Odian, *Principles of Polymerisation*, Wiley-Interscience, 1992.
51. P. J. Flory, *Principles of Polymer Chemistry*, Cornell University Press, 1992.
52. J. C. W. Chien and W. M. Tsai, *Makromol. Chem., Macromol. Symp.*, 1993, **66**, 141-155.

Chapter Five

Experimental details and characterising data

5.1 General methods and instrumentation

All manipulations were carried out using standard Schlenk line or dry-box techniques under an atmosphere of argon or dinitrogen. Solvents were degassed by sparging with dinitrogen and dried by passing through a column of the appropriate drying agent. Toluene was refluxed over sodium and distilled. Deuterated solvents were dried over potassium (C_6D_6) or P_2O_5 ($CDCl_3$ and CD_2Cl_2), distilled under reduced pressure and stored under dinitrogen in Teflon valve ampoules. NMR samples were prepared under dinitrogen in 5 mm Wilmad 507-PP tubes fitted with J. Young Teflon valves. ^{1}H, ^{13}C-{^{1}H} ,^{11}B-{^{1}H}, ^{19}F NMR spectra were recorded on Varian Mercury-VX 300, Varian Unity Plus 500 or on a Bruker avc500 spectrometer fitted with a ^{13}C cryoprobe at RT unless stated otherwise and referenced internally to residual protio-solvent (^{1}H) or solvent (^{13}C) resonances, and are reported relative to tetramethylsilane (δ = 0 ppm). ^{19}F spectra were referenced externally to $CFCl_3$ and ^{11}B spectra were referenced externally to $Et_2O{\cdot}BF_3$. Assignments were confirmed using two dimensional ^{1}H-^{1}H and ^{13}C-^{1}H NMR correlation experiments. Chemical shifts are quoted in δ (ppm) and coupling constants in Hz. Mass spectra were recorded by the mass spectrometry service of the University of Oxford. IR spectra were recorded on Nicolet Magna 560 E.S.P. FTIR, Perkin-Elmer 1710 or (for air-stable, solid samples) Bruker Tensor 27 FT-IR (thin film deposition on diamond ATR module) spectrometers. Air-sensitive samples were prepared in a dry-box as Nujol mulls between NaCl plates, and the data are quoted in wavenumbers (cm^{-1}) within the range 4000−400 cm^{-1}. Elemental analyses were carried out by the Elemental Analysis Service at the London Metropolitan University and Elemental Microanalysis Ltd., Devon.

5.2 Literature preparations and starting materials

$Ti\{NC(Ph)N^{i}Pr_2\}Cl_3$,[1] Cp*Li,[2, 3] Cp^*MCl_3 (M = Zr, Hf),[4] C_5Me_4H-2-C_6H_4CHO,[5] $Ti(NMe_2)_4$[6-8] and 2-(2,3,4,5-tetramethylcyclopentadienyl)ethanamine[9] were prepared according to literature methods. 2,3-Dimethyl-1,3-butadiene, 2,4-hexadiene and 1,3-pentadiene were dried over CaH_2, distilled under reduced pressure and stored under dinitrogen in J. Young Teflon valve ampoules (2,3-dimethyl-1,3-butadiene may only be stored for a few months in the absence of a stabilizer before undergoing self-polymerisation). All other reagents were purchased from Alfa Aesar or Sigma-Aldrich or kindly donated by LANXESS Elastomers and used directly or degassed as appropriate before use.

5.3 Experimental details for Chapter Two

$HNC(Ph)N^iPr_2$ (1)

This compound was prepared by adaptation of a patented procedure.[10] To a toluene (250 mL) solution of diisopropylamine (22.4 mL, 0.16 mol) at 50 ^oC was added MeMgBr (50 mL, 3.0 M in Et_2O, 0.15 mol). Following stirring at 50 ^oC for 1.5 h, the solution was cooled to 0 ^oC and benzonitrile (15.4 mL, 0.15 mol) was added dropwise. The solution was allowed to warm to RT and was stirred for a further 16 h. The reaction was then quenched with water (100 mL) and the organic phase separated from the aqueous layer which was then back extracted with Et_2O (2 x 50 mL). The combined organic phases were then dried over Na_2SO_4 and the volatiles removed under reduced pressure. Vacuum distillation (55-60 ^oC, 10^{-1} mBar) yielded a colourless oil which was mixed with pentane (20 mL) and dried over CaH_2 for 16 h. Following filtration and removal of the pentane *in vacuo*, the product crystallised as a colourless powder. Yield = 14.2 g (50 %). ^1H NMR (C_6D_6, 299.9 MHz, 293 K): 7.18-7.07 (5 H, series of overlapping m, C_6H_5), 5.70 (1 H, br s, NH), 3.44 (2 H, sept, C<u>H</u>Me_2, $^3J = 6.9$ Hz), 1.15 (12 H, d, CH<u>Me</u>$_2$, $^3J = 6.9$ Hz) ppm. ^{13}C-{^1H} NMR (C_6D_6, 293 K): 167.4 (HN<u>C</u>(Ph)N^iPr_2), 142.4 (*i*-C_6H_5), 128.7 (*o*- or *m*-C_6H_5), 128.0 (*m*- or *o*-C_6H_5), 126.0 (*p*-C_6H_5), 48.5 (<u>C</u>HMe_2), 20.9 (CH<u>Me</u>$_2$) ppm. IR (NaCl plates, Nujol mull, cm^{-1}): 3315 (w, υ(N-H)), 1616 (w), 1496 (m), 1364 (s), 1315 (m), 1260 (m), 1218 (s), 1179 (s), 1162 (s), 1148 (m), 1131 (m), 1083 (s), 1032 (s), 1024 (m), 918 (w), 904 (w), 869 (w), 827 (m), 773 (s), 701 (s), 675 (m), 668 (w), 613 (s). Anal. Found (calcd. For $C_{13}H_{20}N_2$): C, 76.50 (76.42); H, 9.90 (9.87); N, 13.79 (13.71) %. FI-HRMS: *m/z* = 204.1629 (calcd. For $[C_{13}H_{20}N_2]^+$ *m/z* = 204.1626). Single crystals suitable for X-ray diffraction were grown by slow cooling of the molten compound.

$CpTi\{NC(Ph)N^iPr_2\}Cl_2$ (2)

This compound may be prepared by adaptation of a patented procedure (Method A)[10] or *via* an alternative procedure (Method B).

Method A: To a stirring toluene (20 mL) suspension of $CpTiCl_3$ (4.00 g, 18.2 mmol) and N,N-diisopropylbenzamidine (**1**) (3.73 g, 18.2 mmol) was added an excess of triethylamine (15.3 mL, 110 mmol). The orange-red solution was stirred for 16 h after which time the volatiles were removed *in vacuo*. The resulting orange solid was extracted into hot (*ca.* 80 ºC) toluene (4 x 20 mL) and the solution was concentrated

to *ca.* 15 mL and stored at -30 ºC for 2 d resulting in crystallisation of the title compound as a deep red solid which was isolated and dried *in vacuo*. Yield = 3.5 g (50 %).

Method B: To a stirring THF (20 mL) solution of $Ti\{NC(Ph)N^iPr_2\}Cl_3$ (2.00 g, 5.60 mmol) was added dropwise a THF (20 mL) solution of NaCp (0.50 g, 5.60 mmol). Following stirring of the deep red solution for 16 h, the volatiles were removed under reduced pressure and the solids extracted into toluene (4 x 20 mL) and filtered through Celite. The toluene solution was concentrated to *ca*. 25 mL and stored at -30 ºC for 2 d resulting in crystallisation of the title compound as a deep red solid which was isolated and dried *in vacuo*. Yield = 0.78 g (35 %).

^{1}H NMR (C_6D_6, 299.9 MHz, 253 K): 7.13-6.92 (5 H, series of overlapping m, C_6H_5), 6.02 (5 H, s, C_5H_5), 3.26 (1 H, sept, C<u>H</u>Me_2 *cis* to C_6H_5, ^3J = 6.7 Hz), 2.82 (1 H, br s, C<u>H</u>Me_2 *trans* to C_6H_5), 1.62 (6 H, d, CH<u>Me</u>$_2$ *trans* to C_6H_5), 0.46 (6 H, d, CH<u>Me</u>$_2$ *cis* to C_6H_5, ^3J = 6.7 Hz) ppm. ^{13}C-{^{1}H} NMR (C_6D_6, 75.4 MHz, 233 K): 165.8 (N<u>C</u>(Ph)N^iPr_2), 138.5 (*i*-C_6H_5), 129.1 (*o*- or *m*-C_6H_5), 128.8 (*m*- or *o*-C_6H_5), 125.8 (*p*-C_6H_5), 115.3 (C_5H_5), 52.6 (<u>C</u>HMe_2 *cis* to C_6H_5), 48.4 (<u>C</u>HMe_2 *trans* to C_6H_5), 19.9 (CH<u>Me</u>$_2$ *trans* to C_6H_5), 19.4 (CH<u>Me</u>$_2$ *cis* to C_6H_5) ppm. IR (NaCl plates, Nujol mull, cm^{-1}): 1517(s), 1493(m), 1442(s), 1351(s), 1184(w), 1154(m), 1104(w), 1031(m), 1021(m), 893(m), 845(w), 813(m), 787(m), 735(w), 700(m), 667(m). Anal. Found (calcd. For $C_{18}H_{24}Cl_2N_2Ti$): C, 56.07 (55.84); H, 6.26 (6.25); N, 7.23 (7.24) %. EI-MS: *m/z* = 286 (25 %, $[M - N^iPr_2]^+$), 183 (95 %, $[M - NC(Ph)N^iPr_2]^+$).

$Cp^*Ti\{NC(Ph)N^iPr_2\}Cl_2$ (3)

This compound was prepared by adaptation of a patented procedure.[10] To a stirring toluene (50 mL) suspension of Cp^*TiCl_3 (1.45 g, 5.01 mmol) and N,N-diisopropylbenzamidine (**1**) (1.00 g, 4.89 mmol) was added an excess of triethylamine (2.50 mL, 18.1 mmol). The resulting orange/red solution was stirred for 16 h after which time the volatiles were removed *in vacuo.* The resulting orange solid was extracted into toluene (2 x 15 mL) and n-hexanes (15 mL) and solution was stored at -30 ºC for 2 d resulting in crystallisation of the desired compound. Yield = 1.23 g (54 %). ^{1}H NMR (Toluene-d_8, 299.9 MHz, 253 K): 7.42-7.05 (5 H, series of overlapping m, C_6H_5), 3.51 (1 H, sept, C<u>H</u>Me_2 *cis* to C_6H_5, ^3J = 6.3 Hz), 3.02 (1 H, br s, C<u>H</u>Me_2 *trans* to C_6H_5), 1.94 (15 H, s, C_5Me_5), 1.59 (6 H, d, CH<u>Me</u>$_2$ *trans* to C_6H_5), 0.60 (6 H,

d, CH$\underline{Me}_2$ *cis* to C_6H_5, ^3J = 6.3 Hz) ppm. ^{13}C-{^1H} NMR (Toluene-d_8, 253 K): 164.5 (N$\underline{C}$(Ph)N^{i}Pr$_2$), 138.4 (*i*-C_6H_5), 128.7 (*o*- or *m*-C_6H_5), 128.5 (*m*- or *o*-C_6H_5), 126.1 (*p*-C_6H_5), 110.1 ($\underline{C}_5Me_5$), 52.5 ($\underline{C}HMe_2$ *cis* to C_6H_5), 47.8, ($\underline{C}HMe_2$ *trans* to C_6H_5), 20.0 (CH$\underline{Me}_2$), 12.6 ($C_5\underline{Me}_5$) ppm. IR (NaCl plates, Nujol mull, cm^{-1}): 1694 (m), 1523 (s), 1336 (s), 1260 (w), 1098 (w), 1074 (w), 1104(w), 1031 (m), 1021 (m), 922 (w), 894 (m), 783 (s), 707 (w), 697 (w), 661 (m). Anal. Found (calcd. For $C_{23}H_{34}Cl_2N_2Ti$): C, 60.32 (60.41); H, 7.36 (7.49); N, 5.94 (6.13) %. EI-MS: *m/z* = 253 (80 %, [*M* – NC(Ph)N^{i}Pr$_2$]$^+$), 203 (60 %, [NC(Ph)N^{i}Pr$_2$]$^+$), 135 (100 %, [Cp*]$^+$), 100 (80 %, [N^{i}Pr$_2$]$^+$), 77 (60 %, [Ph]$^+$). Single crystals suitable for X-ray diffraction were grown from a toluene/n-hexanes solution at -80 ^{o}C.

Cp*Ti{NC(Ph)N^{i}Pr$_2$}Me$_2$ (4)

To a stirring toluene (15 mL) solution of Cp*Ti{NC(Ph)N^{i}Pr$_2$}Cl$_2$ (**3**) (1.00 g, 2.20 mmol) was added dropwise MeLi (2.80 mL, 1.6 M in Et$_2$O, 4.40 mmol) and the resulting solution was stirred for 16 h. The volatiles were then removed *in vacuo* and the yellow solid was then extracted into n-hexanes (50 mL). Concentration of the solution to *ca.* 15 mL and subsequent storage at -30 °C for 24 h resulted in crystallisation of the desired product as large yellow crystals which were isolated and dried *in vacuo*. Yield = 0.37 g (40 %). ^1H NMR (Toluene-d_8, 299.9 MHz, 233 K): 7.23-6.95 (5 H, series of overlapping m, C_6H_5), 3.60 (1 H, sept, C$\underline{H}$Me$_2$ *cis* to C_6H_5, ^3J = 6.1 Hz), 2.91 (1 H, br s, C$\underline{H}$Me$_2$ *trans* to C_6H_5), 1.83 (15 H, s , C_5Me_5), 1.72 (6 H, d, CH$\underline{Me}_2$ *trans* to C_6H_5), 0.64 (6 H, d, CH$\underline{Me}_2$ *cis* to C_6H_5, ^3J = 6.1 Hz), 0.53 (6 H, s, TiMe) ppm. ^{13}C-{^1H} NMR (Toluene-d_8, 233 K): 160.9 (N$\underline{C}$(Ph)N^{i}Pr$_2$), 141.9 (*i*-C_6H_5), 128.1 (*o*- or *m*-C_6H_5), 127.5 (*m*- or *o*-C_6H_5), 126.1 (*p*-C_6H_5), 118.9 ($\underline{C}_5Me_5$), 51.7 ($\underline{C}HMe_2$ cis to C_6H_5), 47.6 (TiMe), 46.5 ($\underline{C}HMe_2$ *trans* to C_6H_5), 19.9 (CH$\underline{Me}_2$), 11.7 ($C_5\underline{Me}_5$) ppm. IR (NaCl plates, Nujol mull, cm^{-1}): 1563 (s), 1506 (w), 1323 (s), 1261 (w), 1132 (w), 1094 (w), 1034 (m), 1023 (m), 886 (m), 782 (s), 696 (m), 666 (m). Anal. Found (calcd. For $C_{25}H_{40}N_2Ti$): C, 71.90 (72.10); H, 9.80 (9.68); N, 6.80 (6.73) %. EI-MS: *m/z* = 203 (5 %, [NC(Ph)N^{i}Pr$_2$]$^+$), 135 (5 %, [Cp*]$^+$), 103 (100 %, [NCPh]$^+$), 77 (70 %, [Ph]$^+$). Single crystals suitable for X-ray diffraction were grown from a pentane solution at -30 °C.

Cp*Ti{NC(Ph)N^{i}Pr$_2$}(η-2,3-C$_4$H$_4$Me$_2$) (5)

To a stirring solution of Cp*Ti{NC(Ph)N^{i}Pr$_2$}Cl$_2$ (**3**) (2.00 g, 4.37 mmol) and 2,3-dimethyl-1,3-butadiene (4.00 mL, 35.0 mmol) in toluene (30 mL) at 0 ºC was added dropwise two equivalents of ^{n}BuLi (5.45 mL, 1.6 M in n-hexanes, 8.74 mmol) which resulted in the solution changing colour from orange-red to green. The solution was allowed to warm slowly to RT and was stirred for 16 h. Removal of the volatiles *in vacuo* afforded a green-blue solid which was extracted into pentane (4 x 20 mL). After filtration, the pentane solution was concentrated to 30 mL and cooled to -30 ºC resulting in crystallisation of the desired complex after 24 h. The dark green crystalline material was isolated and dried *in vacuo*. Yield = 1.09 g, (53 %). ^{1}H NMR (C$_6$D$_6$, 299.9 MHz, 293 K): 7.06-6.95 (5 H, series of overlapping m, C$_6$H$_5$), 3.96 (2 H, sept, C<u>H</u>Me$_2$, ^{3}J = 7.0 Hz), 2.45 (1 H, d, C$_4$<u>H</u>$_4$Me$_2$ (*syn*), ^{2}J = 7.2 Hz), 2.33 (1 H, d, C$_4$<u>H</u>$_4$Me$_2$ (*syn*), ^{2}J = 7.4 Hz), 2.19 (3 H, s, C$_4$H$_4$<u>Me</u>$_2$), 2.02 (3 H, s, C$_4$H$_4$<u>Me</u>$_2$), 1.87 (15 H, s , C$_5$Me$_5$), 1.05 (6 H, d, CH<u>Me</u>$_2$, ^{3}J = 7.1 Hz), 1.00 (6 H, d, CH<u>Me</u>$_2$, ^{3}J = 6.9 Hz), 0.70 (1 H, d, C$_4$<u>H</u>$_4$Me$_2$ (*anti*), ^{2}J = 7.2 Hz), 0.58 (1 H, d, C$_4$<u>H</u>$_4$Me$_2$ (*anti*), ^{2}J = 7.4 Hz) ppm. ^{13}C-{^{1}H} NMR (C$_6$D$_6$, 293 K): 160.3 (N<u>C</u>(Ph)N^{i}Pr$_2$), 142.3 (*i*-C$_6$H$_5$), 128.5 (*o*- or *m*-C$_6$H$_5$), 128.0 (2,3-<u>C</u>$_4$H$_4$Me$_2$), 127.5 (*m*- or *o*-C$_6$H$_5$), 127.3 (*p*-C$_6$H$_5$), 126.3 (2,3-<u>C</u>$_4$H$_4$Me$_2$), 117.3 (<u>C</u>$_5$Me$_5$), 69.3 (1,4-<u>C</u>$_4$H$_4$Me$_2$), 67.4 (1,4-<u>C</u>$_4$H$_4$Me$_2$), 46.5 (<u>C</u>HMe$_2$), 24.9 (C$_4$H$_4$<u>Me</u>$_2$), 24.5 (C$_4$H$_4$<u>Me</u>$_2$), 24.1 (CH<u>Me</u>$_2$), 22.5 (CH<u>Me</u>$_2$), 12.1 (C$_5$<u>Me</u>$_5$) ppm. IR (NaCl plates, Nujol mull, cm^{-1}): 1653 (m), 1589 (s), 1541 (w), 1272 (s), 1026 (w), 1157 (m), 800 (w), 783 (m), 702 (s), 653 (w). Anal. Found (calcd. For C$_{29}$H$_{44}$N$_2$Ti): C, 74.29 (74.34); H, 9.39 (9.47); N, 6.05 (5.98) %. EI-MS: *m/z* = 468 (5 %, [*M*]$^{+}$), 386 (35 %, [*M* – C$_4$H$_4$Me$_2$]$^{+}$), 223 (10 %, [*M* – C$_4$H$_4$Me$_2$ – Ph – 2^{i}Pr]$^{+}$), 100 (80%, [N^{i}Pr$_2$]$^{+}$). Single crystals suitable for X-ray diffraction were grown from a pentane solution at RT.

Cp*Ti{NC(Ph)N^{i}Pr$_2$}(η-1,4-C$_4$H$_4$Me$_2$) (6)

To a stirring solution of Cp*Ti{NC(Ph)N^{i}Pr$_2$}Cl$_2$ (**3**) (6.50 g, 14.2 mmol) and 2,4-hexadiene (13.0 mL, 114 mmol) in toluene (50 mL) at 0 ºC was added dropwise two equivalents of ^{n}BuLi (17.8 mL, 1.6 M in n-hexanes, 28.4 mmol) which resulted in the solution turning a darker colour. The solution was allowed to warm slowly to RT and was subsequently heated at 90 ºC for 8 h after which time the solution had turned dark green. Removal of the volatiles *in vacuo* afforded a green solid which was extracted into pentane (5 x 20 mL). After filtration, the solution was concentrated to *ca.* 30 mL

and was cooled to -80 ºC yielding green crystals which were isolated and dried *in vacuo*. Yield = 2.15 g (35 %). ^{1}H NMR (Toluene-d_8, 299.9 MHz, 253 K): 7.12-6.95 (5 H, series of overlapping m, C_6H_5), 5.76 (1 H, m, 2,3-$C_4\underline{H}_4Me_2$), 5.48 (1 H, m, 2,3-$C_4\underline{H}_4Me_2$), 3.46 (2 H, sept, C$\underline{H}$Me$_2$, ^{3}J = 6.7 Hz), 1.93 (3 H, d, $C_4H_4\underline{Me}_2$, ^{3}J = 6.2 Hz), 1.80 (15 H, s , C_5Me_5), 1.64 (3 H, d, $C_4H_4\underline{Me}_2$, ^{3}J = 6.0 Hz), 0.97 (12 H, app t, CH$\underline{Me}_2$, ^{3}J = 6.6 Hz, 6.8 Hz), 0.56 (1 H, m, 1,4-$C_4\underline{H}_4Me_2$), 0.35 (1 H, m, 1,4-$C_4\underline{H}_4Me_2$) ppm. (Resonances corresponding to minor isomer: 1.76 (s, C_5Me_5), 1.07 (br s, CH$\underline{Me}_2$) ppm) ^{13}C-{^{1}H} NMR (Toluene-d_8, 233 K): 157.6 (N$\underline{C}$(Ph)N^{i}Pr$_2$), 143.0 (*i*-C_6H_5), 127.9 (*o*- or *m*-C_6H_5), 127.3 (*m*- or *o*-C_6H_5), 127.0 (*p*-C_6H_5), 122.5 (2,3-$\underline{C}_4H_4Me_2$), 122.2 (2,3-$\underline{C}_4H_4Me_2$), 115.8 ($\underline{C}_5Me_5$), 74.1 (1,4-$\underline{C}_4H_4Me_2$), 74.5 (1,4-$\underline{C}_4H_4Me_2$), 46.8 ($\underline{C}$HMe$_2$), 22.7 ($C_4H_4\underline{Me}_2$), 21.8 ($C_4H_4\underline{Me}_2$), 18.0 (CH$\underline{Me}_2$), 17.8 (CH$\underline{Me}_2$), 11.0 ($C_5\underline{Me}_5$) ppm. IR (NaCl plates, Nujol mull, cm^{-1}): 1593 (s), 1302 (m), 1282 (m), 1208 (w), 1158 (m), 1084 (w), 917 (w), 881 (w), 814 (m), 841 (w), 783 (m), 701 (m), 657 (w). Anal. Found (calcd. For $C_{29}H_{44}N_2Ti$): C, 74.40 (74.34); H, 9.30 (9.47); N, 5.85 (5.98) %. EI-MS: *m/z* = 468 (5 %, [*M*]$^{+}$), 386 (20 %, [*M* – $C_4H_4Me_2$]$^{+}$), 223 (35 %, [*M* – $C_4H_4Me_2$ – Ph – 2^{i}Pr]$^{+}$), 100 (60%, [N^{i}Pr$_2$]$^{+}$). Single crystals suitable for X-ray diffraction were grown from a pentane solution at -30 ºC.

Cp*Ti{NC(Ph)N^{i}Pr$_2$}(η-1,4-C$_4$H$_4$Ph$_2$) (7)

To a stirring solution of Cp*Ti{NC(Ph)N^{i}Pr$_2$}Cl$_2$ (**3**) (1.00 g, 2.19 mmol) and 1,4-diphenyl-1,3-butadiene (0.45 g, 2.19 mmol) in toluene (30 mL) at 0 ºC was added dropwise two equivalents of ^{n}BuLi (2.70 mL, 1.6 M in n-hexanes, 4.37 mmol) which resulted in the solution changing colour from orange-red to dark brown. The solution was allowed to warm slowly to RT and was stirred for 20 h after which time the opaque solution had turned dark green. Removal of the volatiles *in vacuo* afforded a dark green-brown solid which was extracted into pentane (3 x 20 mL). After filtration, the solvent was removed *in vacuo* and the resulting dark solid was isolated. Uncomplexed diene was removed by sublimation (100 ºC, 10^{-1} mBar, dry ice/acetone cold finger, 8 h). Subsequent recrystallisation from pentane (15 mL) at -30 ºC allowed isolation of analytically pure **7**. Yield = 0.41 g (39 %). ^{1}H NMR (Toluene-d_8, 299.9 MHz, 253 K): 7.26-6.87 (15 H, series of overlapping m, C_6H_5), 6.25 (1 H, m, 2,3-$C_4\underline{H}_4Ph_2$), 5.87 (1 H, m, 2,3-$C_4\underline{H}_4Ph_2$), 3.72 (2 H, br m, C$\underline{H}$Me$_2$), 2.20 (1 H, m, 1,4-$C_4\underline{H}_4Ph_2$), 1.98 (1 H, m, 1,4-$C_4\underline{H}_4Ph_2$), 1.68 (15 H, s , C_5Me_5), 0.95 (12 H, app t, CH$\underline{Me}_2$, ^{3}J = 5.9 Hz, 6.2 Hz) ppm. (Resonance corresponding to minor isomer: 1.59

(s, C_5Me_5) ppm) ^{13}C-{^1H} NMR (Toluene-d_8, 253 K): 158.8 (N<u>C</u>(Ph)N^{i}Pr$_2$), 145.5 (*i*-C_6H_5 of $C_4H_4Ph_2$), 145.3 (*i*-C_6H_5 of $C_4H_4Ph_2$), 140.5 (*i*-C_6H_5 of NC(Ph)N^{i}Pr$_2$), 127.8 (Ph), 127.7 (Ph), 127.0 (Ph), 125.9 (Ph), 124.8 (Ph), 122.5 (2,3-<u>C</u>$_4H_4Ph_2$), 122.3 (Ph), 122.2 (Ph), 119.4 (2,3-<u>C</u>$_4H_4Ph_2$), 118.2 (<u>C</u>$_5Me_5$), 81.6 (1,4-<u>C</u>$_4H_4Ph_2$), 80.3 (1,4-<u>C</u>$_4H_4Ph_2$), 45.1 (<u>C</u>HMe$_2$), 23.2 (CH<u>Me</u>$_2$), 22.3 (CH<u>Me</u>$_2$), 11.1 (C_5<u>Me</u>$_5$) ppm. IR (NaCl plates, Nujol mull, cm^{-1}): 1568 (s), 1297 (m), 1087 (m), 790 (s), 741 (w), 698 (m). Anal. Found (calcd. For $C_{39}H_{48}N_2Ti$): C, 79.11 (79.03); H, 8.11 (8.16); N, 4.80 (4.73) %. EI-MS: *m/z* = 592 (5 %, $[M]^+$), 386 (20 %, $[M - C_4H_4Ph_2]^+$), 223 (65 %, $[M - C_4H_4Ph_2 - Ph - 2^iPr]^+$), 100 (30 %, $[N^iPr_2]^+$). Single crystals suitable for X-ray diffraction were grown from a pentane solution at -30 ^oC.

CpTi{NC(Ph)N^{i}Pr$_2$}(η-1,4-C$_4$H$_4$Me$_2$) (8)

To a solution of CpTi{NC(Ph)N^{i}Pr$_2$}Cl$_2$ (**2**) (0.50 g, 1.30 mmol) in toluene (30 mL) cooled to 0 ºC was added 2,4-hexadiene (0.97 mL, 8.50 mmol). Immediately two equivalents of ^{n}BuLi (2.1 mL, 1.6 M in n-hexanes, 3.4 mmol) were added dropwise which resulted in the solution changing colour from red to dark brown. The solution was allowed to warm slowly to RT and was subsequently heated at 90 ºC for 8 h after which time it had turned dark green. Removal of the volatiles *in vacuo* afforded a green solid which was extracted into pentane (3 x 20 mL). After filtration through Celite, the solution was concentrated to 20 mL and was cooled to -30 ºC yielding green crystals which were isolated and dried *in vacuo*. Yield = 0.36 g (53 %). ^1H NMR (C_6D_6, 299.9 MHz, 253 K): 7.48-7.14 (5 H, series of overlapping m, C_6H_5), 6.06 (5 H, s, C_5H_5), 5.99 (2 H, d, 2,3-C_4<u>H</u>$_4Me_2$, ^3J = 8.8 Hz), 3.52 (2 H, sept, C<u>H</u>Me$_2$, ^3J = 6.7 Hz), 2.15 (6 H, d, C_4H_4<u>Me</u>$_2$, ^3J = 6.1 Hz), 1.33 (12 H, d, CH<u>Me</u>$_2$, ^3J = 6.7 Hz), 1.02 (2 H, dq, 1,4-C_4<u>H</u>$_4Me_2$, ^3J = 6.1 Hz, 8.8 Hz) ppm. ^{13}C-{^1H} NMR (C_6D_6, 75.4 MHz, 293 K): 159.7 (N<u>C</u>(Ph)N^{i}Pr$_2$), 143.0 (*i*-C_6H_5), 128.1 (*o*- or *m*-C_6H_5), 127.1 (*m*- or *o*-C_6H_5), 126.0 (*p*-C_6H_5), 122.5 (2,3-<u>C</u>$_4H_4Me_2$), 107.0 (<u>C</u>$_5H_5$), 74.4 (1,4-<u>C</u>$_4H_4Me_2$), 48.2 (<u>C</u>HMe$_2$), 21.7 (CH<u>Me</u>$_2$), 18.8 (η-1,4-C$_4$H$_4$<u>Me</u>$_2$) ppm. IR (NaCl plates, Nujol mull, cm^{-1}): 1587 (s), 1313 (s), 1210 (m), 1190 (w), 1070 (w), 1035 (m), 1023 (m), 916 (w), 906 (w), 884 (m), 839 (m), 814 (m), 796 (s), 778 (s), 697 (m), 662 (m), 587 (m). Anal. Found (calcd. For $C_{24}H_{34}N_2Ti$): C, 72.46 (72.45); H, 8.52 (8.60); N, 7.15 (7.03) %. EI-MS: *m/z* = 398 (50 %, $[M]^+$), 316 (90 %, $[M - C_4H_4Me_2]^+$). Single crystals suitable for X-ray diffraction were grown from a pentane solution at -30 ^oC.

Cp*Ti{NC(Ph)N^{i}Pr$_2$}{η^3-CH$_2$C(Me)C(Me)CH$_2$BAr$^F_3$} (9)

To a solution of Cp*Ti{NC(Ph)N^{i}Pr$_2$}(η-2,3-C$_4$H$_4$Me$_2$) (**5)** (0.30 g, 0.64 mmol) in toluene (20 mL) was added BAr$^F_3$ (0.33 g, 0.64 mmol) in toluene (20 mL). After *ca.* 30 s the solution changed to a darker colour. It was stirred for a further 2 h and the volatiles were removed *in vacuo*. The resulting green solid was washed with pentane (3 x 15 mL) and dried *in vacuo*. Yield = 0.51 g (81 %). ^{1}H NMR (Toluene-d_8, 299.9 MHz, 233 K): 7.21-6.62 (5 H, series of overlapping m, C$_6$H$_5$), 4.26 (1 H, sept, C<u>H</u>Me$_2$, ^{3}J = 6.3 Hz), 3.16 (1 H, br m, C<u>H</u>Me$_2$), 1.87 (3 H, s, CH$_2$C(Me)C(<u>Me</u>)CH$_2$BAr$^F_3$), 1.78 (1 H, d, C<u>H</u>$_2$C(Me)C(Me)CH$_2$BAr$^F_3$, ^{2}J = 8.3 Hz), 1.58 (15 H, s , C$_5$Me$_5$), 1.25 (1 H, d, C<u>H</u>$_2$C(Me)C(Me)CH$_2$BAr$^F_3$, ^{2}J = 8.3 Hz), 1.14 (6 H, app t, CH<u>Me</u>$_2$, ^{3}J = 6.5 Hz, 6.3 Hz), 1.11 (3 H, s, CH$_2$C(<u>Me</u>)C(Me)CH$_2$BAr$^F_3$), 0.89 (1 H, app d, CH$_2$BAr$^F_3$, ^{3}J = 10.0 Hz), 0.68 (6 H, app t, CH<u>Me</u>$_2$, ^{3}J = 6.1 Hz, 6.5 Hz), -0.51 (1 H, br m, CH$_2$BAr$^F_3$) ppm. ^{13}C-{^{1}H} NMR (Toluene-d_8, 75.4 MHz, 233 K): 164.5 (N<u>C</u>(Ph)N^{i}Pr$_2$), 148.1 (br, C$_6$F$_5$), 140.6 (CH$_2$<u>C</u>(Me)C(Me)CH$_2$BAr$^F_3$), 139.7 (C$_6$F$_5$), 137.0 (*i*-C$_6$H$_5$), 136.9 (C$_6$F$_5$), 129.2 (*o*- or *m*-C$_6$H$_5$), 128.4 (*m*- or *o*-C$_6$H$_5$), 127.2 (*p*-C$_6$H$_5$), 123.0 (<u>C</u>$_5$Me$_5$), 122.7 (CH$_2$C(Me)<u>C</u>(Me)CH$_2$BAr$^F_3$), 79.8 (<u>C</u>H$_2$C(Me)C(Me)CH$_2$BAr$^F_3$), 47.3 (<u>C</u>HMe$_2$), 46.3 (<u>C</u>HMe$_2$), 23.8 (CH<u>Me</u>$_2$), 23.4 (CH<u>Me</u>$_2$), 21.3 (CH$_2$C(<u>Me</u>)C(Me)CH$_2$BAr$^F_3$), 19.2 (CH$_2$C(Me)C(<u>Me</u>)CH$_2$BAr$^F_3$), 11.7 (C$_5$<u>Me</u>$_5$) ppm (<u>C</u>H$_2$BAr$^F_3$ and *i*-C$_6$F$_5$ were not observed). ^{19}F NMR (Toluene-d_8, 282.2 MHz, 353 K): -130.1 (m, *o*-F, 6 F), -160.8 (m, *p*-F, 3 F), -165.4 (m, *m*-F, 6 F) ppm. ^{11}B NMR (Toluene-d_8, 96.2 MHz, 293 K): -12.0 ppm. IR (NaCl plates, Nujol mull, cm^{-1}): 1515 (s), 1493 (w), 1315 (m), 1278 (w), 1136 (m), 1086 (s), 1026 (w), 978 (s), 762 (w), 688 (w). Anal. Found (calcd. For C$_{47}$H$_{44}$BF$_{15}$N$_2$Ti): C, 57.78 (57.60); H, 4.61 (4.52); N, 2.78 (2.65) %. EI-MS: *m/z* = 512 (100 %, [B(C$_6$F$_5$)$_3$]$^+$), 203 (60 %, [NC(Ph)N^{i}Pr$_2$]$^+$), 135 (50 %, [Cp*]$^+$), 100 (90%, [N^{i}Pr$_2$]$^+$), 77 (60 % [Ph]$^+$). Single crystals suitable for X-ray diffraction were grown from a benzene solution at RT.

Cp*Ti{NC(Ph)N^{i}Pr$_2$}{η^3-Et(CH)$_3$CH$_2$BAr$^F_3$} (10)

To a solution of Cp*Ti{NC(Ph)N^{i}Pr$_2$}(η-1,4-C$_4$H$_4$Me$_2$) (**6**) (0.30 g, 0.64 mmol) in toluene (20 mL) was added BAr$^F_3$ (0.33 g, 0.64 mmol) in toluene (20 mL). After *ca.* 30 seconds the solution changed to a darker green colour. It was stirred for a further 2 h and the solvent was removed *in vacuo*. The resulting green solid was washed with pentane (3 x 15 mL), dried *in vacuo*. Yield = 0.58 g (93 %). ^{1}H NMR (Toluene-d_8,

299.9 MHz, 343 K): 7.08-6.92 (5 H, series of overlapping m, C_6H_5), 5.22 (1 H, dd, EtCHC<u>H</u>, ^3J = 12.0 Hz, 14.1 Hz), 4.24 (1 H, br m, C<u>H</u>$CH_2BAr^F_3$, ^3J = 12.0 Hz), 3.94 (2 H, br m, C<u>H</u>Me_2), 3.00 (1 H, m, C<u>H</u>Et), 1.56 (15 H, s , C_5Me_5), 0.94 (6 H, d, CH<u>Me</u>$_2$, ^3J = 6.9 Hz), 0.85 (6 H, d, CH<u>Me</u>$_2$, ^3J = 6.9 Hz), 0.75 (2 H, br m, <u>CH_2</u>Me), 0.52 (3 H, t, diene CH_2<u>Me</u>, ^3J = 7.4 Hz), 0.20 (1 H, br m, $CH_2BAr^F_3$), 0.03 (1 H, br m, $CH_2BAr^F_3$) ppm. ^{13}C-{^{1}H} NMR (Toluene-d_8, 75.4 MHz, 253 K): 165.0 (N<u>C</u>(Ph)N^{i}Pr$_2$), 148.5 (C_6F_5), 140.6 (*i*-C_6H_5), 139.8 (C_6F_5), 137.0 (C_6F_5),), 131.2 (EtCH<u>C</u>H), 129.2 (*o*- or *m*-C_6H_5), 128.3 (*m*- or *o*-C_6H_5), 128.0 (*p*-C_6H_5), 125.6 (<u>C</u>H$CH_2BAr^F_3$), 123.1 (<u>C_5</u>Me_5), 96.6 (<u>C</u>HEt), 47.1 (<u>C</u>HMe_2), 26.1 (CH<u>Me</u>$_2$), 23.2 (<u>C</u>H_2Me), 18.3 (CH_2<u>Me</u>), 14.5 (CH<u>Me</u>$_2$), 11.9 (C_5<u>Me</u>$_5$) ppm (<u>C</u>$H_2BAr^F_3$ and *i*-C_6F_5 were not observed). ^{19}F NMR (Toluene-d_8, 282.2 MHz, 293 K): -126.9 (m, *o*-F, 6 F), -156.0 (m, *p*-F, 3 F), -160.0 (m, *m*-F, 6 F) ppm. ^{11}B NMR (C_6D_6, 96.2 MHz, 293 K): -12.1 ppm. IR (NaCl plates, Nujol mull, cm^{-1}): 1537 (m), 1512 (m), 1317 (s), 1274 (m), 1210 (w), 1138 (w), 1080 (s), 888 (w), 839 (m), 791 (m), 706 (w), 658 (w). Anal. Found (calcd. For $C_{47}H_{44}BF_{15}N_2Ti$): C, 57.60 (57.60); H, 4.73 (4.52); N, 2.86 (2.65) %. EI-MS: *m/z* = 512 (90 %, $[B(C_6F_5)_3]^+$), 203 (30 %, $[NC(Ph)N^iPr_2]^+$), 100 (50%, $[N^iPr_2]^+$). Single crystals suitable for X-ray diffraction were grown from a pentane solution at -30 ^{o}C.

Cp*Ti{NC(Ph)N^{i}Pr$_2$}{η^3-Me(CH)$_3$CH$_2$BAr$^F_3$} (11)

To a solution of Cp*Ti{NC(Ph)N^{i}Pr$_2$}Cl$_2$ (**3**) (0.81 g, 1.77 mmol) in toluene (30 mL) cooled to 0 ºC was added 1,3-pentadiene (0.90 mL, 8.85 mmol). Immediately two equivalents of ^{n}BuLi (2.20 mL, 1.6 M in n-hexanes, 3.54 mmol) were added dropwise which resulted in the solution changing colour from red to dark green. It was allowed to warm slowly to RT and was subsequently heated at 85 ºC for 8 h. Removal of the volatiles *in vacuo* afforded a green sticky substance which was extracted into pentane (3 x 20 mL) and the solution was filtered. The pentane was then removed *in vacuo* leaving the crude diene complex as a dark green oil. This was extracted into toluene (20 mL) and a solution of BAr^F_3 (0.91 g, 1.77 mmol) in toluene (20 mL) was added. After *ca.* 30 seconds the solution changed to a darker green colour. It was stirred for a further 2 h and the solvent was removed *in vacuo*. The resulting green solid was washed with pentane (3 x 15 mL) and dried *in vacuo*. Yield = 1.23 g (72 %). ^{1}H NMR (Toluene-d_8, 499.9 MHz, 243 K): 7.24-6.67 (5 H, series of overlapping m, C_6H_5), 5.03 (1 H, dd, EtCHC<u>H</u>, ^3J = 12.0 Hz, 14.5 Hz), 3.97 (1 H, br m, C<u>H</u>$CH_2BAr^F_3$), 3.67 (1 H,

br m, C<u>H</u>Me$_2$), 3.00 (1 H, br m, allylic C<u>H</u>Me), 2.98 (1 H, sept, C<u>H</u>Me$_2$, ^{3}J = 6.0 Hz), 1.41 (15 H, s , C$_5$<u>Me</u>$_5$), 1.16 (3H, br d, CH<u>Me</u>$_2$), 0.91 (3 H, d, CH<u>Me</u>$_2$, ^{3}J = 7.5 Hz), 0.65 (3 H, d, CH<u>Me</u>$_2$, ^{3}J = 6.0 Hz), 0.62 (3 H, br m, allylic CH<u>Me</u>), 0.48 (1 H, br m, CH$_2$BAr$^F_3$), 0.30 (3H, br d, CH<u>Me</u>$_2$), -0.51 (1 H, br m, CH$_2$BAr$^F_3$) ppm. ^{13}C-{^{1}H} NMR (Toluene-d_8, 75.4 MHz, 248 K): 165.0 (N<u>C</u>(Ph)N^{i}Pr$_2$), 148.6 (C$_6$F$_5$), 140.6 (*i*-C$_6$H$_5$), 139.7 (C$_6$F$_5$), 136.8 (C$_6$F$_5$), 132.4 (EtCH<u>C</u>H), 128.0 (*o*- or *m*-C$_6$H$_5$), 127.7 (*m*- or *o*-C$_6$H$_5$), 127.2 (*p*-C$_6$H$_5$), 125.6 (<u>C</u>HCH$_2$BAr$^F_3$), 122.9 (<u>C</u>$_5$Me$_5$), 89.3 (allylic <u>C</u>HMe), 47.2 (<u>C</u>HMe$_2$), 34.5 (<u>C</u>HMe$_2$), 22.9 (allylic CH<u>Me</u>), 20.3 (CH<u>Me</u>$_2$), 19.0 (CH<u>Me</u>$_2$), 17.1 (CH<u>Me</u>$_2$), 14.4 (CH<u>Me</u>$_2$), 11.7 (C$_5$<u>Me</u>$_5$) ppm (<u>C</u>H$_2$BAr$^F_3$ and *i*-C$_6$F$_5$ were not observed). ^{19}F NMR (Toluene-d_8, 282.2 MHz, 243 K): -132.0 (m, *o*-F, 6 F), -161.1 (m, *p*-F, 3 F), -165.2 (m, *m*-F, 6 F) ppm. ^{11}B NMR (Toluene-d_8, 96.2 MHz, 293 K): -7.1 ppm. IR (NaCl plates, Nujol mull, cm^{-1}): 1512 (s), 1308 (s), 1274 (m), 1208 (w), 1195 (w), 1139 (m), 1080 (s), 1025 (m), 974 (s), 880 (w), 843 (m), 758 (w), 747 (w), 702 (w), 660 (m). Anal. Found (calcd. For C$_{46}$H$_{42}$BF$_{15}$N$_2$Ti): C, 56.75 (57.16); H, 4.49 (4.38); N, 2.93 (2.90) %. EI-MS: *m/z* = 512 (90 %, [B(C$_6$F$_5$)$_3$]$^+$), 203 (40 %, [NC(Ph)N^{i}Pr$_2$]$^+$), 100 (40%, [N^{i}Pr$_2$]$^+$), 77 (40 % [Ph]$^+$). Single crystals suitable for X-ray diffraction were grown from a benzene solution at RT.

CpTi{NC(Ph)N^{i}Pr$_2$}{η^3-Et(CH)$_3$CH$_2$BAr$^F_3$} (12)

To a solution of CpTi{NC(Ph)N^{i}Pr$_2$}(η-1,4-C$_4$H$_4$Me$_2$) (**8**) (0.40 g, 1.00 mmol) in n-hexanes (20 mL) was added BAr$^F_3$ (0.51 g, 1.00 mmol) in n-hexanes (20 mL). immediately a dark green solid precipitated. The solution was stirred for a further 30 min at RT and stored for a subsequent 16 h at -30 ºC. The precipitate was collected by filtration, washed with pentane (3 x 20 mL) and dried *in vacuo*. Yield = 0.71 g (78 %). ^{1}H NMR (Toluene-d_8, 299.9 MHz, 223 K): 7.14-6.37 (5 H, series of overlapping m, C$_6$H$_5$), 5.37 (5 H, s , C$_5$H$_5$), 4.70 (1 H, dd, EtCHC<u>H</u>, ^{3}J = 11.8 Hz, 14.1 Hz), 3.99 (1 H, m, C<u>H</u>CH$_2$BAr$^F_3$), 3.10 (1 H, br m, C<u>H</u>Et), 3.03 (1 H, br m, C<u>H</u>Me$_2$), 2.61 (1 H, br m, C<u>H</u>Me$_2$), 1.37 (3 H, d, CH<u>Me</u>$_2$, ^{3}J = 6.0 Hz), 1.02 (3 H, d, CH<u>Me</u>$_2$, ^{3}J = 7.2 Hz), 0.92 (2 H, m, <u>CH$_2$</u>Me), 0.57 (3 H, t, CH$_2$<u>Me</u>, ^{3}J = 7.2 Hz), 0.49 (3 H, br d, CH<u>Me</u>$_2$), 0.37 (3 H, br d, CH<u>Me</u>$_2$), -0.07 (1 H, br m, CH$_2$BAr$^F_3$), -1.14 (1 H, br m, CH$_2$BAr$^F_3$) ppm. (Resonance corresponding to minor isomer: 5.58 (5 H, s , C$_5$H$_5$) ppm) ^{13}C-{^{1}H} NMR (Toluene-d_8, 75.4 MHz, 223 K): 163.9 (N<u>C</u>(Ph)N^{i}Pr$_2$), 148.5 (C$_6$F$_5$), 139.7 (C$_6$F$_5$), 137.6 (*i*-C$_6$H$_5$), 136.3 (C$_6$F$_5$), 129.3 (EtCH<u>C</u>H), 128.1 (*o*- or *m*-C$_6$H$_5$), 127.8 (*m*- or *o*-C$_6$H$_5$), 125.6 (*p*-C$_6$H$_5$), 111.3 (<u>C</u>$_5$H$_5$), 106.1 (<u>C</u>HCH$_2$BAr$^F_3$), 96.9 (<u>C</u>HEt),

52.7 (<u>C</u>HMe$_2$), 46.6 (<u>C</u>HMe$_2$), 23.3 (CH<u>Me</u>$_2$), 22.8 (diene <u>C</u>H$_2$Me), 19.3 (CH<u>Me</u>$_2$), 18.9 (CH<u>Me</u>$_2$), 17.6 (diene CH$_2$<u>Me</u>), 14.6 (CH<u>Me</u>$_2$) ppm (<u>C</u>H$_2$BAr$^F{}_3$ and *i*-C$_6$F$_5$ were not observed). ^{19}F NMR (Toluene-d_8, 282.2 MHz, 223 K): -132.4 (m, *o*-F, 6 F), -159.8 (m, *p*-F, 3 F), -164.4 (m, *m*-F, 6 F) ppm. (Resonances corresponding to minor isomer: -132.8 (m, *o*-F, 6 F), -160.3 (m, *p*-F, 3 F), -164.9 (m, *m*-F, 6 F) ppm.) ^{11}B NMR (C$_6$D$_6$, 96.2 MHz, 293 K): -12.4 ppm. IR (NaCl plates, Nujol mull, cm^{-1}): 1419 (s), 1262 (m), 1152 (m), 1078 (s), 1023 (w), 960 (s), 842 (w), 811 (m), 778 (m), 697 (w). Anal. Found (calcd. For C$_{42}$H$_{34}$BF$_{15}$N$_2$Ti): C, 55.60 (55.41); H, 3.59 (3.76); N, 2.97 (3.08) %. EI-MS: *m/z* = 512 (80 %, [B(C$_6$F$_5$)$_3$]$^+$), 167 (100 %, [C$_6$F$_5$]$^+$), 100 (100%, [N^{i}Pr$_2$]$^+$). Single crystals suitable for X-ray diffraction were grown from pentane solution at RT.

Cp*Ti{NC(Ph)N^{i}Pr$_2$}{η^3-CH$_2$C(Me)C(Me)CH$_2$BAr$^F{}_3$}(^{t}BuNC) (13)

To a solution of Cp*Ti{NC(Ph)N^{i}Pr$_2$}{η^3-CH$_2$C(Me)C(Me)CH$_2$BAr$^F{}_3$} (**9**) (0.50 g, 0.51 mmol) in toluene (15 mL) was added ^{t}BuNC (57.7 μL, 0.51 mmol). The solution immediately turned from green to dark red. After addition of n-hexanes (5 mL) the solution was left to stand for 16 h resulting in crystallisation of a red solid which was isolated, washed with n-hexanes (3 x 10 mL) and dried *in vacuo*. Yield = 0.39 g (72 %). Single crystals suitable for X-ray diffraction were grown from a toluene/n-hexanes solution at RT. Compound exists as a mixture of diastereomers in solution at 243 K: **13A** and **13B** in a ratio 60:40.

Common data: ^{19}F NMR (Toluene-d_8, 282.2 MHz, 293 K): -130.1 (br m, *o*-F, 6 F), -164.2 (br m, *p*-F, 3 F), -167.4 (br m, *m*-F, 6 F) ppm. ^{11}B NMR (Toluene-d_8, 96.2 MHz, 293 K): -13.4 ppm. IR (NaCl plates, Nujol mull, cm^{-1}): 2171 (s, υ(C≡N)), 1640 (w), 1617 (w), 1510 (m), 1419 (s), 1153 (s), 1075 (s), 1033 (w), 971 (s), 888 (m), 843 (m), 789 (w). Anal. Found (calcd. For C$_{52}$H$_{53}$BF$_{15}$N$_3$Ti): C, 58.54 (58.72); H, 4.92 (5.02); N, 3.85 (3.95) %. EI-MS: *m/z* = 512 (100 %, [B(C$_6$F$_5$)$_3$]$^+$), 203 (100 %, [NC(Ph)N^{i}Pr$_2$]$^+$), 100 (100 %, [N^{i}Pr$_2$]$^+$).

Data for **13A**: ^{1}H NMR (CD$_2$Cl$_2$, 299.9 MHz, 243 K): 7.42-6.88 (5 H, series of overlapping m, C$_6$H$_5$), 4.68 (1 H, sept, C<u>H</u>Me$_2$ *cis* to C$_6$H$_5$, ^{3}J = 6.9 Hz), 3.46 (1 H, br m, C<u>H</u>Me$_2$ *trans* to C$_6$H$_5$), 2.36 (1H, app d, CH$_2$BAr$^F{}_3$, ^{2}J = 9.8 Hz), 2.05 (3 H, s, CH$_2$C(Me)C(<u>Me</u>)CH$_2$BAr$^F{}_3$), 1.91 (1 H, d, C<u>H</u>$_2$C(Me)C(Me)CH$_2$BAr$^F{}_3$, ^{2}J = 7.2 Hz), 1.71 (9 H, s, ^{t}BuNC), 1.55 (15 H, s, C$_5$Me$_5$), 1.48 (3 H, s,

$CH_2C(\underline{Me})C(Me)CH_2BAr^F{}_3$), 1.20 (3 H, d, $CH\underline{Me}_2$ *trans* to C_6H_5, ^3J = 6.5 Hz), 1.12 (3 H, d, $CH\underline{Me}_2$ *trans* to C_6H_5, ^3J = 6.5 Hz), 1.02 (3 H, d, $CH\underline{Me}_2$ *cis* to C_6H_5, ^3J = 6.9 Hz), 0.91 (3 H, d, $CH\underline{Me}_2$ *cis* to C_6H_5, ^3J = 6.9 Hz), 0.87 (1 H, $C\underline{H}_2C(Me)C(Me)CH_2BAr^F{}_3$ (overlapping with $CH\underline{Me}_2$ of **13B**)), -0.27 (1H, app d, ^2J = 9.8 Hz, $CH_2BAr^F{}_3$) ppm. ^{13}C-{^1H} NMR (CD_2Cl_2, 75.4 MHz, 293 K): 160.9 ($N\underline{C}(Ph)N^iPr_2$), 147.8 ($C_6F_5$), 139.5 ($CH_2\underline{C}(Me)C(Me)CH_2BAr^F{}_3$), 138.7 ($C_6F_5$), 136.2 (*i*-$C_6H_5$), 135.5 ($C_6F_5$), 129.1 (*o*- or *m*-$C_6H_5$), 128.3 (*m*- or *o*-$C_6H_5$), 126.4 (*p*-$C_6H_5$), 123.9 ($CH_2C(Me)\underline{C}(Me)CH_2BAr^F{}_3$), 118.9 ($\underline{C}_5Me_5$), 74.3 ($\underline{C}H_2C(Me)C(Me)CH_2BAr^F{}_3$), 58.6 (^{t}BuN$\underline{C}$), 53.3 ($\underline{C}HMe_2$ *trans* to C_6H_5), 47.0 ($\underline{C}HMe_2$ *cis* to C_6H_5), 30.3 ($^t\underline{Bu}$NC), 25.5 ($CH_2C(\underline{Me})C(Me)CH_2BAr^F{}_3$), 22.3 ($CH_2C(Me)C(\underline{Me})CH_2BAr^F{}_3$), 21.7 ($CH\underline{Me}_2$ *trans* to C_6H_5), 21.5 ($CH\underline{Me}_2$ *trans* to C_6H_5), 21.4 ($CH\underline{Me}_2$ *cis* to C_6H_5), 19.9 ($CH\underline{Me}_2$ *cis* to C_6H_5), 11.9 ($C_5\underline{Me}_5$) ppm ($\underline{C}H_2BAr^F{}_3$ and *i*-C_6F_5 were not observed).

Data for **13B**: ^1H NMR (CD_2Cl_2, 299.9 MHz, 243 K): 7.42-6.88 (5 H, series of overlapping m, C_6H_5), 3.39 (2 H, sept, $C\underline{H}Me_2$, ^3J = 7.1 Hz), 2.17 (1 H, d, $C\underline{H}_2C(Me)C(Me)CH_2BAr^F{}_3$, ^2J = 5.5 Hz), 2.01 (1H, app d, $CH_2BAr^F{}_3$, ^2J = 11.7 Hz), 1.86 (3 H, s, $CH_2C(Me)C(\underline{Me})CH_2BAr^F{}_3$), 1.83 (15 H, s , C_5Me_5), 1.68 (3 H, s, $CH_2C(\underline{Me})C(Me)CH_2BAr^F{}_3$), 1.30 (9 H, s, ^{t}BuNC), 1.23 (1 H, $\underline{CH}_2C(Me)$–$C(Me)CH_2BAr^F{}_3$ (overlapping with $CH\underline{Me}_2$ of **13A**)), 0.85 (6 H, d, $CH\underline{Me}_2$, ^3J = 7.5 Hz), 0.81 (6 H, d, $CH\underline{Me}_2$, ^3J = 6.6 Hz), -0.38 (1H, app d, ^2J = 11.7 Hz, $CH_2BAr^F{}_3$) ppm. ^{13}C-{^1H} NMR (CD_2Cl_2, 75.4 MHz, 293 K): 164.0 ($N\underline{C}(Ph)N^iPr_2$), 138.9 ($CH_2\underline{C}(Me)C(Me)CH_2BAr^F{}_3$), 136.3 (*i*-$C_6H_5$), 129.2 (*o*- or *m*-$C_6H_5$), 129.0 (*o*- or *m*-$C_6H_5$), 127.9 ($CH_2C(Me)\underline{C}(Me)CH_2BAr^F{}_3$), 125.4 (*p*-$C_6H_5$), 118.4 ($\underline{C}_5Me_5$), 70.8 ($\underline{C}H_2C(Me)C(Me)CH_2BAr^F{}_3$), 57.8 (^{t}BuN$\underline{C}$), 46.9 ($\underline{C}HMe_2$), 29.6 ($^t\underline{Bu}$NC), 24.6 ($CH_2C(\underline{Me})C(Me)CH_2BAr^F{}_3$), 24.0 ($CH\underline{Me}_2$), 22.2 ($CH_2C(Me)C(\underline{Me})CH_2BAr^F{}_3$), 12.3 ($C_5\underline{Me}_5$) ppm ($\underline{C}H_2BAr^F{}_3$ and C_6F_5 resonances were not observed).

Cp*Ti{NC(Ph)N^{i}Pr$_2$}{η^3-Et(CH)$_3$CH$_2$BAr$^F{}_3$}(^{t}BuNC) (14)

To a solution of Cp*Ti{NC(Ph)N^{i}Pr$_2$}{η^3-Et(CH)$_3$CH$_2$BAr$^F{}_3$} (**10**) (0.50 g, 0.51 mmol) in toluene (15 mL) was added ^{t}BuNC (57.7 µL, 0.51 mmol). The solution immediately turned from green to dark red and on standing at RT for 3 h, dark red crystals of **14** had grown. These were isolated, washed with n-hexanes (3 x 10 mL), and dried *in vacuo*. Yield = 0.42 g (77 %). ^1H NMR (CD_2Cl_2, 499.9 MHz, 293 K): 7.35-6.97 (5 H, series of m, C_6H_5), 4.44 (1 H, dd, EtCHC$\underline{H}$, ^3J = 13.9 Hz, 15.8 Hz),

3.53 (2 H, br m, C<u>H</u>Me$_2$), 3.08 (1 H, app d, CH$_2$BAr$^F_3$, ^{2}J = 10.3 Hz), 2.39 (1 H, m, C<u>H</u>CH$_2$BAr$^F_3$), 1.91 (1 H, app d, CH$_2$BAr$^F_3$, ^{2}J = 10.3 Hz), 1.78 (1 H, m, C<u>H</u>Et), 1.69 (15 H, s, C$_5$Me$_5$), 1.60 (9 H, s, ^{t}BuNC), 1.46 (2 H, br m, <u>CH$_2$</u>Me), 1.27 (6 H, br d, CH<u>Me$_2$</u>), 0.97 (6 H, d, CH<u>Me$_2$</u>, ^{3}J = 7.8 Hz), 0.81 (3 H, t, CH$_2$<u>Me</u>, ^{3}J = 8.2 Hz) ppm. ^{13}C-{^{1}H} NMR (CD_2Cl_2, 125.8 MHz, 293 K): 164.0 (N<u>C</u>(Ph)N^{i}Pr$_2$), 148.8 (C_6F_5), 138.9 (^{t}BuN<u>C</u>), 138.7 (C_6F_5), 138.6 (*i*-C_6H_5), 136.9 (C_6F_5), 129.6 (*o*- or *m*-C_6H_5), 129.1 (*m*- or *o*-C_6H_5), 128.8 (*p*-C_6H_5), 125.8 (<u>C</u>HCH$_2$BAr$^F_3$), 124.8 (EtCH<u>C</u>H), 118.9 (<u>C</u>$_5$Me$_5$), 92.2 (<u>C</u>HEt), 48.1 (<u>C</u>HMe$_2$), 33.0 (<u>C</u>H$_2$BAr$^F_3$), 31.5 (<u>C</u>H$_2$Me), 30.5 (^{t}<u>Bu</u>NC), 21.7 (CH<u>Me$_2$</u>), 21.3 (CH<u>Me$_2$</u>), 19.1 (diene CH$_2$<u>Me</u>), 12.0 (C$_5$<u>Me$_5$</u>) ppm (*i*-C_6F_5 was not observed). ^{19}F NMR (Toluene-d_8, 282.2 MHz, 293 K): -131.3 (m, *o*-F, 6 F), -162.8 (m, *p*-F, 3 F), -166.3 (m, *m*-F, 6 F) ppm. ^{11}B NMR (Toluene-d_8, 96.2 MHz, 293 K): -12.3 ppm. IR (NaCl plates, Nujol mull, cm^{-1}): 2177 (s, υ(C≡N)), 1509 (s), 1331 (s), 1269 (s), 1194 (m), 1158 (m), 1136 (m), 1076 (s), 1026 (w), 918 (m), 885 (w), 789 (w), 758 (w), 726 (s), 571 (m). Anal. Found (calcd. For $C_{52}H_{53}BF_{15}N_3Ti$): C, 58.56 (58.72); H, 5.16 (5.02); N, 3.73 (3.95) %. EI-MS: *m/z* = 512 (100 %, [B(C$_6$F$_5$)$_3$]$^+$), 494 (10 %, [*M* – B(C$_6$F$_5$)$_3$ – tBu]$^+$), 83 (80%, [^{t}BuNC]$^+$), 57 (100 %, [N^{i}Pr]$^+$). Single crystals suitable for X-ray diffraction were grown from a toluene/n-hexanes solution at RT.

Cp*Ti{NC(NMe$_2$)$_2$}Cl$_2$ (15)

This compound was prepared by adaptation of a patented procedure.[10] To a stirring toluene (50 mL) solution of HNC(NMe$_2$)$_2$ (3.50 mL, 27.6 mmol) cooled to -78 ^{o}C was added dropwise ^{n}BuLi (17.3 mL, 1.6 M in n-hexanes, 27.7 mmol). The resulting solution was warmed slowly to RT and stirred for 0.5 h before being added dropwise to a toluene (50 mL) solution of Cp*TiCl$_3$ (8.00 g, 27.6 mmol). The orange-red solution was stirred for 16 h after which time the volatiles were removed *in vacuo*. The resulting orange solid was washed with pentane (3 x 20 mL) and extracted into dichloromethane (5 x 20 mL). Concentration of the solution to *ca*. 20 mL and storage at -30 ^{o}C for 24 h resulted in crystallisation of the desired compound which was subsequently isolated and dried *in vacuo*. Yield = 8.77 g (87 %). ^{1}H NMR (C_6D_6, 299.9 MHz, 293 K): 2.34 (12H, s, NMe$_2$), 2.09 (15H, s, C$_5$Me$_5$) ppm. ^{13}C-{^{1}H} NMR (C_6D_6, 75.4 MHz, 293 K): 159.6 (N<u>C</u>(NMe$_2$)$_2$), 125.7 (<u>C</u>$_5$Me$_5$), 40.0 (NMe$_2$), 13.1 (C$_5$<u>Me$_5$</u>) ppm. EI-MS: *m/z* = 367 (5 %, [*M*]$^+$), 253 (90 %, [*M* –{NC(NMe$_2$)$_2$}]$^+$, 135 (100 % , [Cp*]$^+$), 115 (70 %, [HN<u>C</u>(NMe$_2$)$_2$]$^+$). Anal. Found (calcd. For

$C_{15}H_{27}Cl_2N_3Ti$): C, 48.80 (48.93); H, 7.54 (7.39); N 11.28 (11.41). Single crystals suitable for X-ray diffraction were grown from a benzene solution at RT.

Cp*Ti{NC(NMe$_2$)$_2$}(η-1,4-C$_4$H$_4$Me$_2$) (16)

To a stirring solution of Cp*Ti{NC{NC(NMe$_2$)$_2$}Cl$_2$ (**15**) (0.70 g, 1.90 mmol) and 2,4-hexadiene (2.17 mL, 19.0 mmol) in toluene (15 mL) at 0 ºC was added dropwise two equivalents of ^{n}BuLi (2.38 mL, 1.6 M in n-hexanes, 3.80 mmol) which resulted in the solution turning a darker colour. The solution was allowed to warm slowly to RT and was stirred for 20 h at RT after which time the solution had turned dark green. Removal of the volatiles *in vacuo* afforded a green solid which was extracted into pentane (5 x 15 mL). After filtration, the pentane solution was concentrated to 10 mL and was cooled to -80 ºC yielding green crystals which were isolated and dried *in vacuo.* Yield = 0.31 g (43 %). ^{1}H NMR (C$_6$D$_6$, 299.9 MHz, 293 K): 5.32 (2 H, d, 2,3-C$_4$H$_4$Me$_2$, ^{3}J = 8.8 Hz), 2.24 (12 H, s, NMe$_2$), 1.93 (15 H, s , C$_5$Me$_5$), 1.87 (6 H, d, C$_4$H$_4$Me$_2$, ^{3}J = 5.8 Hz), 0.49 (2 H, dq, 1,4-C$_4$H$_4$Me$_2$, ^{3}J = 5.8 Hz, 8.8 Hz) ppm. (Resonances corresponding to minor isomer: 4.22 (2 H, d, 2,3-C$_4$H$_4$Me$_2$, ^{3}J = 10.2 Hz), 2.56 (12 H, s, NMe$_2$), 2.06 (6 H, d, C$_4$H$_4$Me$_2$, ^{3}J = 5.9 Hz), 1.79 (15 H, s , C$_5$Me$_5$), 1.57 (2 H, br m, 1,4-C$_4$H$_4$Me$_2$) ppm) ^{13}C-{^{1}H} NMR (C$_6$D$_6$, 293 K): 156.3 (NC(NMe$_2$)$_2$), 122.7 (2,3-C$_4$H$_4$Me$_2$), 115.5 (C$_5$Me$_5$), 73.1 (1,4-C$_4$H$_4$Me$_2$), 39.9 (NMe$_2$), 19.1 (C$_4$H$_4$Me$_2$), 11.4 (C$_5$Me$_5$) ppm. (Resonances corresponding to minor isomer: 156.9 (NC(NMe$_2$)$_2$), 114.5 (C$_5$Me$_5$), 111.9 (2,3-C$_4$H$_4$Me$_2$), 70.3 (1,4-C$_4$H$_4$Me$_2$), 40.1 (NMe$_2$), 18.5 (C$_4$H$_4$Me$_2$), 12.1 (C$_5$Me$_5$) ppm) IR (NaCl plates, Nujol mull, cm^{-1}): 1617 (s), 1559 (m), 1421 (s), 1334 (m), 1143 (m), 1109 (s), 1054 (w), 1016 (m), 909 (w), 885 (w), 831 (w), 814 (w), 571 (m). Anal. Found (calcd. For $C_{29}H_{44}N_2Ti$): C, 66.28 (66.48); H, 9.68 (9.83); N, 10.85 (11.08) %. EI-MS: *m/z* = 379 (2 %, [*M*]$^+$), 115 (30 %, [HNC(NMe$_2$)$_2$]$^+$), 82 (20 %, [C$_4$H$_4$Me$_2$]$^+$), 71 (100 %, [HNC(NMe$_2$)]$^+$). Single crystals suitable for X-ray diffraction were grown from a benzene solution at RT.

Cp*Ti{NC(NMe$_2$}{η^3-Et(CH)$_3$CH$_2$BAr$^F_3$} (17)

To a solution of Cp*Ti{NC(Ph)N^{i}Pr$_2$}(η-1,4-C$_4$H$_4$Me$_2$) (**16**) (0.30 g, 0.79 mmol) in toluene (20 mL) was added BAr$^F_3$ (0.40 g, 0.79 mmol) in toluene (20 mL) resulting in a colour change from green to brown. It was stirred for a further 2 h and the volatiles were removed *in vacuo*. The resulting green solid was washed with pentane (3 x 15 mL) and dried *in vacuo*. Yield = 0.55 g (78 %). ^{1}H NMR (C$_6$D$_6$, 299.9 MHz, 293 K):

5.35 (1 H, dd, EtCHC<u>H</u>, ^{3}J = 11.8 Hz, 13.5 Hz), 4.07 (1 H, m, C<u>H</u>CH$_2$BAr$^F_3$), 3.34 (1 H, m, C<u>H</u>Et), 2.33 (6 H, s, N<u>Me</u>$_2$), 2.15 (6 H, s, NMe$_2$), 1.49 (15 H, s , C$_5$<u>Me</u>$_5$), 1.36 (2 H, br m, diene <u>CH$_2$</u>CH$_3$), 1.25 (1 H, br m, CH$_2$BAr$^F_3$), 0.87 (3 H, t, diene CH$_2$<u>Me</u>, ^{3}J = 8.0 Hz), -0.48 (1 H, br m, CH$_2$BAr$^F_3$) ppm. ^{13}C-{^{1}H} NMR (C$_6$D$_6$, 75.4 MHz, 293 K): 162.1 (N<u>C</u>(NMe$_2$)$_2$), 148.9 (C$_6$F$_5$), 138.2 (C$_6$F$_5$), 134.6 (C$_6$F$_5$), 133.8 (EtCH<u>C</u>H), 123.1 (<u>C</u>$_5$Me$_5$), 113.6 (<u>C</u>HCH$_2$BAr$^F_3$), 93.2 (<u>C</u>HEt), 39.4 (N<u>Me</u>$_2$), 22.7 (<u>C</u>H$_2$Me), 18.3 (CH$_2$<u>Me</u>), 12.1 (C$_5$<u>Me</u>$_5$) ppm (<u>C</u>H$_2$BAr$^F_3$ and *i*-C$_6$F$_5$ were not observed). ^{19}F NMR (C$_6$D$_6$, 282.2 MHz, 293 K): -132.1 (m, *o*-F, 6 F), -160.8 (m, *p*-F, 3 F), -165.0 (m, *m*-F, 6 F) ppm. ^{11}B NMR (C$_6$D$_6$, 96.2 MHz, 293 K): -12.7 ppm. IR (NaCl plates, Nujol mull, cm^{-1}): 1641 (w), 1534 (w), 1512 (m), 1260 (s), 1085 (s), 1019 (s), 979 (m), 798 (s). Anal. Found (calcd. For C$_{47}$H$_{44}$BF$_{15}$N$_2$Ti): C, 52.40 (52.55); H, 4.04 (4.18); N, 4.85 (4.71) %. EI-MS: *m/z* = 512 (1 %, [B(C$_6$F$_5$)$_3$]$^+$), 389 (70 %, [*M* – 3C$_6$F$_5$ – H]$^+$, 235 (40 %, [Cp*]$^+$). Single crystals suitable for X-ray diffraction were grown from a benzene solution at RT.

5.4 Experimental details for Chapter Three

Cp*Zr{NC(Ph)N^{i}Pr$_2$}Cl$_2$ (18)

To a stirring toluene (25 mL) solution of HNC(Ph)N^{i}Pr$_2$ (**1**) (2.52 g, 12.4 mmol) was added dropwise at RT MeMgCl (4.10 mL, 3.0 M in THF, 12.4 mmol). The resulting colourless solution was stirred for 10 min and added dropwise to a toluene (20 mL) suspension of Cp*ZrCl$_3$ (4.11 g, 12.4 mmol). After stirring for 16 h, the volatiles were removed *in vacuo* and the resulting yellow-white solid was redissolved in toluene and separated from the insoluble MgCl$_2$ by filtration. The volatiles were then removed *in vacuo* and the solid was washed with pentane (3 x 10 mL) and dried *in vacuo*. Yield = 5.14 g (83 %). ^{1}H NMR (Toluene-d_8, 299.9 MHz, 273 K): 7.40-6.90 (5 H, series of overlapping m, C$_6$H$_5$), 3.50 (1 H, sept, C<u>H</u>Me$_2$ *cis* to C$_6$H$_5$, ^{3}J = 6.6 Hz), 2.93 (1 H, br m, C<u>H</u>Me$_2$ *trans* to C$_6$H$_5$), 1.88 (15 H, s , C$_5$Me$_5$), 1.53 (6 H, d, CH<u>Me</u>$_2$ *trans* to C$_6$H$_5$, ^{3}J = 6.7 Hz), 0.55 (6 H, d, CH<u>Me</u>$_2$ *cis* to C$_6$H$_5$, ^{3}J = 6.6 Hz) ppm. ^{13}C-{^{1}H} NMR (Toluene-d_8, 75.4 MHz, 253 K): 164.4 (N<u>C</u>(Ph)N^{i}Pr$_2$), 141.9 (*i*-C$_6$H$_5$), 129.6 (*o*- or *m*-C$_6$H$_5$), 129.3 (*p*-C$_6$H$_5$), 125.6 (*m*- or *o*-C$_6$H$_5$), 122.8 (<u>C</u>$_5$Me$_5$), 53.0 (<u>C</u>HMe$_2$ *cis* to C$_6$H$_5$), 47.6 (<u>C</u>HMe$_2$ *trans* to C$_6$H$_5$), 20.6 (CH<u>Me</u>$_2$), 11.9 (C$_5$<u>Me</u>$_5$) ppm. IR (NaCl plates, Nujol mull, cm^{-1}): 1653 (m), 1636 (w), 1540 (s), 1339 (s), 1184 (w), 1150 (m), 915 (w), 887 (m), 839 (m), 783 (s), 694 (m), 662 (m). Anal. Found (calcd. For C$_{23}$H$_{34}$Cl$_2$N$_2$Zr): C, 55.27 (55.18); H, 6.77 (6.84); N, 5.52 (5.60) %. EI-MS: *m/z* = 498

(2 %, $[M]^+$), 295 (70 %, $[M - NC(Ph)N^iPr_2]^+$), 203 (45 %, $[NC(Ph)N^iPr_2]^+$), 135 (60 %, $[Cp^*]^+$), 77 (100 %, $[Ph]^+$). Single crystals suitable for X-ray diffraction were grown from a toluene solution at RT.

$Cp^*Hf\{NC(Ph)N^iPr_2\}Cl_2$ (19)

To a stirring toluene (25 mL) solution of $HNC(Ph)N^iPr_2$ (**1**) (2.07 g, 10.1 mmol) was added dropwise at RT MeMgCl (3.35 mL, 3.0 M in THF, 10.1 mmol). The resulting colourless solution was stirred for 10 min and added dropwise to a toluene (20 mL) suspension of Cp^*HfCl_3 (4.25 g, 10.1 mmol). After stirring the reaction mixture for 24 h, the volatiles were removed *in vacuo* and the resulting yellow-white solid was washed with pentane (3 x 10 mL) and extracted into hot (ca. 60 ºC) n-hexanes (4 x 15 mL). The product crystallised on slow cooling of the solution giving the desired complex as a colourless solid which was isolated and dried *in vacuo*. Yield = 4.56 g (77 %). ^{1}H NMR (Toluene-d_8, 299.9 MHz, 253 K): 7.30-6.99 (5 H, series of overlapping m, C_6H_5), 3.56 (1 H, br sept, C<u>H</u>Me_2 *cis* to C_6H_5, $^3J = 6.5$ Hz), 2.98 (1 H, br m, C<u>H</u>Me_2 *trans* to C_6H_5), 1.93 (15 H, s , C_5Me_5), 1.55 (6 H, d, CH<u>Me</u>$_2$ *trans* to C_6H_5, $^3J = 6.6$ Hz), 0.60 (6 H, d, CH<u>Me</u>$_2$ *cis* to C_6H_5, $^3J = 6.5$ Hz) ppm. ^{13}C NMR (Toluene-d_8, 75.4 MHz, 253 K): 166.3 (N<u>C</u>(Ph)N^iPr_2), 142.7 (*i*-C_6H_5), 128.4 (*o*- or *m*-C_6H_5), 128.0 (*m*- or *o*-C_6H_5), 126.1 (*p*-C_6H_5), 120.7 (<u>C</u>$_5Me_5$), 52.4 (<u>C</u>HMe_2 *cis* to C_6H_5), 46.7 (<u>C</u>HMe_2 *trans* to C_6H_5), 19.9 (CH<u>Me</u>$_2$), 11.3 (C_5<u>Me</u>$_5$) ppm. IR (NaCl plates, Nujol mull, cm^{-1}): 1556 (s), 1338 (s), 1260 (m), 1211 (w), 1185 (m), 1151 (s), 1133 (w), 1098 (w), 1033 (s), 1024 (s), 915 (w), 888 (m), 840 (m), 785 (s), 695 (s), 662 (m). Anal. Found (calcd. For $C_{23}H_{34}Cl_2HfN_2$): C, 47.07 (46.99); H, 5.98 (5.83); N, 4.59 (4.76) %. EI-MS: *m/z* = 545 (50 %, $[M - {}^iPr]^+$), 488 (50 %, $[M - N^iPr_2]^+$), 385 (100 %, $[M - NC(Ph)N^iPr_2]^+$). Single crystals suitable for X-ray diffraction were grown from an n-hexanes solution at RT.

$CpTi\{NC(Ph)N^iPr_2\}Me_2$ (20)

To a stirring toluene (15 mL) solution of $CpTi\{NC(Ph)N^iPr_2\}Cl_2$ (**3**) (0.79 g, 2.04 mmol) was added dropwise MeLi (2.55 mL, 1.6 M in Et_2O, 4.08 mmol) and the resulting solution was stirred for 16 h. The volatiles were then removed *in vacuo* and the yellow solid was extracted into pentane (40 mL). Concentration of the solution to *ca.* 15 mL and subsequent storage at -30 °C for 2 d resulted in crystallisation of the desired product as yellow crystals which were isolated and dried *in vacuo*. Yield =

0.40 g (57 %). ^{1}H NMR (Toluene-d_8, 299.9 MHz, 233 K): 7.01-6.84 (5 H, series of overlapping m, C_6H_5), 5.80 (5 H, s , C_5H_5), 3.42 (1 H, sept, C<u>H</u>Me$_2$ *cis* to C_6H_5, ^{3}J = 6.5 Hz), 2.97 (1 H, br m, C<u>H</u>Me$_2$ *trans* to C_6H_5), 1.85 (6 H, d, CH<u>Me</u>$_2$ *trans* to C_6H_5, ^{3}J = 6.7 Hz), 0.75 (6 H, s, TiMe), 0.61 (6 H, d, CH<u>Me</u>$_2$ *cis* to C_6H_5, ^{3}J = 6.5 Hz) ppm. ^{13}C-{^{1}H} NMR (Toluene-d_8, 233 K): 162.7 (N<u>C</u>(Ph)N^{i}Pr$_2$), 141.8 (*i*-C_6H_5), 128.3 (*o*- or *m*-C_6H_5), 127.6 (*m*- or *o*-C_6H_5), 125.0 (*p*-C_6H_5), 110.9 (C_5H_5), 51.7 (<u>C</u>HMe$_2$ *cis* to C_6H_5), 47.0 (<u>C</u>HMe$_2$ *trans* to C_6H_5), 45.3 (TiMe), 19.9 (CH<u>Me</u>$_2$ *trans* to C_6H_5), 19.7 (CH<u>Me</u>$_2$ *cis* to C_6H_5) ppm. IR (NaCl plates, Nujol mull, cm^{-1}): 1557 (s), 1331 (m), 1213 (w), 1187 (m), 1100 (w), 1070 (w), 1035 (m), 1016 (m), 919 (m), 890 (s), 842 (w), 800 (s), 782 (s), 698 (m), 699 (w), 584 (s). Anal. Found (calcd. For $C_{20}H_{30}N_2Ti$): C, 68.99 (69.36); H, 8.58 (8.73); N, 8.17 (8.09) %. EI-MS: *m/z* = 316 (20 %, [*M* – 2Me]$^{+}$), 273 (30 %, [*M* – 2Me – ^{i}Pr]$^{+}$), 216 (40 %, [*M* – 2Me – N^{i}Pr$_2$]$^{+}$), 113 (100 %, [CpTi]$^{+}$).

Cp*Zr{NC(Ph)N^{i}Pr$_2$}Me$_2$ (21)

To a stirring toluene (25 mL) solution of Cp*Zr{NC(Ph)N^{i}Pr$_2$}Cl$_2$ (**18**) (0.50 g, 1.00 mmol) was added dropwise MeMgCl (0.70 mL, 3.0 M in THF, 2.00 mmol) and the resulting solution was stirred for 16 h. The volatiles were then removed *in vacuo* and the oily solid was extracted into pentane (40 mL). The product was isolated as a colourless solid following filtration and removal of the pentane *in vacuo*. Yield = 0.14 g (40 %). ^{1}H NMR (Toluene-d_8, 299.9 MHz, 233 K): 7.19-6.98 (5 H, series of overlapping m, C_6H_5), 3.56 (1 H, sept, C<u>H</u>Me$_2$ *cis* to C_6H_5, ^{3}J = 6.3 Hz), 2.84 (1 H, br sept, C<u>H</u>Me$_2$ *trans* to C_6H_5, ^{3}J = 6.6 Hz), 1.88 (15 H, s , C_5Me_5), 1.72 (6 H, d, CH<u>Me</u>$_2$ *trans* to C_6H_5, ^{3}J = 6.6 Hz), 0.60 (6 H, d, CH<u>Me</u>$_2$ *cis* to C_6H_5, ^{3}J = 6.3 Hz), 0.29 (6 H, s, ZrMe) ppm. ^{13}C-{^{1}H} NMR (Toluene-d_8, 75.4 MHz, 233 K): 161.1 (N<u>C</u>(Ph)N^{i}Pr$_2$), 143.6 (*i*-C_6H_5), 129.4 (*o*- or *m*-C_6H_5), 127.2 (*m*- or *o*-C_6H_5), 125.8 (*p*-C_6H_5), 117.0 (<u>C</u>$_5$Me$_5$), 51.9 (<u>C</u>HMe$_2$ *cis* to C_6H_5), 46.3 (<u>C</u>HMe$_2$ *trans* to C_6H_5), 35.6 (ZrMe), 19.7 (CH<u>Me</u>$_2$), 11.1 (C_5<u>Me</u>$_5$) ppm. IR (NaCl plates, Nujol mull, cm^{-1}): 1568 (s), 1490 (w), 1372 (s), 1323 (s), 1116 (w), 1034 (m), 883 (m), 781 (s), 702 (w), 693 (w), 660 (m). Anal. Found (calcd. For $C_{25}H_{40}N_2Zr$): C, 65.20 (65.30); H, 8.80 (8.77); N, 6.02 (6.09) %. EI-MS: *m/z* = 458 (20 %, [*M*]$^{+}$), 443 (20 %, [*M* – Me]$^{+}$), 428 (10 %, [*M* – 2Me]$^{+}$), 225 (45 %, [Cp*Zr]$^{+}$), 223 (90 %, [*M* – Cp* - N^{i}Pr$_2$]$^{+}$). Single crystals suitable for X-ray diffraction were grown from a pentane solution at RT.

Cp*Hf{NC(Ph)N^{i}Pr$_2$}Me$_2$ (22)

To a stirring toluene (25 mL) solution of Cp*Hf{NC(Ph)N^{i}Pr$_2$}Cl$_2$ (**19**) (0.50 g, 0.85 mmol) was added dropwise MeLi (1.10 mL, 1.6 M in Et$_2$O, 1.70 mmol) and the resulting solution was stirred for 16 h. The volatiles were then removed *in vacuo* and the oily solid was extracted into n-hexanes (40 mL). The product was isolated as a yellow solid following removal of the volatiles *in vacuo*. Yield = 0.23 g (49 %). ^{1}H NMR (Toluene-d_8, 299.9 MHz, 223 K): 7.21-6.97 (5 H, series of overlapping m, C$_6$H$_5$), 3.59 (1 H, sept, C<u>H</u>Me$_2$ *cis* to C$_6$H$_5$, ^{3}J = 6.2 Hz), 2.87 (1 H, br sept, C<u>H</u>Me$_2$ *trans* to C$_6$H$_5$, ^{3}J = 6.5 Hz), 1.90 (15 H, s , C$_5$Me$_5$), 1.68 (6 H, d, CH<u>Me</u>$_2$ *trans* to C$_6$H$_5$, ^{3}J = 6.5 Hz), 0.62 (6 H, d, CH<u>Me</u>$_2$ *cis* to C$_6$H$_5$, ^{3}J = 6.2 Hz), 0.10 (6 H, s, HfMe) ppm. ^{13}C-{^{1}H} NMR (Toluene-d_8, 75.4 MHz, 233 K): 163.7 (N<u>C</u>(Ph)N^{i}Pr$_2$), 144.6 (*i*-C$_6$H$_5$), 128.6 (*o*- or *m*-C$_6$H$_5$), 127.3 (*m*- or *o*-C$_6$H$_5$), 125.6 (*p*-C$_6$H$_5$), (116.4 (<u>C</u>$_5$Me$_5$), 51.8 (<u>C</u>HMe$_2$ *cis* to C$_6$H$_5$), 46.1 (<u>C</u>HMe$_2$ *trans* to C$_6$H$_5$), 45.2 (HfMe), 19.8 (CH<u>Me</u>$_2$), 10.9 (C$_5$<u>Me</u>$_5$) ppm. IR (NaCl plates, Nujol mull, cm^{-1}): 1585 (s), 1325 (s), 1261 (m), 1211 (w), 1187 (w), 1034 (m), 1093 (w), 1024 (m), 885 (w), 798 (m), 782 (s), 702 (w), 660 (m). Anal. Found (calcd. For C$_{25}$H$_{40}$HfN$_2$): C, 54.71 (54.88); H, 7.27 (7.37); N, 4.91 (5.12) %. EI-MS: *m/z* = 548 (80 %, [*M*]$^{+}$), 533 (70 %, [*M* – Me]$^{+}$), 518 (40 %, [*M* – 2Me]$^{+}$), 315 (100 %, [Cp*Hf]$^{+}$).

Cp*Ti{NC(Ph)N^{i}Pr$_2$}(CH$_2$Ph)$_2$ (23)

To a stirring toluene (25 mL) solution of Cp*Ti{NC(Ph)N^{i}Pr$_2$}Cl$_2$ (**3**) (1.50 g, 3.29 mmol) was added dropwise PhCH$_2$MgCl (6.60 mL, 1.0 M in Et$_2$O, 6.57 mmol) resulting in the orange solution turning a darker colour. The mixture was stirred for 16 h after which time the volatiles were removed *in vacuo* and the resulting oily solid extracted into pentane (15 mL). The volatiles were evaporated once more *in vacuo* to remove any residual toluene. The orange solid was extracted into pentane (4 x 20 mL) and filtered through Celite. Following concentration of the solution to 15 mL, it was stored for two days at -80 ºC after which time the product had crystallised as an orange solid which was washed with very cold pentane (2 x 10 mL) and dried *in vacuo*. Yield = 1.65 g (88 %). ^{1}H NMR (Toluene-d_8, 299.9 MHz, 333 K): 7.27-6.95 (15 H, series of overlapping m, C$_6$H$_5$), 4.32 (2 H, br sept, C<u>H</u>Me$_2$, ^{3}J = 7.0 Hz), 2.31 (2 H, d , C<u>H</u>$_2$Ph, ^{2}J = 10.5 Hz), 2.24 (2 H, d , C<u>H</u>$_2$Ph, ^{2}J = 10.5 Hz), 1.88 (15 H, s, C$_5$Me$_5$), 1.24 (12 H, d, CH<u>Me</u>$_2$, ^{3}J = 7.0 Hz) ppm. ^{13}C-{^{1}H} NMR (Toluene-d_8, 75.4 MHz, 233 K): 162.7 (N<u>C</u>(Ph)N^{i}Pr$_2$), 152.7 (*i*-C$_6$H$_5$ of CH$_2$Ph), 140.8 (*i*-C$_6$H$_5$ of

NC(Ph)N^{i}Pr$_2$), 128.2 (Ph), 128.0 (Ph), 127.9 (Ph), 127.8 (Ph), 127.6 (Ph), 127.4 (Ph), 121.1 (C$_5$Me$_5$), 77.7 (CH$_2$Ph), 48.2 (CHMe$_2$), 22.3 (CHMe$_2$), 11.8 (C$_5$Me$_5$) ppm. IR (NaCl plates, Nujol mull, cm^{-1}): 1591 (m), 1537 (s), 1311 (m), 1202 (w), 1133 (m), 1094 (m), 1026 (m), 946 (w), 916 (w), 880 (m), 786 (s), 738 (s), 723 (m), 692 (s), 657 (m). Anal. Found (calcd. For $C_{37}H_{48}N_2Ti$): C, 78.09 (78.15); H, 8.62 (8.51); N, 4.89 (4.93) %. EI-MS: *m/z* = 477 (5 %, [*M* – CH_2Ph]$^+$), 183 (30 %, [*M* – 2CH_2Ph – {NC(Ph)N^{i}Pr$_2$}]$^+$), 91 (100 % [CH_2Ph]$^+$). Single crystals suitable for X-ray diffraction were grown from a pentane solution at RT.

Cp*Zr{NC(Ph)N^{i}Pr$_2$}(CH$_2$Ph)$_2$ (24)

To a stirring toluene (25 mL) solution of Cp*Zr{NC(Ph)N^{i}Pr$_2$}Cl$_2$ (**18**) (1.50 g, 3.00 mmol) was added dropwise PhCH$_2$MgCl (6.00 mL, 1.0 M in Et$_2$O, 6.00 mmol) resulting in the colourless solution turning yellow. The mixture was stirred for 16 h after which time the volatiles were removed *in vacuo* and the resulting oily solid extracted into pentane (15 mL). The volatiles were evaporated once more *in vacuo* to remove any residual toluene. The yellow solid was then extracted into pentane (4 x 20 mL) and filtered through Celite. The solution was concentrated carefully to *ca*. 15 mL and stored for 16 h at -30 ºC. The product was isolated as yellow crystals which were dried *in vacuo.* Yield = 1.30 g (71 %). ^{1}H NMR (Toluene-d_8, 299.9 MHz, 193 K): 7.39-6.93 (15 H, series of overlapping m, C$_6$H$_5$), 3.39 (1 H, sept, CHMe$_2$ *cis* to C$_6$H$_5$ of NC(Ph)N^{i}Pr$_2$, ^{3}J = 5.7 Hz), 2.67 (1 H, br m, CHMe$_2$ *trans* to C$_6$H$_5$ of NC(Ph)N^{i}Pr$_2$), 2.11 (4 H, br s, CH$_2$Ph), 1.72 (15 H, s, C$_5$Me$_5$), 1.51 (6 H, d, CHMe$_2$ *trans* to C$_6$H$_5$ of NC(Ph)N^{i}Pr$_2$, ^{3}J = 6.0 Hz), 0.53 (6 H, br d, CHMe$_2$ *cis* to C$_6$H$_5$ of NC(Ph)N^{i}Pr$_2$, ^{3}J = 5.7 Hz). ^{13}C-{^{1}H} NMR (Toluene-d_8, 75.4 MHz, 213 K): 161.6 (NC(Ph)N^{i}Pr$_2$), 149.3 (*i*-C$_6$H$_5$ of CH$_2$Ph), 142.7 (*i*-C$_6$H$_5$ of NC(Ph)N^{i}Pr$_2$), 130.0 (Ph), 129.4 (Ph), 127.2 (Ph), 127.0 (Ph), 125.7 (Ph), 124.3 (Ph), 118.1 (C$_5$Me$_5$), 63.9 (CH$_2$Ph), 52.0 (CHMe$_2$ *cis* to C$_6$H$_5$ of NC(Ph)N^{i}Pr$_2$), 46.3 (CHMe$_2$ *trans* to C$_6$H$_5$ of NC(Ph)N^{i}Pr$_2$), 19.8 (CHMe$_2$ *cis* to C$_6$H$_5$ of NC(Ph)N^{i}Pr$_2$), 19.5 (CHMe$_2$ *trans* to C$_6$H$_5$ of NC(Ph)N^{i}Pr$_2$), 10.9 (C$_5$Me$_5$) ppm. IR (NaCl plates, Nujol mull, cm^{-1}): 1592 (w), 1541 (m), 1507 (w), 1300 (m), 1135 (m), 786 (s), 743 (s), 727 (m), 695 (s), 657 (w). Anal. Found (calcd. For $C_{37}H_{48}N_2Zr$): C, 72.73 (72.61); H, 7.83 (7.91); N, 4.48 (4.58) %. EI-MS: *m/z* = 250 (10 %, [*M* – 2CH_2Ph – Cp* - ^{i}Pr]$^+$), 207 (40 %, [*M* – 2CH_2Ph – Cp* - 2^{i}Pr]$^+$), 135 (20 %, [Cp*]$^+$), 91 (90 % [CH_2Ph]$^+$), 77 (70 %, [Ph]$^+$), Single crystals suitable for X-ray diffraction were grown from a pentane solution at RT.

Cp*Hf{NC(Ph)N^{i}Pr$_2$}(CH$_2$Ph)$_2$ (25)

To a stirring toluene (25 mL) solution of Cp*Hf{NC(Ph)N^{i}Pr$_2$}Cl$_2$ (**19**) (1.50 g, 2.55 mmol) was added dropwise PhCH$_2$MgCl (5.10 mL, 1.0 M in Et$_2$O, 5.10 mmol) resulting in the colourless solution turning yellow. The mixture was stirred for 16 h after which time the volatiles were removed *in vacuo* and the resulting oily solid extracted into pentane (4 x 20 mL). The product was isolated as a yellow solid following removal of the pentane and drying *in vacuo* for 16 h. Yield = 1.06 g (58 %). ^{1}H NMR (Toluene-d_8, 299.9 MHz, 213 K): 7.32-6.93 (15 H, series of overlapping m, C$_6$H$_5$), 3.44 (1 H, br sept, C<u>H</u>Me$_2$ *cis* to C$_6$H$_5$ of NC(Ph)N^{i}Pr$_2$, ^{3}J = 6.0 Hz), 2.74 (1 H, br sept, C<u>H</u>Me$_2$ *trans* to C$_6$H$_5$ of NC(Ph)N^{i}Pr$_2$, ^{3}J = 6.5 Hz), 1.91 (4 H, br s, C<u>H$_2$</u>Ph), 1.71 (15 H, s, C$_5$Me$_5$), 1.49 (6 H, d, CH<u>Me$_2$</u> *trans* to C$_6$H$_5$ of NC(Ph)N^{i}Pr$_2$, ^{3}J = 6.5 Hz), 0.57 (6 H, br d, CH<u>Me$_2$</u> *cis* to C$_6$H$_5$ of NC(Ph)N^{i}Pr$_2$, ^{3}J = 6.0 Hz) ppm. ^{13}C-{^{1}H} NMR (Toluene-d_8, 75.4 MHz, 233 K): 164.2 (N<u>C</u>(Ph)N^{i}Pr$_2$), 149.9 (*i*-C$_6$H$_5$ of CH$_2$Ph), 143.7 (*i*-C$_6$H$_5$ of NC(Ph)N^{i}Pr$_2$), 129.2 (Ph), 128.6 (Ph), 127.3 (Ph), 125.5 (Ph), 124.8 (Ph), 121.1 (Ph), 117.6 (<u>C</u>$_5$Me$_5$), 72.1 (C<u>H$_2$</u>Ph), 52.1 (<u>C</u>HMe$_2$ *cis* to C$_6$H$_5$ of NC(Ph)N^{i}Pr$_2$), 46.0 (<u>C</u>HMe$_2$ *trans* to C$_6$H$_5$ of NC(Ph)N^{i}Pr$_2$), 19.7 (CH<u>Me$_2$</u> *cis* to C$_6$H$_5$ of NC(Ph)N^{i}Pr$_2$), 19.3 (CH<u>Me$_2$</u> *trans* to C$_6$H$_5$ of NC(Ph)N^{i}Pr$_2$), 10.6 (C$_5$<u>Me$_5$</u>) ppm. IR (NaCl plates, Nujol mull, cm^{-1}): 1594 (w), 1561 (s), 1301 (m), 1260 (s), 1204 (m), 1135 (w), 1095 (m), 1028 (s), 989 (w), 884 (m), 788 (s), 743 (s), 695 (m), 658(w). Anal. Found (calcd. For C$_{37}$H$_{48}$HfN$_2$): C, 63.37 (63.55); H, 6.76 (6.92); N, 3.84 (4.01) %. EI-MS: *m/z* = 609 (20 %, [*M* – CH$_2$Ph]$^{+}$), 518 (15 %, [*M* – 2CH$_2$Ph]$^{+}$), 91 (100 % [CH$_2$Ph]$^{+}$). Single crystals suitable for X-ray diffraction were grown from a benzene solution at RT.

Cp*Zr{NC(Ph)N^{i}Pr$_2$}(η-2,3-C$_4$H$_4$Me$_2$) (26)

To a stirring solution of Cp*Zr{NC(Ph)N^{i}Pr$_2$}Cl$_2$ (**18**) (1.00 g, 2.00 mmol) and 2,3-dimethyl-1,3-butadiene (2.30 mL, 20.0 mmol) in toluene (30 mL) at 0 ºC was added dropwise ^{n}BuLi (2.50 mL, 1.6 M in n-hexanes, 4.00 mmol). It was allowed to warm slowly to RT and was heated at 85 ºC for 16 h after which time the solution had turned dark red. Removal of the volatiles *in vacuo* afforded a dark red solid which was extracted into pentane (3 x 20 mL). After filtration through Celite, the pentane solution was concentrated to 20 mL and was stored at -30 ºC for 16 h resulting in formation of red crystals which were isolated and dried *in vacuo*. Yield = 0.65 g (63 %). ^{1}H NMR (C$_6$D$_6$, 299.9 MHz, 293 K): 7.19-6.99 (5 H, series of overlapping m,

C_6H_5), 3.79 (2 H, sept, C<u>H</u>Me_2, ^3J = 7.0 Hz), 2.48 (2 H, d, C_4<u>H</u>$_4Me_2$ (*syn*), ^2J = 8.5 Hz), 2.11 (6 H, s, C_4H_4<u>Me</u>$_2$), 1.98 (15 H, s, C_5Me_5), 1.03 (12 H, d, CH<u>Me</u>$_2$, ^3J = 7.0 Hz), 0.20 (2 H, d, C_4<u>H</u>$_4Me_2$ (*anti*), ^2J = 8.5 Hz) ppm. ^{13}C-{^{1}H} NMR (C_6D_6, 75.4 MHz, 293 K): 161.4 (N<u>C</u>(Ph)N^{i}Pr$_2$), 144.1 (*i*-C_6H_5), 128.4 (*o*- or *m*-C_6H_5), 127.6 (*o*- or *m*-C_6H_5), 127.5 (*p*-C_6H_5), 124.1 (2,3-<u>C</u>$_4H_4Me_2$), 117.0 (<u>C</u>$_5Me_5$), 58.5 (1,4-<u>C</u>$_4H_4Me_2$), 47.0 (<u>C</u>HMe_2), 24.4 (C_4H_4<u>Me</u>$_2$), 22.5 (CH<u>Me</u>$_2$), 11.8 (C_5<u>Me</u>$_5$) ppm. IR (NaCl plates, Nujol mull, cm^{-1}): 1584 (s), 1362 (s), 1311 (m), 1277 (s), 1192 (w), 1133 (s), 1085 (m), 1071 (w), 1024 (s), 918 (w), 877 (w), 815 (m), 783 (s), 707 (s), 695 (m), 656 (m), 611 (w), 585 (w). Anal. Found (calcd. For $C_{29}H_{44}N_2Zr$): C, 67.87 (68.04); H, 8.53 (8.66); N, 5.34 (5.47) %. EI-MS: *m/z* = 510 (3 %, [*M*]$^+$), 428 (3 %, [*M* – $C_4H_4Me_2$]$^+$), 136 (10 %, [Cp*H]$^+$).]$^+$). Single crystals suitable for X-ray diffraction were grown from a pentane solution at RT.

Cp*Zr{NC(Ph)N^{i}Pr$_2$}(η-1,4-C$_4$H$_4$Ph$_2$) (27)

To a stirring solution of Cp*Zr{NC(Ph)N^{i}Pr$_2$}Cl$_2$ (**18**) (0.47 g, 0.94 mmol) and 1,4-diphenyl-1,3-butadiene (0.17 g, 0.85 mmol) in toluene (30 mL) at 0 ºC was added dropwise ^{n}BuLi (1.25 mL, 1.6 M in n-hexanes, 1.97 mmol). It was allowed to warm slowly to RT and was heated at 90 ºC for 2 h after which time the solution had turned dark red. Removal of the volatiles *in vacuo* afforded a dark red solid which was extracted into pentane (3 x 20 mL). After filtration, the volatiles were again removed *in vacuo* and the crude solid was isolated. Uncomplexed diene was removed by sublimation (100 ºC, 10^{-1} mBar, dry ice/acetone cold finger, 8 h) giving the desired compound as a dark red solid. Yield = 0.21 g (35 %). ^{1}H NMR (C_6D_6, 299.9 MHz, 293 K): 7.40-6.86 (15 H, series of overlapping m, C_6H_5), 6.22 (2 H, d, 2,3-C_4<u>H</u>$_4Ph_2$, ^3J = 8.7 Hz), 3.79 (2 H, sept, C<u>H</u>Me_2, ^3J = 6.9 Hz), 2.01 (2 H, d, 1,4-C_4<u>H</u>$_4Ph_2$, ^3J = 8.7 Hz), 1.85 (15 H, s, C_5Me_5), 1.08 (12 H, d, CH<u>Me</u>$_2$, ^3J = 6.9 Hz) ppm. ^{13}C-{^{1}H} NMR (C_6D_6, 75.4 MHz, 293 K): 161.8 (N<u>C</u>(Ph)N^{i}Pr$_2$), 146.2 (*i*-C_6H_5 of $C_4H_4Ph_2$), 142.2 (*i*-C_6H_5 of NC(Ph)N^{i}Pr$_2$), 133.2 (Ph), 129.0 (Ph), 128.2 (Ph), 127.8 (Ph), 127.2 (Ph), 126.8 (Ph), 124.6 (Ph), 121.7 (Ph), 120.5 (2,3-<u>C</u>$_4H_4Ph_2$), 118.1 (<u>C</u>$_5Me_5$), 73.1 (1,4-<u>C</u>$_4H_4Ph_2$), 46.8 (<u>C</u>HMe_2), 22.4 (CH<u>Me</u>$_2$), 11.0 (C_5<u>Me</u>$_5$) ppm. IR (NaCl plates, Nujol mull, cm^{-1}): 1653 (m), 1576 (s), 1559 (m), 1541 (w), 1506 (w), 807 (m), 699 (m), 668 (m). Anal. Found (calcd. For $C_{39}H_{48}N_2Zr$): C, 73.53 (73.65); H, 7.69 (7.61); N, 4.33 (4.40) %. EI-MS: *m/z* = 634 (25 %, [*M*]$^+$), 428 (15 %, [*M* – $C_4H_4Ph_2$]$^+$), 225 (20 %,

$[Cp^*Zr]^+$), 206 (100 %, $[C_4H_4Ph_2]^+$), 77 (40 %, $[Ph]^+$). Single crystals suitable for X-ray diffraction were grown from a pentane solution at RT.

$Cp^*Zr\{NC(Ph)N^iPr_2\}\{\eta^3\text{-}CH_2C(Me)C(Me)CH_2BAr^F{}_3\}$ (28)

To a solution of $Cp^*Zr\{NC(Ph)N^iPr_2\}(\eta\text{-}2,3\text{-}C_4H_4Me_2)$ (**27**) (0.15 g, 0.29 mmol) in n-hexanes (20 mL) was added $BAr^F{}_3$ (0.15 g, 0.29 mmol) in n-hexanes (20 mL). Immediately, the solution turned from red to orange and a yellow solid precipitated. After 2 h the suspension was filtered and the solid was washed with pentane (3 x 5 mL) and dried *in vacuo*. Yield = 0.25 g (84 %). ^{1}H NMR (Toluene-d_8, 299.9 MHz, 253 K): 7.18-6.75 (5 H, series of overlapping m, C_6H_5), 4.25 (1 H, br m, C<u>H</u>Me_2), 3.20 (1 H, sept, C<u>H</u>Me_2, ^3J = 6.6 Hz), 2.30 (1 H, d, C<u>H</u>$_2$C(Me)C(Me)C$H_2BAr^F{}_3$, ^2J = 8.7 Hz), 1.68 (15 H, s , C_5Me_5), 1.62 (3 H, s, $CH_2C(Me)C($<u>Me</u>$)CH_2BAr^F{}_3$), 1.25 (3 H, s, $CH_2C($<u>Me</u>$)C(Me)CH_2BAr^F{}_3$), 1.17 (6 H, br d, CH<u>Me</u>$_2$), 0.81 (1 H, d, C<u>H</u>$_2$C(Me)C(Me)C$H_2BAr^F{}_3$, ^2J = 8.7 Hz), 0.68 (6 H, d, CH<u>Me</u>$_2$, ^3J = 6.6 Hz), 0.22 (1 H, br m, $CH_2BAr^F{}_3$), - 0.03 (1 H, br m, $CH_2BAr^F{}_3$) ppm. ^{13}C-{^{1}H} NMR (Toluene-d_8, 75.4 MHz, 253 K): 165.3 (N<u>C</u>(Ph)N^iPr_2), 148.5 (C_6F_5), 144.8 (CH_2<u>C</u>(Me)C(Me)$CH_2BAr^F{}_3$), 139.7 (C_6F_5), 139.5 (*i*-C_6H_5), 136.3 (C_6F_5), 128.4 (*o*- or *m*-C_6H_5), 127.2 (*o*- or *m*-C_6H_5), 125.3 (*p*-C_6H_5), 121.5 (<u>C</u>$_5Me_5$), 113.9 ($CH_2C(Me)$<u>C</u>$(Me)CH_2BAr^F{}_3$), 67.3 (<u>C</u>$H_2C(Me)C(Me)CH_2BAr^F{}_3$), 48.0 (<u>C</u>H$Me_2$), 47.2 (<u>C</u>H$Me_2$), 23.8 ($CH_2C($<u>Me</u>$)C(Me)CH_2BAr^F{}_3$), 23.2 (CH<u>Me</u>$_2$), 20.2 (CH<u>Me</u>$_2$), 18.3 ($CH_2C(Me)C($<u>Me</u>$)CH_2BAr^F{}_3$), 11.1 ($C_5$<u>Me</u>$_5$) ppm (<u>C</u>$H_2B^FAr_3$ and *i*-C_6F_5 were not observed). ^{19}F NMR (Toluene-d_8, 282.2 MHz, 293 K) ppm. ^{19}F NMR (Toluene-d_8, 282.2 MHz, 343 K) -130.6 (m, *o*-F, 6 F), -160.6 (m, *p*-F, 3 F), -165.1 (m, *m*-F, 6 F) ppm. ^{11}B NMR (Toluene-d_8, 96.2 MHz, 293 K) -12.0 ppm. IR (NaCl plates, Nujol mull, cm^{-1}): 1641 (s), 1512 (s), 1492 (m), 1320 (s), 1276 (m), 1193 (w), 1157 (w), 1135 (m), 1083 (s), 1031 (w), 976 (s), 882 (m), 797 (m), 786 (w), 762 (w). Anal. Found (calcd. For $C_{47}H_{44}BF_{15}N_2Zr$): C, 54.93 (55.13); H, 4.41 (4.33); N, 2.79 (2.74) %. EI-MS: *m/z* = 512 (10 %, $[B(C_6F_5)_3]^+$), 168 (60 %, $[(C_6F_5H)]^+$), 136 (50 %, $[Cp^*H]^+$), 77 (20 %, $[Ph]^+$). Single crystals suitable for X-ray diffraction were grown from a benzene solution at RT.

NMR tube scale synthesis of $[Cp^*Ti\{NC(Ph)N^iPr_2\}Me][BAr^F{}_4]$ (29)

To a solid mixture of $Cp^*Ti\{\mu\text{-}NC(Ph)N^iPr_2\}Me_2$ (**4**) (30.0 mg, 72.0 μmol) and $[CPh_3][BAr^F{}_4]$ (66.4 mg, 72.0 μmol) was added C_6D_5Cl (0.5 mL) affording a deep red

solution. The solution was then transferred to an NMR tube and the ^{1}H, ^{13}C, ^{19}F and ^{11}B spectra recorded showing complete conversion to **29** and $MeCPh_3$. ^{1}H NMR (C_6D_5Cl, 299.9 MHz, 293 K): 7.25-6.85 (20 H, series of overlapping m, C_6H_5 of $NC(Ph)N^iPr_2$ and $MeC\underline{Ph}_3$), 4.37 (1 H, br sept, $C\underline{H}Me_2$), 3.47 (1 H, sept, $C\underline{H}Me_2$, ^{3}J = 6.5 Hz,), 1.94 (3H, s, $\underline{Me}CPh_3$), 1.50 (15 H, s , $C_5\underline{Me}_5$), 0.93 (6 H, d, $CH\underline{Me}_2$), 0.81 (3 H, s, TiMe), 0.73 (6 H, d, $CH\underline{Me}_2$, ^{3}J = 6.5 Hz) ppm. ^{13}C-{^{1}H} NMR (major isomer) (C_6D_5Cl, 125.7 MHz, 293 K): 169.3 ($N\underline{C}(Ph)N^iPr_2$), 149.2 (*i*-$C_6H_5$ of $MeCPh_3$), 148.8 (d, *o*-C_6F_5, $^{1}J_{CF}$ = 245.8 Hz), 138.7 (d, *p*-C_6F_5, $^{1}J_{CF}$ = 233.6 Hz), 136.7 (d, *m*-C_6F_5, $^{1}J_{CF}$ = 249.5 Hz), 131.5 (*i*-C_6H_5 of $NC(Ph)N^iPr_2$), 131.3 (*m*- or *o*-C_6H_5 of $NC(Ph)N^iPr_2$), 129.9 (*o*- or *m*-C_6H_5 of $NC(Ph)N^iPr_2$), 129.1 (*o*-C_6H_5 of $MeCPh_3$), 128.2 (*p*-C_6H_5 of $NC(Ph)N^iPr_2$), 128.1 (*m*-C_6H_5 of $MeCPh_3$), 126.1 (*p*-C_6H_5 of $MeCPh_3$), 124.7 (*i*-C_6F_5), 122.4 ($\underline{C}_5Me_5$), 68.0 (Me), 53.4 ($\underline{C}HMe_2$), 52.7 ($Me\underline{C}Ph_3$), 52.0 ($\underline{C}HMe_2$), 30.6 ($\underline{Me}CPh_3$), 22.7 ($CH\underline{Me}_2$), 20.1 ($CH\underline{Me}_2$), 11.9 ($C_5\underline{Me}_5$) ppm. ^{19}F NMR (C_6D_5Cl, 282.2 MHz, 293 K) -131.8 (m, *o*-F, 6 F), -162.5 (m, *p*-F, 3 F), -166.3 (m, *m*-F, 6 F) ppm. ^{11}B NMR (C_6D_5Cl, 96.2 MHz, 293 K) -16.0 ppm. ESI^+-MS: m/z = 401.4 (calcd. For $[C_{24}H_{37}N_2Ti]^+$ *m/z* = 401.2).

$[Cp_2Ti_2\{\mu\text{-}NC(Ph)N^iPr_2\}_2Me_2][BAr^F{}_4]_2$ (30)

To a solid mixture of $CpTi\{NC(Ph)N^iPr_2\}Me_2$ (**20**) (0.20 g, 0.58 mmol) and $[CPh_3][B(C_6F_5)_4]$ (0.53 g, 0.58 mmol) was added chlorobenzene (10 mL) at RT. The dark solution was left to stand at RT for 2 h after which time red crystals of the title compound had formed and were isolated and dried *in vacuo*. Yield = 0.37 g (63 %). The compound was insufficiently soluble to obtain satisfactory NMR spectra. IR (NaCl plates, Nujol mull, cm^{-1}): 1644 (s), 1584 (w), 1515 (m), 1376 (m), 1275 (m)1132 (m), 1093 (s), 1023 (w), 977 (s), 927 (w), 909 (w), 821 (m), 775 (m), 756 (m), 749 (m), 702 (m), 661 (m), 611 (w), 602 (w), 574 (m). Anal. Found (calcd. For $C_{86}H_{54}B_2F_{40}N_4Ti_2$): C, 51.30 (51.12); H, 2.84 (2.69); N, 2.90 (2.77) %. ESI^+-MS: m/z = 662.3 (calcd. For $[C_{38}H_{54}N_4Ti_2]^+$ *m/z* = 662.3). EI-MS *m/z*: 512 (10 %, $[B(C_6F_5)_3]^+$), 168 (60 %, $[(C_6F_5H)]^+$), 103 (100 %, $[NC(Ph)]^+$), 77 (60 %, $[Ph]^+$). Single crystals suitable for X-ray diffraction were grown from a chlorobenzene solution at RT.

$[Cp^*{}_2Zr_2\{\mu\text{-}NC(Ph)N^iPr_2\}_2Me_2][BAr^F{}_4]_2$ (31)

To a solid mixture of $Cp^*Zr\{NC(Ph)N^iPr_2\}Me_2$ (**21**) (0.20 g, 0.43 mmol) and $[CPh_3][B(C_6F_5)_4]$ (0.40 g, 0.43 mmol) was added chlorobenzene (10 mL) at RT. The

dark solution was left to stand at RT for 2 h after which time orange crystals of the title compound had formed and were isolated and dried *in vacuo*. Yield = 0.33 g (68 %). The compound was insufficiently soluble to obtain satisfactory NMR spectra. IR (NaCl plates, Nujol mull, cm^{-1}): 1643 (s), 1515 (m), 1349 (w), 1268 (m), 1136 (w), 1085 (s), 1022 (w), 977 (s), 907 (w), 785 (w), 774 (m), 756 (m), 747 (s), 703 (w), 683 (m), 661 (m), 573 (w). Anal. Found (calcd. For $C_{96}H_{74}B_2F_{40}N_4Zr_2$): C, 51.16 (51.30); H, 3.42 (3.32); N, 2.57 (2.49) %. EI-MS: *m/z* = 512 (100 %, $[B(C_6F_5)_3]^+$), 168 (40 %, $[(C_6F_5H)]^+$), 103 (40 %, $[NC(Ph)]^+$), 77 (20 %, $[Ph]^+$). Single crystals suitable for X-ray diffraction were grown from a chlorobenzene solution at RT.

$[Cp^*_2Hf_2\{\mu\text{-}NC(Ph)N^iPr_2\}_2Me_2][BAr^F_4]_2$ (32)

To a solid mixture of $Cp^*Hf\{NC(Ph)N^iPr_2\}Me_2$ (**22**) (0.20 g, 0.37 mmol) and $[CPh_3][B(C_6F_5)_4]$ (0.34 g, 0.37 mmol) was added chlorobenzene (10 mL) at RT. The dark solution was left to stand at RT for 2 h after which time yellow crystals of the title compound had formed and were isolated and dried *in vacuo*. Yield = 0.35 g (79 %). The compound was insufficiently soluble to obtain satisfactory NMR spectra. IR (NaCl plates, Nujol mull, cm^{-1}): 1644 (s), 1583 (w), 1517 (m), 1267 (m), 1085 (s), 1022 (w), 976 (s), 770 (m), 755 (m), 741 (s), 703 (w), 684 (m), 661 (m), 610 (w). Anal. Found (calcd. For $C_{96}H_{74}B_2F_{40}Hf_2N_4$): C, 47.47 (47.60); H, 3.16 (3.08); N, 2.45 (2.31) %. EI-MS *m/z*: 512 (20 %, $[B(C_6F_5)_3]^+$), 168 (30 %, $[(C_6F_5H)]^+$), 57 (60 %, $[N^iPr]^+$), 77 (50 %, $[Ph]^+$). Single crystals suitable for X-ray diffraction were grown from a chlorobenzene solution at RT.

5.5 Experimental details for Chapter Four

$C_5Me_4H\text{-}2\text{-}C_6H_4C(H)N(OMe)$ (33)

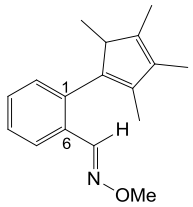

33A

This compound was prepared by adaptation of a patented procedure.[11] To a stirring THF (170 mL) solution of $C_5Me_4H\text{-}2\text{-}C_6H_4CHO$ (14.9 g, 65.6 mmol) was added $H_2NOMe{\cdot}HCl$ (7.14 g, 85.0 mmol), NaOAc (7.03 g, 85.0 mmol) and water (70 mL) and the mixture was stirred for 0.5 h. Following addition of water (60 mL) and EtOAc

(60 mL), the aqueous and organic layers were separated. The organic layer was dried over sodium sulfate and the volatiles were removed *in vacuo*. Addition of toluene (5 mL) followed by removal of the volatiles *in vacuo* was required to remove residual acetic acid to give the title compound as an orange oil. Yield = 17.5 g (77 %). ^{1}H NMR (major isomer **33A** (80 %)) ($CDCl_3$, 299.9 MHz, 293 K): 7.96 (1H, s, C(H)N(OMe)), 7.90 (1H, d, 5-C_6H_4, ^{3}J = 7.8 Hz), 7.33 (1H, dd, 3-C_6H_4, ^{3}J = 7.1 Hz, 7.5 Hz), 7.24 (1H, dd, 4-C_6H_4, ^{3}J = 7.1 Hz, 7.8 Hz), 7.09 (1H, d, 2-C_6H_4, ^{3}J = 7.5 Hz), 3.94 (3H, s, C(H)N(OMe)), 3.07 (1H, br q, CHMe), 1.89 (3H, s, CMeCMeCMe), 1.83 (3H, s, CMeCMeCAr), 1.67 (3H, d, CMeCMeCHMe, ^{4}J = 1.8 Hz), 0.88 (3H, d, CHMe, ^{3}J = 7.5 Hz) ppm. ^{13}C-{^{1}H} NMR (major isomer **33A**) ($CDCl_3$, 75.4 MHz, 293 K): 148.7 (CN), 141.4 (CMeCMeCHMe), 140.3 (CAr), 138.3 (6-C_6H_4), 134.7 (CMeCMeCMe), 134.4 (CMeCMeCAr), 130.5 (1-C_6H_4), 130.3 (2-C_6H_4), 129.4 (3-C_6H_4), 126.7 (4-C_6H_4), 125.7 (5-C_6H_4), 61.9 (OMe), 52.3 (CHMe), 14.1 (CHMe), 12.5 (CMeCMeCHMe), 12.0 (CMeCMeCMe), 11.1 (CMeCMeCAr) ppm. IR (thin film, cm^{-1}): 2961 (s) 2930 (s) 2869 (s) 2817 (m), 1701 (s, υ(C=N)), 1646 (m), 1609 (m), 1478 (m), 1444 (s), 1378 (m), 1338 (m), 1198 (m), 1183 (w), 1056 (s), 980 (w), 957 (w), 917 (s), 847 (m), 761 (s), 638 (w), 625 (m). FI-HRMS: *m/z* = 255.1624 (calcd. For $[C_{17}H_{21}NO]^{+}$ *m/z* = 255.1623).

C_5Me_4H-2-C_6H_4CN (34)

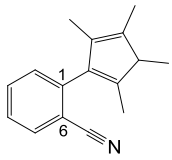

34B

This compound was prepared by adaptation of a patented procedure.[11] LDA was prepared *in situ* by dropwise addition of ^{n}BuLi (121.5 mL, 1.6 M in n-hexanes, 195 mmol) to a solution of diisopropylamine (27.4 mL, 195 mmol) in THF (100 mL) at -78 ºC followed by slow warming to RT. The solution was then cooled to -78 ºC and a solution of C_5Me_4H-2-$C_6H_4C(H)N(OMe)$ (**33**) (16.5 g, 64.6 mmol) in THF (40 mL) was added dropwise. The temperature of the solution was raised slowly to RT and the reaction was quenched by adding toluene (100 mL) and water (100 mL). Separation of the organic and aqueous layers was followed by drying of the organic layer over sodium sulfate. The solvent was removed *in vacuo* to give the title compound as a viscous orange oil. Yield = 13.3 g (92 %). ^{1}H NMR (major isomer

34B (70 %)) ($CDCl_3$, 299.9 MHz, 293 K): 7.66 (1 H, d, 2-C_6H_4, ^3J = 7.8 Hz), 7.53 (1 H, dd, 4-C_6H_4, ^3J = 7.6 Hz, 8.0 Hz), 7.29 (1 H, dd, 3-C_6H_4, ^3J = 7.6 Hz, 7.8 Hz), 7.23 (1 H, d, 5-C_6H_4, ^3J = 8.0 Hz), 3.38 (1H, br q, C<u>H</u>Me, ^3J = 7.5 Hz), 1.91 (3H, d, CMeC<u>Me</u>CHMe, ^4J = 1.2 Hz), 1.86 (3H, d, CHMeC<u>Me</u>CAr, ^4J = 1.2 Hz), 1.67 (3H, s, CMeC<u>Me</u>CAr), 0.92 (3H, d, CH<u>Me</u>, ^3J = 7.5 Hz) ppm. ^{13}C-{^1H} NMR (major isomer **34B**) ($CDCl_3$, 75.4 MHz, 293 K): 142.6 (CMe<u>C</u>MeCHMe), 141.7 (CHMe<u>C</u>MeCAr), 139.5 (<u>C</u>Ar), 137.2 (CMe<u>C</u>MeCAr), 133.3 (2-C_6H_4), 132.4 (1-C_6H_4), 132.3 (4-C_6H_4), 130.7 (5-C_6H_4), 126.8 (6-C_6H_4), 126.4 (3-C_6H_4), 112.2 (CN), 51.3 (<u>C</u>HMe), 14.1 (CH<u>Me</u>), 13.3 (CMeC<u>Me</u>CHMe), 12.0 (CMeC<u>Me</u>CAr), 11.1 (CHMeC<u>Me</u>CAr) ppm. IR (thin film, cm^{-1}): 2223 (s, υ(C≡N)), 1697 (m), 1645 (m), 1597 (m), 1481 (s), 1443 (s), 1379 (m), 1334 (w), 1268 (w), 1185 (w), 1163 (w), 1136 (w), 1104 (w), 1066 (w), 981 (m), 764 (s), 799 (w), 634 (w), 556 (s). FI-HRMS: *m/z* = 223.1366 (calcd. For $[C_{16}H_{17}N]^+$ *m/z* = 223.1361).

C_5Me_4H-2-$C_6H_4C(NMe_2)NH$ (35)

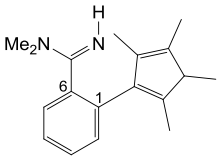

35B

To a stirring THF (80 mL) solution of $LiNMe_2$ (8.26 g, 162 mmol) cooled to -78 ºC was added dropwise a solution of C_5Me_4H-2-C_6H_4CN (**34**) (6.03 g, 27 mmol) in THF (60 mL). Following slow warming to RT, the solution had turned a very dark colour. The solution was then stirred at RT for a further 16 h after which time the solution had turned dark red. Toluene (100 mL) followed by water (200 mL) was added to quench the reaction, the aqueous phase was removed and the organic layer was dried over $MgSO_4$. The solvent was removed *in vacuo* affording a viscous orange oil which was triturated with pentane and dried *in vacuo* giving a waxy orange solid. Yield = 6.86 g (95 %). ^1H NMR (major isomer **35B** (80 %)) (CD_2Cl_2, 299.9 MHz, 243 K): 7.50-7.16 (4 H, series of overlapping m, Ar), 3.16 (3H, s, N<u>Me</u>$_2$)), 2.87 (1H, br q, C<u>H</u>Me, ^3J = 7.1 Hz), 2.54 (3H, s, N<u>Me</u>$_2$), 1.88 (3H, br s, CMeC<u>Me</u>CHMe), 1.84 (3H, br s, CHMeC<u>Me</u>CAr), 1.38 (3H, s, CMeC<u>Me</u>CAr), 0.79 (3H, d, CH<u>Me</u>, ^3J = 7.1 Hz) ppm (NH not observed). ^{13}C-{^1H} NMR (major isomer **35B**) (CD_2Cl_2, 75.4 MHz, 243 K): 166.3 (<u>C</u>N(NMe$_2$)), 142.5 (CMe<u>C</u>MeCHMe), 140.6 (CHMe<u>C</u>MeCAr), 136.0 (<u>C</u>Ar), 134.4 (CMe<u>C</u>MeCAr), 131.4 (Ar CH), 130.9 (Ar CH), 129.0 (1-C_6H_4 or 6-C_6H_4),

127.0 (Ar CH), 126.9 (Ar CH), 125.7 (6-C_6H_4 or 1-C_6H_4), 50.5 (<u>C</u>HMe), 40.4 (N<u>Me</u>$_2$), 39.6 (N<u>Me</u>$_2$), 15.0 (CH<u>Me</u>), 12.5 (CMeC<u>Me</u>CHMe), 12.0 (CMeC<u>Me</u>CAr), 11.2 (CHMeC<u>Me</u>CAr) ppm. IR (thin film, cm^{-1}): 3383 (s, υ(N-H)), 2957 (m), 2870 (m), 1632 (s), 1461 (m), 1453 (m), 1432 (w), 1349 (w), 1251 (s), 1128 (m), 1026 (m), 821 (m), 720 (s). FI-HRMS: *m/z* = 268.1938 (calcd. For $[C_{18}H_{24}N_2]^+$ *m/z* = 268.1939).

C_5Me_4H-2-$C_6H_4C(N^iPr_2)NH$ (36)

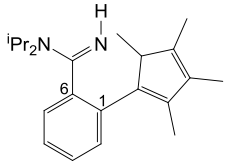

36A

To a stirring THF (60 mL) solution of diisopropylamine (11.5 mL, 81 mmol) cooled to -78 ºC was added dropwise MeMgBr (27 mL, 3.0 M in Et_2O, 81 mmol). The resulting white suspension was allowed to warm slowly to RT. Following 10 min stirring at RT, the suspension was cooled to -78 ºC and a solution of C_5Me_4H-2-C_6H_4CN (**34**) (3.02 g, 13.5 mmol) in THF (40 mL) was added dropwise. Following slow warming to RT, the solution had turned dark red-brown. The solution was then stirred at RT for a further 16 h after which time the solution had turned dark red. Toluene (100 mL) followed by water (200 mL) was added to quench the reaction, the aqueous phase was removed and the organic layer was dried over $MgSO_4$. The solvent was removed *in vacuo* giving a viscous orange oil. The crude product was purified by silica gel column chromatography (5-10 % n-hexanes in Et_2O). Yield = 2.22 g (51 %). ^{1}H NMR (major isomer **36A** (70 %)) ($CDCl_3$, 299.9 MHz, 293 K): 7.34-7.08 (4 H, series of overlapping m, Ar), 3.62 (1H, sept, N(C<u>H</u>Me$_2$)$_2$, ^{3}J = 6.5 Hz), 3.44 (1H, br q, C<u>H</u>Me, ^{3}J = 7.5 Hz), 3.19 (1H, sept, N(C<u>H</u>Me$_2$)$_2$, ^{3}J = 6.5 Hz), 1.85 (3H, s, CMeC<u>Me</u>CMe), 1.83 (3H, s, CMeC<u>Me</u>CAr), 1.67 (3H, br s, CMeC<u>Me</u>CHMe), 1.08 (6H, d, N(CH<u>Me</u>$_2$), ^{3}J = 6.5 Hz), 0.87 (3H, d, CH<u>Me</u>, ^{3}J = 7.5 Hz), 0.74 (6H, d, N(CH<u>Me</u>$_2$), ^{3}J = 6.5 Hz) ppm (NH not observed). ^{13}C-{^{1}H} NMR (major isomer **36A**) ($CDCl_3$, 75.4 MHz, 293 K): 158.8 <u>C</u>N(N^{i}Pr$_2$), 141.6 (CMe<u>C</u>MeCHMe), 139.7 (<u>C</u>Ar), 138.2 (1-C_6H_4 or 6-C_6H_4), 137.6 (CMe<u>C</u>MeCMe), 133.6 (CMe<u>C</u>MeCAr), 130.7 (Ar CH), 128.2 (6-C_6H_4 or 1-C_6H_4), 127.2 (Ar CH), 126.7 (Ar CH), 126.2 (Ar CH), 51.5 (N(<u>C</u>HMe$_2$)$_2$), 51.4 (N(<u>C</u>HMe$_2$)$_2$), 51.0 (<u>C</u>HMe), 15.3 (N(CH<u>Me</u>$_2$)$_2$), 15.1 (CH<u>Me</u>), 14.2 (N(CH<u>Me</u>$_2$)$_2$), 12.3 (CMeC<u>Me</u>CHMe), 12.1 (CMeC<u>Me</u>CMe), 11.3 (CMeC<u>Me</u>CAr) ppm. IR (thin film, cm^{-1}): 3389 (s, υ(N-H)), 2962 (s), 2855 (s), 2753

(m), 1953 (m), 1697 (s), 1621 (s), 1573 (s), 1447 (m), 1367 (m), 1260 (m), 1179 (w), 1026 (s), 921 (w), 802 (s), 761 (s), 733 (m), 699 (m), 680 (w). ESI^+-HRMS: *m/z* = 325.2638 (calcd. For $[C_{22}H_{33}N_2]^+$ *m/z* = 325.2638).

C_5Me_4H-2-$C_6H_4C(NCy_2)NH$ (37)

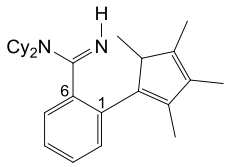

37A

To a stirring THF (100 mL) solution of dicyclohexylamine (26.9 mL, 135 mmol) cooled to -78 ºC was added dropwise MeMgBr (45 mL, 3.0 M in Et_2O, 135 mmol). The resulting yellow solution was allowed to warm slowly to RT. Following 10 min stirring at RT, the solution was cooled to -78 ºC and a solution of C_5Me_4H-2-C_6H_4CN (**34**) (5.02 g, 22.5 mmol) in THF (40 mL) was added dropwise. Following slow warming to RT, the solution had turned dark red-brown. The solution was then stirred at RT for a further 16 h after which time the solution had turned dark red. Water (400 mL) was added to quench the reaction, the aqueous phase was removed and the organic layer was dried over $MgSO_4$. The volatiles were removed *in vacuo* affording a viscous orange oil. The crude product was purified by silica gel column chromatography (5-10 % n-hexanes, 5 % HN^iPr, in Et_2O). Yield = 3.07 g (34 %). ^1H NMR (major isomer **37A** (70 %)) ($CDCl_3$, 299.9 MHz, 293 K): 7.31-7.08 (4 H, series of overlapping m, Ar), 5.78 (1 H, s, NH), 3.46 (1H, qn, C<u>H</u>C_5H_{10}, ^3J = 7.0 Hz), 3.44 (1H, br q, C<u>H</u>Me, ^3J = 7.5 Hz), 2.99 (1H, br m, C<u>H</u>C_5H_{10}), 1.85 (3H, s, CMeC<u>Me</u>CMe), 1.82 (3H, s, CMeC<u>Me</u>CAr), 1.60 (3H, br s, CMeC<u>Me</u>CHMe), 1.74-0.91 (20 H, series of overlapping m for $CHC_5\underline{H}_{10}$), 0.86 (3H, d, CH<u>Me</u>, ^3J = 7.5 Hz) ppm. ^{13}C-{^1H} NMR (major isomer **37A**) ($CDCl_3$, 75.4 MHz, 293 K): 168.3 <u>C</u>N(NCy_2), 142.7 (CMe<u>C</u>MeCHMe), 141.6 (<u>C</u>Ar), 138.2 (1-C_6H_4 or 6-C_6H_4), 133.3 (CMe<u>C</u>MeCMe), 131.1 (CMe<u>C</u>MeCAr), 128.6 (Ar CH), 128.2 (6-C_6H_4 or 1-C_6H_4), 127.5 (Ar CH), 127.0 (Ar CH), 126.5 (Ar CH), 59.7 (<u>C</u>HC_5H_{10}), 51.2 (<u>C</u>HMe), 46.3 (<u>C</u>HC_5H_{10}), 28.1 (CH<u>C</u>$_5H_{10}$), 26.9 (CH<u>C</u>$_5H_{10}$), 26.8 (CH<u>C</u>$_5H_{10}$), 26.5 (CH<u>C</u>$_5H_{10}$), 26.3 (CH<u>C</u>$_5H_{10}$), 26.2 (CH<u>C</u>$_5H_{10}$), 25.6 (CH<u>C</u>$_5H_{10}$), 25.5 (CH<u>C</u>$_5H_{10}$), 22.8 (CH<u>C</u>$_5H_{10}$), 22.7 (CH<u>C</u>$_5H_{10}$), 15.4 (CH<u>Me</u>), 12.8 (CMeC<u>Me</u>CHMe), 12.0 (CMeC<u>Me</u>CMe), 11.2 (CMeC<u>Me</u>CAr) ppm. IR (thin film, cm^{-1}): 3311 (s, υ(N-H)), 3057 (m), 2926 (s), 2853 (s), 1702 (s), 1573 (s), 1484 (m), 1446 (s), 1379 (s), 1326 (m), 1273 (m), 1255 (m),

1194 (s), 1125 (s), 1042 (w), 991 (m), 920 (w), 894 (m), 841 (w), 812 (w), 760 (s), 716 (w), 972 (m), 602 (m). ESI^+-HRMS: *m/z* = 405.3250 (calcd. For $[C_{28}H_{41}N_2]^+$ *m/z* = 405.3264).

(1-C_9H_8OH)-2-$C_6H_4CH(C_2H_4O_2)$ (38)

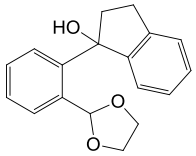

To a stirring Et_2O (400 mL) solution of 2-bromobenzaldehyde ethylene glycol acetal (23.0 g, 100 mmol) cooled to -78 ºC was added dropwise ^{n}BuLi (62.5 mL, 1.6 M in n-hexanes, 100 mmol). Following stirring at -78 ºC for 1 h, a (100 mL) Et_2O solution of 1-indenone (13.3 g, 100 mmol) was added dropwise and the solution was allowed to warm slowly to RT. After 16 h, it was quenched with water (300 mL) and the aqueous and organic layers were separated. Drying of the organic layer over sodium sulfate and concentration of the solution to *ca.* 50 mL *in vacuo* resulted in the title compound crystallizing as a colourless solid which was collected by filtration and dried *in vacuo*. Yield = 16.5 g (59 %). ^{1}H NMR ($CDCl_3$, 299.9 MHz, 293 K): 7.72 (1H, d, Ar, ^3J = 7.7 Hz), 7.29-7.09 (7 H, series of overlapping m, Ar), 6.76 (1H, d, Ar, ^3J = 7.6 Hz), 6.41 (1 H, s, C<u>H</u>($C_2H_4O_2$), 4.14 (2H, m, C_2<u>H_4</u>O_2), 3.96 (2H, m, C_2<u>H_4</u>O_2), 3.21 (1 H, br s, OH), 2.91 (2H, m, CH_2Ar), 2.55 (2H, m, CH_2C(OH)) ppm. ^{13}C-{^{1}H} NMR ($CDCl_3$, 75.4 MHz, 293 K): 148.7 (Ar C_q), 144.2 (Ar C_q), 130.5 (Ar C_q), 129.0 (Ar C_q), 128.9 (Ar CH), 128.8 (Ar CH), 128.3 (Ar CH), 128.1 (Ar CH), 128.0 (Ar CH), 127.6 (Ar CH), 125.4 (Ar CH), 125.0 (Ar CH), 101.8 (<u>C</u>H($C_2H_4O_2$)), 87.1 (COH), 66.0 (<u>C_2</u>H_4O_2), 65.8 0 (<u>C_2</u>H_4O_2), 45.5 (<u>C</u>H_2C(OH)), 30.4 (<u>C</u>H_2Ar) ppm. IR (thin film, cm^{-1}): 3432 (s, υ(O-H)), 2983 (m), 2952 (s), 2926 (m), 2895 (w), 2847 (w), 1603 (w), 1580 (w), 1474 (m), 1451 (m), 1406 (s), 1348 (s), 1287 (s), 1212 (s), 1136 (s), 1091 (s), 1063 (s), 1005 (m), 983 (m), 906 (s), 878 (m), 754 (s), 729 (s), 633 (m), 615 (m). ESI^+-HRMS: *m/z* = 305.1144 (calcd. For $[C_{18}H_{18}NaO_3]^+$ *m/z* = 305.1148). Single crystals suitable for X-ray diffraction were grown by slow evaporation of an acetonitrile solution.

(1-C_9H_7)-2-C_6H_4CHO (39)

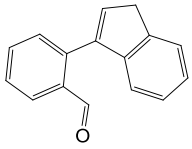

A THF (300 mL) solution of (1-C_9H_8OH)-2-C_6H_4CH($C_2H_4O_2$) (**38**) (16.5 g, 58.4 mmol) was treated with aqueous HCl (6N, 200 ml) and acetone (70 mL). The mixture was stirred for 24 h before toluene (50 mL) was added and the organic and aqueous layers separated. Removal of the volatiles *in vacuo* produced an orange oily material. Purification by silica gel column chromatography (5 % n-hexanes in EtOAc) gave a white powder speculated to be the intramolecular hemiacetal (see Chapter Four) by ^{1}H NMR (and FI-HRMS: *m/z* = 238.0997 (calcd. For $[C_{16}H_{14}O_2]^+$ *m/z* = 238.0994)). Short path distillation (180 ºC, 10^{-6} bar) was required for dehydration giving the title compound as a yellow oil. Yield = 6.10 g (47 %). ^{1}H NMR ($CDCl_3$, 299.9 MHz, 273 K): 10.04 (1H, s, C<u>H</u>O), 8.04 (1H, d, Ar, ^{3}J = 8.0 Hz), 7.67-7.17 (7 H, series of overlapping m, Ar), 6.52 (1H, t, C<u>H</u>CH$_2$, ^{3}J = 2.3 Hz), 3.58 (2H, d, CHC<u>H</u>$_2$, ^{3}J = 2.3 Hz) ppm. ^{13}C-{^{1}H} NMR ($CDCl_3$, 75.4 MHz, 293 K): 192.3 (<u>C</u>HO), 145.3 (Ar C_q), 143.9 (CH<u>C</u>Ar), 141.5 (Ar C_q), 139.8 (Ar C_q), 135.5 (<u>C</u>HCH$_2$), 134.6 (<u>C</u>CHO), 134.0 (Ar CH), 130.3 (Ar CH), 128.2 (Ar CH), 127.6 (Ar CH), 126.7 (Ar CH), 125.6 (Ar CH), 124.2 (Ar CH), 120.3 (Ar CH), 38.9 (CH_2) ppm. IR (thin film, cm^{-1}): 3064 (m), 2847 (m), 2750 (m), 1691 (s, υ(C=O)), 1592 (s), 1457 (s), 1391 (m), 1262 (w), 1248 (w), 1210 (w), 1195 (m), 825 (m), 769 (s), 720 (s), 695 (m), 644 (w), 628 (m), 578 (s). FI-HRMS: *m/z* = 220.0891 (calcd. For $[C_{16}H_{12}O]^+$ *m/z* = 220.0888).

(1-C_9H_7)-2-C_6H_4C(H)N(OMe) (40)

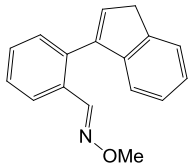

To a stirring THF (200 mL) solution of (1-C_9H_7)-2-C_6H_4CHO (**39**) (6.10 g, 27.7 mmol) was added H_2NOMe·HCl (2.55 g, 30.5 mmol), NaOAc (2.54 g, 30.5 mmol) and water (40 mL) and the mixture was stirred for 2 h. Following addition of toluene (40 mL), the aqueous and organic layers were separated. The organic layer was dried over sodium sulfate and the solvent was evaporated giving the title compound was as an off-white crystalline solid. Yield = 6.20 g, (90 %). ^{1}H NMR ($CDCl_3$, 299.9 MHz,

273 K): 8.11 (1H, s, C(H)N(OMe), 8.03 (1H, d, Ar, ^{3}J = 7.8 Hz), 7.55-7.16 (7 H, series of overlapping m, Ar), 6.46 (1H, t, C<u>H</u>CH_2, ^{3}J = 2.3 Hz), 3.92 (3H, s, OMe), 3.55 (2H, d, CHC<u>H</u>$_2$, ^{3}J = 2.3 Hz) ppm. ^{13}C-{^{1}H} NMR ($CDCl_3$, 75.4 MHz, 293 K): 147.9 (CN), 145.2 (Ar C_q), 144.0 (CH<u>C</u>Ar), 142.9 (Ar C_q), 136.0 (<u>C</u>CN), 134.0 (<u>C</u>HCH_2), 130.6 (Ar C_q), 129.9 (Ar CH), 129.8 (Ar CH), 128.0 (Ar CH), 126.5 (Ar CH), 126.0 (Ar CH), 125.2 (Ar CH), 124.1 (Ar CH), 120.6 (Ar CH), 62.0 (OMe), 38.7 (CH_2) ppm. IR (thin film, cm^{-1}): 3075 (m), 3014 (m), 2990 (m), 2935 (m), 2895 (m), 2819 (m), 1723 (m, υ(C=N)), 1603 (m), 1458 (s), 1385 (w), 1344 (m), 1253 (w), 1203 (w), 1050 (s), 1038 (s), 920 (m), 877 (m), 847 (m), 790 (m), 764 (s), 722 (s), 685 (m), 623 (m). FI-HRMS: *m/z* = 249.1149 (calcd. For $[C_{17}H_{15}NO]^{+}$ *m/z* = 249.1154). Single crystals suitable for X-ray diffraction were grown by slow evaporation of an acetonitrile solution.

(1-C_9H_7)-2-C_6H_4CN (41)

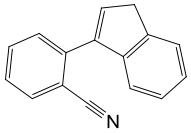

LDA was prepared *in situ* by dropwise addition of ^{n}BuLi (46.2, 1.6 M in n-hexanes, 74.0 mmol) to a solution of diisopropylamine (10.4 mL, 74.0 mmol) in THF (200 mL) at -78 ºC followed by slow warming to RT. The solution was then cooled to -78 ºC and a solution of (1-C_9H_7)-2-C_6H_4C(H)N(OMe) (**40**) (6.10 g, 24.5 mmol) in THF (100 mL) was added dropwise. The temperature was raised to RT and the reaction was quenched by adding toluene (100 mL) and water (100 mL). Separation of the organic and aqueous layers was followed by drying of the organic layer dried over sodium sulfate. The volatiles were then removed *in vacuo* to give the title compound without further purification. Yield = 4.50 g (85 %). ^{1}H NMR ($CDCl_3$, 299.9 MHz, 293 K):7.40-6.84 (8 H, series of overlapping m, Ar), 6.46 (1H, t, C<u>H</u>CH_2, ^{3}J = 2.4 Hz), 3.22 (2H, d, CHC<u>H</u>$_2$, ^{3}J = 2.4 Hz) ppm. ^{13}C-{^{1}H} NMR ($CDCl_3$, 75.4 MHz, 293 K): 144.2 (CH<u>C</u>Ar), 143.5 (Ar C_q), 141.3 (Ar C_q), 139.6 (Ar C_q), 135.2 (<u>C</u>HCH_2), 134.0 (Ar CH), 132.6 (Ar CH), 129.4 (Ar CH), 128.0 (Ar CH), 126.4 (Ar CH), 125.5 (Ar CH), 124.4 (Ar CH), 120.0 (Ar CH), 118.6 (Ar C_q), 112.0 (CN), 38.9 (CH_2) ppm. IR (thin film, cm^{-1}): 3065 (m), 3032 (m), 2226 (s, υ(C≡N)), 1607 (w), 1570 (w), 1488 (m), 1442 (m), 1383 (m), 1339 (w), 1247 (w), 1167 (w), 1089 (w), 1025 (w), 946 (s),

898 (w), 800 (m), 762 (s), 713 (s), 605 (m). FI-HRMS: *m/z* = 217.0887 (calcd. For $[C_{16}H_{11}N]^+$ *m/z* = 217.0891).

±2-(((1R,2S)-1,2,3,4-tetramethyl-5-oxocyclopent-3-en-1-yl)methyl)benzonitrile (42)

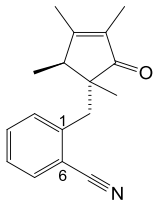

LDA was prepared *in situ* by dropwise addition of ^{n}BuLi (54.3 mL, 1.6 M in n-hexanes, 87.0 mmol) to a solution of diisopropylamine (12.2 mL, 87.0 mmol) in THF (100 mL) at -78 ºC followed by slow warming to RT. The solution was then cooled to -78 ºC and a solution of 2,3,4,5-tetramethylcyclopent-2-enone (10.0 g, 72.4 mmol) in THF (50 mL) was added dropwise. The resulting yellow solution was allowed to warm slowly to RT before being refluxed for a further 16 h. The volatiles were then removed *in vacuo* affording a yellow oil. The oil was extracted into THF (20 mL) and cooled to -78 ºC before a THF (30 mL) solution of 2-(bromomethyl)benzonitrile (14.2 g, 72.4 mmol) was added dropwise. Following slow warming of the orange solution to RT and stirring for 16 h, the volatiles were removed in vacuo affording an orange oily material which was extracted into Et_2O (50 mL) and washed with water (3 x 15 mL). The aqueous phase was removed and the organic layer was dried over sodium sulfate before the solvent was removed *in vacuo*. Recrystallisation from MeOH (15 mL) gave a single diastereomer of the product as large colourless crystals. Yield = 12.3 g (71 %). ^{1}H NMR ($CDCl_3$, 299.9 MHz, 293 K): 7.15 (1H, d, 2-C_6H_4, ^{3}J = 7.8 Hz), 7.01 (1H, dd, 3-C_6H_4, ^{3}J = 7.7 Hz, 7.8 Hz), 6.86 (1H, dd, 4-C_6H_4, ^{3}J = 7.7 Hz, 7.9 Hz), 6.81 (1H, d, 5-C_6H_4, ^{3}J = 7.9 Hz), 2.70 (1H, d, CH_2, ^{2}J = 13.5 Hz), 2.57 (1H, d, CH_2, ^{2}J = 13.5 Hz), 2.14 (1H, q, C<u>H</u>Me, ^{3}J = 7.5 Hz), 1.44 (3H, s, C<u>Me</u>CMeCO), 1.21 (3H, s, CMeC<u>Me</u>CO), 0.64 (3H, s, C(<u>Me</u>)CH_2Ar), 0.62 (3H, d, CHMe, ^{3}J = 7.5 Hz) ppm. ^{13}C-{^{1}H} NMR ($CDCl_3$, 75.4 MHz, 293 K): 211.9 (CO), 171.9 (<u>C</u>MeCMeCO), 142.2 (1-C_6H_4), 133.5 (CMe<u>C</u>MeCO), 132.5 (2-C_6H_4), 132.4 (3-C_6H_4), 131.5 (5-C_6H_4), 127.0 (4-C_6H_4), 118.5 (6-C_6H_4), 113.8 (CN), 51.4 (<u>C</u>(Me)CH_2Ar), 44.9 (<u>C</u>HMe), 41.3 (CH_2), 20.9 (C(<u>Me</u>)CH_2Ar), 14.7 (C<u>Me</u>CMeCO), 13.3 (CH<u>Me</u>), 8.17 (CMeC<u>Me</u>CO) ppm. IR (thin film, cm^{-1}): 3068 (m), 3028 (w), 2869 (s), 2219 (m, υ(C≡N)), 1687 (s, υ(C=O)), 1648 (s), 1598 (w), 1572 (w), 1486 (w), 1449 (m), 1388 (m), 1335 (m),

1299 (w), 1196 (w), 1180 (w), 1129 (w), 1088 (m), 1077 (m), 1042 (m), 1003 (w), 951 (w), 925 (w), 819 (w), 766 (s), 717 (w), 678 (w). ESI$^+$-HRMS: *m/z* = 276.1362 (calcd. For $[C_{17}H_{19}NnaO]^+$ *m/z*: 276.1359). Single crystals suitable for X-ray diffraction were grown by slow evaporation of a methanol solution.

{η^5, η^1-C_5Me_4-2-C_6H_4C(NMe_2)N}TiCl_2 (43)

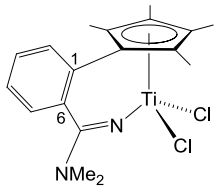

To a stirring toluene (40 mL) solution of Ti(NMe_2)$_4$ (6.10 mL, 25.6 mmol) was added dropwise a toluene (20 mL) solution of C_5Me_4H-2-C_6H_4C(NMe_2)NH (**35**) (6.86 g, 25.6 mmol). The solution immediately turned from orange to dark red and was stirred for a further 6 h at RT. The volatiles were then removed *in vacuo* and the solid extracted into toluene (40 mL). Trimethylsilyl chloride (7.10 mL, 56.3 mmol) was added dropwise and the solution was stirred for a further 16 h. The volatiles were again removed *in vacuo* and the dark red solid extracted into warm (*ca.* 50 ºC) toluene (80 mL). The desired product crystallised after storage at -30 ºC for two days. Following washing thoroughly with pentane (4 x 20 mL) and drying *in vacuo* the product was isolated as an orange microcrystalline powder. Yield = 4.48 g (45 %). ^{1}H NMR (CD_2Cl_2, 299.9 MHz, 293 K): 7.64-7.46 (4H, series of overlapping m, Ar), 3.34 (3 H, s, NMe_2), 3.14 (3 H, s, NMe_2), 2.19 (6 H, s, C<u>Me</u>CMeCAr), 1.73 (6 H, s, CMeC<u>Me</u>CAr) ppm. ^{13}C-{^{1}H} NMR (CD_2Cl_2, 75.4 MHz, 293 K): 168.8 (CN), 138.7 (1-C_6H_4), 135.8 (6-C_6H_4), 132.0 (Ar CH), 131.3 (Ar CH), 130.7 (<u>C</u>MeCMeCAr), 128.7 (CMe<u>C</u>MeCAr), 127.7 (Ar CH), 127.5 (Ar CH), 125.1 (<u>C</u>Ar), 41.7 (NMe_2), 40.1 (NMe_2), 13.1 (CMeC<u>Me</u>CAr), 12.4 (C<u>Me</u>CMeCAr) ppm. IR (NaCl plates, Nujol mull, cm^{-1}): 1573 (s), 1547 (s), 1269 (m), 1248 (m), 1206 (m), 1079 (w), 1019 (m), 953 (w), 918 (w), 880 (m), 823 (s), 774 (w), 760 (s), 712 (m), 673 (w), 595 (m), 536 (m). Anal. Found (calcd. For $C_{18}H_{22}Cl_2N_2Ti{\cdot}0.1(C_7H_8)$): C, 56.98 (56.95); H, 5.82 (5.83); N, 7.02 (7.10) %. EI-MS: *m/z* = 384 (30 %, $[M]^+$), 340 (20 %, $[M - NMe_2]^+$). Single crystals suitable for X-ray diffraction were grown from a benzene solution at RT.

{η^5, η^1-C_5Me_4-2-$C_6H_4C(N^iPr_2)N$}$TiCl_2$ (44)

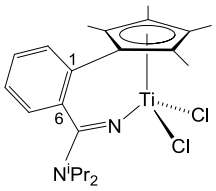

To a stirring toluene (30 mL) solution of $Ti(NMe_2)_4$ (1.60 mL, 6.90 mmol) was added dropwise a toluene (20 mL) solution of C_5Me_4H-2-$C_6H_4C(N^iPr_2)NH$ (**36**) (2.22 g, 6.90 mmol). The solution immediately turned from orange to dark red and was stirred for a further 6 h at RT. The volatiles were then removed *in vacuo* and the solid extracted into toluene (40 mL). Trimethylsilyl chloride (1.90 mL, 15.2 mmol) was added dropwise and the solution was stirred for a further 16 h. The volatiles were again removed *in vacuo* and the dark red solid extracted into benzene (25 mL). The desired product crystallised as a red/orange solid from the concentrated benzene solution (15 mL) and, after washing thoroughly with pentane (4 x 20 mL), was isolated and dried *in vacuo*. Yield = 1.84 g (61 %). ^{1}H NMR (Toluene-d_8, 299.9 MHz, 213 K): 7.15-7.00 (4 H, series of overlapping m, Ar), 3.73 (1 H, sept, C<u>H</u>Me_2 *cis* to Ar, ^3J = 6.0 Hz), 2.75 (1 H, sept, C<u>H</u>Me_2 *trans* to Ar, ^3J = 6.3 Hz), 2.23 (6 H, s, C<u>Me</u>CMeCAr), 1.97 (3 H, s, CMeC<u>Me</u>CAr (closer to Ar)), 1.60 (6 H, br s, two peaks overlapping: 3 H, d, CH<u>Me</u>$_2$ *trans* to Ar and 3 H, s, CMeC<u>Me</u>CAr (further from Ar)), 1.41 (3 H, d, CH<u>Me</u>$_2$ *trans* to Ar, ^3J = 5.9 Hz), 0.76 (3 H, br d, CH<u>Me</u>$_2$ *cis* to Ar, ^3J = 6.0 Hz), 0.43 (3 H, br d, CH<u>Me</u>$_2$ *cis* to Ar, ^3J = 6.0 Hz) ppm. ^{13}C-{^{1}H} NMR (Toluene-d_8, 75.4 MHz, 213 K): 167.6 (CN), 139.0 (1-C_6H_4), 138.1 (6-C_6H_4), 132.0 (Ar CH), 130.6 (Ar CH), 129.9 (Ar CH), 128.0 (<u>C</u>MeCMeCAr), 127.2 (<u>C</u>MeCMeCAr), 126.6 (CMe<u>C</u>MeCAr (further from Ar)), 126.4 (CMe<u>C</u>MeCAr (closer to Ar)), 126.1 (Ar CH), 124.1 (<u>C</u>Ar), 53.6 (<u>C</u>HMe_2 *cis* to Ar), 48.2 (<u>C</u>HMe_2 *trans* to Ar), 20.8 (CH<u>Me</u>$_2$ *cis* to Ar), 20.3 (two peaks overlapping: CH<u>Me</u>$_2$ *cis* to Ar and CH<u>Me</u>$_2$ *trans* to Ar), 18.5 (CH<u>Me</u>$_2$ *trans* to Ar), 14.7 (CMeC<u>Me</u>CAr (closer to Ar)), 13.0 (CMeC<u>Me</u>CAr (further from Ar)), 12.2 (C<u>Me</u>CMeCAr), 11.7 (C<u>Me</u>CMeCAr) ppm. IR (NaCl plates, Nujol mull, cm^{-1}): 1595 (w), 1569 (w), 1304 (s), 1261 (s), 1151 (m), 1083 (m), 1018 (s), 966 (w), 890 (m), 801 (m), 771 (m). Anal. Found (calcd. For $C_{22}H_{30}Cl_2N_2Ti\cdot0.1(C_6H_6)$): C, 60.30 (60.45); H, 6.84 (6.87); N, 5.60 (6.24) %. EI-MS : *m/z* = 440 (3 %, $[M]^+$), 397 (100 %, $[M - {}^iPr]^+$), 340 (70 %,

[*M* – N^iPr_2]$^+$), 305 (30 %, [*M* - N^iPr_2 – Cl]$^+$), 222 (50 %, [*M* – $TiCl_2$ – N^iPr_2]$^+$), 78 (100 %, [Ph]$^+$). Single crystals suitable for X-ray diffraction were grown from a benzene solution at RT.

{η^5, η^1-C_5Me_4-2-$C_6H_4C(NCy_2)N$}$TiCl_2$ (45)

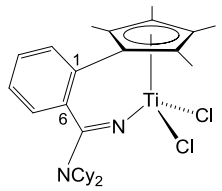

To a stirring toluene (30 mL) solution of $Ti(NMe_2)_4$ (1.80 mL, 7.59 mmol) was added dropwise a toluene (20 mL) solution of C_5Me_4H-2-$C_6H_4C(NCy_2)NH$ (**37**) (3.07 g, 7.59 mmol). The solution immediately turned from orange to dark red and was stirred for a further 6 h at RT. The volatiles were then removed *in vacuo* and the solid extracted into toluene (40 mL). Trimethylsilyl chloride (2.60 mL, 20.4 mmol) was added dropwise and the solution was stirred for a further 16 h. The volatiles were again removed *in vacuo* and the dark red solid washed with pentane (3 x 20 mL) and subsequently extracted into hot toluene (60 mL). The desired product crystallized after storage for 16 h at -30 ºC. The crystals were washed with pentane (3 x 20 mL) and dried *in vacuo*. Yield = 1.26 g (32 %). ^{1}H NMR (CD_2Cl_2, 299.9 MHz, 293 K): 7.60-7.39 (4 H, series of overlapping m, Ar), 3.92 (1 H, br m, C<u>H</u>C_5H_{10}), 2.98 (1 H, br m, C<u>H</u>C_5H_{10}), 2.16 (6 H, s, C<u>Me</u>CMeCAr), 1.91-1.10 (20 H, series of overlapping m for $CHC_5\underline{H}_{10}$), 1.81 (6 H, s, CMeC<u>Me</u>CAr) ppm. ^{13}C-{^{1}H} NMR (CD_2Cl_2, 75.4 MHz, 293 K): 168.7 (CN), 138.9 (1-C_6H_4), 138.5 (6-C_6H_4), 132.6 (Ar CH), 130.5 (Ar CH), 129.3 (<u>C</u>MeCMeCAr), 128.5 (CMe<u>C</u>MeCAr), 126.8 (Ar CH), 126.3 (Ar CH), 125.3 (<u>C</u>Ar), 63.2 (<u>C</u>HC_5H_{10}), 59.7 (<u>C</u>HC_5H_{10}), 32.5 (CH<u>C</u>$_5H_{10}$), 32.3 (CH<u>C</u>$_5H_{10}$), 28.9 (CH<u>C</u>$_5H_{10}$), 28.7 (CH<u>C</u>$_5H_{10}$), 26.7 (CH<u>C</u>$_5H_{10}$), 26.6 (CH<u>C</u>$_5H_{10}$), 26.5 (CH<u>C</u>$_5H_{10}$), 26.1 (CH<u>C</u>$_5H_{10}$), 25.9 (CH<u>C</u>$_5H_{10}$), 25.4 (CH<u>C</u>$_5H_{10}$), 13.6 (CMeC<u>Me</u>CAr), 12.2 (C<u>Me</u>CMeCAr) ppm. IR (NaCl plates, Nujol mull, cm^{-1}): 1569 (m), 1504 (s), 1332 (m), 1317 (s), 1260 (m), 1249 (w), 1160 (w), 1018 (m), 992 (s), 895 (m), 830 (s), 781 (m), 759 (s), 709 (w), 691 (m), 646 (w). Anal. Found (calcd. For $C_{28}H_{38}Cl_2N_2Ti$): C, 64.67 (64.50); H, 7.35 (7.35); N, 5.15 (5.37) %. EI-MS: *m/z* = 520 (3 %, [*M*]$^+$), 437 (100 %, [*M* – Cy]$^+$), 340 (60 %, [*M* – NCy_2]$^+$), 305 (40 %, [*M* – Cl – NCy_2]$^+$). Single crystals suitable for X-ray diffraction were grown by slow cooling of a benzene solution from 70 ºC to RT.

{η^5, η^1-C$_5$Me$_4$-2-C$_6$H$_4$C(NMe$_2$)N}TiMe$_2$ (46)

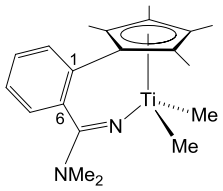

To a stirring toluene (40 mL) solution of {η^5, η^1-C$_5$Me$_4$-2-C$_6$H$_4$C(NMe$_2$)N}TiCl$_2$ (**43**) (1.0 g, 2.60 mmol) was added dropwise two equivalents of MeMgCl (1.73 mL, 3.0 M in THF, 5.20 mmol). Following stirring for 16 h, the volatiles were removed *in vacuo* and the resulting solid extracted into pentane (4 x 20 mL). The desired complex was recrystallised from a concentrated pentane solution (20 mL) at -30 ºC as a yellow-brown powder which was isolated and dried *in vacuo*. Yield = 0.27 g (30 %). ^{1}H NMR (C$_6$D$_6$, 299.9 MHz, 293 K): 7.29 (1 H, d, 2-C$_6$H$_4$, ^{3}J = 7.7 Hz), 7.09 (1 H, dd, 3-C$_6$H$_4$, ^{3}J = 7.7 Hz, 7.8 Hz), 6.95 (1 H, dd, 4-C$_6$H$_4$, ^{3}J = 6.5 Hz, 7.8 Hz), 6.93 (1 H, d, 5-C$_6$H$_4$, ^{3}J = 6.5 Hz), 2.65 (6 H, s, NMe$_2$), 2.19 (6 H, s, C<u>Me</u>CMeCAr), 1.51 (6 H, s, CMeC<u>Me</u>CAr), 0.60 (6 H, s, TiMe) ppm. ^{13}C-{^{1}H} NMR (C$_6$D$_6$, 75.4 MHz, 293 K): 166.3 (CN), 138.6 (1-C$_6$H$_4$), 138.5 (6-C$_6$H$_4$), 132.0 (2-C$_6$H$_4$), 129.0 (3-C$_6$H$_4$), 126.8 (4-C$_6$H$_4$), 125.6 (5-C$_6$H$_4$), 123.8 (CMe<u>C</u>MeCAr), 120.5 (<u>C</u>MeCMeCAr), 119.0 (<u>C</u>Ar), 43.9 (TiMe), 39.2 (NMe$_2$), 11.9 (CMeC<u>Me</u>CAr), 11.7 (C<u>Me</u>CMeCAr) ppm. IR (NaCl plates, Nujol mull, cm^{-1}): 1596 (s), 1570 (s), 1560, 918 (m), 817 (s), 774 (m), 757 (s), 714 (s), 678 (m), 643 (w). Anal. Found (calcd. For C$_{20}$H$_{28}$N$_2$Ti): C, 69.82 (69.77); H, 8.34 (8.20); N, 7.92 (8.14) %. EI-MS: *m/z* = 329 (5 %, [*M* – Me]$^+$), 314 (40 %, [*M* – 2Me]$^+$), 270 (20 %, [*M* – 2Me – NMe$_2$]$^+$). Single crystals suitable for X-ray diffraction were grown from a pentane solution at RT.

{η^5, η^1-C$_5$Me$_4$-2-C$_6$H$_4$C(N^{i}Pr$_2$)N}TiMe$_2$ (47)

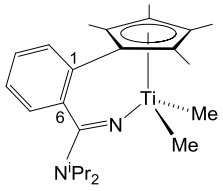

To a stirring toluene (30 mL) solution of {η^5, η^1-C$_5$Me$_4$-2-C$_6$H$_4$C(N^{i}Pr$_2$)N}TiCl$_2$ (**44**) (0.66 g, 1.50 mmol) was added dropwise two equivalents of MeMgCl (1.00 mL, 3.0 M in THF, 3.00 mmol). Following stirring for 16 h, the volatiles were removed *in*

vacuo and the resulting solid extracted into pentane (4 x 20 mL). The desired complex was recrystallised from a concentrated pentane solution (20 mL) at -30 ºC as a yellow powder which was isolated and dried *in vacuo*. Yield = 0.24 g (40 %). ^{1}H NMR (C_6D_6, 299.9 MHz, 293 K): 7.34 (1 H, d, 2-C_6H_4, ^{3}J = 7.6 Hz), 7.14 (1 H, d, 5-C_6H_4, ^{3}J = 7.8 Hz), 7.08 (1 H, dd, 3-C_6H_4, ^{3}J = 7.5 Hz, 7.6 Hz), 6.93 (1 H, dd, 4-C_6H_4, ^{3}J = 7.5 Hz, 7.8 Hz), 3.47 (2 H, br sept, C<u>H</u>Me_2, ^{3}J = 6.0 Hz), 2.20 (6 H, s, C<u>Me</u>CMeCAr), 1.64 (6 H, s, CMeC<u>Me</u>CAr), 1.28 (12 H, br d, CH<u>Me</u>$_2$, ^{3}J = 6.0 Hz), 0.52 (6 H, s, TiMe) ppm. ^{13}C-{^{1}H} NMR (C_6D_6, 75.4 MHz, 293 K): 165.8 (CN), 141.6 (1-C_6H_4), 138.5 (6-C_6H_4), 132.8 (2-C_6H_4), 128.7 (3-C_6H_4), 125.8 (5-C_6H_4), 125.3 (4-C_6H_4), 123.6 (<u>C</u>MeCMeCAr), 120.4 (<u>C</u>Ar), 119.4 (CMe<u>C</u>MeCAr), 50.0 (TiMe), 45.9 (<u>C</u>HMe_2)), 21.1 (CH<u>Me</u>$_2$), 12.5 (CMeC<u>Me</u>CAr), 11.7 (C<u>Me</u>CMeCAr) ppm. IR (NaCl plates, Nujol mull, cm^{-1}): 1570 (w), 1524 (s), 1313 (s), 1220 (w), 1024 (m), 889 (w), 783 (m), 758 (m), 674 (w). Anal. Found (calcd. For $C_{24}H_{36}N_2Ti$): C, 71.65 (71.99); H, 8.84 (9.06); N, 6.89 (7.00) %. EI-MS: *m/z* = 385 (5 %, [*M* – Me]$^{+}$), 370 (40 %, [*M* – 2Me]$^{+}$), 270 (75 %, [*M* – 2Me – N^{i}Pr$_2$]$^{+}$). Single crystals suitable for X-ray diffraction were grown from benzene solution at RT.

{η^5, η^1-C_5Me_4-2-C_6H_4C(NCy$_2$)N}TiMe$_2$ (48)

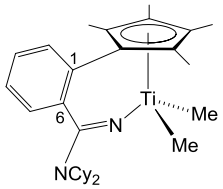

To a stirring toluene (30 mL) solution of {η^5, η^1-C_5Me_4-2-C_6H_4C(NCy$_2$)N}TiCl$_2$ (**45**) (1.00 g, 1.92 mmol) was added dropwise two equivalents of MeLi (2.40 mL, 1.6 M in Et_2O, 3.84 mmol). Following stirring for 3 h, the volatiles were removed *in vacuo* and the resulting solid extracted into n-hexanes (4 x 20 mL). The desired complex was recrystallised from a concentrated n-hexanes solution (30 mL) at -30 ºC as a yellow powder which was isolated and dried *in vacuo*. Yield = 0.34 g (37 %). ^{1}H NMR (C_6D_6, 299.9 MHz, 293 K): 7.35 (1 H, d, 2-C_6H_4, ^{3}J = 7.6 Hz), 7.21 (1 H, d, Ar, 5-C_6H_4, ^{3}J = 7.8 Hz), 7.07 (1 H, dd, 3-C_6H_4, ^{3}J = 7.4 Hz, 7.6 Hz), 6.93 (1 H, dd, 4-C_6H_4, ^{3}J = 7.4 Hz, 7.8 Hz), 3.30 (2 H, br m, C<u>H</u>C_5H_{10}), 2.21 (6 H, s, C<u>Me</u>CMeCAr), 1.69 (6 H, s, CMeC<u>Me</u>CAr), 1.65-0.85 (20 H, series of overlapping m for CHC_5<u>H</u>$_{10}$), 0.53 (6 H, s, TiMe) ppm. ^{13}C-{^{1}H} NMR (C_6D_6, 75.4 MHz, 293 K): 166.0 (CN), 141.4 (1-C_6H_4), 138.6 (6-C_6H_4), 132.9 (2-C_6H_4), 128.7 (3-C_6H_4), 125.5 (5-C_6H_4), 125.2 (4-

C_6H_4), 123.5 (CMeCMeCAr), 120.5 (CAr), 119.5 (CMeCMeCAr), 60.2 (br, CHC_5H_{10}), 46.2 (TiMe), 32.0 (CHC_5H_{10}), 31.4 (CHC_5H_{10}), 25.8 (CHC_5H_{10}), 23.1 (CHC_5H_{10}), 14.3 (CHC_5H_{10}), 12.7 (CMeCMeCAr), 11.8 (CMeCMeCAr) ppm. IR (NaCl plates, Nujol mull, cm^{-1}): 2360 (s), 2340 (m), 1304 (s), 1078 (m), 966 (m), 892 (w), 668 (s), 480 (s). Anal. Found (calcd. For $C_{30}H_{44}N_2Ti$): C, 74.92 (74.98); H, 9.52 (9.23); N, 5.57 (5.83) %. EI-MS *m/z*: 465 (3 %, $[M - Me]^+$), 450 (25 %, $[M - 2Me]^+$), 270 (20 %, $[M - 2Me - NCy_2]^+$). Single crystals suitable for X-ray diffraction were grown from a benzene solution at RT.

2-(2-(2,3,4,5-tetramethylcyclopentadienyl)ethyl)isoindolin-1-imine (49)

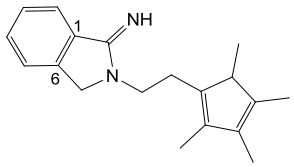

49A

To a stirring toluene (80 mL) solution of 2-(bromomethyl)benzonitrile (5.03 g, 25.7 mmol) was added a toluene (80 mL) solution of 2-(2,3,4,5-tetramethylcyclopentadienyl)ethanamine (4.24 g, 25.7 mmol). The resulting solution was refluxed for 20 h giving the hydrobromide salt of the title compound as a white precipitate which was collected by filtration, washed with Et_2O (3 x 50 mL) and dried *in vacuo*. The salt was then dissolved in chloroform (150 mL) and washed with 4M NaOH solution (40 mL). Following separation of the organic and aqueous layers and drying of the organic phase over Na_2SO_4, the volatiles were removed *in vacuo* giving the title compound as an orange oil. Yield = 3.80 g (53 %). ^{1}H NMR (major isomer **49A** (60 %)) (C_6D_6, 299.9 MHz, 293 K): 7.32 (1H, br s, NH), 7.12-6.88 (4 H, series of overlapping m, Ar), 3.83 (2H, s, ArCH_2N), 3.59 (2H, br m, CH_2CH_2N), 2.79 (1H, q, CHMe, ^{3}J = 7.5 Hz), 2.67 (2H, br m, $CH_2(C_5Me_4H)$, 1.78 (3H, s, CMeCMeCEt), 1.77 (3H, s, CMeCMeCMe), 1.68 (3H, d, CMeCMeCHMe, ^{4}J = 1.7 Hz), 1.08 (3H, d, CHMe, ^{3}J = 7.5 Hz) ppm. ^{13}C-{^{1}H} NMR (major isomer **49A**) (C_6D_6, 75.4 MHz, 293 K): 163.8 (CN), 140.4 (Cet), 138.7 (CMeCMeCHMe), 136.6 (CMeCMeCMe), 134.4 (CMeCMeCEt), 129.7 (1-C_6H_4), 129.6 (Ar CH), 127.6 (Ar CH), 122.7 (Ar), 122.6 (Ar CH), 121.9 (6-C_6H_4), 51.9 (ArCH_2N), 50.1 ($CH_2C_5Me_4H$), 44.2 (CH_2CH_2N), 25.2 (CHMe), 14.4 (CHMe), 11.8 (CMeCMeCHMe), 11.4 (CMeCMeCMe), 11.2 (CMeCMeCEt) ppm. IR (thin film, cm^{-1}): 3254 (m, υ(N-H)), 2958 (s), 2913 (s), 2854 (s), 1636 (s, υ(C=N)), 1591 (m), 1473 (s), 1458 (s), 1365 (m), 1325 (m), 1188 (w),

1142 (w), 1099 (w), 1019 (w), 915 (w), 752 (s), 730 (s), 661 (s). ESI^+-HRMS: *m/z* = 281.2007 (calcd. For $[C_{19}H_{25}N_2]^+$ *m/z* = 281.2012).

{η^5, η^1-C_5Me_4-C_2H_4-$C_8H_7N_2$}$TiCl_2$ (50)

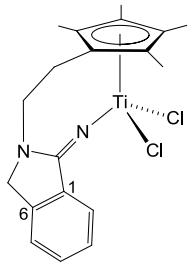

To a stirring THF (30 mL) suspension of NaH (0.36 g, 15.0 mmol) was added a THF (20 mL) solution of 2-(2-(2,3,4,5-tetramethylcyclopentadienyl)ethyl)isoindolin-1-imine (**49**) (2.00 g, 7.1 mmol). The solution was stirred for 16 h at 60 ºC before being cooled to RT and filtered. Trimethylsilyl chloride (1.90 mL, 15.0 mmol) was added dropwise to the solution which was stirred for a further 2 h at RT. The solution was then cooled to -78 ºC and $TiCl_4$ (0.78 mL, 7.13 mmol) was added to it dropwise. The resulting red/orange solution was warmed slowly to RT and stirred for a further 16 h. Removal of the volatiles *in vacuo* afforded a dark brown sticky solid which was washed with n-hexanes (4 x 20 mL) and dried *in vacuo*. Crude yield = 2.20 g (79 %). Spectroscopic data recorded for crude product; assignments for signals thought to correspond to **50**. ^{1}H NMR (C_6D_6, 299.9 MHz, 293 K): 7.14-6.89 (4H, series of overlapping m, Ar), 3.91 (1H, br m, ArC$\underline{H}_2$N), 3.85 (1H, br m, ArC$\underline{H}_2$N), 2.74 ((1H, br m, $CH_2C\underline{H}_2N$), 2.55 (1H, br m, $CH_2C\underline{H}_2N$), 1.85 (3H, s, Me), 1.77 (3H, s, Me), 1.72 (3H, s, Me), 1.63 (3H, s, Me), 1.09 (1H, m, $CH_2(C_5Me_4)$), 0.77 (1H, m, $CH_2(C_5Me_4)$) ppm. ^{13}C-{^{1}H} NMR (C_6D_6, 75.4 MHz, 293 K): 174.8 (CN), 137.9 (1-C_6H_4 or 6-C_6H_4), 134.2 (6-C_6H_4 or 1-C_6H_4), 133.5 ($\underline{C}_5Me_4$), 132.3 (Ar CH), 128.9 (Ar CH), 128.2 (Ar CH), 127.9 ($\underline{C}_5Me_4$), 127.4 ($\underline{C}_5Me_4$), 126.7 ($\underline{C}_5Me_4$), 125.7 (Ar CH), 123.0 ($\underline{C}CH_2CH_2N$), 54.4 (Ar$\underline{C}H_2N$), 52.0 ($CH_2\underline{C}H_2N$), 21.5 ($\underline{C}H_2(C_5Me_4)$), 12.0 ($C_5\underline{Me}_4$), 11.9 ($C_5\underline{Me}_4$), 11.4 ($C_5\underline{Me}_4$), 11.1 ($C_5\underline{Me}_4$) ppm. IR (NaCl plates, Nujol mull, cm^{-1}): 1675 (s), 1616 (w), 1591 (w), 1548 (s), 1307 (w), 1259 (m), 1214 (m), 1178 (w), 1102 (m), 1118 (m), 896 (m), 843 (m), 799 (w), 782 (w), 728 (s), 694 (w), 669 (w). EI-MS: *m/z* = 396 (5 %, $[M]^+$), 361 (5 %, $[M - Cl]^+$), 278 (10 %, $[M - TiCl_2]^+$). EI-HRMS: *m/z* = 396.06 (calcd. For $[C_{19}H_{22}Cl_2N_2Ti]^+$ *m/z* = 396.06).

5.6 General polymerisation procedure

Polymerisation testing was carried out LANXESS Elastomers, The Netherlands, by Mr Ralph Franssen, Mr Philip Kenyon and Mr Hans Leduc under the supervision of Drs Alexandra Berthoud and Martin Zuideveld.

5.6.1 Reagents, cocatalysts and scavengers

Methylaluminoxane (MAO) was purchased from Chemtura as a 10 wt.% aluminium solution in toluene and dosed as a 0.10 M or 1.0 M solution. Isobutylaluminoxane (IBAO-65, 3.5 wt.% Al n-hexanes solution) was purchased from Akzo Nobel and dosed as 0.10 M solutions in n-hexanes or toluene. 4-Methyl-2,6-di-*tert*-butylphenol (BHT, > 99.0 %) was purchased from Sigma-Aldrich and dosed as a 0.20 M solution in n-hexanes. The catalyst precursor solutions were dosed as 1.0 mM solutions in toluene or n-hexanes. $[CPh_3][BAr^F{}_4]$ was dosed as a 2.0 mM solution in toluene. $BAr^F{}_3$ was dosed as a 2.0 mM solution in toluene or n-hexanes. The feed streams (ethylene, propylene, n-hexanes, hydrogen, nitrogen) were purified by contacting with various adsorption media to remove impurities such as water, oxygen and polar compounds. Nitrogen, ethylene and hydrogen were purified using 4Å Molsieves (Merck). Propylene and 2,2,4,6,6-Pentamethylheptane (PMH) were purified using Molsieves 13-X (Merck). Nitrogen, ethylene and propylene were further purified with a copper catalyst (BTS R311 (BASF)). The PMH solvent was additionally stripped with nitrogen. 5-Ethylidene-2-norbornene (ENB) and 5-vinyl-2-norbornene (VNB) were purchased from Ineos and dosed to the reactor as liquids after stripping with nitrogen. In order to avoid mass transfer limitation problems, the total polymer yield in each polymerisation was limited to approximately 10 g after a total polymerisation time of 10 min. The total aluminium concentration in the reactor was kept above 0.45 mM to ensure efficient scavenging.

5.6.2 Ethylene homopolymerisation

The polymerisations were carried out in a 1.5 L batch autoclave equipped with a double intermig stirrer and baffles. The reaction temperature was set to 100 ºC and regulated with a Lauda Thermostat. During polymerisation ethylene was continuously fed to the gas cap of the reactor (500 NL/h). The pressure of the reactor was kept constant by a back-pressure valve. In an inert atmosphere of nitrogen (1.8 bar), the reactor was filled with 700 mL of PMH and IBAO-65. It was heated to 100 ºC while

stirring at 500 rpm, pressurised to 7 bar and conditioned for 15 min until the pressure and temperature remained constant. The catalyst components in PMH solution were then added to the reactor and the catalyst vessel was rinsed with an additional 50 mL PMH. $[CPh_3][BAr^F{}_4]$ was added directly after the precatalyst was dosed. After 10 min, the monomer flow was stopped and the solution was carefully transferred to a 2 L Erlenmeyer flask containing a solution of Irganox-1076 in isopropanol. The reactor was cleaned by stirring the reactor twice for 0.5 h with 750 mL PMH at 150 ºC. All solutions were stabilised with Irganox-1076 in isopropanol and dried overnight at 100 ºC under reduced pressure (< 20 mbar). The polymers were analysed using GPC for molecular weight distributions.

5.6.3 Ethylene-Propylene copolymerisation

Ethylene-propylene batch copolymerisation reactions were carried out in a 2 L autoclave equipped with a double intermig stirrer and baffles. The reaction temperature was set to 90 °C and regulated by a Lauda LTH303 Thermostat. Ethylene and propylene monomers were continuously fed to the gas cap of the reactor during the conditioning period and the polymerisation time. The total monomer flow was kept constant during each experiment (either 500 or 800 NL/h). The pressure of the reactor was kept constant by a back-pressure valve. In an inert atmosphere of nitrogen (1.8 bar) the reactor was filled with 950 ml of PMH solvent, IBAO-65 (Chapter Three) or MAO and BHT (Chapter Four). It was heated to 90 °C while stirring at 1350 rpm, pressurised to 7 bar by feeding ethylene and propylene and conditioned by applying a fixed ratio of ethylene and propylene for 15 min. The catalyst components were then added as PMH solutions to the reactor and the catalyst vessel was rinsed with an additional 50 mL of PMH. $[CPh_3][BAr^F{}_4]$ or $BAr^F{}_3$ was added directly after the precatalyst was dosed. After 10 min of polymerisation time the monomer flow was stopped and the solution was carefully transferred to a 2 L Erlenmeyer flask, containing a solution of Irganox-1076 in isopropanol and dried over night at 100 °C under reduced pressure (< 20 mbar). The polymers were analysed for molecular weight distribution (GPC) and composition (FT-IR).

5.6.4 EPDM copolymerisation

The same procedure was used as for the ethylene-propylene copolymerisation reactions and in addition: 0.70 mL of ENB and 0.70 mL of VNB were added before

heating the reactor to 90 °C and 0.35 NL/h of hydrogen was fed to the reactor together with the ethylene/propylene feed.

5.7 X-ray data collection and processing parameters

Crystals were mounted on glass fibres using perfluoropolyether oil and cooled rapidly in a stream of dinitrogen gas (150 K) from an Oxford Cryostreams unit. Diffraction data were measured using an Enraf-Nonius KappaCCD diffractometer. As appropriate, absorption and decay corrections were applied to the data and equivalent reflections merged.[12] The structures were solved with SIR92[13] and further refinements and all other crystallographic calculations were performed using the CRYSTALS program suite.[14] Other details of structure solutions and refinements (CIF data) are provided in the CD Appendix.

5.8 References for Chapter Five

1. H. Bigmore, DPhil Thesis, University of Oxford, 2007.
2. J. L. Robbins, N. M. Edelstein, S. R. Cooper and J. C. Smart, *J. Am. Chem. Soc.*, 1979, **101**, 3853-3857.
3. C. M. Fendrick, L. D. Schertz, E. A. Mintz, T. J. Marks, T. E. Bitterwolf, P. A. Horine, T. L. Hubler, J. A. Sheldon and D. D. Belin, *Inorg. Synth.*, 1992, **29**, 193-198.
4. P. T. Wolczanski and J. E. Bercaw, *Organometallics*, 1982, **1**, 793-799.
5. D. S. Matharu, D. J. Morris, A. M. Kawamoto, G. J. Clarkson and M. Wills, *Org. Lett.*, 2005, **7**, 5489-5491.
6. D. C. Bradley and I. M. Thomas, *J. Chem. Soc.*, 1960, 3857.
7. G. M. Diamond, R. F. Jordan and J. L. Petersen, *Organometallics*, 1996, **15**, 4030-4037.
8. D. C. Bradley and I. M. Thomas, *J. Chem. Soc.*, 1960, 3857 - 3861.
9. D. van Leusen, D. J. Beetstra, B. Hessen and J. H. Teuben, *Organometallics*, 2000, **19**, 4084-4089.
10. E. G. Ijpeij, P. J. H. Windmuller, H. J. Arts, F. Van der Burgt, G. H. J. Van Doremaele and M. A. Zuideveld, *LANXESS ELASTOMERS, WO/2005/090418*, 2005.
11. H. Hanaoka, E. Yoshikawa and Y. Imamoto, *Sumitomo Chemical Co., WO2003024983A1*, 2003.

12. Z. Otwinowski and W. Minor, *Processing of X-ray Diffraction Data Collected in Oscillation Mode*, Academic Press, New York, 1997.
13. A. Altomare, G. Cascarano, C. Giacovazzo and A. Guagliardi, *J. Appl. Crystallogr.*, 1994, **27**, 1045-1050.
14. P. W. Betteridge, J. R. Carruthers, R. I. Cooper, K. Prout and D. J. Watkin, *J. Appl. Crystallogr.*, 2003, **36**, 1487.